Damage Detection in Structures

using

Natural Frequency Measurements

A thesis submitted to the

School of Aerospace, Civil and Mechanical Engineering

University of New South Wales

Australian Defence Force Academy
for the degree of Doctor of Philosophy

by

Laxmikant Kannappan

December 2008

Certificate of Originality

I hereby declare that this submission is my own work and to the best of my knowledge it contains no material previously published or written by another person, nor material which to a substantial extent has been accepted for the award of any other degree or diploma at UNSW or any other educational institution, except where due acknowledgement is made in the thesis. Any contribution made to the research by colleagues, with whom I have worked at UNSW or elsewhere, during my candidature, is fully acknowledged.

I also declare that the intellectual content of this thesis is the product of my own work, except to the extent that assistance from others in the projects design and conception or in style, presentation and linguistic expression is acknowledged.

Laxmikant Kannappan

Abstract

In the last two decades, the emphasis in aircraft maintenance has been on developing on-line structural health monitoring systems to replace conventional non destructive inspection techniques which require considerable down-time, human effort and cost. Vibration based damage detection is one of the most promising techniques for implementation in Structural Health Monitoring *(SHM)*. In vibration based methods, the presence of damage is detected by monitoring changes in one of the dynamic parameters of the structure, resonant frequencies, modeshapes or damping characteristics. Compared to modeshape based methods, frequency based methods have the advantage that measurements need to be taken only at a single location. Previous developments on frequency based techniques have relied on Finite Element Model updating; analytical techniques have hitherto been restricted to beams due to the complexity in developing equations for cracked two dimensional structures. In this thesis the analytical approach using an energy formulation is extended to plates with through-thickness cracks, where modeshapes from either numerical modelling or experimental measurements can be employed to determine the energy of vibration. It is demonstrated that by using a hybrid approach, incorporating experimentally measured modeshapes along with measured changes in frequencies, the damage parameters can be estimated without resorting to theoretical modelling or numerical analysis. The inverse problem of finding the crack location, size and orientation from measured changes in frequencies is addressed using minimisation techniques.

The forward problem and the inverse algorithm is first validated using numerical simulation and experimental testing of beams with edge cracks and centre cracks. The application of the methodology to the two dimensional case is then validated

by numerical simulation and experimental modal analysis of plates with through-thickness cracks. A statistical procedure is developed for determination of the 90/95 probability of crack detection and the minimum detectable crack size in both cases. It is demonstrated that the measurement of frequency changes can be successfully employed to detect and assess the location and size of cracks in beams and plates, using modeshapes from theory, *Finite Element Analysis (FEA)* or measurements.

Publications arising from the thesis work

A number of peer-reviewed papers have been published based on the work presented in this thesis. They are listed here for reference.

Conference papers

1. Kannappan, L., Shankar, K., Sreenatha, A.G., **Damage detection using frequency measurements**, 25th International Modal Analysis Conference (IMAC-XXV), Orlando, Florida, USA, February 1922, 2007.

2. Kannappan, L., Shankar, K., **Frequency measurement based damage detection methods applied to different cracks configurations**, 48th AIAA/ASME/ASCE/AHS/ASC Structures, Structural Dynamics, and Materials Conference, Hawaii, USA, April 23-26, 2007.

3. Kannappan, L., Shankar, K., Sreenatha, A.G., **Detection of centre cracks in cantilever beams using frequency measurements**, 7th international conference on Damage Assessment of Structures (DAMAS), Torino, Italy, June 25-27, 2007.

4. Kannappan, L., Shankar, K., Sreenatha, A.G., **Detection of multiple cracks in cantilever beams using frequency measurements**, 13th International Conference on Experimental Mechanics (ICEM13), Alexandroupolis, Greece, July 1-6, 2007.

5. Kannappan, L., Shankar, K., Sreenatha, A.G., **Experimental verification of detection of centre cracks in cantilever beams using energy methods**, International Conference on Advanced Technology in Experimental Mechanics (ATEM07) and 6th Asian Conference on Experimental Mechanics (ACEM6), Fukuoka, Japan, September 12-14, 2007.

6. Kannappan, L., Shankar, K., ***Nondestructive inspection of plates using frequency measurements***, Australian congress of applied mechanics (ACAM07), Brisbane, Australia, December 10-12, 2007.

7. Kannappan, L., Shankar, K., ***Structural integrity assessment of plates using vibration monitoring I:Theory and Simulation***, 13th Australian International Aerospace Congress (AIAC-13), Health and Usage Monitoring, Melbourne, Australia, March 9-12, 2009. (Accepted and to be published)

8. Kannappan, L., Shankar, K., ***Structural integrity assessment of plates using vibration monitoring II:Experiments***, 13th Australian International Aerospace Congress (AIAC-13), Health and Usage Monitoring, Melbourne, Australia, March 9-12, 2009. (under review)

Journal paper

1. Kannappan, L., Shankar, K., Sreenatha, A.G., ***Crack detection using frequency measurements - Theory, experiments and analysis***, Journal of Sound and Vibration (under review).

Acknowledgements

This thesis is set in Adobe using LaTeX. Figures were drawn with xfig or Dia and converted to EncapsulatedPostScript files. Graphs were created with MATLAB and converted to EncapsulatedPostScript files.

Contents

Contents

List of Tables

List of Figures

Nomenclature

Acronyms and abbreviations

Acronyms	Description
AE	Acoustic Emission
ANOVA	ANalysis Of VAriance
APDL	Ansys Parametric Design Language
AR	Auto Regressive
ARX	Auto Regressive Exogenous
ARMA	Auto Regressive Moving Average
CDF	Curvature Damage Factor
CF	Carbon Fibre
CFRP	Carbon Fibre Reinforced Plastic
CVM	Comparative Vacuum Monitoring
CWT	Continuous Wavelet Transform
DI	Damage Index
DIM	Damage Index Method
DLAC	Damage Location Assurance Criterion
DOF	Degrees Of Freedom
EDM	Electric Discharge Machining
EMA	Experimental Modal Analysis
FD	Finite Difference
FDAC	Frequency Domain Assurance Criterion
FE	Finite Element
FEA	Finite Element Analysis

FEM	Finite Element Method
FFT	Fast Fourier Transform
FOS	Fibre Optic Sensor
FRF	Frequency Response Function
GA	Genetic Algorithm
LEFM	Linear Elastic Fracture Mechanics
LISA	Local Interaction Simulation Approach
LS	Least Square
MAC	Modal Assurance Criterion
MDC	Minimum Detectable Crack size
MLP	Multi Layer Perceptron
NDE	Non-Destructive Evaluation
NDI	Non-Destructive Inspection
NN	Neural Network
NSGA	Non-dominated Sorting Genetic Algorithm
POD	Proper Orthogonal Decomposition
PVDF	Poly Vinylidene Flouride
PZT	Plumbum (Lead) Zirconate Titanate
RBF	Radial Basis Function
RC	Reinforced Concrete
RHS	Right Hand Side
RMS	Root Mean Square
SD	Standard Deviation
SHM	Structural Health Monitoring
SIF	Stress Intensity Factor
SNR	Signal to Noise Ratio
SQP	Sequential Quadratic Programming
TOF	Time of Flight

Symbols

Symbols	*Description*
A	Full area of the crack
a	Crack length in case of part-through edge cracks (for beams)
b	Crack length of through-thickness centre cracks (for beams)
	Crack length of through-thickness cracks (for plates)
D	$=Eh^3/12(1-\nu^2)$, Flexural rigidity of the plate
E	Young's Modulus
f_L	"90/95" lower limit frequency
$f(a/h)$	Geometry factor for beams with part through edge cracks
$f(b/W)$	Geometry factor for beams with through-thickness cracks
$g(a/h)$	Integral of the form factor for beams with edge cracks
$g(b/W)$	Integral of the form factor for beams with centre cracks or plates with through-thickness crack
h	Thickness of beam
	Thickness of plate
I	Second moment of area
K_I	Mode I Stress Intensity Factor
L	Length of beam
	Length of plate
$M_n(x)$	Bending moment at any point x along the length of the beam
M_o	Moment resultant (moment per unit width) at the crack location
W	Width of beam
	Width of plate
U_n	Strain energy of the undamaged structure in n^{th} mode
U_n^*	Strain energy of the damaged structure in n^{th} mode
x_c	Crack location along x-axis (for both beams and plates)
y_c	Crack location along y-axis (for plates only)

α_c	Crack location normalised to x-axis (for plates), x_c/L
β_c	Crack location normalised to y-axis (for plates), y_c/W
γ	Normalised crack length; b/W for beams and plates with centre cracks and through-thickness crack respectively
ΔU_n	$= U_n^* - U_n$, Difference between the strain energies of the damaged and the undamaged structure, equal to the strain energy stored in the crack in its nth mode
ζ	Running variable representing the instantaneous crack length
μ	Mean frequency
ν	Poisson's ratio
ρ	Density
ϕ	Crack orientation
χ_{RMS}	Root Mean Square *(RMS)* value of the curvature distribution over the entire length of the beam or area of the plate
χ_c	Curvature at the location of the crack
ψ	Modeshape deflection of undamaged structure
ψ^*	Modeshape deflection of damaged structure
ω_n	Natural frequency of the uncracked structure in the nth mode
ω_n^*	Natural frequency of the cracked structure in the nth mode

CHAPTER 1

Introduction

1.1 Introduction

Structural ageing and cyclic loading cause structures to develop fatigue cracks. Cracks can also be initiated due to defects in manufacturing and environmental conditions. Progressive growth of these cracks can result in failure of the structure. It is critical to prevent catastrophic failures by periodically inspecting the structure for cracks and other damages. Especially in aircraft structures, early damage detection is absolutely vital as it involves human safety. It is estimated that 27% of the cost of the average life cycle of an aircraft is spent on inspecting the structure for damage [1]. Due to the current practices of damage detection used in aircraft maintenance, a significant portion of the aircraft's life is spent as down-time while it is being inspected to ensure structural integrity. The traditional Non-Destructive Inspection *(NDI)* techniques, developed in the first half of the twentieth century, are labour intensive, time consuming and hence costly.

Therefore the ability to ensure the integrity of structures while they are still in operation and on a continuous, real-time basis, is desirable. The last two decades has seen a spurt in research and development in Structural Health Monitoring *(SHM)* systems that offer the capability of monitoring the integrity of the structure in real-time and in situ with minimum down-time and human labour involved. *SHM* involves integration of sensors, data processing, telemetry, modern computational hardware and decision-making algorithms. Conventional *NDI* techniques are not suitable candidates for on-line implementation and new techniques are sought after

for adoption to *SHM*. One of the early techniques to be seriously considered as a candidate for *SHM* is vibration monitoring. Because of their high sensitivity, whole field coverage and ease of application, vibration based techniques are still highly promising as candidates for *SHM*. Unlike other potential techniques for implementation in *SHM* such as Lamb waves, Fibre optics and impedance methods, vibration monitoring does not require a source of excitation; the vibration resulting from operation of the equipment such as aircraft may be employed to extract the natural frequencies for monitoring.

The principle behind vibration based damage assessment is that any damage changes the local stiffness and energy dissipation characteristics which results in changes in the natural frequencies, modeshapes and damping parameters of the structure. By monitoring the change in any or all of these parameters, damage can be identified and assessed. While damping is highly sensitive to damage, damping parameters are not easy to measure and are significantly influenced by environmental factors, loading and boundary conditions. The presence of a local defect produces only a small local variation in the modal deflection, but this shows up sharply in the second derivative of the deflection function. Thus variations in modeshapes can provide definite indications of the presence and location of the damage. However, a major disadvantage is that modeshape measurements are prone to noise. The differences in the values of modeshape deflections of the damaged and undamaged structures are often of the same order of magnitude or lower than the noise level in the measurements, making it difficult to identify small defects reliably and often producing false alarms. The accuracy of modeshape measurements depends highly on the number and distribution of the measurement points employed. Further, modeshape methods require arduous and meticulous measurement of displacements or accelerations over the entire surfaces of the undamaged and damaged structures. On the other hand, frequency based damage detection methods are easier to implement in practice since they only require measurement of resonant frequencies which can be performed quickly using a single sensor at a single location. Further, changes in modal frequencies can be recorded with greater accuracy and more reliably as the effect of external noise is minimal in comparison to modeshape measurements.

Hence, a damage detection technique incorporating the measurement of natural frequencies is explored in this thesis.

1.2   Scope of thesis

The aim of this thesis is to develop and extend the use of frequency based damage assessment for health monitoring in structures. Two approaches currently employed in this area are the use of numerical modelling and analytical formulation. In the former, a Finite Element model which accurately matches the dynamic properties of the undamaged structure is created and then progressively updated using trial and error or sensitivity analysis until the frequencies of the updated model match the measured frequencies of the damaged structure. Current analytical methods using frequency measurements are limited to one dimensional beam structures, mainly due to the difficulty of formulating the governing equations for vibrations of plates with damage. In the present work, a theoretical approach using energy formulation for beams with edge cracks is extended to beams with centre cracks and further developed to through-thickness cracks in plates. This is possible since the energy formulation does not require solution of the governing equations for vibration of the plate; the frequency changes can be related to modal curvatures which may be obtained numerically or experimentally. The methodology for solving the inverse problem i.e., determining the crack size, location and orientation from measured frequency changes, is formulated using different minimisation techniques.

1.3   Thesis outline

An overview of literature relating to potential *SHM* techniques is presented in Chapter 2 followed by a detailed survey of literature on vibration based damage detection techniques including modeshape based methods and frequency based methods. A preliminary study of comparison between modeshape based and frequency based methods using *FE* modelling and experimental testing is presented in Chapter 3. The theoretical model using the energy formulation for beams with centre cracks and plates with through-thickness cracks is developed in Chapter 4. Methodologies for solution to the inverse problem are also presented. Chapter 5 describes

the validation of the theory for beams using numerical simulation. The validation using experimental testing on beams is presented in Chapter 6. In Chapter 7, an attempt is made to conduct a statistical analysis on experimental data to determine the probability of crack detection and minimum detectable crack size. Chapters 8 and 9 respectively deal with validation of the theoretical model for plates using *Finite Element Analysis (FEA)* and experimentation. The efficacy of the gradient based minimisation technique (Sequential Quadratic Programming) in solving the inverse problem of determining the damage parameters from measured frequency changes is also demonstrated. Conclusions and recommendations for future work are presented in Chapter 10.

CHAPTER 2

Literature review

2.1 Introduction

Non-Destructive Inspection (NDI) has played a major role in the service of aircraft, particularly since the introduction of the damage tolerance philosophy of maintenance. Traditional *NDI* techniques such as magnetic particle inspection, eddy current inspection, ultrasonic testing, radiography and the liquid penetrant method, which were introduced during the first and second world wars, are still extensively used for inspection of cracks in metallic aircraft structures. Some of these techniques such as ultrasonic testing and radiography have also been adapted for damage detection in composite structures. While individual methods may have their own limitations and drawbacks, these conventional methods complement each other and, together, provide a comprehensive system of inspection for ensuring structural integrity. However, the last three decades have seen a move towards the introduction of Structural Health Monitoring *(SHM)* systems. They essentially involve embedding a *Non-Destructive Evaluation (NDE)* system (or a set of *NDE* systems) into a structure to allow continuous remote monitoring for damage with minimal human intervention [1]. The conventional *NDI* techniques, although highly sensitive, are not easily amenable to on-line implementation for the following reasons:

- Most of the techniques listed above, with the exception of radiography have been developed for localised inspection which requires some a priori knowledge of the location of damage. Application over wider areas requires movement of the probe in a systematic manner which requires mechanical effort and is

time consuming. Although radiography is a whole field inspection technique, its hazardous nature eliminates any possibility of it being implemented as an on-line technique.

- Most conventional *NDI* techniques, in particular radiography, require the use of large pieces of equipment, a string of instrumentation and/or a variety of consumables (eg. dye penetrant for liquid penetrant inspection).

- Traditional *NDI* techniques are dependent on skilled mechanical labour and human intervention for both application of the technique and interpretation of the indications.

- Since the conventional techniques were developed before the advent of modern electronics, they are not easily adaptable to modern methods of data acquisition and storage and interpretation through intelligent information systems.

For the above reasons, researchers have resorted to looking elsewhere for *SHM* systems that can be employed on-line, require minimal human intervention, can be monitored remotely in real-time and through the use of intelligent data interpretation systems. Techniques potentially considered for *SHM* include Fibre optic sensors, Acoustic Emission, Lamb waves, Comparative Vacuum Monitoring, Impedance methods and Vibration monitoring systems. This thesis focuses on vibration based techniques, however, a brief review of the state of the art of some of the other techniques is presented in Section 2.2. Vibration techniques of damage detection are based on monitoring changes in the vibration characteristics of the structure introduced by the damage. Vibration parameters that may be monitored include modal frequencies, modeshapes, damping characteristics, time response and frequency response functions of the structure. Vibration methods other than frequency based techniques and other auxiliary methods are described in Section 2.3. Literature on frequency based methods which form the subject of this thesis is comprehensively dealt with in Section 2.4.

2.2 Potential *SHM* techniques

It is estimated that a quarter of an aircraft's life cycle cost is spent for inspection and repair [1]. Industry has been searching for ways in which the cost, effort and time associated with aircraft maintenance can be reduced without compromising passenger safety. In particular, in the current economic climate, the high cost associated with aircraft down-time and the human effort required for traditional aircraft maintenance systems is of great concern. On-line Structural Health Monitoring systems, offering the benefits of reduced aircraft down-time, reduced human intervention, electronic information storage and the other advantages mentioned above, have been touted as the solution to this. Worden and Dulieu-Barton [2] provide an overview of a typical *SHM* system and describe its components. The following subsections present a review of literature on potential *SHM* techniques other than vibration based methods (which are presented elsewhere).

2.2.1 Fibre Optic Sensors

Fibre Optic Sensors *(FOS)* were one of the first to be advocated as potential on-line health monitoring devices. They have been employed in a variety of health monitoring applications to monitor parameters such as temperature, pressure, strain and moisture content [3]. It may be noted that any of these can be used as indicators of health of the structure or a potential threat to it. For instance, a sudden increase in temperature or pressure may indicate a potential fire hazard; an abrupt change in strain can indicate the possibility of an overload on the structural component which may lead to damage or even catastrophic failure. Optical fibres are usually embedded into composites made of fibre reinforced laminates during the manufacturing stage. It is claimed that since the optical fibres are of the same dimensions as that of the fibre reinforced laminates, they do not significantly affect the structural properties of the composite. The fibres are interrogated with coherent light from lasers and optical sensors are employed to monitor either the transmitted or reflected light coming out of the optic fibres. It is proposed that the output of the *FOS* can be continuously monitored by an on-board computer even when the aircraft is in flight. The most common application of optical fibres is for strain measurement. Fibre optic Bragg gratings are employed for this purpose [4, 5, 6, 7, 8]. Although

strain measurement is not the same as damage detection, monitoring strain can be employed for detection of damage when it occurs, as described above.

FOS have also been proposed as damage detection systems for low velocity impact damage of composite structures [9]. This is based on monitoring the light transmitted through the fibres which records a sudden drop if an optical fibre is damaged in the vicinity of the impact location. By having a grid of fibres covering a wide area, such as that of an aircraft wing, the damage location can also be identified. Lee [10], Rao [11], Dudderar [12], Casas and Cruz [13] and Majumder *et al.* [14] have published extensive reviews on application of *FOS*.

Due to their high sensitivity and their suitability for continuous maintenance-free monitoring, *FOS* have often been applied in the monitoring of bridges [11, 13, 14, 15, 9]. But one of the main disadvantages of the *FOS* is that the fibres have to be embedded during the manufacturing phase itself and, hence, cannot be applied to existing, ageing fleets of aircraft or structures [16]. Moreover, the surface-bonded fibres are insensitive to internal damage in the structure [16].

2.2.2   Acoustic Emission

In acoustic emission, the rapid release of elastic energy stored in the structure due to crack growth, called an Acoustic Emission *(AE)* event, is used to identify and locate the occurrence or growth of discontinuity [17, 18, 19, 20, 21]. Once this event occurs, acoustic waves propagate in concentric circles for isotropic material or in a pattern dominated by the internal structure (unidirectional laminate, woven fibre, etc.) for non-isotropic materials.". Thus, by using a number of sensors and the time of arrival of the energy bursts at each sensor, the location of the discontinuity can be determined. Though this technique promises to be effective in crack detection, it cannot be used to locate or assess an existing defect, unless the defects size increases and results in an *AE* event. Also, to find the extent of damage, the emission behaviour of a structure with similar material properties must be studied in the laboratory. Using different damage scenarios, a database of the energy released as a function of crack sizes and locations relative to the sensor positions is created.

2.2.3   Lamb wave based methods

Lamb waves refer to the elastic waves propagating in a thin plate with free boundaries [22]. Two types of Lamb waves are used in damage detection: symmetric and asymmetric. When Lamb waves are generated within the material of a known wave frequency (and a known velocity), using the Time Of Flight *(TOF)* information and the attenuation in the signal received, damage can be located and assessed [23]. Two methods are commonly used: the echo pulse method where a single transducer is used as both the actuator and the sensor and the shadow method where an actuator and a sensor are placed on opposite edges of the plate [22]. Excellent reviews of Lamb wave based damage detection technology are given by Ajay and Cesnik [23, 24] and Su *et al.* [25].

Guided Lamb waves have been proposed for *SHM* applications using piezoelectric sensors permanently attached to thin panels such as aircraft wing skins in a rectangular or circular array. The omnidirectional characteristics of circular elements were found to be well-suited for application to large areas [26, 27, 28]. Giurgiutiu *et al.* [29] and Purekar *et al.* [30] have used spatially compact linear arrays. Malyrenko *et al.* [31, 32] have developed tomographic algorithms to construct images using data from elements arranged on the periphery of the interrogation area. While the above approaches require a fairly large number of array elements for reasonable accuracy in locating the damage, more recent techniques using a sparse array of circular elements over a large area in combination with special algorithms to generate images have been investigated [33]. Kim *et al.* [34] proposed a novel signal-conditioning method in which they separated the symmetric and asymmetric modes using two sensors to record the Lamb wave signals.

Kessler [1, 35] used Lamb waves for damage detection in quasi-isotropic plates and cylinders made from graphite epoxy laminates, aluminium honeycomb, Nomex and Rohacell cores. Different types of damage (holes, matrix cracks and delamination) were considered. Though they successfully located the damage in all cases, they could not quantitatively establish its severity (the area of delamination or the size of the hole) from the energy content of the fringe pattern in the reflected waves obtained from either the composite plates or the cylinders.

Lee and Staszewski [36,37] studied a simulation technique for the propagation of Lamb waves over thin plates using the Local Interaction Simulation Approach *(LISA)* which they validated experimentally. On the basis of good agreement between the simulation and experimental results, they proposed that *LISA* is more suited to wave propagation studies than the Finite Element Method *(FEM)* or the Boundary Element Method.

Koh *et al.* [38] conducted *FEA* using PAFEC software to study the effect of local stiffness changes and presence of delaminations on transmission of Lamb waves. They simulated various scenarios of *Barely Visible Impact Damage* and computed the power transmitted through the damage. They observed that the normalised power transmitted across the damage decreased with decreasing stiffness. Koh *et al.* [39] studied the effect of disbond growth beneath a composite repair patch on the magnitude of power transmitted using numerical simulation and experiments and concluded that power measurement is efficient in detecting disbonds.

Yuan *et al.* [40] used Lamb waves together with Neural Network *(NN)* to determine the location and size of the damage in impact-damaged honeycomb sandwich and carbon fibre composites. They trained the *NN* with experimental data and successfully applied the method to detect similar damages in composite panels.

Su and Ye [25, 41, 42, 43] also used *NN* along with Lamb waves but trained the network with a large set of data generated by numerical simulation of Carbon Fibre *(CF)* composite panels with various levels of delamination damage. They also demonstrated that with training of *NN* using simulation, Lamb waves can be successfully employed to detect and characterise delamination damage in composites.

2.2.4   Comparative vacuum monitoring

A relatively new technique proposed for *SHM* is the Comparative Vacuum Monitoring *(CVM)* where a vacuum is maintained within a small-volume chamber between the test surface and a pressure sensor. Any leakage from within the chamber due to the crack, changes the vacuum inside the chamber and the pressure difference is used to quantify the damage [44].

Wishaw and Barton [45] conducted *CVM* experiments on specimens containing cracks as small as 250 microns and demonstrated that *CVM* can detect cracks which are not easily detectable by conventional *NDI* techniques such as eddy current and ultrasonic inspection. Roach *et al.* [46] conducted an extensive study of application of *CVM* technique to airframe components. Together with the University of Arizona they conducted fatigue tests on simulated aircraft panels with *CVM* sensors embedded along the riveted joints. Through-thickness cracks were allowed to grow and pressure readings recorded periodically. On the basis of extensive statistical analyses, they reported that cracks as small as 0.02" (0.5mm) were detected with a 90% probability with 95% confidence. They implemented this technique in real commercial aircraft for periodic measurements but, to date, no results have been reported on the progress of this research.

The *CVM* technique seems promising, as it is sensitive to cracks as small as 0.25mm, but it requires the approximate location of damage to be known a priori. The sensors used in this technique can be left in-situ for periodic monitoring [45], but installing them along all the rivet holes is not feasible. Moreover, common damage modes in composites, such as delamination, which occur below the surface, cannot be detected as this technique is limited to identifying surface cracks.

2.2.5 Impedance based methods

Impedance based *SHM* involves monitoring variations in the mechanical impedance of the structure caused by the presence of damage. The impedance is measured by electromechanical coupling using Plumbum (Lead) Zirconate Titanate *(PZT)* patches [47, 48]. The *PZT* patch acts both as an actuator and a sensor, exciting the structure at very high frequencies, typically greater than $30KHz$. At this level, the wavelength of excitation is small and the sensitivity to minor defects is high. The impedance response is measured continuously by the patch; any sudden change in impedance provides the indication of occurrence of damage. Park *et al.* [49] provide an excellent overview of the impedance based health monitoring technique.

Chaudhry *et al.* [50] implemented the impedance based technique to monitor the structural integrity of the tail section of a Piper Model 601P airplane. They simulated damage by loosening various bolts both near and far from the *PZT* sensor.

11

They were able to identify all the near-field damage cases but none of the far-field damage cases. They concluded that the damage detection capability of impedance based technique is *highly localised.* In contrast, Andrew *et al.* [51] conducted experiments on thin aluminium plates and reported that higher impedance signatures were observed for far field damages, although they could not provide an explanation for this abnormal behaviour.

Most researchers using impedance based techniques for damage detection use high frequency ranges ($> 30KHz$) in their experiments because of the high sensitivity of impedance signatures to damage at those frequencies and their low sensitivity to boundary condition changes. But, this restricts the technique to localised areas [49]. Some investigators propose a combination of two different methods for near- and far-field damage detection or the integration of impedance based techniques with soft computing techniques like *NN* or evolutionary programming.

Park *et al.* [47] integrated the impedance based technique with Frequency Response Function *(FRF)* data to detect and characterise damage. Giurgiutiu *et al.* [52] proposed the use of the impedance based technique in combination with the guided wave (Lamb wave) propagation. Lopes *et al.* [53] used impedance signatures in combination with *NN* to detect damage in the form of bolt loosening in truss structures. Xu *et al.* [54] formulated impedance based damage detection as an optimisation problem and solved it using evolutionary algorithm.

2.3   Vibration based methods

Vibration based methods rely on the fact that damage causes a local change in the stiffness and material properties of the structure which, in turn, changes its dynamic characteristics, *viz.* natural frequencies, damping characteristics and modeshapes. The changes in these dynamic properties can be employed to detect the presence and characterise the damage. In general, vibration based damage detection techniques may be categorised into methods based on damping measurements, those based on measurement of modeshapes, frequency response and time response methods and techniques based on measurement of frequencies. The last of these, being the subject of this thesis, is reviewed in detail in the next section. Other vibration based methods are discussed below.

Over the past two decades, vibration based damage detection techniques have been studied extensively and have found increasing applications in the aeronautical, civil and mechanical engineering fields. Zou *et al.* [55], Doebling *et al.* [56,57], Sohn *et al.* [58], Carden and Fanning [59], Dimarogonas [60] and Montalvao *et al.* [61] provide excellent reviews of vibration based damage detection methods.

2.3.1 Methods based on measurement of damping characteristics

Damping measurements are not explored as much as other modal parameters for damage detection [58] and only a few researchers have tried to implement this procedure. One of its greatest advantages is that it is sensitive to the non-linear, dissipative effects that cracks produce. The damping in a structure changes significantly due to the initiation of cracks as well as their growth. A small, visually undetectable damage which produces only a negligible change in frequency can produce upto a 50% change in the damping ratio values [62].

Modena *et al.* [62, 63] developed two theories using damping ratios to detect and locate damage. In the first, they used specific damping and, in the second, friction damping. As the authors intended to incorporate these techniques for implementation in Reinforced Concrete *(RC)* manufacturing industries, they first applied them to successfully detect damage in a 5.8mX1.2m *RC* beam.

Kawiecki [16] also proposed the use of damping ratios for damage detection. The author conducted experiments on metal beams and metal blanks used in the manufacture of 3.5" floppy disks. Modal analysis was performed using an array of *PZT* transducers, one of which acted as an actuator. Damage was simulated by bonding a 0.5mm thick Dyad 606 viscoelastic patch. The author measured the damping ratios on the beam using patches of different sizes to represent the different levels of damage. It was concluded that the damping ratio measurements were easy to perform and could be used reliably for damage detection but no procedures for locating or characterising damage were provided.

Damping ratio measurements are found to be highly sensitive to very small abnormalities which is of interest to the *SHM* community. Unfortunately, damping measurements are highly inconsistent [64] since damping characteristics are also

easily affected by environmental factors such as temperature, pressure and humidity and more so by minor variations in boundary changes. They are also complex in nature to deduce [55], thus requiring significant advances in technology and analytical tools before they can be implemented in practice.

2.3.2 Modeshape based methods

Modeshape methods are based on the fact that damage in a structure produces a change in the local stiffness, which in turn affects the local curvature and hence the modal deflection at the damage location. Modeshape based damage detection techniques essentially involve monitoring the deflections or curvatures to identify sudden changes which are indicative of the presence of the damage. This is best done by comparing the modal deflections or curvatures of the undamaged and the damaged structures. The simplest approach is to plot the absolute differences in modeshape deflections [65]. An alternative approach is to employ the Modal Assurance Criterion *(MAC)* which is the dot product of the two vectors representing the deflections of the damaged and the undamaged structures [65, 66, 67]. If the *MAC* value is close to 0, there is no correlation between the vectors and, if it is equal to 1, then the vectors are identical. Thus the presence of damage is indicated by a low value of *MAC*. Note that the use of *MAC* suffers from the drawback that the damage location is not identified directly.

In general, monitoring changes in deflections is not very effective since the changes in deflection caused by the damage are small. Identifying changes in curvatures is much more effective due to the direct relationship between curvature and stiffness and the fact that damage introduces a local change in stiffness. Since deflection is the second integral of curvature, small changes in curvature get smoothed out in the deflection function. Hence, most modeshape methods are based on monitoring changes in curvature [68, 69, 70, 71, 72, 73, 74, 75, 76, 77, 78, 79, 80]. The simplest approach once again, is to plot the curvatures of the undamaged structure and that of the structure suspected to have damage on top of each other and look for discrepancies (see Fig. 3.4). However, since the magnitude of the difference in curvatures is small relative to the absolute values of the curvatures, it is much more effective

to plot the difference in curvatures as a function of the beam coordinate and look for significant variations (see Fig. 3.5).

Based on *FEA* results, Pandey *et al.* [68] showed that the use of curvature differences is more effective in detecting damage than the *MAC* method. Curvature based methods have the added advantage that the location of damage is readily identified as soon as a significant difference in curvature is observed. Note that in the methods described so far, the differences in deflections or curvatures are plotted separately in each mode. Other researchers contend that a more effective means to highlight the presence of a damage is to combine the curvature differences in a number of modes. Wahab and Roeck [70] have introduced a parameter combining the differences in several modes, called the *Curvature Damage Factor (CDF)* method while Stubbs *et al.* [69] employ a more complex method called the *Damage Index Method (DIM)*). These are described in greater detail in Section 3.2.

Lestari and Qiao [72] compared the *DIM and CDF* methods by applying them to a fibre-reinforced polymer *(FRP)* composite beam containing impact damage and delamination. The damage location could not be conclusively determined due to the presence of a large number of peaks in the plots obtained from those methods. They concluded that the lower modes were more reliable and suggested increasing the sensor density in order to obtain less noisy modeshapes and increase the reliability of these methods. Hamey *et al.* [73] conducted similar experiments on carbon/epoxy composite beams containing delamination, impact damage and saw cut. They used Poly Vinylidene Fluoride *(PVDF)* sensors to measure the responses and hence the modeshapes. Though they claim that the *DIM* is better than the other methods, its deceptive peaks of almost equal magnitudes in other locations can lead to false alarms unless there is prior knowledge of the location of damage in the structure.

Choi and Stubbs [74] made a comparison of the compliance method and the curvature methods. The compliance method is the application of a biharmonic differential operator to the modeshape deflection. Using modeshapes of simply-supported plates obtained from simulations, they reported that the compliance method performs better than the curvature method. Park *et al.* [76] used the *DIM* to detect damage in a complex 3-D truss structure. They applied it to modeshape

data obtained from *FEA* and damage was detected with no false alarms. When they applied the same algorithm to experimentally obtained modeshapes, only large damages could be detected successfully and, in cases where the damage was small, false alarms arose due to the noise contained in the modeshapes.

Zimmerman and Kaouk [81] employed *FEA* based updating technique using both eigen values (frequencies) and eigen vectors (modeshapes) of the undamaged and damaged structures. Kim *et al.* [77], Jauregui and Farrar [78], Farrar and Jauregui [79] and Cornwell *et al.* [80] also employed modal updating techniques in conjunction with various modeshape based methods and concluded that the *DIM* yielded the best results. Note that, since modeshape methods are based on observations of change in deflections or curvatures, any noise in the measurement data can mask the damage signature or lead to false alarms. Eliminating the noise by filtering runs the risk of removing the damage signature also. This may be improved by using a large array of sensors and instrumentation that provide measurements with minimum noise.

2.3.3   Frequency response and Time response based methods

Owolabi *et al.* [82] used *Frequency Response Function (FRF)* data to identify damage in simply-supported and clamped-clamped beams. First, they created a database of changes in the normalised amplitudes of the *FRF* (ratio of the amplitude of cracked beam to that of the uncracked beam) in the first three modes, as a function of crack location and size from experiments. This database was used to identify, detect and locate damage in a blind specimen. Davis and Wicks [83] used Frequency Domain Assurance Criterion *(FDAC)* to differentiate undamaged and damaged structures. *FDAC* is similar to *MAC* in that, a *FDAC* value of 1 indicates perfect correlation and 0 no correlation. Using this technique, the authors could qualitatively assess the severity of damage present in cylindrical test specimens. Herszberg *et al.* [84] also observed significant changes in *FRF*s obtained from undamaged and damaged beams. Damage was introduced by artificially delaminating the composite beams. Comparing the *FRF*s of control and damaged beams, the presence of disbond was identified irrespective of the location of the sensor-actuator pair.

Lately, time domain based vibration signals are extensively used as a means of system identification and thus damage detection. These techniques are highly sensitive to damage as they use raw data; modal parameters like frequencies and modeshape measurements suffer from the fact that a lot of important information is lost in the processing of the time series data required to obtain them. One of the significant disadvantages of time domain based techniques is that damage information can be extracted qualitatively but not quantitatively and the processing time is considerably high. More importantly, these techniques are highly dependent on environmental factors and the input excitation.

Sohn *et al.* [85] used time response of the damaged and undamaged beams along with statistical pattern recognition techniques for damage detection. Using Auto-Regressive *(AR)* model and Auto Regressive Exogenous *(ARX)* model, they were able to observe differences in the signals between the undamaged and damaged parts of the fast patrol boat. Sohn and Farrar [86] and Sohn *et al.* [87] use the *AR* and *ARX* models in combination with a *NN* to identify damage in a 8-DOF spring mass system.

Nair *et al.* [88] proposed a novel method using the Auto Regressive Moving Average *(ARMA)* to locate and quantify damage in a 2X2-bay structure. Damage was simulated by removing braces or loosening bolts in the structure. Shane and Jha [89] compared the results from an *AR* and a Proper Orthogonal Decomposition *(POD)* model applied to time series data obtained from undamaged and damaged composite wings simulated in *FEA*. Two damage cases were analysed: delamination at the root and delamination at the wing tip. The authors found that the *POD* model was able to distinguish the changes caused by damage better than the *ARMA*.

Many other researchers reported using time domain based techniques for damage detection: Garibaldi *et al.* [90] - Canonical Variate Analysis; Garibaldi *et al.* [91] - *ARMA* and Stochastic Subspace Identification - Balanced Realisation; and Abe *et al.* [92] - Ibrahim's time domain method [93]. They reported that significant changes were observed when comparing the damaged and undamaged signals. But no concrete steps for the implementation of these techniques to locate or characterise damage were suggested.

2.3.4 Wavelet based methods

There is a vast amount of literature on vibration based techniques using Fourier analysis and modal property extraction, but very few researchers have used wavelet-analysis based techniques for damage detection. Vill [94] first introduced the concept of time-frequency analysis in which the signal is filtered at different frequency bands and the energy content is obtained as a function of time and frequency. In short, the signal in time is broken down into a two-dimensional function of time and frequency [95]. Wavelet analysis can be used either as a signal processing tool for filtering noise where another technique is used for fault detection [35, 96] or the wavelet coefficients can be used directly for damage detection [97, 98].

Okafor and Dutta [99] used discrete wavelet transform to detect damage in a cantilever beam. They performed wavelet analysis on the response-time signal obtained from a laser vibrometer and calculated the wavelet coefficients. The beam was excited using a *PZT* patch bonded to both the undamaged and damaged beams and, by comparing their wavelet coefficients, damage was located accurately. The authors observed that very little information regarding damage was present in the modeshapes results. They also showed that the amplitude of the wavelets increased with increasing damage which could be used to find the extent of the damage.

Kessler [1, 35] and Yan *et al.* [100] used wavelet analysis as a signal processing tool in combination with the Lamb waves based method for damage detection. Kessler [1, 35] used this combined approach to detect the presence of damage in composite panels. Yan *et al.* [100] used wavelet transforms to filter the group velocities of the Lamb wave signals and, thus, the Time of flight *TOF*. With these measurements (wavelet coefficients and *TOF*) obtained from a graphite-epoxy composite plate and integrated into the Genetic Algorithm *(GA)*, they determined the damage location and size.

Biemans *et al.* [101] monitored crack growth on an aluminium plate using wavelet analysis. Strain data was collected at different stages of the damage using 5 *PZT* sensors, one being an actuator. They also defined the *Damage Index, DI* as a Euclidean distance between the mean vectors of the variance taken from the wavelet coefficients of the damaged and undamaged plate. Melhem and Kim [102, 103]

applied both the Fourier transform and wavelet analysis for damage detection in a concrete pavement and a simply-supported concrete beam. The Fourier analysis did not show differences in the frequencies before and after the damage, but the Continuous Wavelet Transform *(CWT)* showed considerable changes.

Sung *et al.* [104] used *PZT* sensors to detect the propagation of acoustic waves due to the initiation of impact damage on a composite plate. As the transient *AE* signals obtained from the damaged structure were very complicated for the analysis and characterisation of the damage, it was processed using the *CWT*. Significant changes in the energies of the wavelets after impact and their increasing amplitudes with increases in the energy of the impact were observed.

Yan and Yam [105] proposed the use of changes in the energy distribution of wavelets at different frequencies to identify damage. The undamaged structure was excited with a known force and the energy of the structural vibration response signals at different frequencies were measured using wavelet analysis. They observed that the wavelet energy distribution in the damaged structure changed significantly compared to that in the undamaged structure. They conducted experiments on a composite plate and showed that damage as small as 1% (the ratio of damage size to total size of the structure) could be detected. Yam *et al.* [106] used the same technique but integrated it with *NN* for solving the inverse problem of characterising damage in a *PVC* sandwich plate.

Usually, in any fault detection method, feature extraction plays a very important role. Features are key components which mark significant changes in their properties before and after damage. In wavelet analysis, in order to classify and characterise damage, either the wavelet coefficients themselves [105] or the energy in the wavelets [106] can be used. Other methodologies using wavelet analysis are also employed by researchers to detect damage.

Since the signals obtained for machinery diagnostics are supposed to contain very low signal-to-noise ratios, *(SNR)*, Lin and Qu [97] suggested using the wavelet transform for denoising and fault feature extraction. They proposed an improvement to the *soft-thresholding denoising method* by using Morlet wavelets and the *CWT* for impulse component extraction. They applied this technique for fault detection

to a roller bearing and a gear box. In the former, when the roller passed through the damage, an impulse appeared. By identifying the presence of an impulse signature in the signal, the damage location was determined. The presence of a broken tooth in a gear box was also determined by applying Morlet wavelets to denoise the signals obtained.

2.3.5 *Electrical analogy as a damage detection technique*

Akgun and Ju [107] developed a method for detecting multiple cracks in a beam using electrical analogy. Just as cracks are represented as rotational springs in mechanical analogy, the authors simulated a crack as a resistor. They divided the beam into a number of segments, each represented by a T-circuit consisting of a resistor representing damage. They derived a relationship between the electrical circuit using Kirchoff's voltage law and the Euler-Bernoulli shape function and, from the solution, determined the location and size of the damage.

Song *et al.* [108] used the correlation between damage in a mechanical structure and changes in electrical resistance in a circuit to detect damage. The behaviour of failure progress in Carbon Fibre reinforced Plastic *(CFRP)* composites was studied under monotonic and cyclic tensile loading. The relationship between the strain-producing damage and the electrical resistance changes was correlated and a *NN* was trained using the strain/resistance data. By monitoring changes in electrical resistance, the extent of damage was predicted. The *NN* was tested with experimental data and good agreement was obtained suggesting that measurement of electrical resistances can be used for damage detection.

2.4 Frequency based methods

Damage detection methods employing measurement of changes in frequencies are based on the fact that a damage reduces the local stiffness of the structure and thereby affects its resonant frequencies. Vandiver [109] was the first to examine the changes in frequencies due to the presence of damage. The author noticed upto 17% change in the frequency in the first mode by removing members from a numerical model representing an offshore light station tower that he was investigating. While

a reduction in modal frequencies is indicative of damage, the real inverse problem consists not only of identifying that a damage exists but also determining its location and size. To fully characterise the damage by solving the inverse problem, two different approaches are used: the model-updating technique and the analytical approach.

In the model based approach, a numerical model is developed whose dynamic characteristics perfectly match those of the undamaged structure. Then, the stiffness of the elements of the undamaged model are progressively altered until good agreement is obtained with the responses measured on the damaged structure [110]. Note that the damage is modelled as a variation in the stiffness of the local elements. When the response of the damaged model match those of the damaged structure, the location of the damage and the reduction in stiffness representing the severity of the damage are known. The analytical approach involves modelling the crack as discontinuity in stiffness and deriving the resonant frequencies of the cracked structure theoretically. These equations are used again for solving the inverse problem of characterising damage based on the measured dynamic responses.

2.4.1 Finite Element Analysis based approach

In the model based approach, the numerical model is tuned so that it reproduces the measured responses of the undamaged structure. Then, some of its physical properties are changed, mainly the stiffness of its elements, such that it produces modal data comparable to those measured from the damaged structure [111, 112]. Natural frequencies are generally used for this model based approach [113] but, in some cases, either modeshapes [114] or both frequencies and modeshapes are employed [81, 112, 115].

Cawley and Adams [113] are two of the early researchers who used the *FEA* based approach. They devised the model updating procedure to find the location and extent of damage contained in both an aluminium plate and a cross-ply *CFRP* plate. They performed experiments on the undamaged and damaged plates in a constant temperature enclosure. They modelled the undamaged structure numerically using the *FEM*s. The *FE* program was run iteratively for different damage scenarios by changing the locations and stiffness of the elements until the natural

frequencies obtained from the model matched those from the damaged structure in every mode. Excellent agreement in predicting the location and size of the damage was reported by using this technique for damage detection.

Lee and Chung [116] used sensitivity analysis for finding the location and extent of cracks. They reduced the computation time by finding approximate locations using a rank ordering technique, i.e., the order in which the frequency in each mode changed for different crack locations. They performed numerical analysis on a cracked beam to extract the first four natural frequencies and ranked them according to the percentage changes from the baseline of the undamaged beam's frequency. They compared each rank with the list of ranks created previously to find the approximate location of the damage. Then, the crack was modelled in that approximate location using *FEA* to further iteratively find the exact location and size of the damage.

Mottershead and Friswell [112, 115] provide an excellent review of different model updating methods. Sinha and Friswell [117] provide an overview of a model updating technique using both the trial and error and sensitivity methods. Sensitivity based updating is a form of model updating where the pattern of sensitivity, with respect to the location and size of the crack and the different modes, is calculated beforehand and the resulting information used in the model updating routine [112]. Brownjohn *et al.* [118] provide a summary of model updating procedures with an emphasis on civil structure condition monitoring. They explain the procedure of model updating based damage detection using results obtained from controlled laboratory modal analysis experiments on a steel portal frame.

Friswell and Penny [119] studied different crack modelling approaches, as applied to model updating techniques. Damage can be modelled as elements with reduced stiffness or by using a rotational spring and fracture mechanics. They claimed that the rotational spring method is tedious when applied to *FE* techniques as it needs a *FE* node at the location of the crack and a separate algorithm to relate the spring stiffness to the crack length. They conducted experiments on a 1000mmX25mmX50mm cantilever beam and compared the results obtained from Young's Modulus reduction approach to those from the fracture mechanics

approach of Christides and Barr [120]. The results obtained from both techniques were comparable but the fracture mechanics approach was found to be more tedious in terms of both complexity and computation. Therefore, they concluded that a simple open crack, modelled by reducing the stiffness of its elements, is sufficient for low-frequency health monitoring applications.

Zimmerman and Kaouk [81] used the matrix updating method where a damage or a perturbation matrix was computed using changes in the measured modal data before and after damage. The inverse problem was solved as an optimisation problem in which the error between the undamaged and damaged mass, the stiffness and the damping matrices, $[\Delta M]$, $[\Delta K]$ and $[\Delta C]$, were minimised. They found a matrix of the minimum norm representing damage, using both the eigen values and eigen vectors of the undamaged and damaged structures. They studied the effect of measurement noise by *corrupting* the numerically obtained eigen vectors and good results were obtained for noise levels of upto 5%. They also conducted experiments on an 8-bay truss and accurately identified the location of the damage.

Shi *et al.* [121] proposed the use of modeshapes, combined with natural frequency data, for accurate damage detection and characterisation. They used Multiple Damage Location Assurance Criterion (MDLAC), introduced by Messina *et al.* [122], and compared the modeshapes of a truss before and after damage, to locate the damage approximately. Once the approximate location was determined, the authors used natural frequency data, from before and after damage, in a *FEA* algorithm to determine the extent of damage in the structure.

Ren and Roeck [123,124] employed the use of both frequencies and modeshapes to update the numerical model representing the undamaged structure. They claimed that, by employing both the frequencies and the modeshapes, the results would be more accurate. They implemented this technique on a numerical model of a simply-supported beam and a two-span continuous beam with multiple damage elements. The damage locations were accurately detected in the case of the numerical model even after they added a 2% random noise to both the frequencies and modeshapes results. However, when they applied the technique to a 6m long reinforced concrete beam, they could not localise or quantify the damage. Since the updating technique

also used experimental modeshapes, it may have been sensitive to the noise in the modeshapes which could be a possible explanation for the poor results.

Keye [125] used modal damping as a parameter to update the model and detect damage. The author implemented it on a *CFRP* composite panel which was damaged (induced delamination) using a steel ball impact. The *FE* model of the structure in its undamaged state was obtained from MSC-NASTRAN. A model updating procedure was carried out using modeshapes and natural frequencies so that the model exactly reproduced the real structure. Then, the damping values of the damaged *CFRP* panel obtained from the real structure were used again in the model updating algorithm to detect the damage location; this was determined accurately from the updated model compared to the non-updated, initial *FE* model.

Wu and Li [126] used a 2-stage sensitivity based updating procedure for damage detection in the *IASC-ASCE* (International Association for Structural Control-American Society of Civil Engineers) *SHM* benchmark structure. The *IASC-ASCE* structure is a 4 storey, 2-bay by 2-bay steel frame construction. In the first stage, the connection stiffness between the beam-column joint and the stiffness of the frames was established for the undamaged structure using *FEA*. A sensitivity matrix of frequencies and modeshapes was obtained in terms of the updating parameters, namely, Young's Modulus and the stiffness of various members of the truss structure. In the second stage, by applying the sensitivity based updating procedure, the location of damage in the frame was successfully identified based on the reduction in stiffness. Damage was simulated by removing the braces from the steel structure or by loosening the bolts at the beam-column joints. They used the first five natural frequencies for model updating as they claimed that the measurements of modal frequencies are much more reliable than those of modeshapes.

Khiem and Lien [127] modelled crack as a spring and used both the *FEM* and the analytical solution of the cracked Euler-Bernoulli beam theory to detect multiple damages present in a cantilever beam. They employed an analytical model incorporated in a *FEA* to calculate the stiffness matrix and thus found the locations and extent of multiple cracks in a cantilever beam. A similar study was carried out by Krawczuk [128], but for thin plate structures containing a through-thickness

crack. Only a forward analysis of the calculation of changes in frequencies from the crack parameters was studied. Analytical equations were derived for the element's flexibility matrix and implemented in a Finite Element model to calculate the natural frequencies of the cracked plate. Modal analysis using commercial *FEA* software (ABAQUS) was also carried out and the results were compared with those obtained from the flexibility matrix based *FEA*. Comparable results were obtained from the model with less computational effort as the need for refined mesh around the cracks tips in commercial *FEA* software was eliminated.

Hao and Xia [129] used *GA* instead of conventional gradient based minimisation techniques to minimise the error between the measured vibration data and the *FEM*. Once the baseline, undamaged model was updated, damage detection was realised using frequencies and modeshapes, both separately and simultaneously, in a cantilever beam and on a one-span portal frame. The authors observed that, by using a combination of frequencies and modeshapes, with increased weights for the lower order modeshapes, the location of the damage was detected accurately.

Abdel Wahab [110] studied the effects of including curvatures in sensitivity based model updating for damage detection in a simply-supported beam. Damage was modelled at the centre of the beam by reducing the stiffness of that element by 50%. The author used both natural frequencies and modeshapes for model updating and determined the damage location. Then, modal curvatures were included in the updating algorithm to study the convergence rate. Though modal curvatures are sensitive to damage, the author concluded that their inclusion as a parameter in the updating algorithm did not help the rate of convergence.

Friswell and Penny [130] and Friswell [131] point out the disadvantages and drawbacks associated with model updating procedures. They observe that the new element matrix, including damage, is not necessarily positive-definite and new modes may be introduced into the frequency of interest. Also, as this does not ensure connectivity between the elements of the structure [130, 131], the whole damage detection procedure will fail. Usually, a penalty function, the error between the measured and the predicted values, is minimised. However, finding the global minima of the error function can be tedious and can cause incorrect results for the location and size of the damage if the solution gets stuck in a local minimum.

Model updating requires an accurate model representing the real structure. More often than not, changes in the measured quantities due to the presence of damage are smaller than the differences between the measurements from the real structure and the numerical model [131]. Friswell [131] also indicated that model updating methods are useful mainly for structural modification, vibration stability or the annulment of differences between the measured and the analytical models when using vibration parameters and they are not necessarily suited for the detection of small damage.

2.4.2   Analytical approach

2.4.2.1   Equilibrium method using spring analogy

In most of the analytical studies concerned with vibration based damage detection, cracks are modelled as rotational springs with stiffness inversely proportional to their size. When a modelled spring is relatively stiff, the additional displacement due to the presence of a crack is small and so is the damage size. But an increase in deflection (rotation) due to a reduction in the spring's stiffness indicates a larger damage. Chondros and Dimarogonas [132] were one of the first researchers to use and prove the technique of modelling cracks as changes in local flexibility by using a spring. They simulated damage in welded joints by introducing part-through cracks at the fixed end of a cantilever beam welded to the vibrating table. They performed vibration experiments and empirically derived a relationship between changes in the frequencies and the stiffness of the spring used. They provided nomograms relating changes in the frequencies, the spring constant and the depth of the crack.

In contrast to the empirical approach, Adams *et al.* [133] analytically derived a relationship using the receptances of the structure on either side of the spring representing the crack. Using two modal frequencies obtained from the axial vibrations of the bar, damage was located using the point of intersection of the curves obtained from the relationship between the spring stiffness and the receptances at any location along the length of the bar. They conducted a experiments on an aluminium bar and a camshaft with and without damage and successfully located the damage in all cases. They also showed that the stiffness was inversely proportional to the damage, but no exact method to quantitatively assess the damage was proposed.

Christides and Barr [120] developed a cracked Euler-Bernoulli beam vibration theory, studying the effect of the presence of a crack on the vibration parameters. They assumed that the effect of the crack on the stress distribution would decay exponentially with the distance from the crack as calculated from experimental data. Though this theory was a significant step in developing the cracked beam theory, the estimation of the decay constant from a series of experiments and its application to finding changes in the frequencies was perceived by Chondros *et al.* [134] as a serious limitation. Hence, Chondros *et al.* [134] developed a continuous crack beam vibration theory using the principles of fracture mechanics instead of experimental data. Experiments were conducted on beams containing single-edge and double-edge fatigue cracks to extract their natural frequencies which proved that the continuous cracked beam vibration theory was closer to the experimental data than the method proposed by Christides and Barr [120].

Rizos *et al.* [135], Ostachowicz and Krawczuk [136], Liang *et al.* [137, 138, 139] and Nandwana and Maiti [140] employed the spring analogy and the Euler-Bernoulli vibration theory to determine the frequencies simply-supported and cantilever beams with edge cracks. They also employed fracture mechanics relationship (see theory developed in Chapter 4 and Appendix D) to relate the size of the crack to the stiffness of the spring. Rizos *et al.* [135] employed the Newton-Raphson method to solve the inverse problem. Ostachowicz and Krawczuk [136] analysed only the forward problem but extended the study to the case of a cantilever beam containing two cracks. Liang *et al.* [137, 138] introduced a graphical solution to the inverse problem by plotting spring stiffness *vs* the beam coordinates and using their intersection point to identify the location and size of the damage. Nandwana and Maiti [140] and Patil and Maiti [141] extended the equilibrium theory proposed by Liang *et al.* to develop analytical models for cracks in stepped cantilever beams and beams with variable depth. Nandwana and Maiti [142] used the same theory to predict the locations of through-thickness (centre) cracks. To determine the length of through-thickness centre cracks, they used the formulation for edge cracks given by Ostachowicz and Krawczuk [136] which is questionable.

Lele and Maiti [143] extended the equilibrium technique with the rotational spring analogy to cracks in short beams. In short beams, shear deformation and

rotational inertia cannot be neglected as they are in Euler-Bernoulli theory; hence, they used the Timoshenko beam theory. It was also demonstrated that the predictions from the Timoshenko beam theory were in better agreement with the experimentally measured frequencies than those given by the Euler-Bernoulli theory for short beams.

Loya *et al.* [144] obtained the bending mode natural frequencies of a beam using the Timoshenko beam theory. In the short beam theory by Lele and Maiti [143], they did not allow for displacements in the beam segments due to the presence of cracks. Loya *et al.* [144] modelled cracks with two springs, one extensional and the other rotational which permitted discontinuities in both vertical displacement and rotation due to bending. Using this extended theory, they solved the forward problem of finding the natural frequencies of a simply-supported short beam containing cracks of different sizes at different locations.

Williams *et al.* [145] created a new parameter called the Damage Location Assurance Criterion *(DLAC)*, the values of which range from 0 to 1. This is similar to the *MAC* proposed by Allemang and Brown [66], but uses natural frequencies before and after damage in lieu of modeshapes.

$$
DLAC(j) = \frac{\left|\{\Delta f\}^T \cdot \{\delta f_j\}\right|^2}{\left(\{\Delta f\}^T \cdot \{\Delta f\}\right) \cdot \left(\{\delta f_j\}^T \cdot \{\Delta f_j\}\right)} \tag{2.1}
$$

where Δf is the experimentally determined frequency change vector and δf is the analytical frequency change vector for each location, j, as previously determined from a numerical simulation. *FEA* was performed using ABAQUS software and a database was created with 40 potential damage locations and the first 27 transverse modal frequencies. Experiments were also conducted to verify the effectiveness of this new parameter. It was found that the accuracy of damage location predictions increased with the increasing number of modes used.

2.4.2.2   *Energy Method applied to beams*

Lord Rayleigh was the first to formulate the vibration theory using energy principles in which he stated that "When the expressions of kinetic and potential energy of a

system moving about a configuration of stable equilibrium are given, the possible frequencies of vibration are determined by an algebraic equation of degree (in the square of the frequency) equal to the number of independent motions of which the system is capable" [146]. For multiple Degrees Of Freedom *(DOF)* systems, a function for modeshape deflections is assumed such that it satisfies the boundary conditions of the structure. This function is substituted in both the kinetic and potential energy equations, by solving which, the frequencies can be obtained. In the second of his series of papers [147], Lord Rayleigh estimated the natural frequencies of a square plate using the above-mentioned energy principle.

Gudmundson [148] provided vibration theory for a cracked beam using energy principles. He derived a relationship between the strain energy stored in the crack and the total strain energy in the structure by considering the geometrical changes in the structure (presence of cracks or notches) as perturbations of the undamaged structure. If ω_n is the natural frequency of the undamaged structure, ω_n^* the natural frequency of the structure with the crack, U the total strain energy in the undamaged structure, ΔU_n the strain energy stored in the crack, ΔU_c the strain energy stored in the cut-away geometry, ΔT_c the kinetic energy stored in the cut-away geometry, then ω^* can be expressed as [148]

$$\omega_n^{*2} = \omega_n^2 \left[1 - \frac{\Delta U_n + \Delta U_c - \Delta T_c}{U} \right] \tag{2.2}$$

where the suffix n, indicates the mode number.

Since volume does not change in the case of a crack in the structure, ΔU_c and ΔT_c vanish, and thus

$$\omega_n^{*2} = \omega_n^2 \left[1 - \frac{\Delta U_n}{U_n} \right] \tag{2.3}$$

Using Eqn. [2.3], longitudinal frequencies were calculated for bars with centre cracks and holes, and transverse frequencies for beams with edge cracks. The author validated these theoretical predictions by comparing them to frequencies extracted from *FEA* and good agreement was observed.

Hu and Liang [149] proposed a theory to find the locations and sizes of multiple edge cracks in beams using the rotational spring analogy. They proposed two

approaches which resulted in the same end equations. They used Castigliano's theorem and Gudmundson's theory [148] to derive a relationship between changes in the natural frequencies and the strain energy in structures with and without cracks. They validated their theory by performing numerical analyses on a simply-supported beam containing two cracks. Using the natural frequencies obtained from the numerical model, they successfully identified the crack locations and sizes using the graphical approach [137, 138].

Patil and Maiti [150, 151, 152, 153] extended the energy formulation of Hu and Liang [149] with the spring analogy to characterise multiple cracks in beams on elastic foundations, beams with multiple pin supports and stepped cantilever beams. In the above studies, the crack size was determined from the stiffness of the rotational spring using the relationship derived by Ostachowicz and Krawczuk [136].

2.4.2.3   *Analytical methods for plates*

The analytical methods described so far using equilibrium and energy methods have only been developed for one dimensional structures i.e., beams. Damage detection in plates using vibration parameters have mainly been restricted to empirical methods using modeshape measurements or model-updating in which a *FE* model is updated to match measured frequencies and/or modeshapes. Analytical modelling for cracked plates using classical or higher order plate theories has received very little attention compared to the modelling of cracked beams. This is possibly due to the complexity of the theoretical formulation of vibration of plates with cracks and difficulty in solving these equations. Moreover, solving the inverse problem is also very tedious due to the increase in the number of unknown variables. The vibration of plates without damage has been studied extensively using both *FEA* and analytical approaches. Leissa [154, 155] has published a collection of solutions to the vibration of plates with different geometries and boundary conditions.

Chondros and Dimarogonas [156] were one of the first to investigate the effect of cracks on the frequencies of plates. They conducted experiments on circular plates containing crack at the periphery where the plate was welded to a rigid support and presented nomograms relating natural frequency changes in the first three modes to the crack length. Anifantis *et al.* [157] studied the effect of a crack on the natural

frequencies of an annular plate. Crack was simulated as a perturbation in the local stiffness which was computed using fracture mechanics theory for beams with an edge crack. Implementing the change in stiffness in *FEA*, they predicted changes in the natural frequencies due to the presence of cracks. Note that this may be considered a semi-analytical approach as only the relationship between cracks size and its compliance was obtained from theory, the rest of the analysis was conducted using *FEA*.

Banks and Emeric [158] use Galerkin's method to determine the effect of edge cracks on the natural frequencies of cantilevered plates. The crack was modelled by removing local elements in the Finite Dimensional solution of the plate equations. The inverse problem was solved using a 2-step optimisation algorithm (Nelder-Mead algorithm) to search the data generated from the analytical results. In the first step, the lower frequencies were used to predict an approximate location. In the second step, all the remaining modes were used to improve the accuracy of determining the crack location. Once the location was determined, damage size was ascertained from the previously established database of frequency changes *vs* damage sizes. The methodology was validated by experiments on cantilever plates with edge cracks using *PZT* patches for frequency measurements. It may be noted that due to the cantilever boundary conditions, the theory developed is closer to that of beams rather than plates with multiple edges constrained. Ma and Huang [159] studied the effect of through-thickness cracks in cantilever plates employing *FEA* and compared the results to measurements on square aluminium plate with Electronic Speckle Pattern Interferometry. They showed that cracks perpendicular to the direction of the clamped edge had a negligible effect on natural frequency changes, but cracks parallel to the clamped edge had significant effects. However, they did not provide any means to solve the inverse problem of determining crack sizes and locations from measured frequencies.

As seen from above, analytical approaches to the solution of the forward problem i.e., the determination of the presence of damage in plates using frequency changes, have mainly been restricted to beam-like cantilevered plates [158]. Others have created databases relating the changes in frequencies to defects in plates using experimentation [156] or using *FE* modelling. This thesis aims to fill the gap by

extending the theoretical approach to predicting the changes in frequencies due to defects in plates. Once the forward problem in solved or a database of frequency changes relating to crack sizes and locations is created using experimentation or numerical modelling, the inverse problem of assessing damage size and location from known frequency changes can be addressed by various means, such as least square identification, *NN*, *GA* and fuzzy logic. Applications of intelligent algorithms to solve the inverse problem are discussed in the next section.

2.5   Intelligent algorithms for solution to inverse problem

The highly non-linear nature of the relationship between the vibration responses and the damage parameters makes the inverse problem difficult to solve. In general, in a two dimensional structure, there are four crack parameters to be determined, x and y coordinates of the crack location, crack orientation and size. A combination of these parameters produces a change in modal frequency. However, the change in frequency due to a given crack is different in different modes. Hence we may use measured changes in frequencies in multiple modes to solve the inverse problem. Algorithms like *NN*, *GA* and fuzzy logic have been used extensively as means of pattern recognition for damage detection. Typically, in *NN* or fuzzy logic based diagnostic systems, a database of modal parameters corresponding to damage at various locations and of varying sizes, obtained from numerical or analytical modelling or from experiments, is used to *train* the system. A dataset of modal parameters corresponding to a crack scenario is input to the trained system and the inverse problem of determining the location and size of the damage is solved.

Ganguly [160] proposed the use of a fuzzy logic system for the health monitoring of a helicopter rotor. The author extracted the first four modes of the natural frequency shifts for a cantilever beam before damage using *FEA*. Natural frequencies were also extracted from 20 damage cases and a fuzzy rule base was developed. The author reported that the fuzzy logic system successfully located the damage even when the frequencies were contaminated by adding noise of upto 3%. To tune the fuzzy rules for the fuzzy logic based system, Pawar and Ganguly [161] proposed the use of the *GA* as opposed to manual tuning which can be time-consuming and not necessarily accurate. They tested the proposed self-rule-generating genetic coded

algorithm for a cantilever beam with damage at various locations and of different sizes. Even with upto 20% noise in the measurements, they obtained a 100% success rate in locating the damage. Since fuzzy logic was used, only *fuzzified* output value for the damage size was obtained, i.e., the damage size was not obtained quantitatively but qualitatively. They also applied this algorithm to faulty measurement data, to high noise data (upto 30%) and to non-uniform beams. They located the damage accurately for most cases ($> 95\%$).

Reddy and Ganguly [162] generated natural frequency data for a cantilever beam using *FEA*. Damage was simulated by reducing the stiffness of the elements and the database was created by damaging one of the 20 beam elements with various levels of damage. A Radial Basis Function *(RBF) NN* was trained with the generated data and, by using the first 4 transverse mode frequencies, damage at various locations and of different sizes was identified and assessed accurately. Suresh *et al.* [163] used a two-stage modular *NN* to detect damage present in a cantilever beam. They generated natural frequency data for different damage cases using the analytical model of representing damage as a spring. They compared the results obtained from two *NN*s; the Multiple Layer Perceptron *(MLP)* and the *RBF*. In both cases, the *NN* architecture consisted of two stages: the first used the first three frequency changes to find the location and then, employing just one of the modes of frequency change, the second found the size of the damage. The *RBF* network produced better results and took less training time than did the *MLP* network.

Krawczuk *et al.* [164] used both *GA* and *NN* to solve the inverse problem of detecting delamination in a glass-epoxy composite beam. They derived an equation for extracting the natural frequencies of a composite beam containing delamination. They created a database of the first four frequencies (for 2277 damage cases) using the derived analytical procedure after which a *NN* was trained. They also used the *GA* to solve the inverse problem using that equation. The objective function used in the *GA* was the *DLAC* proposed by Messina *et al.* [122]. They validated both these techniques by using two test cases where the frequencies of the damaged beam were also obtained from the analytical model. In comparison, the results obtained from the *GA* were more promising than those from the *NN*.

Hatem *et al.* [165] used different kinds of *NN* for training, and the *GA* for searching through a database of natural frequency values, to detect damage in a graphite/epoxy composite beam. Four types of damage were studied; a hole with different diameters; delamination with different areas; and surface and through-cracks of different lengths, all at different locations. The database was created using a commercial *FE* software, I-DEAS. For finding damage, five different variants of the *NN* were used for training and the *GA* was used for searching through the database. One of the *NN*s, the generalised regression network, showed better results in solving the inverse problem but, in general, none of the techniques provided promising results in locating or characterising the damage. The authors claimed that a more extensive database was needed to characterise the damage accurately, but no information regarding the number of damage cases required to train the *NN* was presented.

Apart from these methods, where intelligent algorithms are used for searching a database of known damage cases, the *NN* and the *GA* are also used for pattern recognition from complex Lamb wave signals, acoustic emission signals or signal analysis [40, 41, 42, 43].

2.6 Conclusion

In the foregoing sections, a survey of literature on damage detection techniques applicable to *SHM* was presented. Techniques other than vibration based methods were covered briefly in Section 2.2. Vibration methods using damping measurements, modeshape measurements, time and frequency response and wavelet analysis were described in Section 2.3. Modeshape based methods of damage detection suffer from a serious disadvantage in that modeshapes cannot be estimated as accurately as natural frequencies. Studies have shown that the error associated with measuring modeshapes can be as high as 100% [57]. Since modeshape methods use differences in modeshape deflections or curvatures for detecting damage, the damage signature can be masked by the noise in the measurements data. Further, abrupt changes in deflections or curvatures due to noise can often lead to false alarms. Filtering the noise in modeshape measurements while retaining the damage signature cannot be

easily achieved. Measuring modeshape deflections in a real structure is also cumbersome and time consuming as it requires measurements at multiple points and the accuracy of the modeshapes is highly dependent on the number of measurement points.

Frequency based methods on the other hand require measurements at only a single location. Also, measurements of frequencies are less susceptible to noise. For this reason, change in frequency is a more reliable indicator for damage detection. However, unlike modeshape based methods, the identification of the location of the damage is not readily achieved when using frequency measurements. Solution to the inverse problem of determining the location and size of the damage requires the use of data from multiple modes and can be quite involved. Research using frequency measurements for damage detection has mainly concentrated on *FE* based model updating techniques. Analytical approach has been restricted to beams of various geometries and different boundary conditions. For the detection of defects in plates, the approach so far has been to use model updating or the use of experimentally or numerically generated databases with pattern recognition algorithms.

CHAPTER 3

Preliminary study: Investigations on modeshape methods

3.1 Introduction

The work described in this chapter was motivated by the ultimate objective of being able to detect damage in structures using vibration parameters. The literature review in the previous chapter indicated that vibration based damage detection methods are of two main types: those based on the measurement of modeshapes and those based on the measurement of frequencies. A preliminary study is conducted to investigate the applicability and efficacy of both methods using numerical simulation as well as experimental testing. In the following section, the theoretical basis for modeshape based damage detection techniques is presented. In later sections, results from the numerical simulation and experiments are presented. A comparison of the two techniques is made, leading to the conclusion that frequency measurement is easier to implement in practice, more reliable and repeatable, albeit having its own disadvantages.

3.2 Damage detection using modeshapes - Theory

The occurrence of damage alters the dynamic properties of a structure, such as its natural frequencies, modeshapes and damping characteristics, due to the reduction in stiffness at the location of the damage. By comparing these properties to those of the undamaged structure, damage can be located and assessed. Wolff and Richardson [65] proposed comparing the measured modeshapes directly to detect damage, while Pandey *et al.* [68] proposed the use of the curvatures of the modeshapes for

that purpose. The latter also observed that the curvatures of the modeshapes are highly sensitive to the presence of damage due to the direct relationship of damage to stiffness. Many researchers have used this technique and verified it experimentally [73, 56, 71, 72, 77, 78, 80, 76] while some have extended it in order to improve its sensitivity [70, 69]. Variations in curvature based techniques, namely the *Damage Index Method (DIM)* and the *Curvature Damage Factor (CDF)* method, were proposed by Stubbs *et al.* [69] and Wahab and Roeck [70] respectively. In the *DIM*, the modeshape curvatures for each mode are calculated at each point and represented as functions of the total modal stiffness in that mode. Using the *CDF*, the curvatures of the modeshapes at each location are averaged for all the modes used. Both these cases allow for the normalising of the effects of cracks in different modes.

If ψ is the modeshape deflection, the absolute change in deflection is obtained as

$$\Delta\psi = \psi - \psi^* \tag{3.1}$$

where ψ and ψ^* are modeshape deflections of the undamaged and damaged structure respectively.

The modeshape curvature can be obtained from the deflection shape by numerical differentiation (central difference approximation). Since the damage causes a change in local stiffness, there will be a significant difference between the curvatures of the undamaged and the damaged structures at the location of the damage. Either the two curvatures or the difference between them along the length of the beam or over the surface of the structure can be plotted and the location of the damage determined from the position of the maximum difference in the curvatures. It may also be possible to estimate the size of the damage from the magnitude of the differences between the curvatures since a larger defect would, theoretically, cause a greater change in local stiffness, if some prior calibration is done. One may be able to locate the damage in this manner by plotting changes in the curvatures in a single mode of vibration; however, depending on its location, damage of the same size can have varying effects on the curvatures of different modes and may not affect some modes; it would, therefore, be more fruitful to examine the curvature differences in several modes.

A simple means of combining the effect of the damage in different modes is the use of the *CDF* [70] which is the average of the differences in the curvatures between the damaged and undamaged beams in all the modes being examined and is given by

$$CDF(x) = \frac{1}{N} \sum_{i=1}^{N} |\psi_i'' - \psi_i''^*| \tag{3.2}$$

where N is the number of modes being examined and double prime ($''$) indicating second differentiation with respect to the beam coordinate (x). By plotting the *CDF* along the length of the beam to determine the damage location, it is not necessary to examine each individual mode separately.

Stubbs *et* al. [69] proposed a more elaborate means of combining the effect of the damage on curvatures in several different modes, called the *DIM*. This is a non-dimensional parameter derived from the curvature differences of all the modes examined and is indicative of the magnitude of the damage. The fraction of modal stiffness in any mode, and at any location, is normalised to the total modal stiffness in that mode. A ratio of this quantity for the undamaged and damaged structures yields the *DIM*. By plotting the *DIM* across the surface of the whole structure, and locating its maximum, the location of the damage can be determined and its size estimated [69].

3.3   Assessment of modeshape methods by numerical simulation

To assess the applicability of the above modeshape based methods to damage detection, *FEA* using commercial software *(ANSYS Version 11)* is performed on a cantilever beam 600mm long, 50mm wide and 3.2mm thick made from aluminium alloy Al 7075-T6 (*Young's Modulus*, $E = 69.6GPa$; *Poisson's ratio*, $\nu = 0.3$; *and density*, $\rho = 2772.53Kg/m^3$). *SHELL93* is used to model the beam as it allows the modelling of through-thickness cracks for analysis of the damaged beam. Convergence analysis is conducted on the *FE* model of the undamaged beam in order to choose an appropriate mesh size. The initial *FE* model is meshed with 12 elements along the length of the beam. The natural frequencies of the first five

bending modes are extracted. Consequently, the number of elements used is doubled and the natural frequencies are extracted until the *RMS* errors for the first three bending modes, when compared to those obtained from the previous run, are within 0.05%. It can be seen from Fig. 3.1 that a converged solution is obtained for a mesh containing 1536 elements along the length where the *RMS* error is only 0.045%. Further *FEA* conducted on beams with similar dimensions, is modelled with 1536 elements along their lengths.
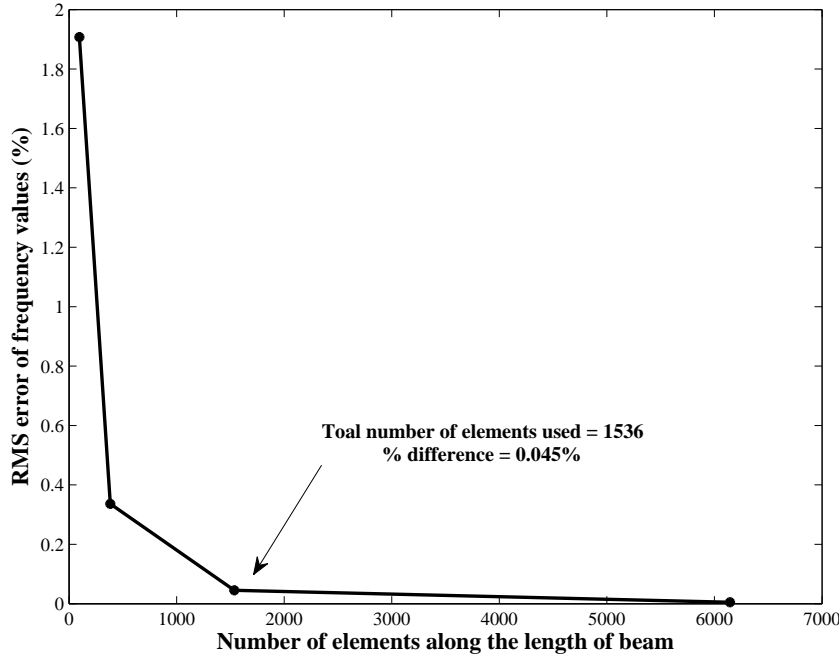
Figure 3.1: Convergence plot for choosing appropriate mesh size

To simulate damage, a through-thickness crack is modelled along the centre-line of the beam at 100mm from the fixed end (17% of the length of the beam). The crack is 20mm long (40% of the width of the beam) and is modelled by separating the nodes along its length. The crack tips are modelled using quarter-point singular elements. The natural frequencies are extracted from *ANSYS* and the modeshapes of the first three transverse modes are also extracted. In the experiments conducted (see Section 3.4), modeshapes are measured at 15mm intervals along the length of the beam. Hence, in numerical simulations too, deflections in each mode are extracted at 40 points along the length of the beam. The normalised beam deflection values of the damaged and undamaged beams are plotted together for the comparison of modes 1, 2 and 3 in Figs. 3.2(a) - 3.2(c).

(a) Mode1

(b) Mode2

(c) Mode3
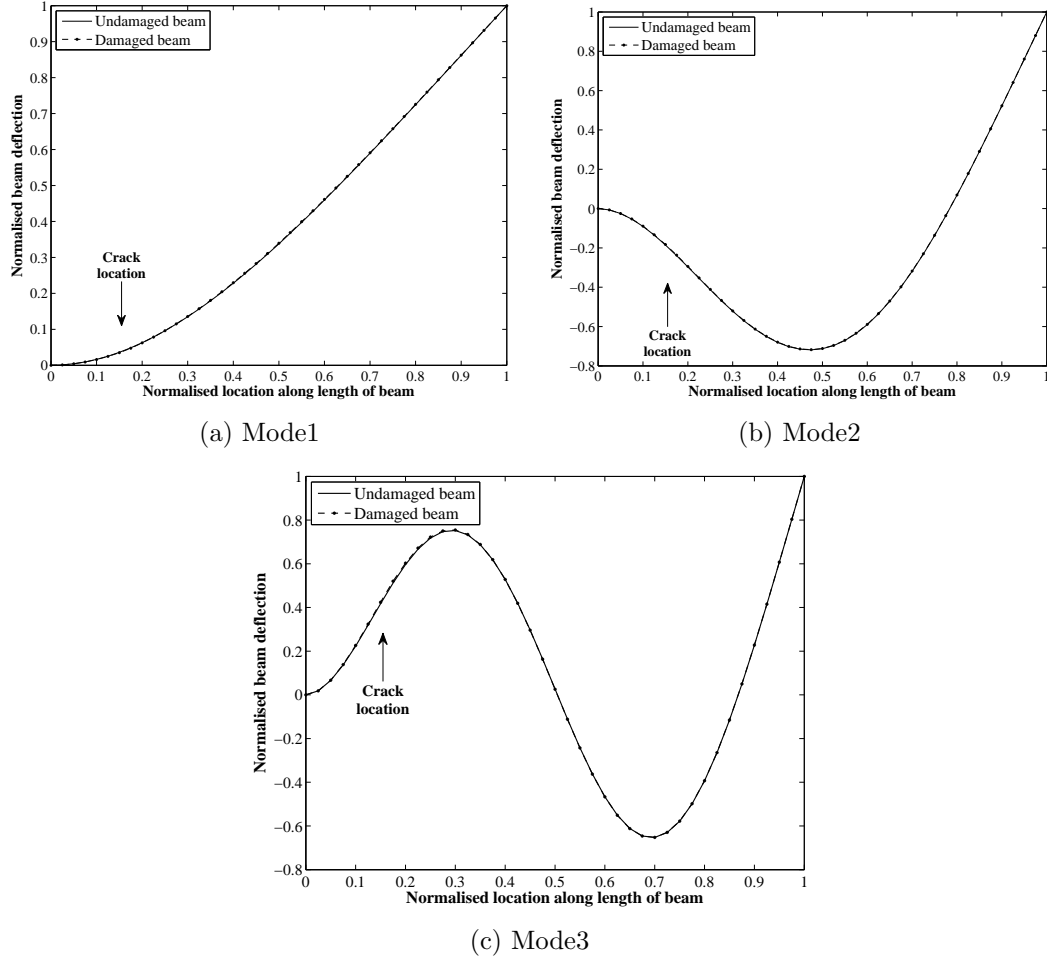
Figure 3.2: Normalised beam deflections of undamaged and damaged beams from *FEA* (crack length = 40% of beam width)

The modeshape deflections of the damaged and undamaged beams in Figs. 3.2(a) - 3.2(c) appear to be identical as no differences among them are discernible at the location of the damage or elsewhere. In order to examine whether this is due to variations in the deflections being too small compared to the magnitudes of the deflections, the magnitude differences in the normalised modeshape deflections of the undamaged and damaged beams are plotted for the first three modes in Figs. 3.3(a) - 3.3(c).

The magnitude differences in the deflections show peaks in the vicinity of the damage location and, except in the case of mode 1 (Fig. 3.3(a)), the peaks are much higher than the values of the differences in deflections along the rest of the beam. This indicates that there is a noticeable difference in the beam deflection at the location of the damage which could be used to detect the damage and determine its location.

(a) Mode1
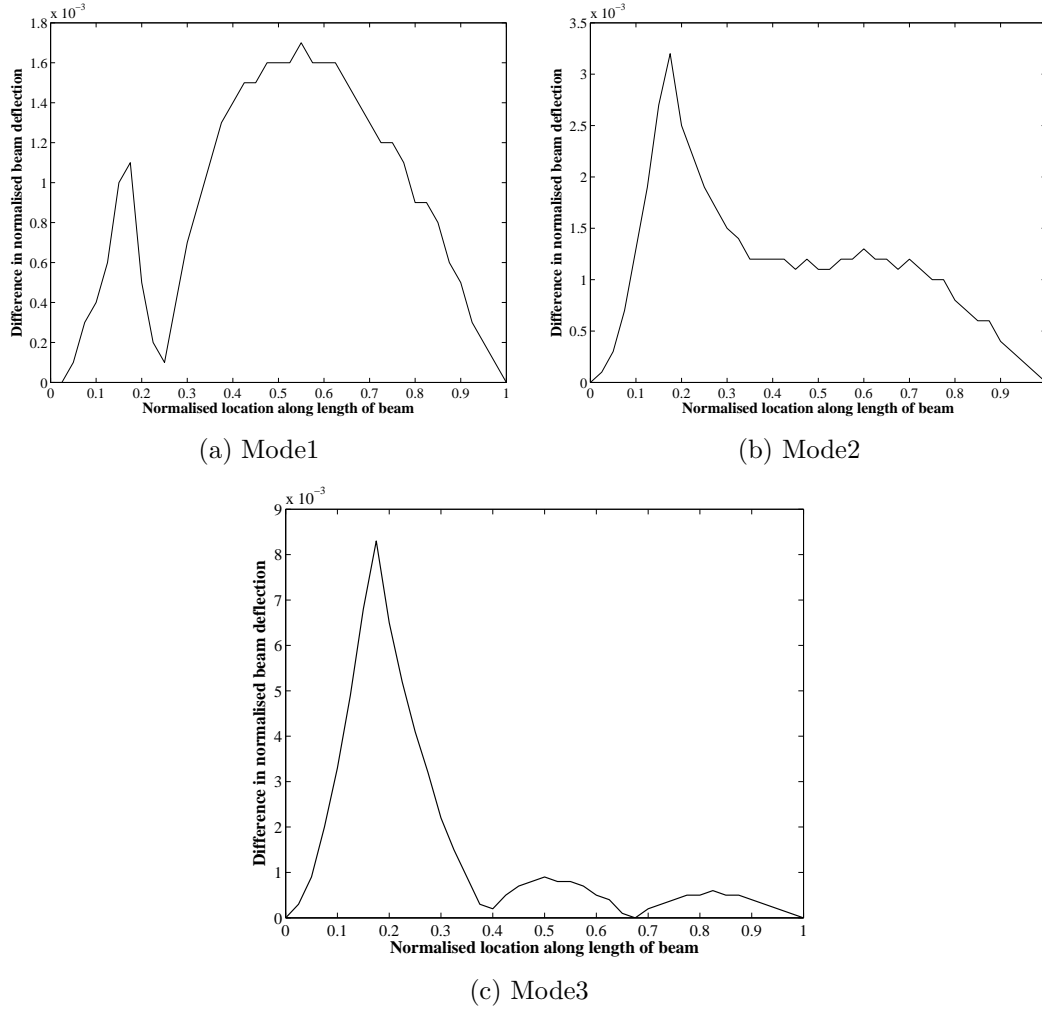
(b) Mode2

(c) Mode3

Figure 3.3: Magnitude differences in normalised beam deflections of damaged and undamaged beams from *FEA* (Crack location = 17% of beam length, crack length = 40% of beam width) (a) Mode 1, (b) Mode 2, (c) Mode 3

The modeshape curvatures of the undamaged and damaged beams for modes 1, 2 and 3 are plotted in Figs. 3.4(a) - 3.4(c) and it can be seen that at least in mode 1 there is a considerable difference unlike the modeshape deflections. The differences in curvatures of the modeshapes in the damaged and undamaged beams for modes 1, 2 and 3 are shown in Figs. 3.5(a) - 3.5(c). It is clear that they are more sensitive to damage in the structure, as there is a distinct peak in each mode at the location of the damage. The magnitude of the curvature difference at the peak is higher for higher modes, e.g., almost 5 times higher in mode 3 than in mode 1. This, of course, is dependent on the location of the damage. It is also noteworthy that the peaks are narrower in the case of curvatures than in the case of differences in deflections (Figs. 3.3(a) - 3.3(c)), indicating that the effect on the curvatures is

more localised. The peaks in Figs. 3.5(a) - 3.5(c) provide encouragement for the application of modeshape curvature measurements to damage detection.

(a) Mode1
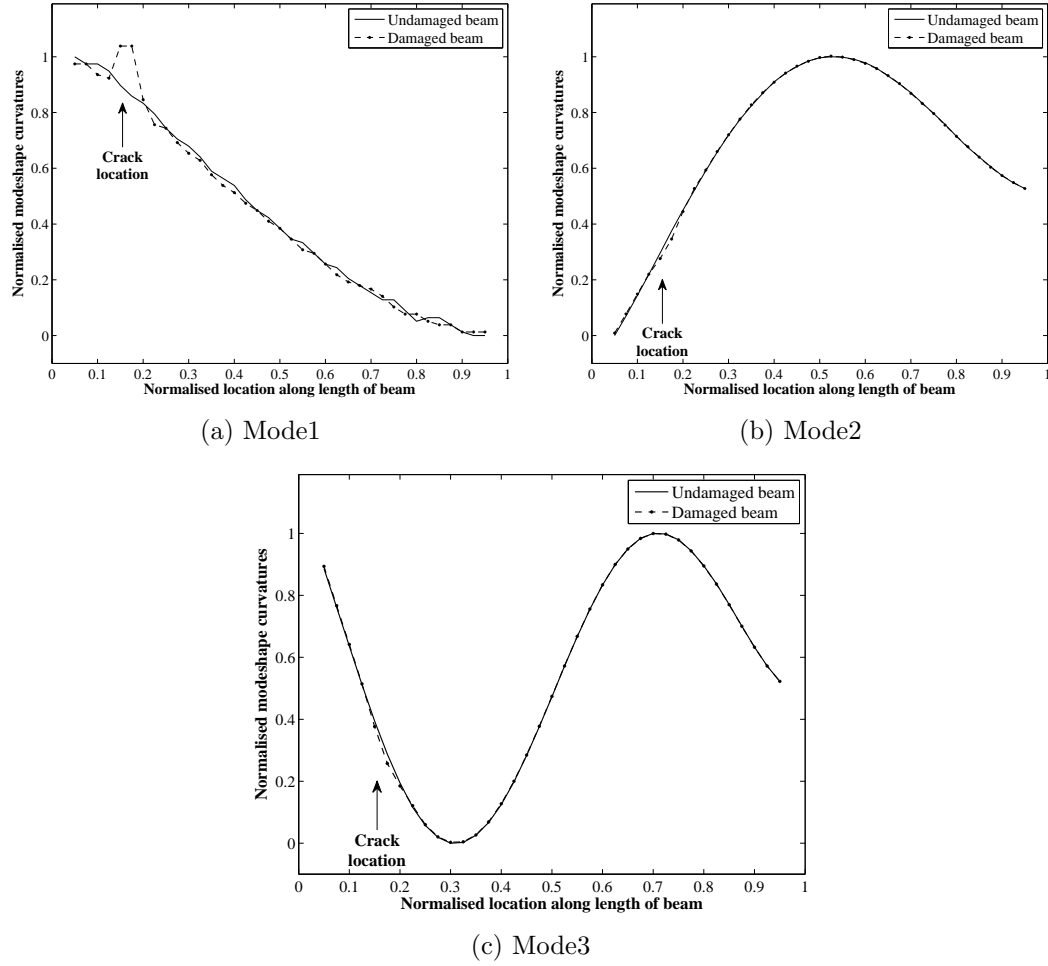
(b) Mode2

(c) Mode3

Figure 3.4: Normalised modeshape curvatures of damaged and undamaged beams from *FEA* (Crack location = 17% of beam length, crack length = 40% of beam width) (a) Mode 1, (b) Mode 2, (c) Mode 3

(a) Mode1
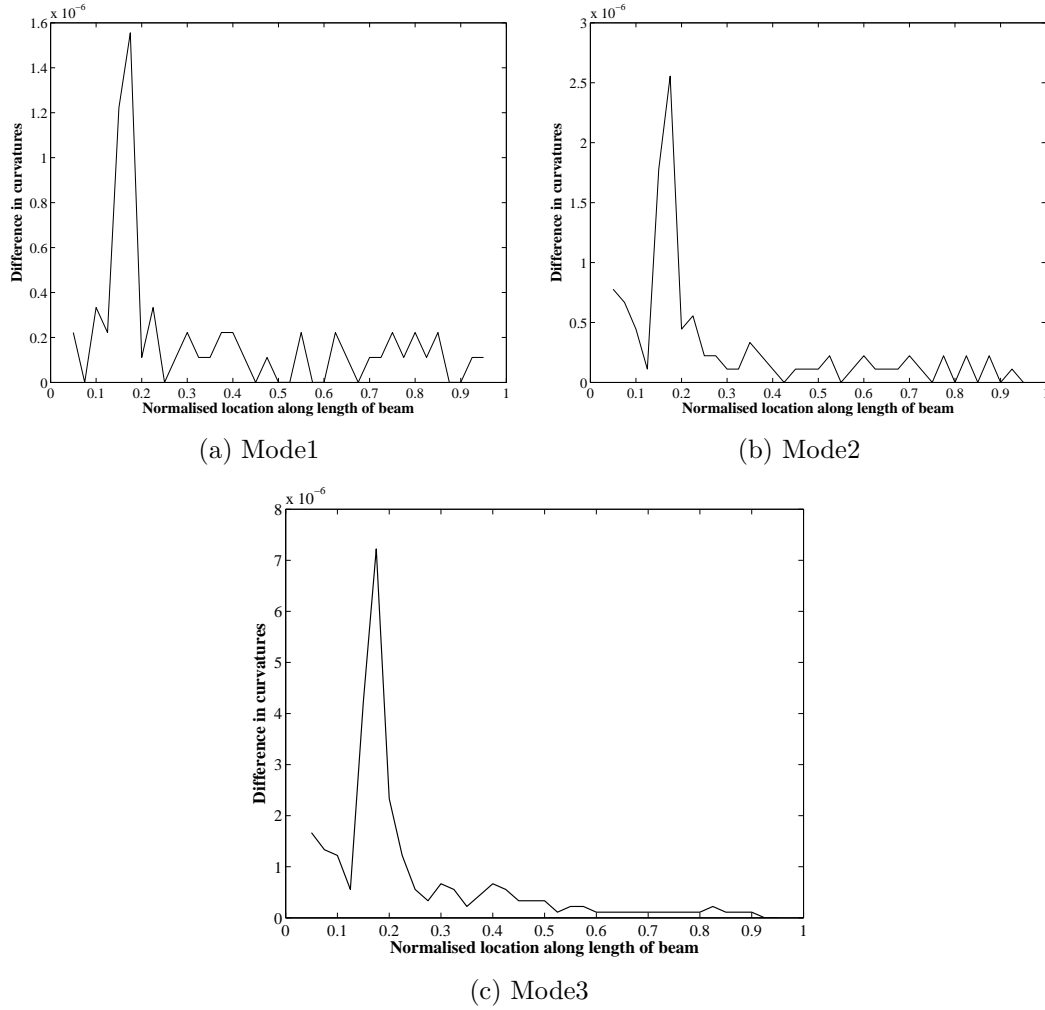
(b) Mode2

(c) Mode3

Figure 3.5: Magnitude differences in modeshape curvatures of damaged and undamaged beams from *FEA* (Crack location = 17% of beam length, crack length = 40% of beam width) (a) Mode 1, (b) Mode 2, (c) Mode 3

The *CDF* and the *DIM* for the same beam are calculated and are plotted in Figs. 3.6 and 3.7 respectively. Both show distinct peaks at the location of the damage, similar to those seen in the curvature differences plotted in Figs. 3.5(a) - 3.5(c). Thus, these variations also appear to be equally as good as the differences in curvatures for damage detection. The modeshapes obtained from the experiments are incorporated into these techniques and the results are presented in subsequent sections.
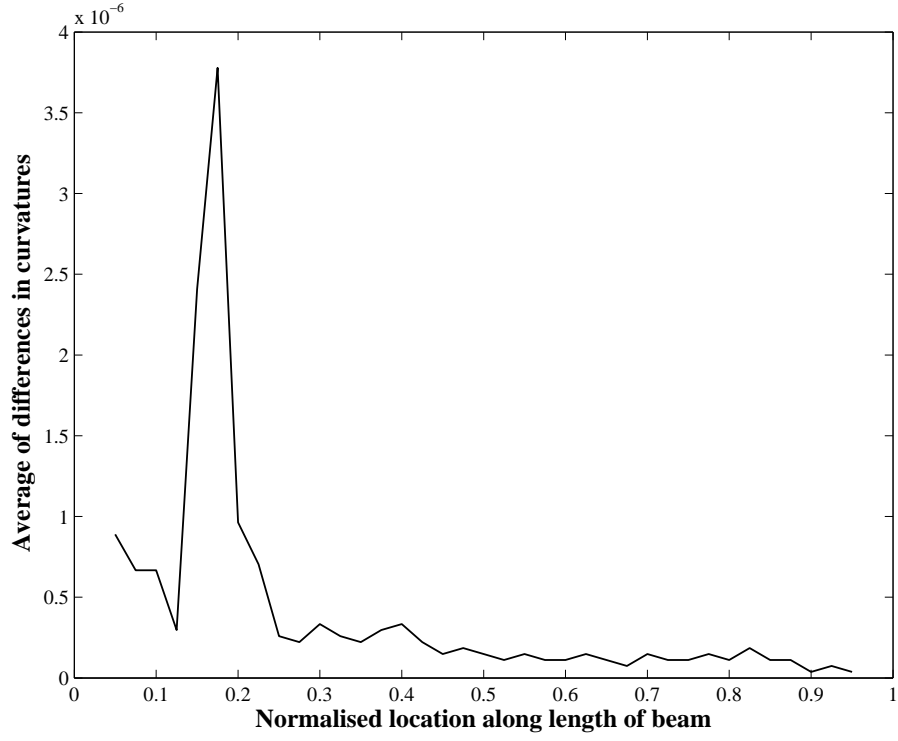
Figure 3.6: *CDF* for beam with crack from *FEA* (Crack location = 17% of beam length, crack length = 40% beam width)
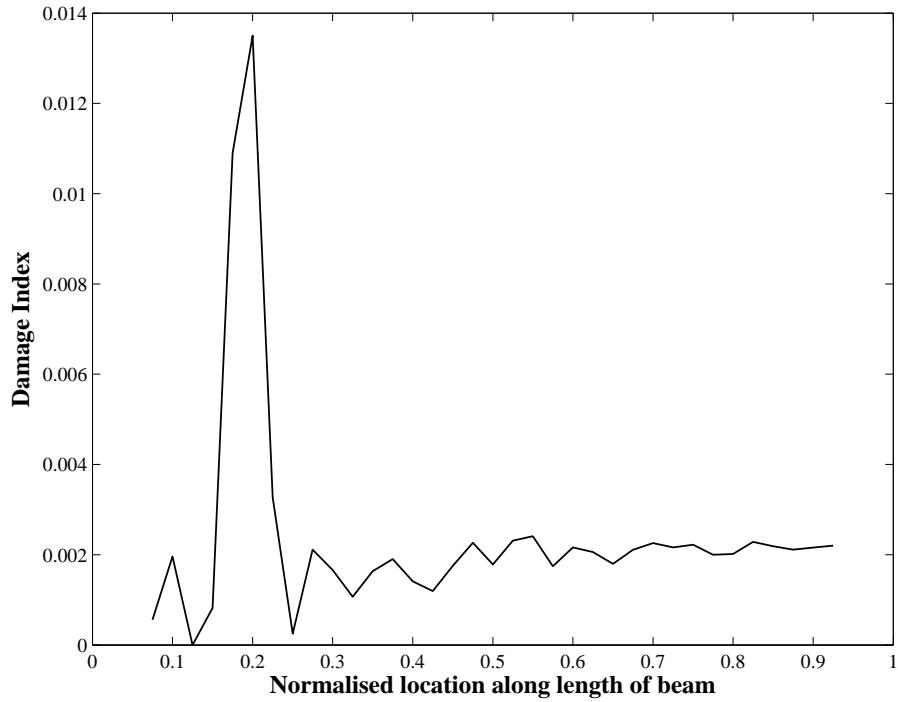
Figure 3.7: *DI* for beam with crack from *FEA* (Crack location = 17% of beam length, crack length = 40% of beam width)

3.4 Assessment of modeshape methods by experiments

3.4.1 Experimental apparatus and procedure

In Experimental Modal Analysis *(EMA)*, a known excitation is applied to a structure and its response is measured; from this, the vibration parameters such as the natural frequencies, modeshapes and damping characteristics, can be extracted. *EMA* can be performed with the point of excitation fixed and the responses measured at different locations or with the point of excitation moved along the structure while the response measured is fixed. In the experiments conducted here, the former method of measuring the responses at different points along the length of the beam with the excitation source fixed is used. A schematic of the experimental set-up is illustrated in Fig. 3.8.
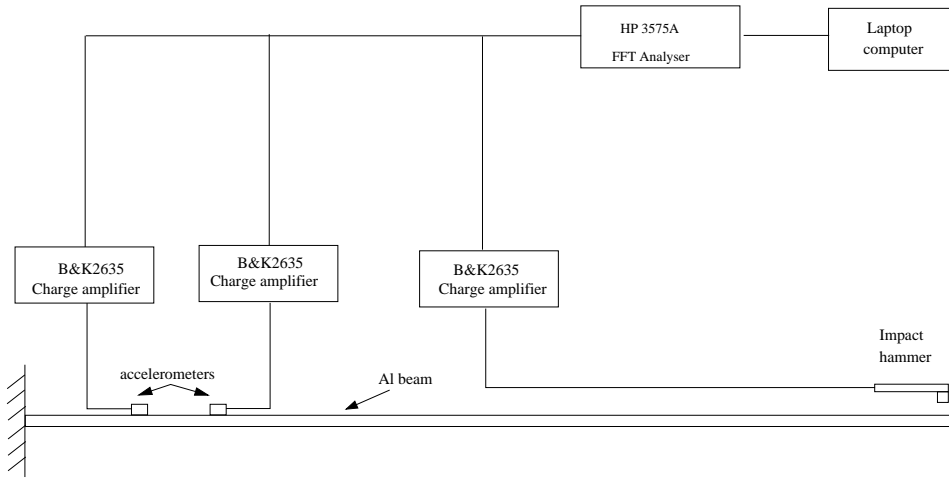
Figure 3.8: Schematic of Experimental Set-up

The aluminium beam specimen, the clamping rig and the instrumentation and accessories used in the modal analysis experiments are shown in Fig. 3.9. The beam used is made of aluminium 7075-T6, with Young's Modulus $69.6GPa$, Poisson's ratio 0.3, density $2772.53Kg/m^3$3 and the same geometry ($L = 600mm$, $W = 50mm$, $h = 3.2mm$) as used in the numerical modelling. Experiments are conducted on beams in their pristine states and then on damaged beams with simulated cracks located at 100mm from the fixed end (17% of the length of the beam) whose size is 40% of the width of the beam. Cracks are simulated by machining a rectangular slot, 20mmX0.2mm, symmetrically along the centre-line of the beam width.

Figure 3.9: Experimental set-up for modal analysis of beam specimen

A calibrated impact hammer, *(B&K 8202)*, is used to excite the beam and the responses are measured at 41 equally-spaced points along its length. The output responses are measured as acceleration signals using two miniature accelerometers, *(B&K 4374)*. Both the input excitation and the output responses are amplified using three charge amplifiers, *(B&K 2635)*, measured for 4 seconds, and recorded by a HP 3566A 8-channel FFT analyser. The frequency range for the experiments is $0\text{-}800Hz$, with 3200 spectral lines resulting in $0.25Hz$ spectral line spacing. A force/impulse window is applied to the input signal from the impact hammer and an exponential window is applied to outputs from the two accelerometers. The free end of the beam is chosen as the excitation point since it is not a node in any of the modes for a cantilever beam. Up to 10 spectral averages are taken at each measurement point. The average of 10 measurements at each measurement point was deemed sufficient to provide enough accuracy as the frequency response function appeared to converge when 10 measurements were taken and did not improve significantly with further increase in the number of measurements over which the averages were taken. Increasing the number of measurements for averaging would not have reduced the noise in extracted mode shapes to any significant level, whereas it would have considerably increased the duration of the tests. Averaging removes random noise

and randomly excited non-linearities from the cross-power spectra of each signal pair. After the measurements are taken at all 41 points, the vibration parameters are extracted using a frequency domain based curve-fitting software *StarModal v5.3*. A rational, polynomial curve-fitting method is used for extracting the vibration parameters. From the resonant peaks in the averaged Frequency Response Functions *(FRFs)* of each measurement point, the modal natural frequencies are identified. Curve-fitting bands are placed around each resonant peak to obtain other modal information. This process is repeated for measurements obtained from every point to extract information on the modeshapes and accurate natural frequencies.

3.4.2   Damage identification with modeshapes from experiments

The modal deflections of the original beam and the beam with the crack obtained from experiments are plotted together for comparison of modes 1, 2, and 3 in Figs. 3.10(a), 3.10(b) and 3.10(c) respectively.

It is obvious from the plots that the measured modal deflections have the same shapes as those predicted by the *FEA*, but are quite noisy compared to them. It is not easy to identify the presence of the crack or determine its location by comparing the measured deflection plots of the cracked beam with those of the uncracked beam.

The magnitude differences in the normalised modeshape deflections from *EMA* of the beams with and without cracks are plotted together for the first three modes in Figs. 3.11(a), 3.11(b) and 3.11(c) respectively. While the plots of the magnitude differences in modal deflections predicted by the *FEA* exhibit peaks and, therefore, some promise for identifying the damage location (especially in the higher modes), it is obvious that the plots of the differences in measured modal deflections in Fig. 3.11 are too noisy to indicate either the presence, or the location, of cracks.

(a) Mode1

(b) Mode2

(c) Mode3
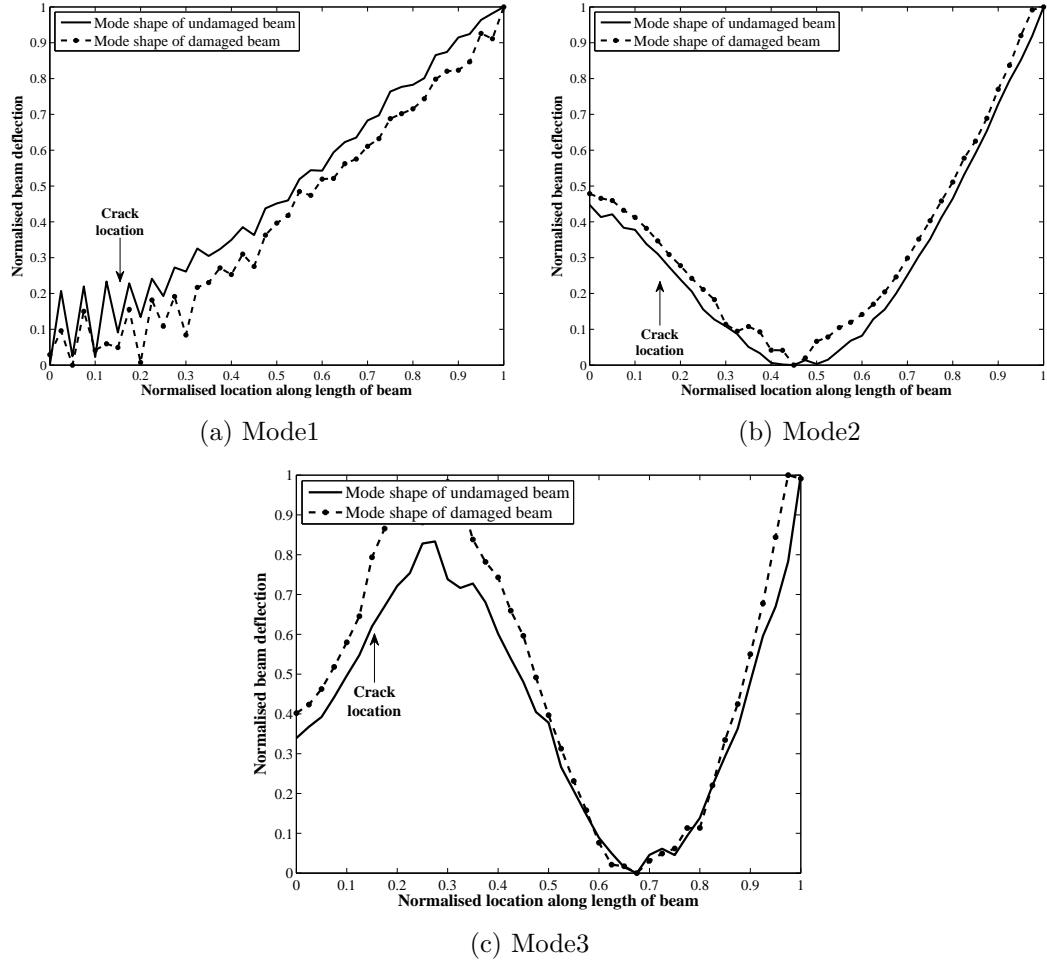
Figure 3.10: Normalised beam deflections of undamaged and damaged beams from experiments (crack length = 40% of beam width)

(a) Mode1

(b) Mode2

(c) Mode3
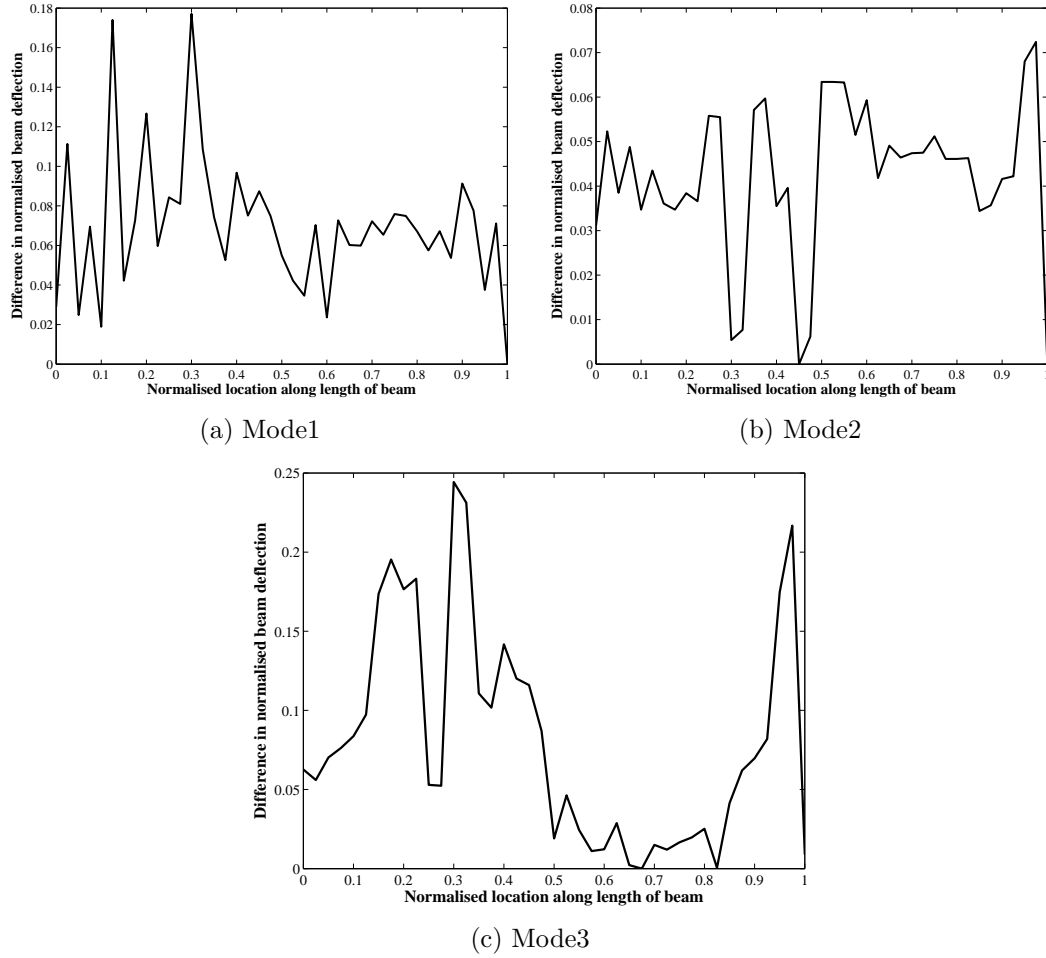
Figure 3.11: Magnitude differences in normalised beam deflections of damaged and undamaged beams from experiments (Crack location = 17% of beam length, crack length = 40% of beam width)

Differences in the magnitudes of the curvatures computed from the measured modal deflections of the cracked and uncracked beams are plotted for modes 1, 2 and 3 in Figs. 3.12(a), 3.12(b) and 3.12(c) respectively. In mode 1, there are larger peaks away from the crack location than in the vicinity of the crack, in mode 2, there are two big peaks to the right of the crack location and, in mode 3, the largest difference in the curvatures lies to the right of the crack with a peak at about $0.3L$ (30% of the length of the beam) instead of the expected $0.17L$ (17% of the length of the beam). Thus, the differences in the measured curvatures in mode 3 would lead to a crack being identified in an erroneous location, while those in mode 2 would indicate the presence of two cracks further to the right of the location of the actual crack.

(a) Mode1

(b) Mode2

(c) Mode3
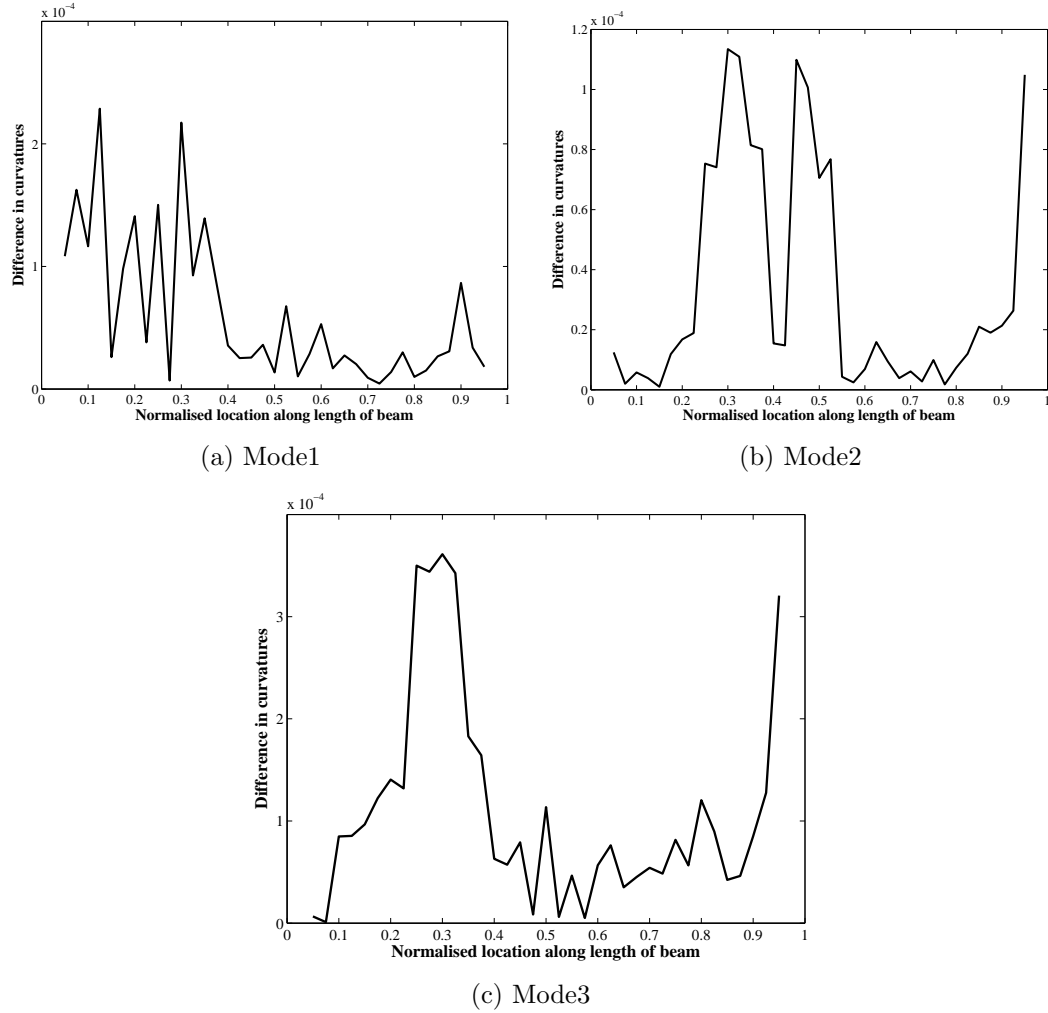
Figure 3.12: Magnitude differences in modeshape curvatures of damaged and undamaged beams measured from experiments (Crack location = 17% of beam length, crack length = 40% of beam width)

Figs. 3.13 and 3.14 show the *CDF* and the *DI* respectively which are calculated using the curvatures from the measured deflections of the cracked and uncracked beams. It can be seen that, the *CDF* shows a peak to the right of the real damage location similar to the curvature differences in modes 2 and 3 (Figs. 3.12(b) and 3.12(c)), the *DI* plot in Fig. 3.14 shows numerous peaks, with the largest being around $0.3L$ from the clamped end. Thus, it would appear that the *CDF* and *DIM* are no more successful in determining the presence of damage or identifying its location in a real application than is the plotting of the differences in the curvatures.
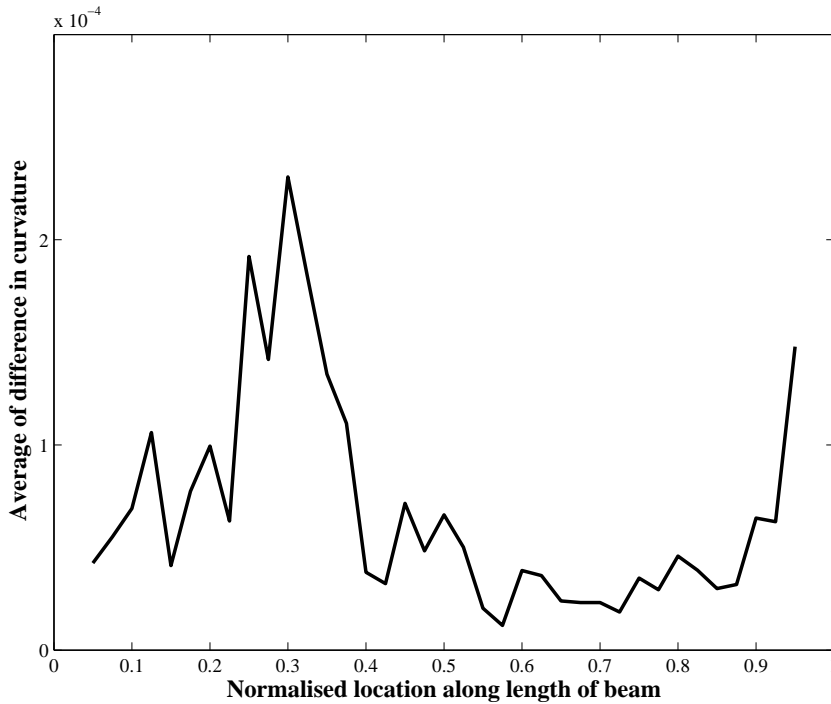
Figure 3.13: *CDF* for beam with crack from experiments (Crack location = 17% of beam length, crack length = 40% beam width)

These results indicate that curvatures obtained from measured modal deflections cannot be reliably used to detect damage. This is mainly because the variations in deflection measurements, i.e., the noise in the data, become amplified each time the modeshape is differentiated (with small ups and downs producing positive and negative derivatives); also, differentiating twice to obtain curvatures worsens the situation. If the damage signature is sufficiently strong, i.e., if the variation in the measured deflections caused by the damage is large compared to the noise in the
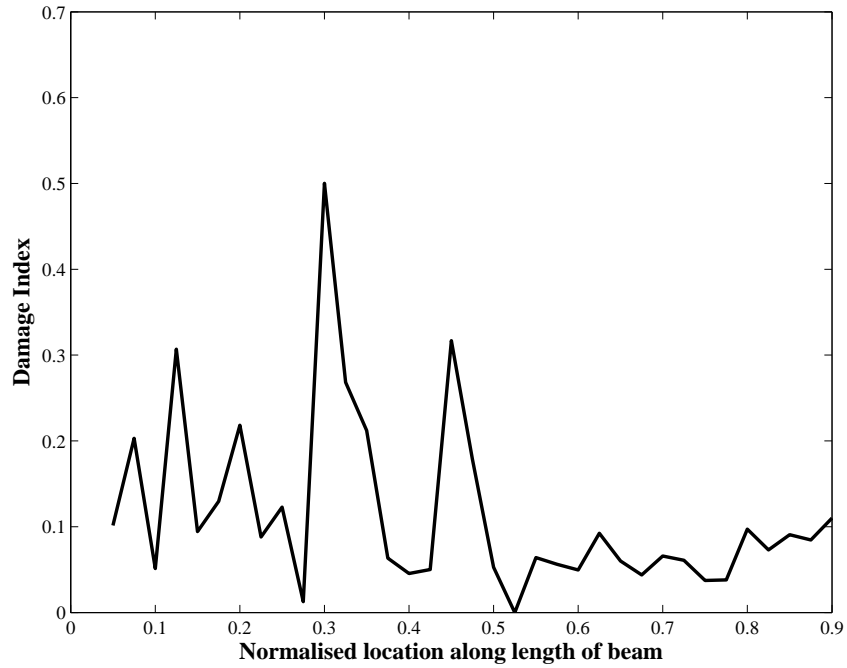
Figure 3.14: *DI* for beam with crack from experiments (Crack location = 17% of beam length, crack length = 40% beam width)

data, an attempt to filter the noise and smoothen the modeshapes before differentiating them could be made; however, in the present case, the crack extending over 40% of the beam width and located at 17% of the length from the fixed end of the cantilever does not reduce the local stiffness sufficiently to produce a change in the deflection pattern that is higher than the noise level. Thus, it appears that, without a major advancement in technology which would allow measurements of vibration data with high sensitivities and much lower noise levels, the application of modeshape measurements for the non-destructive inspection of realistic flaws in real structures will not be practical.

The above measurements, using *EMA* and data analysis, were repeated on the same beam to check whether any experimental errors were made the first time and to see whether the results could be improved. The results were similar, with the identification of the presence of the crack inconclusive for the most part due to the noise in the data. It was, however, interesting to note that the peaks in the curvature difference plots, indicating the damage location, appeared different to those from the first set of experiments which shows that the results of the modeshape methods are not necessarily repeatable, possibly due to the random nature of the noise in the data. Some more experiments were conducted on beams with cracks machined at

different locations but of the same size (40% of beam width); once again, identification of the presence of a crack was largely inconclusive. These experiments provide further evidence that the modeshape methods cannot be reliably and effectively employed for damage detection in real structures due to the low sensitivity of the curvature changes to the damage and the high degree of noise in the data collected. In the subsequent section, the effect of an alternate dynamic parameter, i.e., natural frequency changes, is investigated for possible implementation in damage detection.

3.5   Use of natural frequencies for damage detection

The numerical simulations and *EMA* performed to obtain modeshape data also provided natural frequency values for the damaged and undamaged beams. The frequencies predicted by the *FEA* for the undamaged beam and the beam with damage (crack size of 40% of beam width located at 17% of length of beam from fixed end) for the first six modes are shown in Table. 3.1 and plotted as a bar chart in Fig. 3.15. In the plot, for easy comparison, the frequencies of the beam with damage are normalised with respect to the frequencies of the undamaged beam.

Table 3.1: Frequencies extracted from *FEA*

	Uncracked beam	Cracked beam (located at 17% length and size 40% width)	% change compared to undamaged beam frequency
Mode1	7.24	7.14	1.37
Mode2	45.36	45.31	0.12
Mode3	127.07	126.95	0.10
Mode4	249.26	247.70	0.63
Mode5	412.61	408.64	0.96
Mode6	617.36	612.71	0.75
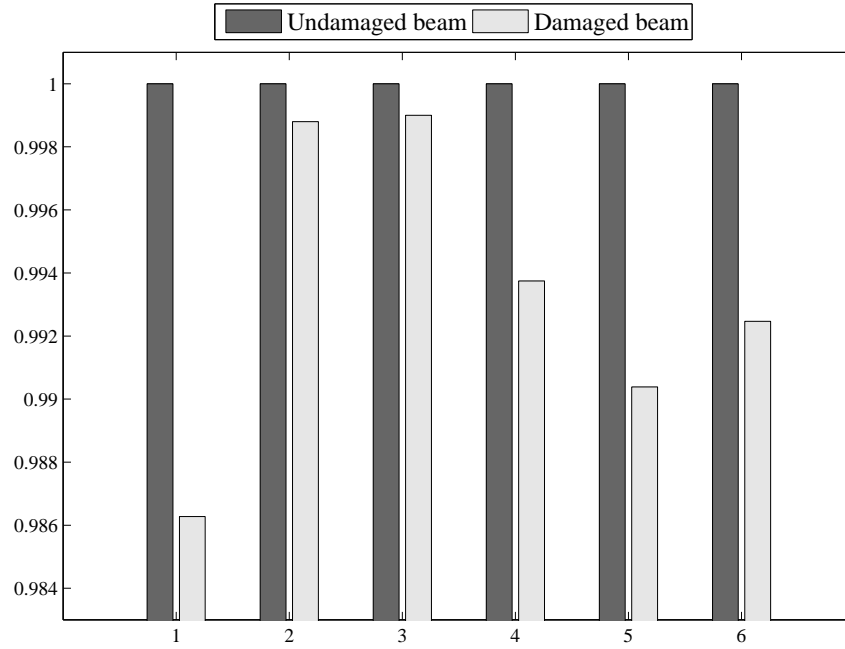
Figure 3.15: Comparison of natural frequencies obtained from *FEA*

The first six frequencies measured by *EMA* on the cantilever aluminium beam specimens, with and without a crack, are listed in Table. 3.2. These frequency values are averaged over measurements taken at 41 locations in two trials. The Standard Deviation *(SD)* of data from the two trials are also listed in the table. The mean values of the measured frequencies, normalised with respect to those of the undamaged beam are plotted as a bar chart in Fig. 3.16, with the scatter bars indicating standard deviations above and below the mean of the measured data.

Table 3.2: Frequencies measured from experiments

	Undamaged beam		Damaged beam (located at 17% length and size 40% width)		% change compared to undamaged beam frequency
	Average	*SD*	Average	*SD*	
Mode1	7.11	0.000	7.005	0.007	1.48
Mode2	44.61	0.000	44.525	0.021	0.19
Mode3	125.005	0.007	124.715	0.064	0.23
Mode4	245.215	0.007	243.285	0.078	0.79
Mode5	406.26	0.014	401.97	0.113	1.06
Mode6	608.175	0.035	603.695	0.219	0.74

SD ⇒ *Standard Deviation*
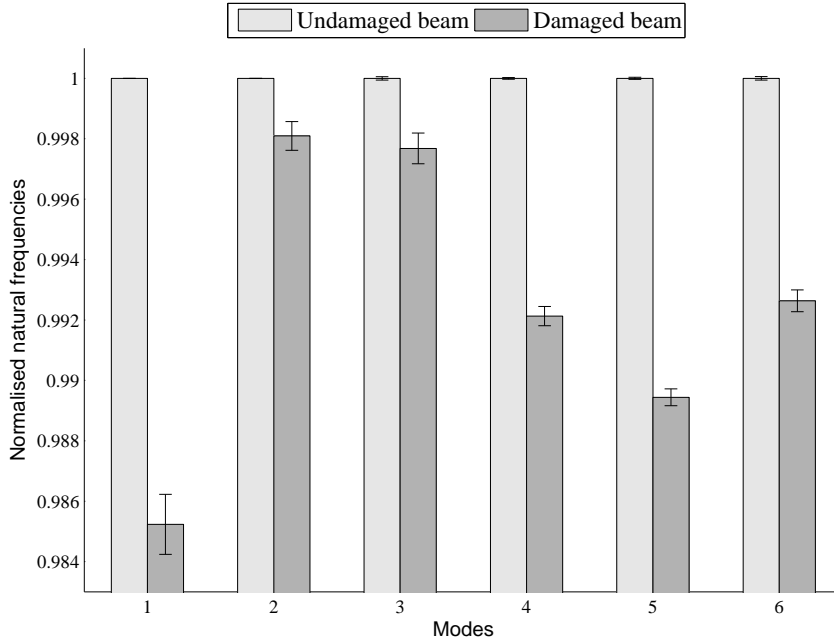
Figure 3.16: Comparison of natural frequencies obtained from experiments

It can be seen that the differences in the mean frequencies between the uncracked and cracked beams are larger in magnitude than the scatter in the data in each mode. This strongly suggests that frequency changes can be used as reliable indicators of the presence of damage in the structure, at least for the case of a defect of size 40% of the width of the beam and located at 17% of the beam length from the fixed end.

This is in line with the findings of Doebling *et al.* [57] that natural frequency changes due to the presence of damage are *statistically more significant* compared to changes in modeshapes and their derivatives.

3.6 Conclusion

A survey of the literature indicated that modeshape methods offer some promise for damage detection. Further, they have the advantage that, once the presence of damage is detected by changes in the modal deflection or the curvature, its location is also identified; whereas, by employing frequency based methods, even if the presence of damage is indicated by a change in the frequency, further investigation or analysis has to be conducted in order to identify its location. Hence, the applicability of modeshape methods for damage detection has been investigated first in

this preliminary study. The numerical simulation using *ANSYS* showed that the presence of damage and its location can be identified with some degree of certainty using curvature based methods. The application of those methods to a real case was then tested by *EMA* on a beam in the laboratory, with a simulated crack of the same size and at the same location as the numerical model. However, the curvatures determined from the modal deflections, measured over 41 points along the length of the beam, proved to be too noisy, drowning out the effect of the damage on the beam stiffness and, therefore, any resulting variations in the modal curvatures. The use of modal deflections was quite futile; even the curvature based methods (differences in curvatures, *CDF* and *DIM*) produced results with many false peaks and at the wrong locations. This preliminary study thus leads to the conclusion that the application of modeshape methods for damage detection in practice is quite unreliable and has limited success, unless techniques for obtaining measurements with more sensitivity and less noise can be employed.

Although the use of frequency measurements for damage detection has the disadvantage that, even if the presence of damage is detected, further analysis has to be carried out to determine its location and size, the measurement of natural frequencies needs only one sensor and can be measured relatively quickly and reliably. Further, the data obtained in this preliminary study show that natural frequency measurements are repeatable and capture the changes due to the presence of damage. Considering these advantages and the lack of success with modeshape methods, further research in this thesis is focused on the application of frequency measurements for the detection of damage, the determination of its location and the assessment of its severity. The methods developed are first validated using numerical simulation and then their practical applicability is verified on actual structures, i.e., beam and plate components.

Chapter 4

Change in frequencies due to damage in a structure: Theory

4.1   Introduction

This chapter presents details of the theoretical background for damage detection in beams and plates. A small crack in a beam or a plate has virtually no effect on its mass, but produces a significant reduction in the local stiffness of the structure. This causes a change in the natural frequencies of the structure. Usually the damaged structure has a lower natural frequency compared to its undamaged counterpart. It has been shown that the change in natural frequency can be related to the change in energy of vibration in the structure. The energy of vibration is higher in a damaged structure due to its lower stiffness (higher flexibility). Due to a local reduction in stiffness there is also a discontinuity in the slope (gradient of deflection) of the structure at the location of damage. In previous studies on beams [132,133,136,135, 138,140], the crack was modelled as a rotational spring and the increase in energy of the damaged structure was accounted for as the energy accumulated in the rotational spring at the location of damage. The stiffness of the spring is inversely proportional to size of the crack.

The essential relationship between the change in frequency and the change in vibrational energy of the damaged structure, also forms the basis of the methodology proposed in the present study. However, instead of modelling the crack as a spring, the change in energy of the damaged structure is directly obtained from Linear Elastic Fracture Mechanics *(LEFM)* as the energy stored in the crack. This opens the methodology for application to two dimensional structures, wherein a small

crack anywhere on the plate does not produce a discontinuity in the gradient of deflection over the entire width and the spring analogy may not be compatible with physical reality. In the following sections, the theory is first developed for transverse vibration of beams containing edge cracks (also designated as part-through cracks), then extended to beams containing through-thickness centre cracks and, finally, to transverse vibration of plates containing through-thickness cracks.

The problem of determining changes in resonant frequencies due to an edge crack in a beam has been dealt with using a spring model and a force equilibrium approach by [136, 142, 135, 138]. Hu and Liang [149] and Patil and Maiti [152, 150] implemented the spring model for the same case using an energy approach. In both cases, a methodology was also provided for solution to the inverse problem, i.e., for determining the crack size and location from the measured frequency changes. Gudmundson [148] has addressed the problem of frequency changes due to an edge crack in a beam without the spring model by using perturbation theory and implementing Stress Intensity Factor *(SIF)* solutions for edge cracks in semi-infinite field. He extended this approach for centre cracks in bars subjected to tension and for beams with circular holes. He does not, however, provide solution to the inverse problem.

The theory developed herein is along the lines of Gudmundson [148] for edge cracks in beams, but is applicable to beams with cracks of finite size. In the present study, for the first time, it is shown that changes in resonant frequencies are related to the normalised curvature at the crack location through a damage index parameter which is indicative of the severity of the crack. This approach has also been extended for the first time to centre cracks in beams and to through-thickness cracks in two dimensional structures i.e., plates. Further, the solution to the inverse problem for beams with edge and centre cracks is presented in Section 4.6.1 using an approach similar to that employed previously [136, 142, 135, 138, 149, 152, 150]. The solution to the inverse problem for plates however requires extension from one dimensional to two dimensional, involving four unknowns instead of two. This is presented in Section 4.6.2.

4.2 Relationship between change in frequency and incremental energy

Gudmundson [148] employed a first order perturbation theory to predict the changes in resonant frequencies of a structure due to cracks, notches and other geometrical changes. He showed that eigen frequency changes are dependent on the difference in strain energy of the cracked and uncracked structure. The natural frequencies in transverse vibration of a beam with a crack, can be expressed in terms of the energy stored in the crack and the vibrational energy of the structure as [148]

$$\frac{\omega_n^{*2}}{\omega_n^2} = 1 - \frac{\Delta U_n}{U_n} \tag{4.1}$$

where,

ω_n is the natural frequency of the uncracked structure in the nth mode ;

ω_n^* is the natural frequency of the cracked structure in the nth mode ;

U_n is the strain energy of the undamaged structure in n^{th} mode; and

U_n^* is the strain energy of the damaged structure in n^{th} mode; and

$\Delta U_n = U_n^* - U_n$, is the difference between the strain energies of the damaged and the undamaged structure, equal to the strain energy stored in the crack in its nth mode.

Using Binomial expansion,

$$\frac{\omega_n^*}{\omega_n} = 1 - \frac{1}{2}\left[\frac{\Delta U_n}{U_n}\right] - \frac{1}{8}\left[\frac{\Delta U_n}{U_n}\right]^2 + \cdots$$

Neglecting higher order terms and rearranging we get

$$\frac{\Delta\omega_n}{\omega_n} = \frac{1}{2}\frac{\Delta U_n}{U_n} \tag{4.2}$$

where, $\Delta\omega_n$ is the *reduction* in frequency of the damaged beam from that of the undamaged beam, i.e., $\Delta\omega_n = \omega_n - \omega_n^*$.

The energy stored in the crack, i.e., the change in strain energy due to formation of the crack (ΔU_n), can be expressed in terms of the *Stress Intensity Factor (SIF)* at the crack tip, shown by Kobayashi [166], as

$$\Delta U_n = \frac{1}{E} \int^{A} K_I^2 dA \tag{4.3}$$

where, E is the young's modulus and the integral is taken over the full area of the crack, A. K_I is the mode I *SIF* at the crack tip for a beam or plate in bending. Mode I *SIF* can be obtained for different crack configurations from fracture mechanics theory.

The strain energy in the undamaged state, U_n, is computed from the transverse deflection (modeshape) of the structure.

4.2.1 Energy of vibration for beams

Assuming conservation of energy, the total energy in a beam undergoing transverse vibration can be expressed in terms of the bending strain energy at its extremum positions. Thus the vibration energy in the nth mode, U_n, is given by

$$U_n = \frac{1}{2EI} \int_0^L M_n(x)^2 dx$$

where EI is the bending stiffness, E the Young's Modulus and I the second moment of area of the cross section of the beam. $M_n(x)$, the bending moment at any point x along the length of the beam in the nth mode, is related to the curvature (second derivative of deflection) by $M_n(x) = EI \left[d^2\psi/dx^2 \right]_n$, ψ being the deflection (modeshape) of the beam in the nth mode.

$$\therefore U_n \;=\; \frac{1}{2} EI \int\limits_0^L \left[d^2\psi/dx^2 \right]_n^2 dx \tag{4.4}$$

Noting that the Root Mean Square *(RMS)* value of the curvature distribution, over the entire length of the beam, is given by

$$\chi_{RMS} \;=\; \sqrt{\frac{1}{L} \int\limits_0^L [d^2\psi/dx^2]_n^2 \, dx} \tag{4.5}$$

the vibration energy in the beam may be expressed as

$$U_n \;=\; \frac{1}{2} EIL\chi_{RMS}^2 \tag{4.6}$$

The *RMS* value of the curvature χ_{RMS} can be obtained using Eqn. [4.5] from the modal deflections of the beam. The modal deflections depend on the boundary conditions of the beam and can be derived theoretically, obtained numerically or through measurements.

4.2.2 Energy of vibration for plates

The total energy in a plate undergoing transverse vibration can be expressed in terms of the bending strain energy at its extreme points of motion. The bending strain energy stored in the plate is obtained using *Kirchhoffs classical plate theory* [167,168] as

$$U_n = \frac{1}{2} D \int\limits_0^W \int\limits_0^L \left\{ \left(\frac{\partial^2\psi}{\partial x^2} + \frac{\partial^2\psi}{\partial y^2} \right)^2 - 2\left(1-\nu\right) \left[\frac{\partial^2\psi}{\partial x^2}\frac{\partial^2\psi}{\partial y^2} - \left(\frac{\partial^2\psi}{\partial x\partial y} \right)^2 \right] \right\} dxdy \tag{4.7}$$

where, $\psi(x,y)$ is the deflection in the nth mode at location (x,y), L and W are the length and width of the plate, ν is the Poisson's ratio and D is the flexural rigidity of the plate given by

$$D = Eh^3/12(1-\nu^2) \tag{4.8}$$

where h is the thickness of the plate and E the Young's Modulus.

Using the notation

$$\chi_{RMS} = \sqrt{\frac{1}{LW} \int_0^W \int_0^L \left\{ \left(\frac{\partial^2 \psi}{\partial x^2} + \frac{\partial^2 \psi}{\partial y^2} \right)^2 - 2(1-\nu) \left[\frac{\partial^2 \psi}{\partial x^2} \frac{\partial^2 \psi}{\partial y^2} - \left(\frac{\partial^2 \psi}{\partial x \partial y} \right)^2 \right] \right\} dxdy}$$

(4.9)

the vibrational energy of the plate may be succinctly expressed as

$$U_n = \frac{1}{2} DLW \chi_{RMS}^2$$

(4.10)

Note that, χ_{RMS} in this case, represents the RMS value of the effective curvature distribution over the entire surface of the plate.

4.3 Theory for beam with edge crack

The theory for predicting the change in frequencies in terms of the damage size and location is presented in this section for the case of edge crack in a beam subjected to transverse vibrations. Theory for edge cracks has been developed earlier using the spring analogy in [140, 142, 138, 136] and using the energy approach by Gudmundson in [148]. An energy approach, similar to Gudmundson [148], is used here to develop equations which maintain the commonality with the theory developed for through-thickness cracks in beams and plates in subsequent sections.
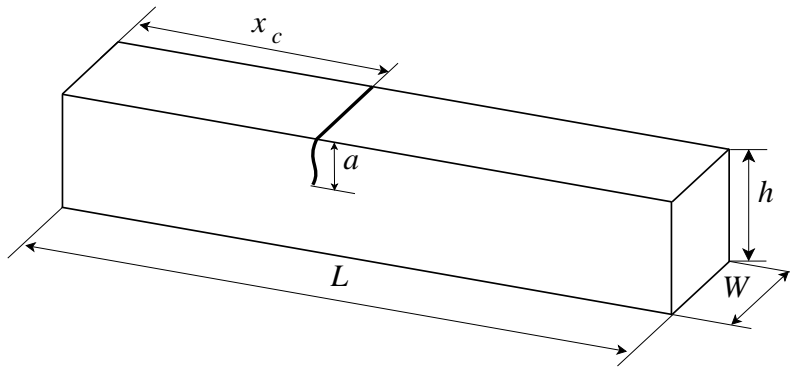
Figure 4.1: Beam with edge crack

4.3.1 Beam with infinitesimal edge crack

Initially, the equations are derived for a small edge crack in a semi-infinite beam to illustrate the salient points in the development of the theory.

A crack of length (depth) a is located at a distance of x_c from one end of the beam. The crack runs along the full width, W, of the beam as shown in Fig. 4.1. When subjected to transverse vibrations, the mode I *SIF* at the crack tip is a function of the bending moment at the location of the crack and for an infinitesimally small crack is given by [169]

$$K_I = 1.12\sigma_g\sqrt{\pi a} \tag{4.11}$$

The gross stress, σ_g, is given by $\sigma_g = 6M_o/h^2$, where M_o is the moment resultant (moment per unit width) at the location of the crack. Note that the constant 1.12 is the geometry correction factor for an edge crack in a semi-infinite beam. Substituting for σ_g, the *SIF* is obtained as

$$K_I = 1.12\frac{6M_o}{h^2}\sqrt{\pi a} \tag{4.12}$$

The moment stress resultant M_o can be expressed in terms of the curvature at the location of the crack as,

$$M_o = \frac{EI}{W}\chi_c \tag{4.13}$$

where I is the second moment of area given by $Wh^3/12$ and χ_c is the curvature of the uncracked beam at the location of the crack given by

$$\chi_c = \left[d^2\psi_c/dx^2\right] \tag{4.14}$$

Substituting Eqns. [4.12] and [4.13] in Eqn. [4.3], the energy stored in the crack is obtained as

$$\Delta U_n = \frac{3\pi EI}{2h}1.12^2a^2\chi_c^2 \tag{4.15}$$

Substituting for total energy of the beam from Eqn. [4.6] and change in energy from Eqn. [4.15] in Eqn. [4.2], the change in frequency due to the presence of the damage is obtained as

$$\frac{\Delta\omega}{\omega} = \left[1.12^2 \left(\frac{3\pi}{2} \right) \left(\frac{a^2}{Lh} \right) \right] \left[\frac{\chi_c}{\chi_{RMS}} \right]^2 \tag{4.16}$$

Eqn. [4.16] shows that the change in frequency due to the presence of damage is a function of the ratio of the curvature (of the uncracked beam) at the location of the crack to the RMS value of the curvature distribution over the whole structure. This term is independent of the size of the crack and can be obtained from the modeshape deflections of the uncracked beam for each mode of vibration.

The constant of proportionality, given by the factor inside the square brackets, is a function of the size of the crack relative to the length and height of the beam (a^2/Lh). This factor is an indication of the severity of the crack and may be designated as *Damage Index (DI)*, given by

$$Damage\ Index,\ DI \ = \ 1.12^2 \left(\frac{3\pi}{2} \right) \left(\frac{a^2}{Lh} \right) \tag{4.17}$$

Thus the change in frequency in the nth mode due to the presence of the crack can be expressed as

$$\left[\frac{\Delta\omega}{\omega} \right]_n \ = \ DI \left[\frac{\chi_c}{\chi_{RMS}} \right]_n^2 \tag{4.18}$$

Eqn. [4.18] relating the change in natural frequencies to the damage parameter DI and the normalised curvature at the location of the damage (relative to the average curvature of the structure and represented by χ_{RMS}), is quite general and applicable to other structures as well.

4.3.2 Beams with cracks of finite length

The geometry correction factor of 1.12 is appropriate only for very small edge cracks i.e., when $a/h \approx 0$. For larger cracks in beams of finite depth, the geometry factor

66

is a function of the crack size to the beam depth (a/h) ratio and may be expressed as,

$$f(a/h) = C_1 - C_2(a/h) + C_3(a/h)^2 - C_4(a/h)^3 + \cdots$$

In this case, Eqn. [4.15] takes the form

$$\Delta U_n = \frac{3\pi EI}{h} \chi_c^2 \int_0^a \zeta f(\zeta/h)^2 d\zeta \tag{4.19}$$

where, ζ is the running variable representing the instantaneous crack length as shown in Fig. 4.2.
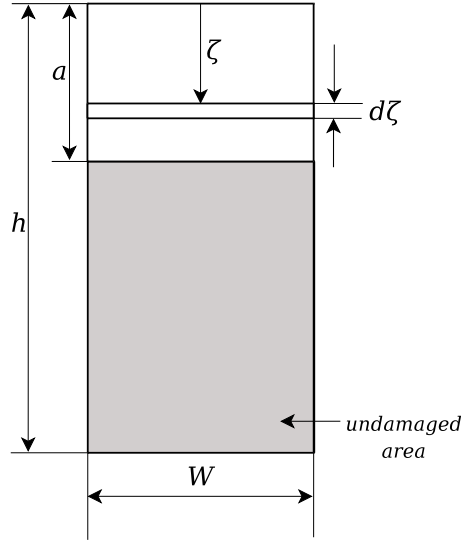
Figure 4.2: Cross section at the location of the edge crack

The integral on the right side of Eqn. [4.19] may be expressed as

$$a^2 g(a/h) = \int_0^a \zeta f(\zeta/h)^2 d\zeta \tag{4.20}$$

(Note that in the case of $a/h \approx 0$, $g(a/h) = \frac{1.12^2}{2}$). Hence, DI for a through-thickness crack of finite size is given by

$$Damage\ Index,\ DI = \frac{3\pi a^2}{Lh} g(a/h) \tag{4.21}$$

Gustafson [170] as well as Anifantis and Dimarogonas [171] have given the following expression for the geometry factor for edge cracks in beams subjected to transverse bending

$$f(a/h) = 1.13 - 1.374(a/h) + 5.74(a/h)^2 - 4.46(a/h)^3 \qquad (4.22)$$

Substituting this in Eqn. [4.20], the function $g(a/h)$ is obtained as

$$
\begin{aligned}
g(a/h) &= 0.64 - 1.035(a/h) + 3.72(a/h)^2 - 5.18(a/h)^3 + 7.55(a/h)^4 \\
&\quad - 7.33(a/h)^5 + 2.5(a/h)^6 \qquad (4.23)
\end{aligned}
$$

From Eqn. [4.21] it can be seen that the *Damage Index (DI)* is independent of material properties of the beam and the location of crack. It is only a function of crack size relative to the length and depth of the beam i.e., the ratios a/L and a/h. It may be noted that the damage index increases with the square of the crack size. The effect of the damage decreases with increasing length and height of the beam.

The curvature ratio $\left[\frac{\chi_c}{\chi_{RMS}}\right]_n$ is independent of the material properties and the crack size. It can be computed from the modeshape curvatures which are dependant on the boundary conditions and the mode of vibration. The magnitude of the curvature χ_c depends on the location of the crack as well as the mode of vibration. For instance, the curvature at the mid point of a simply-supported beam is maximum in mode 1 and vanishes for mode 2 (the mid point is an antinode for deflection in mode 1 and a node in mode 2). This means that a crack located at the mid point of a simply-supported beam will influence the mode 1 frequency significantly, but will have no effect on the second mode frequency.

Further, the damage index parameter, *DI*, is independent of the boundary conditions of the beam, i.e., it would remain the same whether the beam is simply supported or built-in. The boundary conditions will influence the normalised curvature term, χ_c/χ_{RMS}, and hence affect the change in modal frequencies.

4.4 Theory for beam with through-thickness centre crack

The change in frequency due to the presence of a through-thickness centre crack, located at a distance x_c from the edge of a beam as shown in Fig. 4.3, can be obtained in a similar manner as shown above. The *SIF* for through-thickness cracks in beams is the same as that for centre cracks in plates given by Boduroglu and Erdogan [172] and may be expressed as

$$K_I = \frac{6M_o}{h^2} f(\gamma) \sqrt{b/2} \tag{4.24}$$

where, M_o is the moment per unit width, $\gamma = b/W$, b is the crack length and $f(\gamma)$ is a function of the crack length to width ratio (b/W). Expressions for f have been provided by several authors for thin and thick plates [172, 173, 174, 175]. It may be noted that the expressions for *SIF* in Eqns. [4.12] and [4.24] are the solutions for stress intensity factors in mode I for a beam or a plate in bending. The opening mode fracture is caused by tensile stresses which may be caused by bending or in-plane tension, and in general the mode I *SIF* is a function of both in-plane and bending tensile stresses. However, in the case of a beam subjected to lateral vibrations, the deformation is predominantly pure bending and there are no tensile loads causing in-plane stresses. Hence the *SIF* in Eqns. [4.12] and [4.24] are obtained purely from the bending moments due to the lateral vibration. If the plate or beam is thick, then *SIF*s due to shear stresses in the tearing mode may also become significant and may have to be taken into consideration; but this combined mode is not considered in the present formulation.
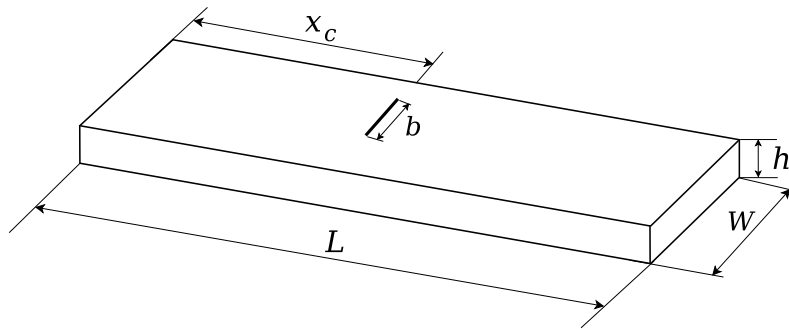
Figure 4.3: Beam with through-thickness centre crack

Note that the finite width correction factor, $f(\gamma)$, becomes unity for an infinitesimally small crack as $\gamma \approx 0$, as expressed by Zehnder and Hui [174, 175].

Substituting the above equation for K_I in Eqn. [4.3],

$$\Delta U = \frac{36M_o^2}{Eh^4} \int_A f(\zeta/W)^2 \zeta dA$$

where, ζ is a running variable representing the instantaneous crack length, as shown in Fig. 4.4.
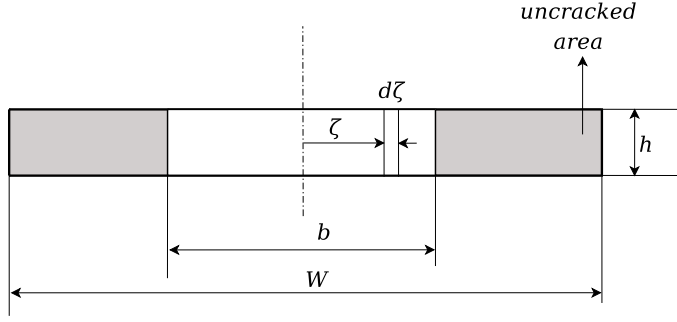
Figure 4.4: Cross section at the location of the centre crack

Substituting $dA = hd\zeta$,

$$
\begin{aligned}
\Delta U &= \frac{72M_o^2}{Eh^3} \int_0^{b/2} f(\zeta/W)^2 \zeta d\zeta \\
&= \frac{9M_o^2}{Eh^3} b^2 g(\gamma)
\end{aligned}
\tag{4.25}
$$

where

$$\int_0^{b/2} f(\zeta/W)^2 \zeta d\zeta = (b^2/8)g(\gamma) \tag{4.26}$$

Substituting for M_o as $\frac{EI}{W}\chi_c$ from Eqn. [4.13], we get,

$$\Delta U = \frac{3EI}{4W} b^2 g(\gamma)\chi_c^2 \tag{4.27}$$

Substituting for total energy of the beam from Eqn. [4.6] and change in energy from Eqn. [4.27] in Eqn. [4.2], the change in frequency due to the presence of the damage is obtained as

$$\left[\frac{\Delta\omega}{\omega}\right]_n = DI \left[\frac{\chi_c}{\chi_{RMS}}\right]_n^2$$

70

This equation is identical to Eqn. [4.18] given in Section 4.3. *DI* is now given by

$$Damage\ Index,\ DI = \frac{3b^2 g(\gamma)}{4LW} \tag{4.28}$$

The damage index for the beam with centre crack given by Eqn. [4.28] is similar in form to *DI* for edge cracks given by Eqn. [4.21]. *DI* for centre cracks is proportional to the relative crack sizes, b/W and b/L.

Boduroglu and Erdogan [172] have expressed the function $f(\gamma)$ for through-thickness cracks to be used in Eqn. [4.24] using polynomials whose coefficients are dependant on the width to thickness ratio (W/h) of the plate. These functions and their integrals $g(\gamma)$ are provided in Appendix A.

For thin plates, Wilson and Thompson [173, 176] have provided an expression for *SIF* of through-thickness cracks of the form

$$K_I = \left[\frac{1+\nu}{3+\nu}\right] \frac{6M_o}{h^2} f_1(\gamma) \sqrt{\pi b/2} \tag{4.29}$$

where

$$f_1(\gamma) = 12\gamma^5 - 14.7\gamma^4 + 5.6\gamma^3 + 0.02\gamma^2 + 0.002\gamma + 1.$$

Eqn. [4.29] can be expressed in the same form as that of Eqn. [4.24], by assigning

$$f(\gamma) = \left[\frac{1+\nu}{3+\nu}\right] \sqrt{\pi} f_1(\gamma).$$

and the corresponding $g(\gamma)$ can be derived.

4.5   Theory for plate with through thickness crack

The solution for *SIF* for through thickness cracks in plates is the same as that given in Eqn. [4.24] for beams with centre cracks. The finite width correction factors $(f(\gamma))$ are the same as those of beams with centre cracks, given in Appendix A. Thus the energy stored in the crack is expressed by the same equation as that for beams with centre cracks, Eqn. [4.27]. The length of the crack is denoted by b, the crack location is identified by the x and y co-ordinates of its mid point, x_c and y_c and h is the thickness of the plate. The functions $g(\gamma)$ are also obtained by the integration of the $f(\gamma)$ over the length of the crack as given by Eqn. [4.26] and presented in Appendix A. Note that M_o is the moment stress resultant or the moment per unit width acting along n, the direction of the normal to the crack, as shown in Fig. 4.5. M_o can be expressed in terms of the moments M_x and M_y along x and y axes respectively and twisting moment M_{xy} as [168]

$$M_o \;=\; M_x sin^2\phi + M_y cos^2\phi + 2M_{xy} sin\phi cos\phi \tag{4.30}$$

where, ϕ denotes the angle of orientation of the crack with respect to the x-axis.

The moment resultants are related to the curvatures and the twist by

$$\begin{aligned}
M_x &= -D\left(\frac{\partial^2\psi}{\partial x^2} + \nu\frac{\partial^2\psi}{\partial y^2}\right) \\
M_y &= -D\left(\frac{\partial^2\psi}{\partial y^2} + \nu\frac{\partial^2\psi}{\partial x^2}\right) \\
M_{xy} &= -D(1-\nu)\frac{\partial^2\psi}{\partial x\partial y}
\end{aligned} \tag{4.31}$$

where D is the flexural rigidity given by Eqn. [4.8].

Substituting Eqns. [4.31] in [4.30], we get

$$\begin{aligned}
M_o = \quad &-D\left[\left(\frac{\partial^2\psi}{\partial x^2} + \nu\frac{\partial^2\psi}{\partial y^2}\right)sin^2\phi + \left(\frac{\partial^2\psi}{\partial y^2} + \nu\frac{\partial^2\psi}{\partial x^2}\right)cos^2\phi \right.\\
&\left. +2\left(1-\nu\right)\frac{\partial^2\psi}{\partial x\partial y}sin\phi cos\phi\right]_{@x=x_c \text{ and } y=y_c}
\end{aligned} \tag{4.32}$$
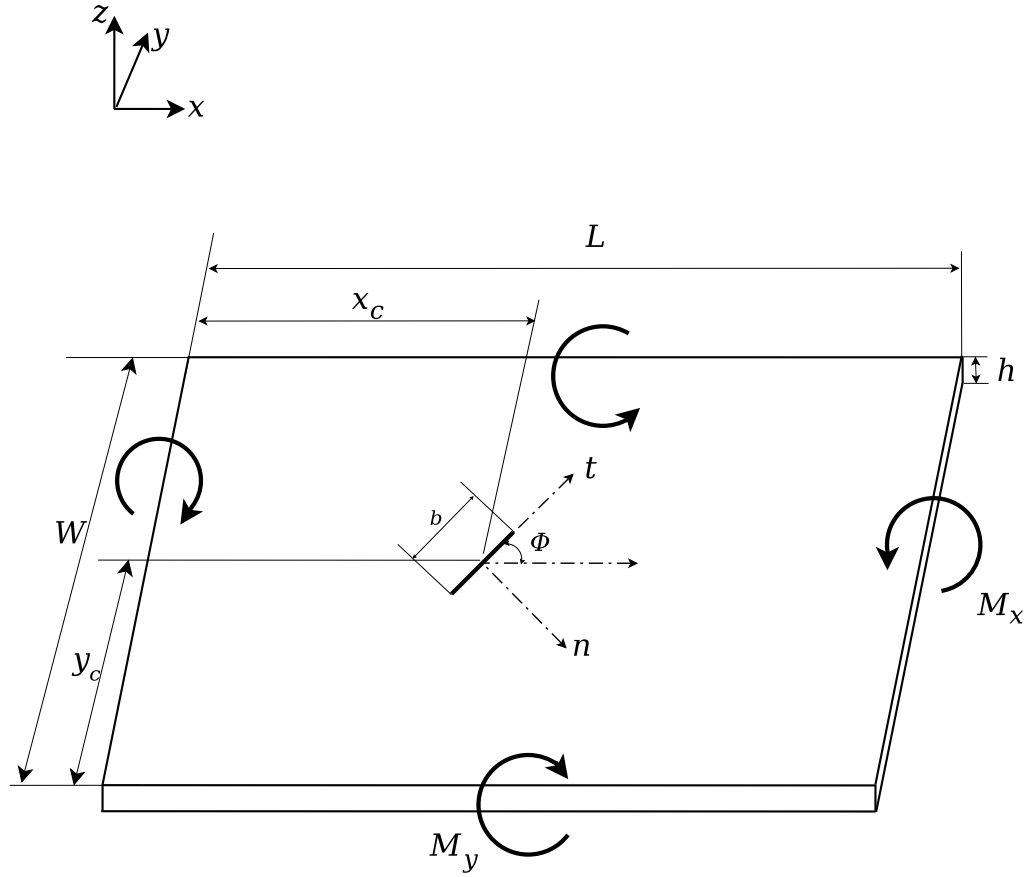
Figure 4.5: Figure showing plate with coordinate system and sign conventions

Substituting for M_o in Eqn. [4.25], the strain energy stored in the crack may be written as

$$\Delta U = \frac{3b^2 g(\gamma)}{4(1-\nu^2)} D \chi_c^2 \tag{4.33}$$

where χ_c is the effective curvature normal to the crack at its centre given by

$$\chi_c = \left(\frac{\partial^2 \psi}{\partial x^2} + \nu \frac{\partial^2 \psi}{\partial y^2}\right) sin^2\phi + \left(\frac{\partial^2 \psi}{\partial y^2} + \nu \frac{\partial^2 \psi}{\partial x^2}\right) cos^2\phi$$
$$+ 2\left(1-\nu\right) \frac{\partial^2 \psi}{\partial x \partial y} sin\phi cos\phi \tag{4.34}$$

Substituting for the total energy of the plate from Eqn. [4.10] and the change in energy from Eqn. [4.33] into Eqn. [4.2], the change in frequency due to presence of a through-thickness crack in a plate is obtained as

$$\frac{\Delta \omega_n}{\omega_n} = DI \left[\frac{\chi_c}{\chi_{RMS}}\right]_n^2$$

73

This equation is also identical to Eqn. [4.18], given in Section 4.3. The *DI* for through-thickness cracks in plates is given by

$$DI = \frac{3b^2 g(\gamma)}{4(1 - \nu^2)LW} \tag{4.35}$$

Note that the expression for *DI* is the same as that of Eqn. [4.28], except for the factor $(1 - \nu^2)$ in the denominator due to the two dimensional nature of the plate.

The finite width correction factor $f(\gamma)$ and the function $g(\gamma)$ become equal to unity as γ approaches 0 i.e., for small cracks.

It may be noted that the change in frequency of a plate is a function of four crack parameters, x and y coordinates of the crack x_c, y_c, the crack length b and orientation of the crack ϕ. *DI* is independent of both the location and the orientation of the crack and is dependent only on the crack size relative to the length and width of the plate. For a given crack size, the change in frequency is governed by the effective curvature, χ_c, normalised with respect to the mean curvature over the entire surface of the plate denoted by χ_{RMS}. χ_c is a function of the crack location as well as its orientation.

4.6   Solution to the inverse problem

The change in natural frequencies due to the presence of a crack in a beam or plate can be calculated from Eqn. [4.18] wherein the determination of *DI* requires the use of appropriate expression for the *SIF* solution. The forward problem is a direct application of the theory and thus relatively simple. The inverse problem of determining the crack location and size, and orientation in the case of plates, from changes in natural frequencies is, however, not straightforward. The methodology for solution of the inverse problem is presented below for each of the above cases.

4.6.1   Inverse problem for beams

The inverse problem for beams consists of solving for the location for the crack, x_c, and the relative crack length (equal to a/h for edge cracks and b/w for centre cracks), from known or measured values of changes in frequency. Since there are two unknowns this requires the use of at least two values of change in frequencies which may be obtained from measurements in two different modes. The expression for change in frequencies, Eqn. [4.18], may be rewritten as

$$DI = \frac{\left[\frac{\Delta\omega}{\omega}\right]_n}{\left[\frac{\chi_c}{\chi_{RMS}}\right]_n^2} \tag{4.36}$$

In Eqn. [4.36], DI is a function of only the size of the crack and the normalised curvature term is a function of the location of the crack and the mode of vibration. The normalised curvature term in the denominator can be determined from the deflections on the beam derived analytically, computed numerically or measured experimentally on the undamaged beam for each individual mode for the whole length of the beam. For any given mode, DI can be computed as a function of the beam locations from Eqn. [4.36]. All curves of DI plotted as functions of the location for two or more different modes will intersect at a common point, since the actual crack location and DI which is a function of the crack size are independent of the vibration mode. If we use only two modes, the curves may intersect at more than one point. The use of three or more modes ensures the determination of a unique solution for the location and size of the damage. The solution to the inverse problem for beams may thus be obtained graphically from the intersection of three or more DI plots as illustrated in Fig. 4.6. In practice, due to errors in measurement or round off errors in calculation, three curves may not all pass through the same point but are more likely to intersect with each other at neighbouring points forming a small triangle. In solving the inverse problems of beams graphically, the centroid of the triangle thus formed, is taken to be the final solution whose x and y values respectively represent the crack location and DI.

The solution to the inverse problem in beams may also be obtained numerically by the least square method, minimising the differences in DI between the different
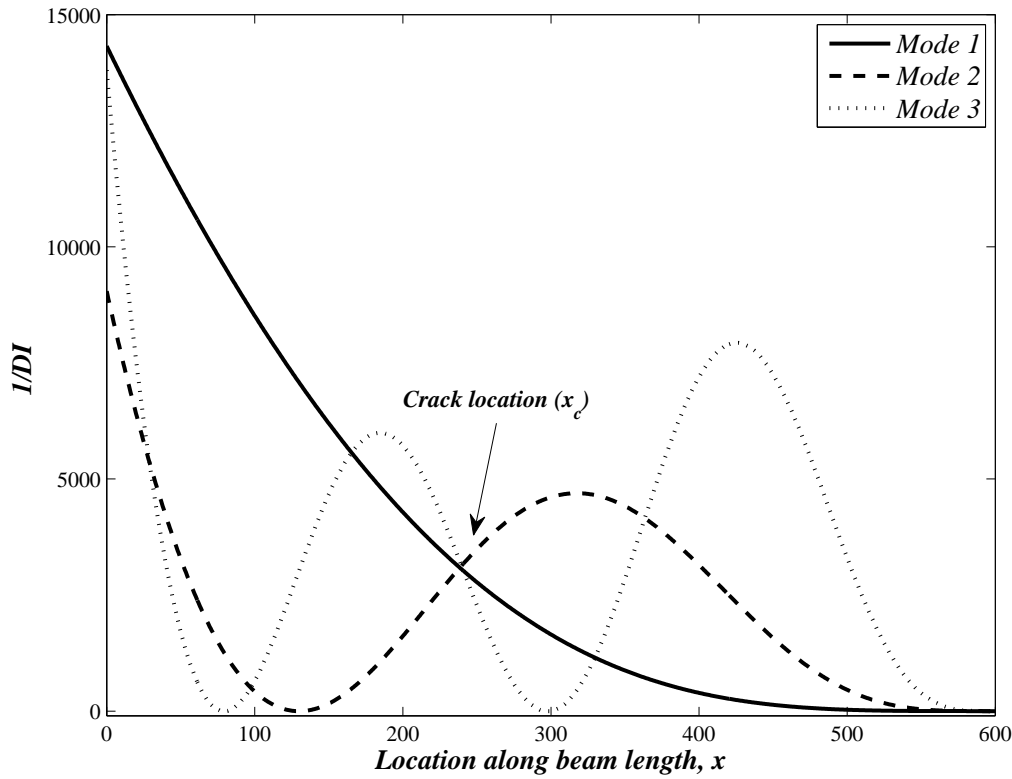
Figure 4.6: A typical *DI vs x* plot

modes. The *RMS* value of the distances between the *DI* curves of the different modes plotted against the beam coordinate (x) may be expressed as

$$d_{RMS}(x) = \frac{1}{n}\sqrt{\sum_{i=1}^{n-1}\sum_{j=i+1}^{n}[DI_i(x) - DI_j(x)]^2} \qquad (4.37)$$

where n is the total number of modes.

Computing the value of d_{RMS} from Eqn. [4.37] as a function of the beam coordinate (x), we can easily identify its minimum value which will provide us with the closest solution to the inverse problem, i.e., the values of DI and x_c, the damage index parameter and the location of the crack in the beam.

It is seen that the graphical solution using the centroid of the triangle of the intersection points and the numerical solution using the least square method, given by Eqn. [4.37], lead to predictions for crack location and size which are nearly the same and have discrepancies of similar magnitude with the actual values (compare Figs. B.1(a), B.1(b), B.2(a) and B.2(b) in Appendix B). So either method may be used in practice.

4.6.2   Inverse problem for plates

For plates, the inverse problem consists of solving for four unknowns, the coordinates of the crack (x_c, y_c), its orientation (ϕ) and crack size (b). In general, we need atleast four values of change in frequencies for the solution to this problem. If one of the four variables is known, the other three can be determined using a graphical technique similar to that described for beams in the previous section. For example, if the orientation of the crack is known, DI can be plotted as a function of x and y for each mode and the intersection point of three such surface plots will give us the values of x_c, y_c and DI of the crack. This is employed in Chapter 8 to find the location and size of cracks which are known to be parallel to the edges of the rectangular plate.

The solution to the inverse problem for plates may also be obtained numerically using a least square *(LS)* technique similar that used in beams by finding the minimum value of the RMS distance which may now be expressed as

$$d_{RMS}(x,y,\phi) = \frac{1}{n}\sqrt{\sum_{i=1}^{n-1}\sum_{j=i+1}^{n}[DI_i(x,y,\phi) - DI_j(x,y,\phi)]^2} \qquad (4.38)$$

Note, however, that the d_{RMS} value now is a function of three variables rather than that of a single variable as in beams. Hence determining the minimum value of d_{RMS} in Eqn. [4.38] would require the use of a minimisation technique.

The four-variable problem of determining x_c, y_c, ϕ and b from measured changes in frequencies can be directly formulated and solved as a minimisation problem. The residual, i.e. the error between the measured change in frequencies and the frequency change predicted from theory (Eqn. [4.18]) for each mode i may be expressed as

$$R_i(x_c, y_c, \phi, b/W) \;=\; \left[\frac{\Delta\omega}{\omega}\right]_{i(measured)} - DI\left[\frac{\chi_c}{\chi_{RMS}}\right]_i^2 \qquad (4.39)$$

The objective function for the minimisation problem may now be expressed as

$$F = \frac{1}{n}\sqrt{\sum_{i=1}^{n} R_i^2} \qquad (4.40)$$

where n is the total number of modes.

The damage detection problem involves finding the optimum crack parameters, x_c, y_c, ϕ and b/W such that F is the minimum. Techniques like *Sequential Quadratic Programming (SQP)* and computational intelligence based methods such as *Genetic Algorithms (GA)* can be used to solve the inverse problem. For n values of difference in modal frequencies between the undamaged and damaged plate, n equations can be formed based on Eqn. [4.40]. In this study, three different kinds of minimisation algorithms are used; *SQP*, *GA* and a combination of both.

SQP is a *gradient* based optimisation method which iteratively improves the solution by moving a random probable solution along the direction of the greatest decrease in function value [177, 178, 179, 180]. For damage detection in plates, the four-variable problem is first solved using *SQP fmincon*, a built-in function of the optimisation toolbox in *MATLAB*. *SQP* is an efficient algorithm but suffers the common disadvantage of gradient based techniques where the solution gets stuck on local minima depending on the starting point. Hence gradient based methods are not ideal when the objective function is multi-modal (i.e., have multiple minima). In such cases, *GA* can be used to find the global minimum. *GA*s are a class of population based methods in which a set of solutions evolve over generations, unlike the point improvement method [181, 182]. In this study, such an algorithm, developed by Deb [183, 184] and called *NSGA-II*, is investigated for solving the damage detection problem. This and other black-box based algorithms identify an approximate region for the minimum solution in the first few generations but, finding the *exact solution* needs a large number of generations as they do not use the information from the search space characteristics. Moreover, these techniques are computationally intensive and time-consuming. Hence, a combined 2-step *GA-SQP* approach, which reduces processing time and improves the efficiency of the search process, is proposed. A comparison between the three minimisation techniques is presented in Chapter 8.

4.7   Conclusion

In this chapter, a theoretical relationship between change in frequencies and damage parameters is developed, based on the axiom that the change in frequencies is

directly proportional to the change in energy due to the presence of a crack. It is shown that in all cases the normalised change in frequency is a function of the curvature at the location of the damage, normalised with respect to the mean curvature of the whole structure, in any particular mode. The constant of proportionality, expressed as *DI*, is directly proportional to the size of the damage relative to the dimensions of the structure, modified by the form factor of the *SIF* solution.

It is shown that the same relationship is applicable to edge cracks and centre cracks in beams and to through-thickness cracks in plates, with the difference only in the expression for *DI*. Once the crack size and location are known, and the finite width correction factor is determined using equations of *LEFM*, the forward problem of predicting resonant frequency changes in different modes becomes straight forward.

The inverse problem of determining the location and crack size for beams may be solved graphically or numerically from 3 or more values of measured changes in frequency. In the case of plates, three different methods, using *SQP*, *GA* and a combination of the two, are proposed for the solution of the inverse problem which involves solving for the four unknowns, the x and y coordinates of the crack location, its size and orientation.

One of the main advantages of the approach developed herein is that, only the curvatures of the *undamaged* structure are required for solving for the damage parameters from measured frequency changes. The curvatures can be determined by double differentiation from distributions of modal deflections over the undamaged structure which may be obtained from measurements, numerical modelling or theoretical analysis. Previous reports on frequency based techniques of damage detection have mainly relied on theoretical analysis for determination of the curvatures. This restricted the theoretical development hitherto to simple one dimensional cases. The recognition that changes in frequency due to damage are directly proportional to the normalised curvatures and that the latter can be obtained from numerical or experimental analysis allows the extension and application of the technique to cases of complex geometry. It will be shown in subsequent chapters that either numerical or experimental data for modeshapes can be employed successfully to predict damage size and location.

The application of the methodology is implemented using *FEA* and experimental measurements in Chapters 5 and 6, respectively, for beams. Data from numerical simulation and experimental modal analysis on plates are employed in chapters 8 and 9, respectively, for demonstration of application to two dimensional cases.

CHAPTER 5

Validation of analytical model for beams using *FEA*

5.1   Introduction

The theory for predicting change in frequencies due to the presence of damage was developed for beams with edge cracks and centre cracks and for plates with through-thickness cracks. It was shown that, the ratio of the change in frequency to the original frequency in any mode can be expressed as a function of a damage parameter *(DI)* and the curvature at the location of the crack normalised with the Root Mean Square *(RMS)* value of the curvature over the entire structure, as given by Eqn. [4.18]. In this chapter, we use numerical simulation to assess the validity of this relationship and the accuracy of Eqn. [4.18] by modelling edge cracks and centre cracks in beams using *Finite Element Analysis (FEA)*.

Chapter 4 also describes the approach for solving the inverse problem. The applicability of this technique for determining the location and size of damage is also verified, using beams with simulated cracks in *FEA*.

5.2   Description of Finite Element Modelling

The numerical modelling was conducted using the commercial software *ANSYS Version 11*. Macros were written using *Ansys Parametric Design Language (APDL)* to do the preprocessing work such as geometry definition, input of material properties, creating the mesh and setting boundary condition. The *ANSYS* modal analysis

capability was employed to extract the modal parameters, *viz.* the resonant frequencies and the corresponding modeshape deflections. Subsequently curvature values are computed from modeshape deflections using central difference as given by

$$\psi_i'' = \frac{(\psi_{i-1} - 2\psi_i + \psi_{i+1})}{h^2} \tag{5.1}$$

where, ψ is the deflection modeshape, ψ'' its second derivative with respect to x at any point i along the length of the beam and h is the distance between two node points.

5.2.1 Modelling of edge cracks in simply-supported beams

To study the effect of edge cracks on natural frequencies, simply-supported beams were modelled in *ANSYS* with material properties of steel matching those measured on the experimental samples (see section 6.2). The beam dimensions were: length=600mm, width=25mm and thickness=10mm. The beam was modelled in 2-D in elevation so that edge cracks running partially through the thickness could be modelled as shown in Fig. 5.1.
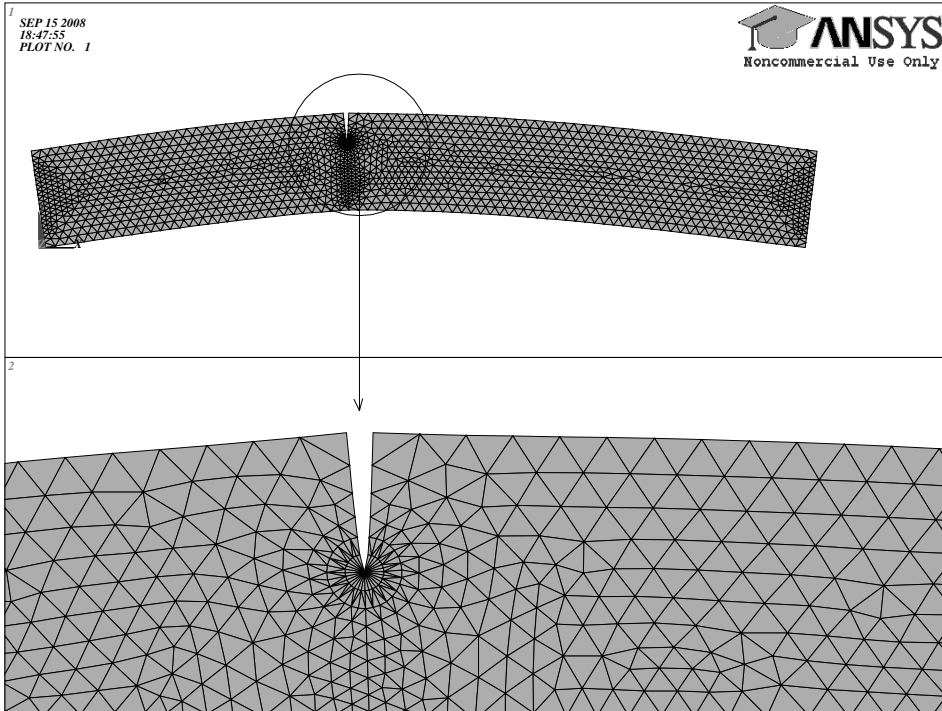
Figure 5.1: *FE* model of beam containing through-width edge crack

Plane stress elements were used as they support in-plane deflections (in-plane bending); hence *PLANE2* element type, with an option to specify thickness, is chosen. To model cracks, the nodes along the crack length were separated and crack tips were modelled using singular elements (KSCON option in *ANSYS*).

A convergence analysis was conducted on the Finite Element *(FE)* model of the undamaged beam in order to choose an appropriate mesh size. The initial *FE* model was meshed with 12 elements along the length of the beam. The number of elements used in each model was then doubled in each subsequent model. The natural frequencies in the first three modes of each model were compared to those of the previous one. To study the convergence, the Root Mean Square *(RMS)* value of the differences between natural frequencies of successive models ($i-1$ and i) were computed using the Eqn. [5.2].

$$RMS\ error = \frac{1}{3}\sqrt{\sum_{m=1}^{3}\left(\omega_{m,i-1} - \omega_{m,i}\right)^2} \tag{5.2}$$

where m is the mode number.

The *RMS* error is plotted against the number of elements in Fig. 5.2. It can be seen from Fig. 5.2, that a converged solution is obtained for a mesh containing 1152 elements where the *RMS* error is less than 0.05%. Further increases in mesh size do not significantly improve the accuracy of the results while they increase the computational time exponentially. Therefore subsequent investigations on simply-supported beams with edge cracks were conducted using a mesh containing 1152 elements.
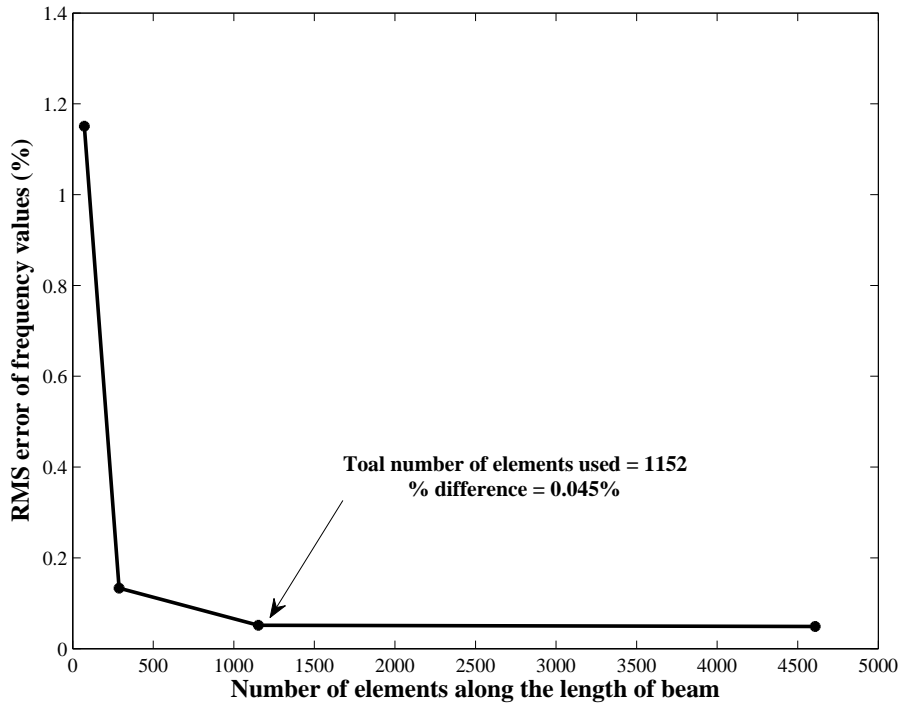
Figure 5.2: Convergence plot for choosing appropriate mesh size

The natural frequencies for the first 10 modes for the simply-supported beam obtained from *ANSYS* with 1152 plane stress elements (*PLANE2*) are listed in Table 5.1 along with values obtained from Euler-Bernoulli theory [185, 186]. The percentage differences between the frequencies obtained from *FEA* and theory are shown in the right hand side column. It can be seen that the discrepancy increases with increase in mode order. The highest difference between the theory and *FEA* is of the order of 20%, obtained for the tenth mode. The natural frequency values obtained using one dimensional beam elements (*BEAM3*), modelled with 600 elements, are also compared in Table 5.1. It can be seen that the results from *BEAM3* agree closely to the theoretical values, the highest difference being 8%, but these elements cannot be used to simulate beams with edge cracks, running partially through the thickness.

Table 5.1: Comparison of frequencies from *FEA* and theory for simply-supported beam

Mode	*Theory** (Hz)	Frequencies from *FEA* (Hz)		%difference from theory	
		PLANE2	BEAM3	PLANE2	BEAM3
1	156.26	155.78	156.02	0.31	0.15
2	625.05	617.5	622.77	1.21	0.37
3	1406.35	1369.19	1396.29	2.64	0.72
4	2500.18	2386.92	2470.16	4.53	1.22
5	3906.54	3641.9	3835.65	6.77	1.85
6	5625.41	5103.36	5481.98	9.28	2.62
7	7656.81	6741.14	7396.68	11.96	3.52
8	10000.73	8526.99	9565.84	14.74	4.55
9	12657.18	10435.05	11974.52	17.56	5.7
10	15626.14	12443.99	14473.5	20.36	7.96

*Euler-Bernoulli theory

Ten different cases of simply-supported beams having edge cracks were modelled in *FEA* with different values of crack size and location. The normalised crack location, x_c/L, and the normalised crack length, a/h, for these ten cases are presented in Table 5.2 along with the values of natural frequencies for the first three modes obtained from the *ANSYS* modal analysis. The natural frequencies of the undamaged beam are also shown for comparison. Table 5.2 lists the resonant frequency for the first three modes.

Table 5.2: Natural frequencies of simply-supported beams with edge cracks

Damage case	Crack location, x_c/L	Crack length, a/h	Natural frequencies from *FEA* (Hz)		
			Mode1	Mode2	Mode3
Undamaged beam			155.784	617.503	1369.193
1	0.05	0.05	155.758	617.139	1367.440
2	0.05	0.1	155.745	616.939	1366.498
3	0.1	0.1	155.697	616.268	1363.892
4	0.1	0.2	155.508	613.602	1353.033
5	0.1	0.3	155.174	608.913	1334.277
6	0.2	0.05	155.701	616.578	1366.406
7	0.2	0.15	155.243	611.940	1356.605
8	0.2	0.25	154.325	602.950	1338.577
9	0.85	0.05	155.726	616.743	1366.252
10	0.4	0.1	155.145	616.284	1365.737

For a given damage location, the percentage change in frequency increases with increase in damage size in all modes, as is to be expected, noting that the damage parameter is directly proportional to the crack size. However, even for a given crack size, the variations of frequency change with crack location and modeshape are not monotonic and are interrelated. This is because the frequency change is proportional to the normalised curvature which is a function of the crack location and mode of vibration as seen from Eqn. [4.18].

5.2.2 *Modelling of centre cracks in cantilever beams*

Through-thickness centre cracks were modelled in cantilever aluminium beams with material properties matching those determined from the experimental models (see section 6.2). The beams modelled had a length of 600mm, width of 60mm and thickness equal to 5mm. Initially natural frequencies were obtained for undamaged beam using three different element types: *SHELL63*, *SHELL93* and *BEAM3*. The first two are two dimensional shell elements whereas *BEAM3* is one dimensional beam element. The number of elements over the whole length of the beam for models with the *SHELL63* and *SHELL93* types was 1536 whereas 600 beam elements were employed in the third case. The natural frequencies obtained from *ANSYS* with these three element types for the first 10 modes are listed in Table 5.3 along with natural frequencies computed using Euler-Bernoulli theory [185,186]. The discrepancy between the *FEA* results and the theoretical predictions are shown are shown in the right hand side columns for the three cases.

Table 5.3: Comparison of frequencies from *FEA* and theory for cantilever beam

Mode	*Theory** *(Hz)*	Frequencies from *FEA* (Hz)			%difference from theory		
		SHELL63	SHELL93	BEAM3	SHELL63	SHELL93	BEAM3
1	*11.24*	11.34	11.32	11.24	0.89	0.71	0.00
2	*70.45*	71.01	70.93	70.44	0.79	0.68	0.01
3	*197.26*	199.03	198.67	197.21	0.90	0.71	0.03
4	*386.54*	390.74	389.7	386.38	1.09	0.81	0.04
5	*638.98*	647.52	645.04	638.56	1.34	0.94	0.07
6	*954.53*	969.96	964.91	953.61	1.62	1.07	0.10
7	*1333.2*	1358.58	1349.39	1331.42	1.90	1.19	0.13
8	*1774.9*	1813.72	1798.33	1771.87	2.19	1.29	0.17
9	*2279.8*	2335.59	2311.37	2274.79	2.45	1.35	0.22
10	*2847.8*	2924.28	2887.98	2840.02	2.69	1.37	0.27

*Euler-Bernoulli theory

In all three cases the deviation from the theory increases with increasing mode order. The *BEAM3* elements provide the best results with a maximum discrepancy of only 0.27% for the tenth mode. However, we cannot model through-thickness cracks if the beam is modelled using *BEAM3* elements. Among the shell elements, *SHELL93* offers better accuracy than *SHELL63* (1.37% compared to 2.69% for the 10th mode). Hence all future modelling of beams with centre cracks was conducted using triangular *SHELL93* elements in the *FEA*.

The crack is modelled by separating the nodes along the length of the crack with the crack tips modelled using singular elements, as shown in Fig. 5.3. Ten different cases of beams with centre cracks were modelled in *FEA* with different values of crack size and location. The normalised crack location, x_c/L, and the normalised crack length, b/W, for these ten cases are presented in Table 5.4, along with the values of natural frequencies for the first three modes obtained from *ANSYS* modal analysis. The natural frequencies of the undamaged beam is also presented.
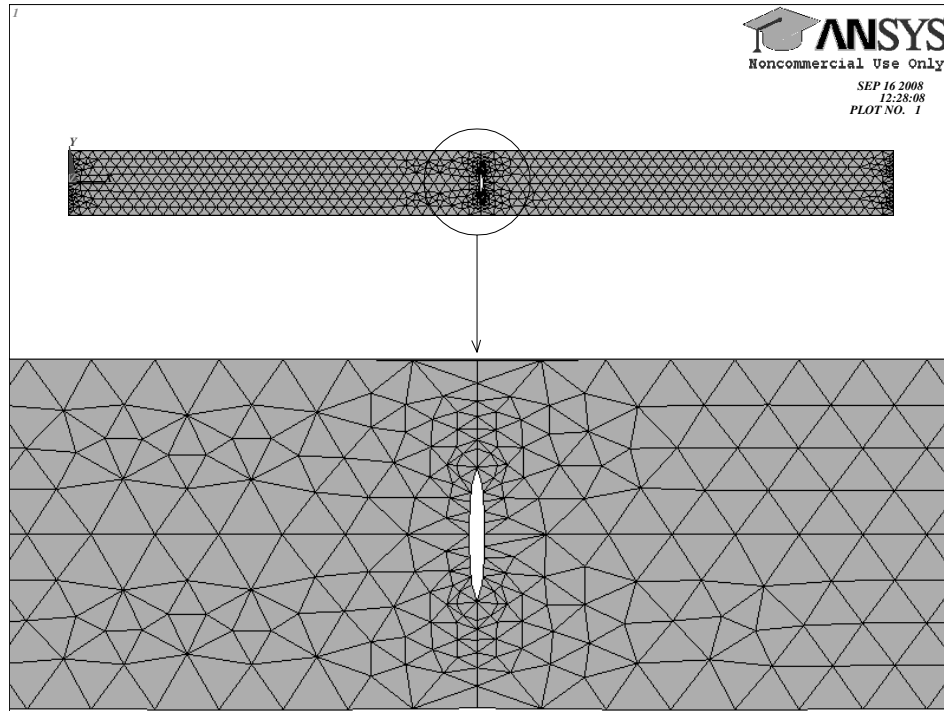
Figure 5.3: Model of beam containing through-thickness centre crack

Table 5.4: Natural frequencies of cantilever beams with centre cracks

Damage case	Crack location, x_c/L	Crack length, b/W	Natural frequencies from *FEA* (Hz)		
			Mode1	Mode2	Mode3
Undamaged beam			11.324	70.929	198.675
1	0.05	0.05	11.318	70.902	198.626
2	0.05	0.1	11.302	70.834	198.500
3	0.1	0.1	11.305	70.883	198.649
4	0.1	0.25	11.225	70.693	198.535
5	0.1	0.5	10.948	70.054	198.142
6	0.25	0.1	11.313	70.927	198.524
7	0.25	0.25	11.265	70.916	197.900
8	0.4	0.05	11.323	70.914	198.646
9	0.4	0.1	11.319	70.873	198.571
10	0.4	0.25	11.295	70.642	198.139

5.3   Validation of Eqn. [4.18]

5.3.1   *Linearity of frequency change with square of normalised curvature*

Eqn. [4.18] establishes that the normalised frequency change is related to the curvature at the damage location normalised with the average curvature through the constant of proportionality, *Damage Index (DI)*, which is fixed for a given crack size. Therefore the normalised change in frequency must vary linearly with the square of the normalised curvature for any given crack size. The data from the above *FEA* is employed to verify this.

Fig. 5.4 shows the plot of normalised modal frequency changes ($\Delta\omega/\omega$) obtained from *FEA* against the square of the normalised curvature values (χ_c^2/χ_{RMS}^2) for a centre crack of length, $b = 0.05W$, located at $x_c = 0.05L$ (damage case 1) in a cantilever beam. The mode numbers are indicated by numerals along the plot. It can be seen that the x and y values for the first five modes fall on a straight line confirming the veracity of the linear relationship expressed in Eqn. [4.18].

Note that the gradient of this line is the magnitude of the damage index parameter *DI*. The values from the higher order modes deviate from the straight line indicating that they may not provide an accurate value for *DI*. This is probably due to the fact that the frequencies predicted by *FEA* are, in general, more inaccurate for higher order modes, with the magnitude of error rising with increasing mode
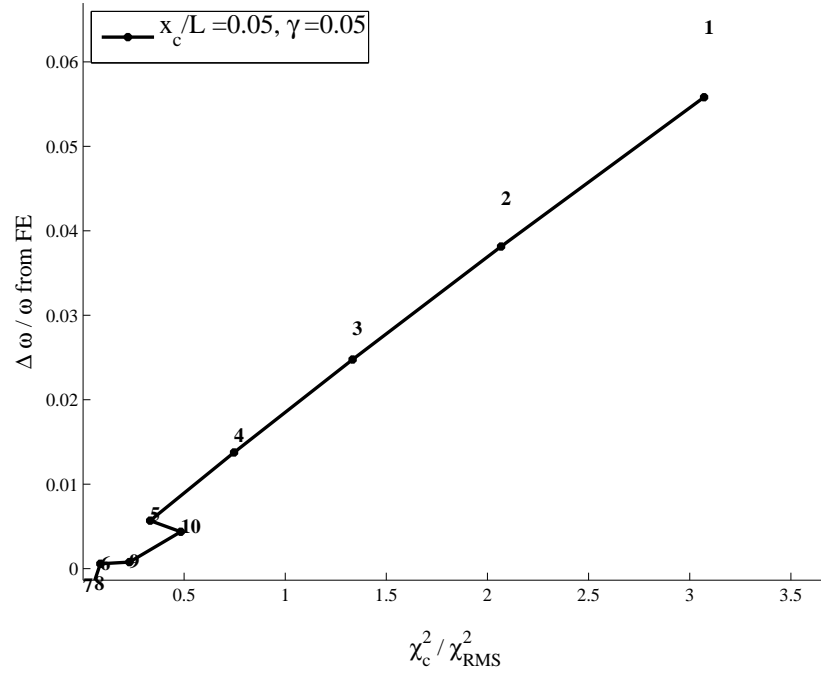
Figure 5.4: Variation of normalised change in frequency with normalised curvature

order [187, 188, 189]. Similar analysis was conducted for the remaining nine damage cases in Table 5.4. Their results are presented in Appendix C and show a similar trend to that in Fig. 5.4. These results indicate that the use of data from higher order modes will not necessarily increase the accuracy of damage detection based on the solution for Eqn. [4.18]. Noting that three modal values are sufficient for determining the damage location and size uniquely, optimum accuracy is likely to be achieved by using only the first 3 or 4 modes.

5.3.2 Relation of DI to crack location and size

$\Delta\omega/\omega$ is plotted against χ_c^2/χ_{RMS}^2 for a centre crack of size $\gamma = b/W = 0.1$ for various locations, x_c, in Fig. 5.5 using only the first four modes. The values of DI, obtained from the gradients of these plots, are listed in Table 5.5 along with their mean. It can be seen that, DI values obtained from these four different crack locations are very nearly the same. This confirms that the magnitude of DI is independent of the crack location.
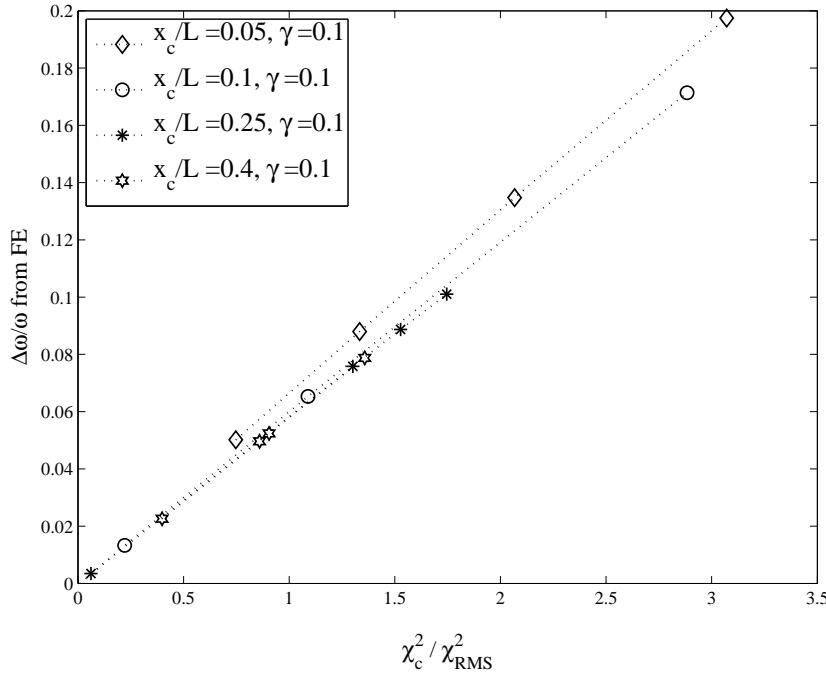
Figure 5.5: Variation of frequency change with curvature for damage of same size ($\gamma = 0.1$) at different locations

Table 5.5: Comparison of *DI* from theory and *FEA* for γ=0.1

Damage case	Crack location, x_c/L	*DI* from the model
2	0.05	0.063
3	0.1	0.060
6	0.25	0.058
9	0.4	0.059
	Mean	0.060

($\Delta\omega/\omega$) is plotted against $(\chi_c/\chi_{RMS})^2$, for different damage cases with increasing crack size, in Fig. 5.6, using only the first four modes. For two cases, the damage is located at $x_c = 0.05L$ and for the remaining two cases at $x_c = 0.1L$. The values of *DI*, obtained from the gradients of their trend lines are plotted in Fig. 5.7 against values of b^2/LW. These data fall in a straight line, as can be seen from the fitted trend line, and its high r-squared value. This demonstrates that the linear relationship between *DI* and b^2/LW, suggested by Eqn. [4.28], is indeed appropriate.
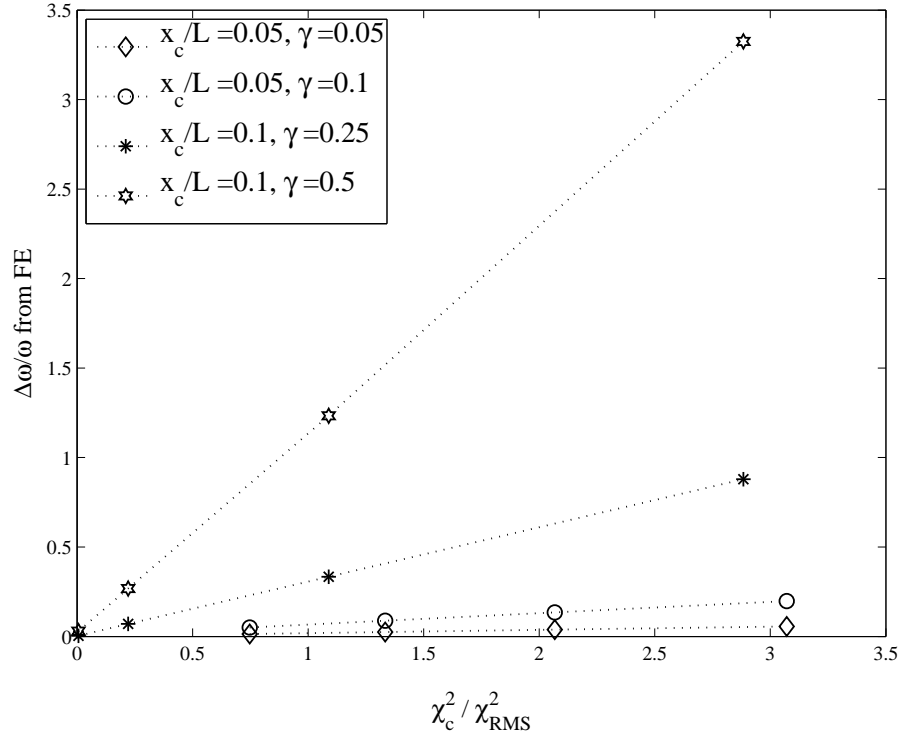
Figure 5.6: Variation of frequency change with curvature for damages of different size
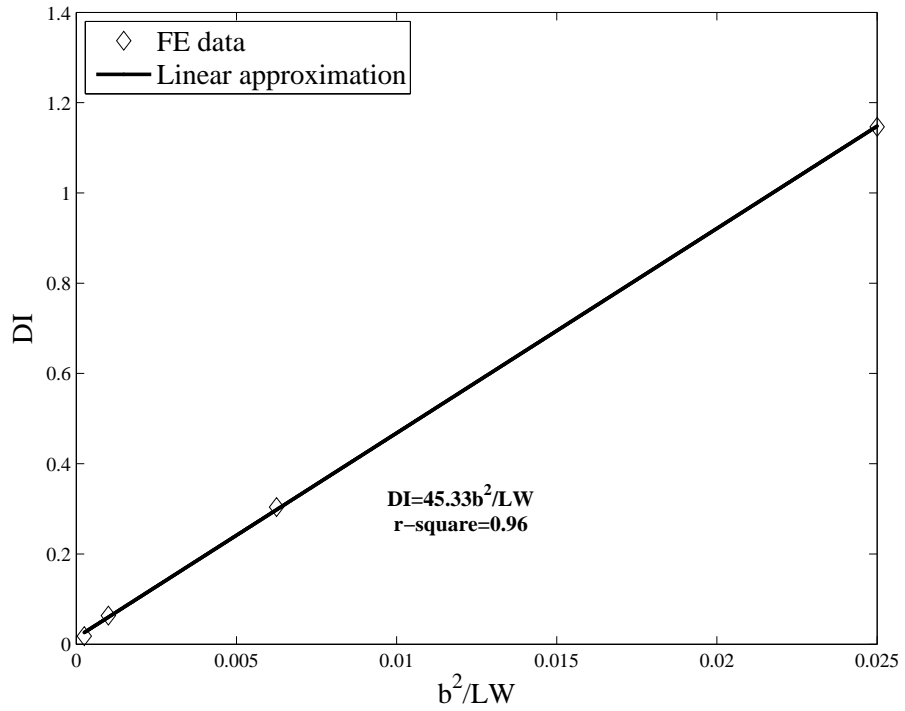
Figure 5.7: Variation of DI with b^2/LW

5.4 Comparison between theory and *FEM* - Forward problem

5.4.1 Centre cracks in cantilever beams

In the forward problem, the size of centre crack and location are known. The *DI* can be determined from Eqn. [4.28] from known crack size and the normalised curvature can be obtained from Eqns. [4.14] and [4.5] for each mode as a function of the crack location. Using these we can predict the normalised frequency change as a function of location along the beam for any given crack size from Eqn. [4.18]. Values of $\Delta\omega/\omega$, calculated in this manner from Eqn. [4.18] for a constant $b/W \; (= 0.1)$, are plotted in Fig. 5.8 as a function of the normalised x-coordinate for modes 1, 2 and 3. The normalised values of the change in frequency obtained from *FEA* for damage cases 2, 3 and 6 in Table 5.4, which have cracks of same size ($b = 0.1W$) located at three different positions ($x_c/L = 0.05, 0.1 \; and \; 0.25$), are also marked with symbols in the Fig. 5.8 for comparison.
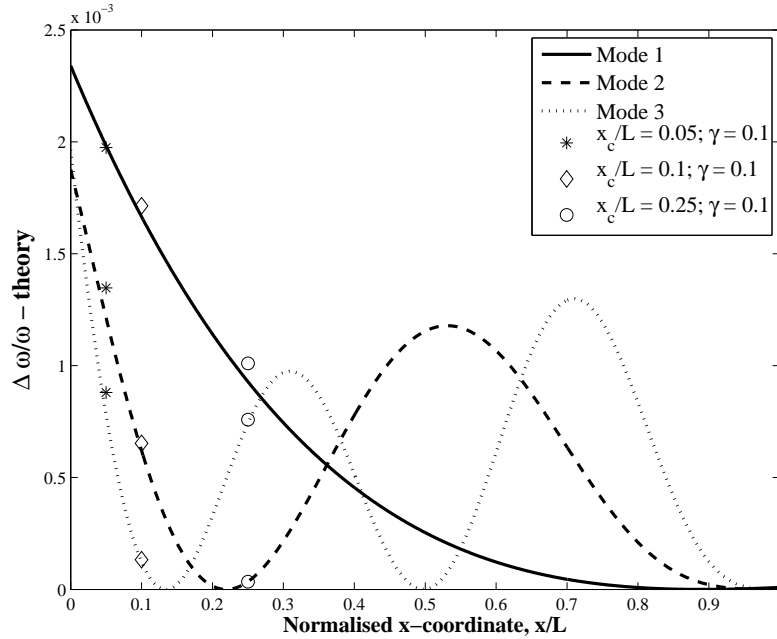
Figure 5.8: Variation of natural frequencies of cantilever beam with respect to crack location for constant crack length; Symbols $*$, $\Diamond$ and $\bigcirc$ indicate results from *FEA*

Fig. 5.9 shows plots of $\Delta\omega/\omega$, calculated from Eqn. [4.18], for a constant value of crack location, $(x_c = 0.1L)$, as a function of the normalised crack length (b/W) for the first three modes. The normalised values of the change in frequency obtained from *FEA* for damage cases 3, 4 and 5 in Table 5.4, which have cracks of different sizes $(b = 0.1W, \ 0.25W \ and \ 0.5W)$, located at the same position $(x_c/L = 0.1)$ are marked with symbols in the same figure.
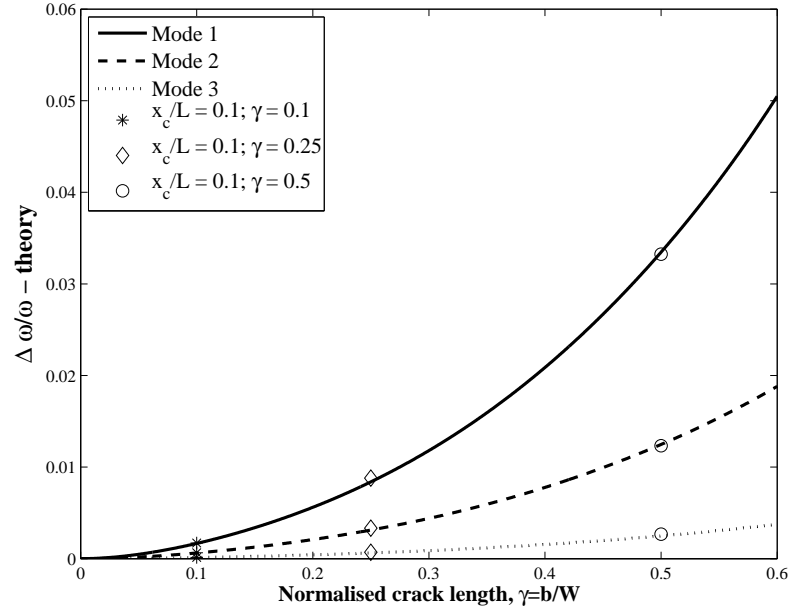
Figure 5.9: Variation of natural frequencies of cantilever beam with respect to crack length for constant location; Symbols $*$, $\Diamond$ and $\bigcirc$ indicate results from *FEA*

It can be seen, in both Figs. 5.8 and 5.9, that the normalised frequency changes predicted from *FEA*, lie on the curves predicted by the theory for each of the three modes, indicating good agreement between theoretical predictions for frequency changes and and the *FEA* simulation.

5.4.2 Edge cracks in simply-supported beams

For a known damage size and location, *DI* can be determined for edge cracks from Eqn. [4.21], and the normalised curvatures from Eqns. [4.14] and [4.5]. For a particular size of edge crack, the normalised frequency change is calculated as a function of crack locations along the beam length for a simply-supported beam using Eqn. [4.18]. The change in frequency values $(\Delta\omega/\omega)$ of the first three modes calculated for a constant crack size $(a/h = 0.1)$ are plotted in Fig. 5.10 as a

function of the normalised x locations. It can be seen that the change in normalised frequencies for the first mode is almost negligible at the ends of the beam and maximum at the centre of the beam; whereas for the second mode, they vanish at the ends of the beam and also at the centre of the beam, which is a node of that mode. (Note that the curves are plotted only upto $x_c/L = 0.6$ in Fig. 5.10; but will be symmetrical about the mid-point $x_c/L = 0.5$ of the simply-supported beam).
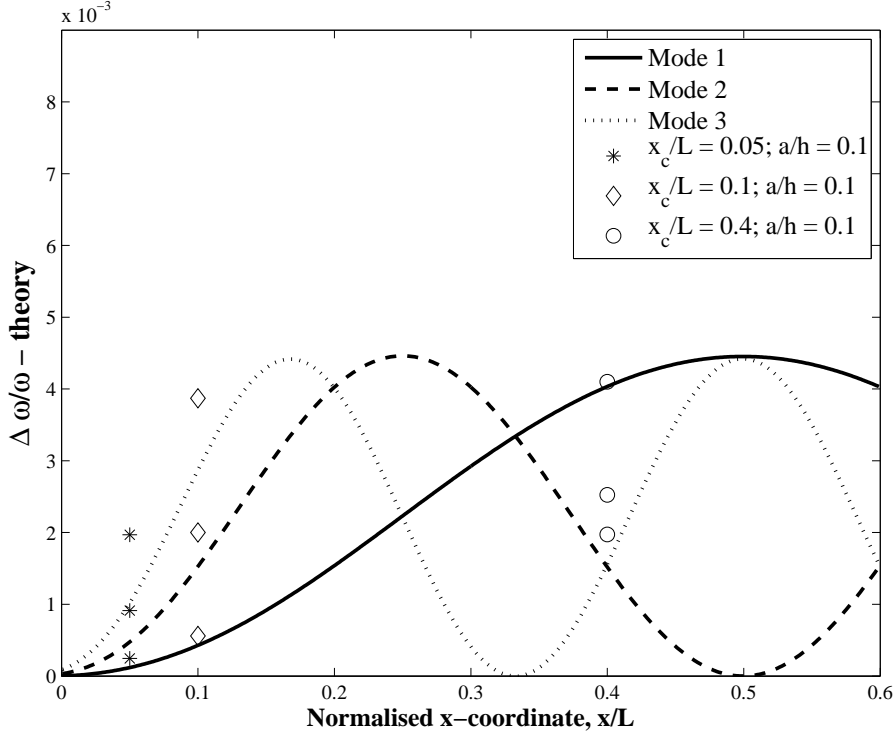
Figure 5.10: Variation of natural frequencies of simply-supported beam with respect to crack location for constant crack length; Symbols ∗, ◇ and ◯ indicate results from *FEA*

The normalised values of the change in frequency obtained from *FEA* for damage cases of same size ($a = 0.1h$) (damage case 2, 3 and 10 in Table 5.2) are also marked with symbols in the Fig. 5.10 for comparison. It should be noted that the locations of crack in each case is different ($x_c/L = 0.05$, 0.1 *and* 0.4) and only the crack size is constant for the three cases. It can be seen in Fig. 5.10 that, the normalized changes in frequencies predicted by the finite element simulations for the cracks modelled at the different locations lie reasonably close to the curves predicting the normalised frequency changes obtained from Eqn. [4.18] based on the current theoretical formulation.

For a particular crack location ($x_c = 0.1L$), the normalised change in frequencies are calculated as a function of crack length using Eqn. [4.18]. Fig. 5.11 shows the trend of normalised change in frequencies in the first three modes as a function of the normalised crack length (a/h), for a constant value of crack location. For each mode, the frequency changes calculated increase with increasing crack lengths, as shown in Fig. 5.11.
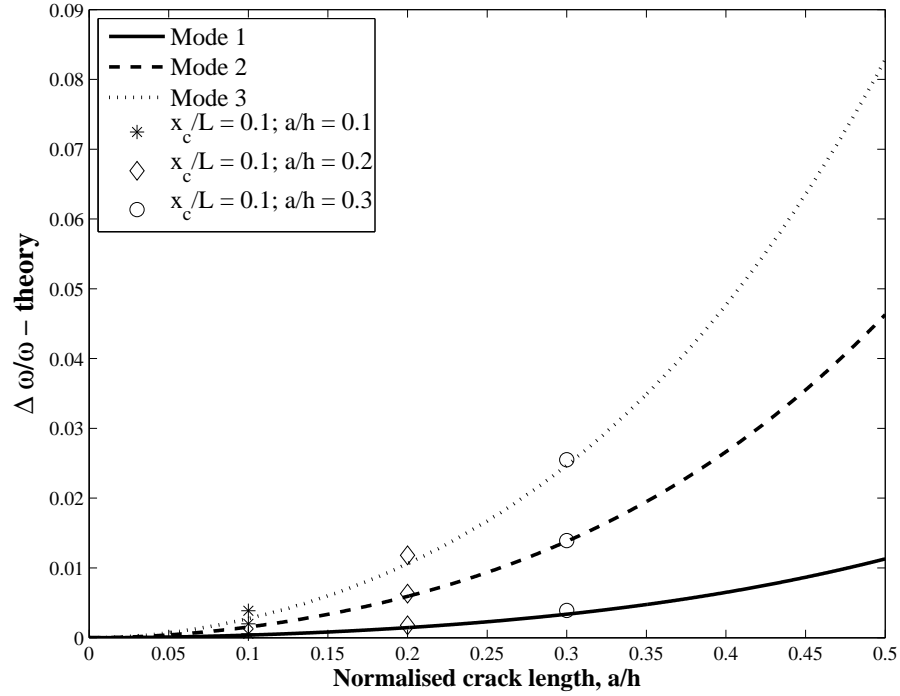
Figure 5.11: Variation of natural frequencies of simply-supported beam with respect to crack length for constant location; Symbols $*$, $\Diamond$ and $\bigcirc$ indicate results from *FEA*

Natural frequency data obtained from *FEM* are also available for a constant crack location and varying width in Table 5.2. Damage cases 3, 4 and 5 have cracks located at $x_c/L = 0.1$, but of varying crack lengths, $a = 0.1h$, $0.2h$ and $0.3h$. $\Delta\omega/\omega$ values are calculated from the data for these cases and marked in the same figure (Fig. 5.11) with symbols.

It can be observed from the figure that the normalised frequency changes predicted from *FEA* lie on the curves representing change in frequencies computed from the proposed theory. This provides sufficient indication that the solutions to forward problem based on the theory developed are comparable to those predicted by *FE* modelling of beams with edge cracks.

5.5 Comparison between theory and FEM - Inverse problem

5.5.1 Estimation of discrepancies between predicted and actual values

In this section and elsewhere in the thesis the efficacy of the proposed method for detecting cracks in beams and plates is assessed by comparing the predicted values of crack parameters such as crack location, size and orientation (in the case of cracks in plates) to their actual or measured values. The comparison is done in terms of the differences between predictions and actual values, normally termed "errors in prediction". The common practice for determination of "error" or the discrepancy in prediction is to divide the difference between the predicted (theoretical) and the actual (measured) value by the actual value and multiply it by 100, so the error is expressed as a percentage of the actual value. This approach has two drawbacks, particularly when it is applied to Non-Destructive Inspection *(NDI)* or crack detection techniques. The first is that estimated "percentage error" value becomes co-ordinate dependent, and the second is that it gives rise to exaggerated and spurious magnitudes of apparent discrepancies.

For example, consider a cantilever beam with a length of 11m in which an edge crack is located at a distance of 1m from the fixed end. Let us say that the crack detection technique using measured frequency changes estimates the crack to be located at a distance of $2m$ from the fixed end. In this case the percentage error of the estimated crack location obtained by the traditional method is [(2-1)/1]*100, i.e. 100%, if the distances are measured from the fixed end. On the other hand, if the distances are measured from the free end of the beam, the percentage error in locating the crack is [(10-9)/10]*100, i.e. only 10%. This shows that in cases where the magnitude of measured parameters are co-ordinate dependent, the percentage error calculated in the traditional way is also co-ordinate dependent. This is obviously undesirable and inappropriate, for we would like to establish the accuracy or reliability of a measurement technique or theoretical model independent of the co-ordinate system used for measurements. In particular, where the accuracy of the system depends on the actual location of the crack and its orientation, since both influence the shifts in frequencies, using a co-ordinate dependent system will make

it impossible to isolate the influence of the actual crack location and orientation on the accuracy of the technique.

Even in situations where the parameter is not co-ordinate dependent, such as the width of a crack, the traditional percentage error formula has the drawback that the magnitude of the error tends to infinity as the magnitude of the measured parameter becomes smaller and smaller. In *NDI* applications, where one is concerned about comparison between sensitivities and uncertainties in measurement, it is more useful and practical to express the "errors" in absolute terms rather than as percentages of the actual crack size.

Both these drawbacks can be addressed by using the absolute differences between the predicted and actual values to estimate the error or discrepancy. However, if the difference in absolute magnitudes is used directly, the magnitude of the error will depend on the units employed. This can be avoided by using normalised values. If the parameters concerned are normalised with respect to a common denominator, such as the length of the beam, then the calculated error or discrepancy between predictions and measurement will be unit independent, co-ordinate independent as well as independent of the actual magnitude of the parameter being estimated.

For this reason, the discrepancies between predicted and actual values, estimated and measured parameters, through out this thesis are calculated as the absolute differences between normalised values. Since the magnitudes are quite small in most cases, for ease of appreciation, the discrepancies are expressed in terms of percentages, i.e. the absolute differences between the normalised values are multiplied by 100. This method of expressing errors or discrepancies between theoretical and measured values has been employed by many other researchers in non-destructive inspection, especially in applications of vibration methods [150, 143]. In order to clarify that the errors calculated in the rest of this thesis are absolute differences between normalised values expressed as a percentage (multiplied by 100) the term "Normalised Discrepancy (per cent)" has been employed rather than "percentage error" in all the Tables and the text.

For estimation of the *Normalised Discrepancy* values, the crack locations are normalised with the length of the beam, the crack sizes with the beam width and the crack orientation by ninety degrees.

In general, the normalised discrepancy is obtained as:

$$\text{Normalised Discrepancy for parameter } X \text{ (per cent)} = \left(\frac{X_a}{X_0} - \frac{X_p}{X_0} \right) * 100 \quad (5.3)$$

where,

X_a = the actual value of parameter X,

X_p = the predicted value of parameter X, and

X_0 = constant value against which parameter X is normalised.

$X_0 = L$ for crack location, $X_0 = W$ for crack size and $X_0 = 90$ when crack orientation is measured in degrees.

5.5.2 Centre cracks in cantilever beams

The data obtained from the *FE* models, listed in Table 5.4, is also used to verify the proposed solution to the inverse problem for beams with centre cracks. From the changes in frequencies in the first 3 modes obtained from *FEA*, the crack location and *DI* were determined using the graphical technique (centroid of intersection points) described in Section 4.6.1. The crack size b/W was then calculated from *DI* using Eqn. [4.28] for each of these ten cases. The values of the crack location normalised to the beam length, x_c/L, and the crack size, b/W, predicted by the solution to the inverse problem are presented along with the actual values employed in the *FEA* in Table 5.6. The normalised discrepancy between the predicted values and the actual values in the models are also listed for the ten cases.

Note that the normalised discrepancies between the actual and predicted values in Table 5.6 are calculated as the absolute difference between their normalised values listed in the preceding columns, as described in Section 5.5.1.

From Table 5.6, it can be seen that the maximum normalised discrepancy in predictions for crack location is only 0.2% while the maximum normalised discrepancy in predicted crack sizes is 0.7% in all the ten cases. It is also seen that the normalised discrepancy in estimation of crack sizes increases with increasing crack lengths, while there is no apparent correlation between the magnitude of normalised discrepancy and location of crack.

Table 5.6: Predictions for crack size and location using inverse algorithm for beams with centre cracks

Damage case	Crack location, x_c/L			Crack size, γ		
	Actual	Predicted	Normalised Discrepancy (per cent)	Actual	Predicted	Normalised Discrepancy (per cent)
1	0.05	0.050	0.0	0.05	0.052	0.2
2	0.05	0.050	0.0	0.1	0.105	0.5
3	0.1	0.101	0.1	0.1	0.102	0.2
4	0.1	0.100	0.0	0.25	0.257	0.7
5	0.1	0.100	0.0	0.5	0.497	0.3
6	0.25	0.251	0.1	0.1	0.101	0.1
7	0.25	0.252	0.2	0.25	0.255	0.5
8	0.4	0.402	0.2	0.05	0.050	0.0
9	0.4	0.401	0.1	0.1	0.100	0.0
10	0.4	0.401	0.1	0.25	0.254	0.4

5.5.3 Inverse problem for edge cracks in simply-supported beams

The data obtained from the *FE* models of beams with edge cracks presented in Table 5.2 is employed to gauge the applicability of the theory to crack detection. The normalised crack locations and the normalised crack sizes obtained by solution of the inverse problem, using frequency changes extracted from *FEA* for the first 3 modes, are shown in Table 5.7 along with the actual values of crack location and size used in the *FE* models of the ten cases of edge cracks. The normalised discrepancies in predicting location and size of the crack are presented in the 4th and 7th columns respectively.

Table 5.7: Predictions for crack size and location using inverse algorithm for beams with edge cracks

Damage case	Crack location, x_c/L			Crack size, γ		
	Actual	Predicted	Normalised Discrepancy (per cent)	Actual	Predicted	Normalised Discrepancy (per cent)
1	0.05	0.071	2.1	0.05	0.082	3.2
2	0.05	0.067	1.7	0.1	0.109	0.9
3	0.1	0.088	1.2	0.1	0.130	3.0
4	0.1	0.095	0.5	0.2	0.218	1.8
5	0.1	0.099	0.1	0.3	0.306	0.6
6	0.2	0.173	2.7	0.05	0.066	1.6
7	0.2	0.201	0.1	0.15	0.152	0.2
8	0.2	0.208	0.8	0.25	0.242	0.8
9	0.85	0.879	2.9	0.05	0.076	2.6
10	0.4	0.407	0.7	0.1	0.106	0.6

It appears that the normalised discrepancies in predictions of crack locations as well as crack sizes for beams with edge cracks are higher, in general, than those for beams with centre cracks. This may be a result of the different boundary conditions applied to the beams in the two cases. The maximum normalised discrepancies in predictions for crack location for the edge cracks is 2.9% (case 9) while that in predictions of crack size is 3.2% (case 1). It may however be noted that these normalised discrepancies are still acceptable and attest to the high accuracy of the predictions of crack location and size obtained using the theory in Chapter 4.

The theory presented in Chapter 4 was developed using the energy approach. Many researchers have implemented frequency based damage detection for beams with edge cracks using the equilibrium approach and spring model [138,135,136,140], also described in Appendix D. Figs. 5.12(a) and 5.12(b), respectively, compare the normalised discrepancy predicted by the present method using energy approach with those predicted using the equilibrium approach. It can be seen that the discrepancies from actual values are of the same order in both cases. This demonstrates that the theory and the methodology proposed in the present work is as good as those reported by previous researchers. The main benefit of the present approach is that it could easily be extended to centre cracks in beams and through-thickness cracks in plates, whereas the application of the equilibrium approach was limited to edge cracks in beams.
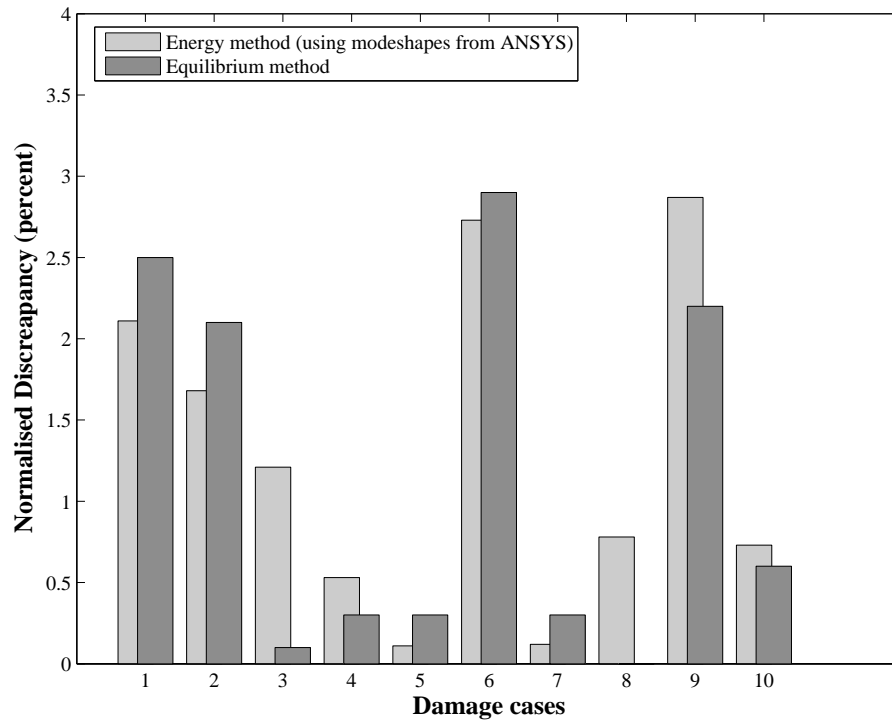
(a) Normalised discrepancy in predicting crack locations
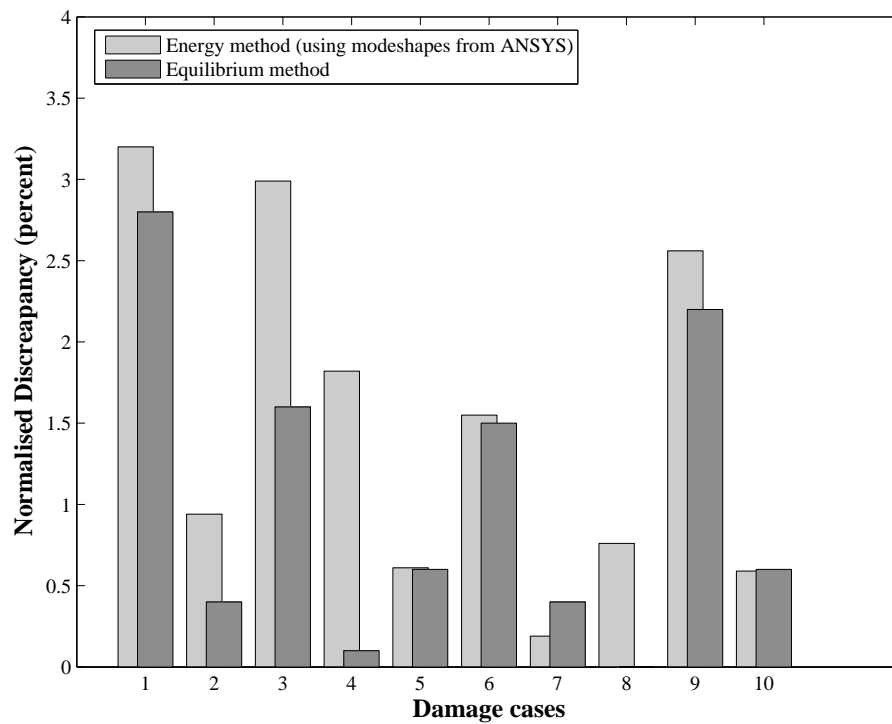
(b) Normalised discrepancy in predicting crack sizes

Figure 5.12: Comparison of normalised discrepancy in estimating locations and sizes of edge cracks - equilibrium method and energy technique

101

5.6   Conclusion

The validation of the theory developed, using *FEA* simulation, was presented in this chapter. Using *FEA* results from ten damage cases, it was shown that the relationship between the normalised frequency change and the square of the normalised curvature at the crack location is linear for a given size and location, as predicted by Eqn. [4.18]. The gradient of this linear relationship is the *Damage Index, DI*, which is also linearly related to the square of the crack length, as suggested by Eqns. [4.21] and [4.28].

Frequency changes predicted by solution to the forward problem, given by Eqn. [4.18], are shown to be in good agreement with those calculated from *FEA* of beam models with edge and centre cracks. The *FEA* data was also employed to assess the applicability of the inverse algorithm for predicting the crack location and size from the change in frequencies. It is seen that the predictions of the crack size and locations obtained by solving the inverse algorithm are within 3.5% of the actual values used in the *FE* models. This provides a high level of confidence in the applicability of the technique for detection of cracks in real structures. The validity of the damage detection methodology is further verified, by conducting experimental modal analysis on beams with edge and centre cracks, in the next chapter.

CHAPTER 6

Verification of analytical model for beams using experiments

6.1   Introduction

This chapter presents the outcomes of experimental investigations on damage detection in beams. Natural frequencies and modeshapes are measured on beams with and without cracks using *Experimental Modal Analysis (EMA).* The measured changes in frequencies are compared to predictions from the theory using Eqn. [4.18], to gauge the accuracy of the theory in predicting the effect of damage in real structures on their natural frequencies.

However, the real intended application of the theory is to detect the presence of damage and assess its location and size, without knowing them a priori. For this, we use the methodology of solving the inverse problem i.e., estimating the damage location and size from the measured changes in frequencies. The damage locations and sizes predicted in this manner are compared to their actual values in the beam specimens employed for the *EMA*. As seen in Eqn. [4.18], the change in normalised energy is a function of the curvature at the crack location normalised with respect to the average *(RMS)* value of the curvature distribution in the beam. Since, the effect of the damage on the magnitude of the curvatures along the length of the beam, including that at the crack location, is very small, it is postulated that the curvature terms employed for application of the methodology to damage detection, can be obtained from *Finite element Analysis (FEA)* or measurements on the damaged or undamaged structure. This hypothesis is verified by comparing the accuracies of the predictions using curvatures from *FEM* to those obtained with measurements on the uncracked as well as the cracked beams.

6.2   Description of set-up and test specimens

All experiments were conducted on cantilever beams. The study on centre cracks are conducted on aluminium alloy beams while beams of industry grade mild steel were used for investigations on edge cracks. The elastic properties of the materials were determined by static cantilever bending tests on coupons cut from the same stock. The test coupons were instrumented with uni-axial strain gauges for this purpose. The Young's Moduli were determined by comparing the measured strains to those predicted by Simple Beam Theory [190]. The density was obtained by weighing the samples in a laboratory scale with an accuracy of $\pm$ 1g and using vernier callipers to measure the transverse dimensions. The measured values of the Young's Modulus of the aluminium alloy and steel specimens were $69.6GPa$ and $192.3GPa$, respectively. The measured densities of the aluminium and steel materials were $2772Kg/m^3$ and $7808Kg/m^3$, respectively. The specimen geometry and test set-ups used are described below.

6.2.1   Centre cracks

The aluminium beam specimens employed for studies on centre cracks had a length of 600mm, width of 50mm and thickness of 3.2mm. In all, seven samples were used. *EMA* was conducted on five of the seven samples before introducing the damage to determine the modal parameters of the uncracked beams. Rectangular slots of different lengths were machined through the thickness of the beams at predetermined locations on the seven samples, to simulate seven different cases of centre crack damage. The slots were machined using a die-sink *Electric Discharge Machining (EDM)* process which allowed the creation of slots with a width of only 0.08mm, providing a good replication of cracks in real structures. A special fixture was designed and manufactured with six bolts to provide clamping to the fixed end of the beam. A typical experimental set-up for the study on centre cracks, with the thin aluminium beam and its clamping fixture, is shown in Fig. 6.1. A typical *EDM* slot simulating a centre crack in an aluminium beam is shown in Fig. 6.2.

Figure 6.1: Experimental set-up for aluminium beams (centre crack specimens)
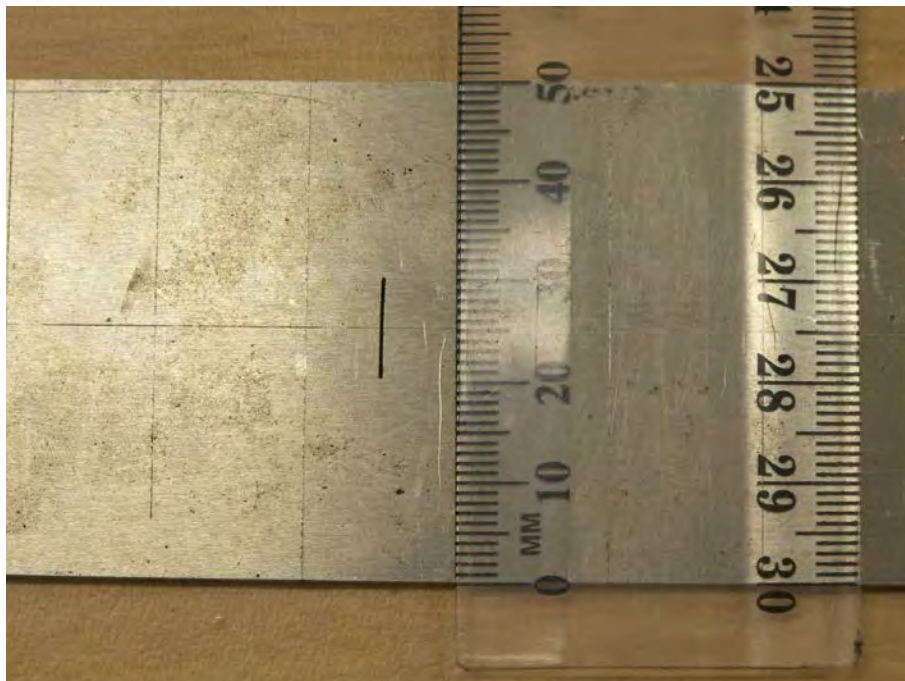
Figure 6.2: Typical centre crack in aluminium specimen

6.2.2 Edge cracks

The study on the effect of edge cracks on natural frequencies was conducted on steel beam specimens with a length of 500mm, width of 10mm and thickness of 24.9mm. Thicker samples were used for experiments with edge cracks so that cracks of different depths across the thickness could be simulated. Before introducing the damage, *EMA* was conducted on five samples to determine the modal parameters of the uncracked steel beams. Slots of different depths running across the full width of the beams were machined at predetermined locations on ten samples to simulate ten different cases of damage (edge crack). Since it is difficult to employ the die-sink *EDM* process to create part-through cracks, the slots representing the edge cracks were machined using a wire-cut *EDM* process, which resulted in a slot width of 0.16mm.

The experimental set-up for *EMA* for the study on beams with edge cracks is shown in Fig. 6.3. A close-up of the fixture for clamping the thick steel beams is shown in Fig. 6.4.

Figure 6.3: Experimental set-up for steel beams (edge crack specimens)

Figure 6.4: Close-up view of clamping fixture

6.3   Procedure for Experimental Modal Analysis

For the *EMA*, the beam samples were excited using a calibrated impact hammer, *B&K 8202*, and the response was measured using *B&K 4374* miniature accelerometers mounted on the beams using bee's wax. The measurements were restricted to a range of 0-400Hz for the aluminium beams while a range of 0-1600Hz was used for the steel beams due to their higher stiffness. Different tips were used for the hammer employed for excitation based on the frequency band. A rubber tip was used for aluminium beams and a plastic tip for steel beams. The input was measured by the accelerometer attached to the impact hammer. The signals from all sensors were conditioned using *B&K 2635* charge amplifiers. The time response is converted by a data analyser (*HP 3566A FFT analyser*) to *Frequency Response Function (FRF)* which is then fed into a commercial modal analysis software, *StarModal v5.3*, for modal parameter extraction. The frequency range for each mode in the *FRF* was set and by curve fitting the *FRF*, the natural frequencies and modeshapes were extracted. For the current study, polynomial curve fitting method was consistently specified for all measurements for data extraction. Measurement of frequencies can be accomplished with measurement at only a single location, but for modeshape

extraction, data has to be obtained from different points along the length of the beam. This can be accomplished using either a rowing hammer or rowing response method. In the former, the location of the accelerometer is fixed and the beam is excited at different points along its length; while, in the rowing response method, the excitation point is fixed and the response is measured at different points along the length of the beam. In the present study, the latter technique was employed for modeshape extraction in both cases. The point of excitation was chosen to be at the free end of the beams at it is not a node of any mode and hence frequencies in all modes are excited. For frequency measurements, the accelerometer was also placed close to the free end to capture the response measurements. For modeshape measurements, the response was measured over 41 points along the length of the beam. The frequency values of the undamaged beams were obtained by taking five measurements on five beams without cracks and using the average of all twenty five values. In the case of damaged beams, the frequencies were obtained by taking the average of ten measurements on each of the beams. Before each trial, the beam was removed from the fixture and bolted again. The averaging process tends to smooth out variations due to small changes in dimensions and due to minor changes in the boundary conditions.

6.4   Experimental validation of the forward problem

In this section, the validity of the theory proposed in Sections 4.3 and 4.4 is assessed by comparing the measured changes in frequencies to those predicted by Eqn. [4.18]. The magnitude of *DI* is calculated from the dimensions of the crack using Eqns. [4.21] and [4.28] for different crack configurations; and the normalised curvature is determined from deflection functions given by Euler-Bernoulli theory [185, 186]. The theoretical predictions for the frequency changes are then obtained by a straight forward application of Eqn. [4.18].

6.4.1 Beams with centre cracks

The natural frequencies in the first three modes, extracted using StarModal software, from the measured *FRF*s, for the undamaged aluminium beam and the seven damage cases of centre cracks are presented in Table 6.1. The damage locations and the crack lengths for the seven cases are presented in columns 2 and 3. The normalised frequency changes obtained by direct application of Eqn. [4.18] for the seven cases are presented graphically along side the measured values for modes 1, 2 and 3 in Figs. 6.5(a), 6.5(b) and 6.5(c) respectively. Scatter bars equal to the standard deviation of the change in frequencies for the measured values are also presented. It can be seen that there is good agreement between the predicted and the measured values of frequency changes in most cases. The small discrepancies observed could be attributed to the noise in measurements and to the uncertainties and the possible differences in the dimensions and mechanical properties of the actual experimental samples and those assumed in the theory. It can also be observed that, for damage case 1, 2 and 3, the change in frequencies continue to increase with progressing damage size for the cracks located at $x_c = 0.167L$. The same can be observed for damage case 6 and 7, for location $x_c = 0.417L$. Overall, the predicted theoretical change in frequencies are within the range of values measured from experiments.

Table 6.1: Natural frequencies of cantilever beams with centre cracks

Damage case	Crack location, x_c/L	Crack length, $\gamma = b/W$	Natural frequencies from *EMA*		
			Mode1	Mode2	Mode3
Undamaged beam			7.151	45.074	126.468
1	0.167	0.1	7.136	45.042	126.354
2	0.167	0.2	7.117	45.026	126.350
3	0.167	0.4	7.061	44.975	126.238
4	0.250	0.4	7.081	45.009	125.386
5	0.333	0.4	7.092	44.887	125.282
6	0.417	0.2	7.137	44.926	126.198
7	0.417	0.4	7.108	44.737	126.128
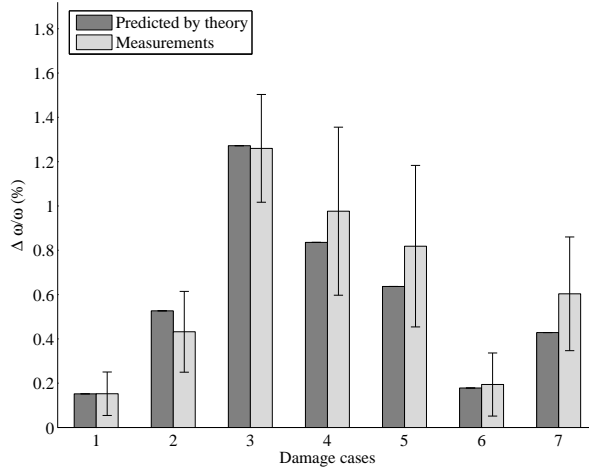
(a)
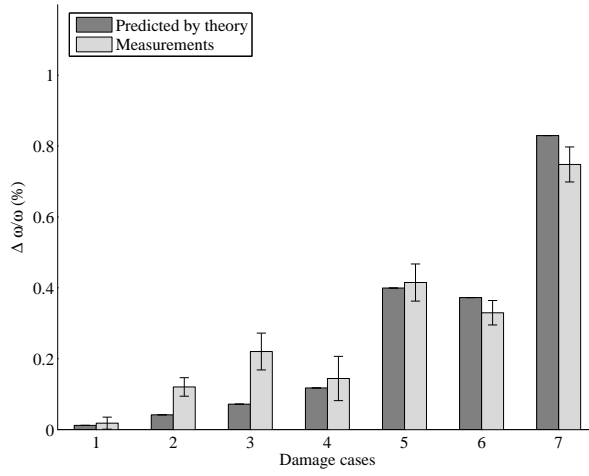
(b)
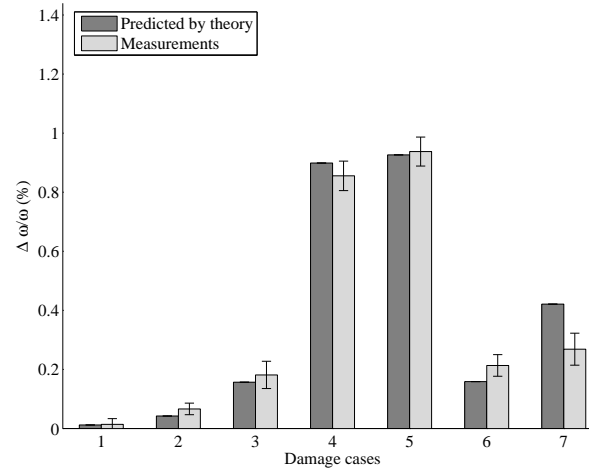
(c)

Figure 6.5: Comparison of measured changes in frequencies with theoretical predictions on beams with centre cracks (a) Mode 1, (b) Mode 2, (c) Mode 3

6.4.2   Beams with edge cracks

The natural frequencies in the first three modes were measured experimentally on the undamaged steel beams and those containing edge cracks for the ten damage cases are presented in Table 6.2. The normalised frequency changes, obtained by direct application of Eqn. [4.18] for the ten cases, are plotted along side the measured values for modes 1, 2 and 3 in Figs. 6.6(b), 6.6(b) and 6.6(b), respectively. Again, it can be seen that most of the measured values are in good agreement with those predicted by theory. The changes in frequencies for beams with edge cracks are considerably higher (about 5 times) compared to beams with centre cracks for the same size of damage. The maximum change in frequencies measured is 9% for mode 1 in damage case 4. However, it should be noted that this change in the first mode for case 4 is much more than the predicted value. It can also be seen that, for damage cases 8, 9 and 10, where the crack is located at $x_c = 0.5L$, the measured changes in frequencies in mode 3 are less than 1%. The theoretical predictions for change in frequencies in mode 3 for cases 8, 9 and 10 are zero because the midpoint of the cantilever beam is a node and any damage at this location will not have any effect on the frequency in the third mode.

Table 6.2: Natural frequencies of cantilever beams with edge cracks

Damage case	Crack location, x_c/L	Crack length, a/h	Natural frequencies from *EMA*		
			Mode1	Mode2	Mode3
Undamaged beam			77.68	482.59	1338.71
1	0.05	0.08	76.75	479.79	1331.38
2	0.05	0.16	75.34	477.46	1326.41
3	0.05	0.24	73.77	475.06	1319.91
4	0.05	0.32	70.86	470.12	1314.72
5	0.25	0.16	76.38	481.51	1322.93
6	0.25	0.24	75.19	480.84	1310.02
7	0.25	0.32	74.55	480.09	1294.59
8	0.5	0.16	77.10	477.30	1335.30
9	0.5	0.24	76.71	471.98	1332.78
10	0.5	0.32	75.70	461.55	1324.68
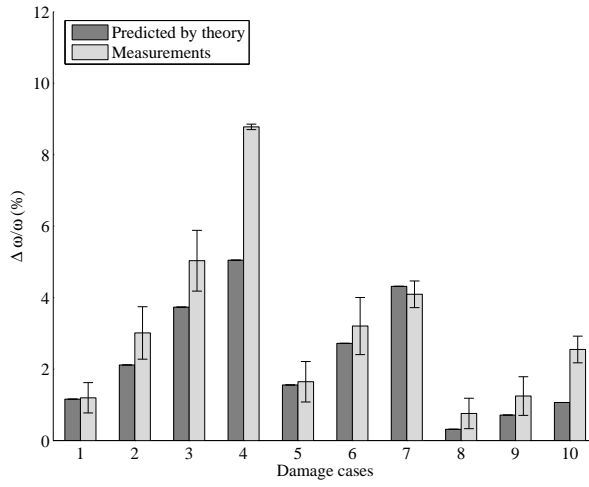
(a)
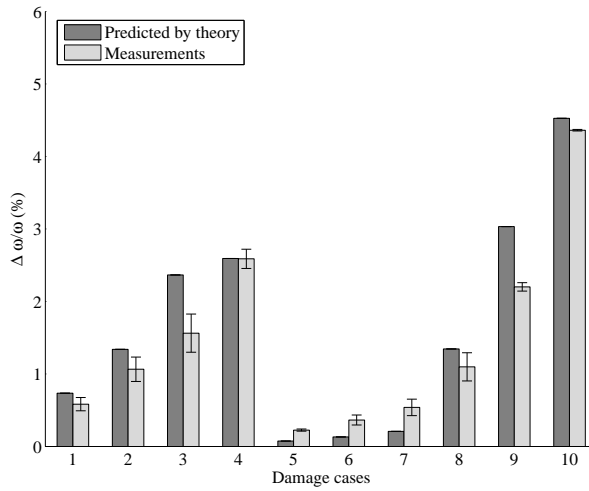
(b)
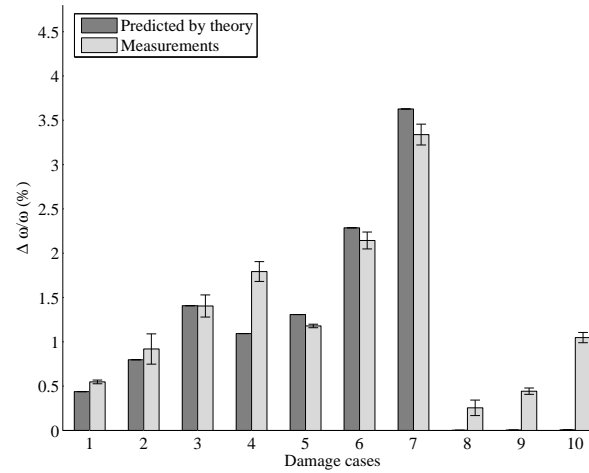
(c)

Figure 6.6: Comparison of measured changes in frequencies with theoretical predictions on beams with edge cracks (a) Mode 1, (b) Mode 2, (c) Mode 3

6.5 Experimental validation of the inverse problem

The inverse problem is the determination of damage location and size from the measured changes in natural frequencies, which is the real purpose of the *NDI* methodology developed. In this section, the *DI* and the crack location are obtained by inverse solution of Eqn. [4.18] using the graphical method. The procedure for the solution of the inverse problem consists of plotting *DI* as a function of the x-coordinate along the length of the beam, using Eqn. [4.36], for the first three modes. The solutions for the location of the crack and the corresponding *DI* is given by triangular intersection of these three curves, as described in Section 4.6.1. To do this, the normalised curvature value on the *RHS* of Eqn. [4.36] may be obtained as a function of the beam coordinate from theory, *FEA* or measured modeshape distribution. Results are presented in this section using curvature distributions obtained from *FEA* and experimental measurements on the undamaged as well as two cases of damaged beams.

The size of the crack, b/W or a/h, is calculated from the estimated value of *DI* using Eqn. [4.28] for centre cracks and Eqn. [4.21] for edge cracks. The *RHS* of these equations contain the function g, which is a polynomial function in b/W or a/h. The value for the crack size b/W or a/h, is obtained by solving for the roots of this polynomial using secant method and inverse quadratic interpolation, provided as function *fzero* in *Matlab*.

6.5.1 Centre cracks

The finite width correction factor, f, for centre crack specimens is a function of the beam thickness or more precisely the ratio W/h, where W is the beam width and h is the thickness (see Eqn. [A.1] in Appendix A). The actual value of the ratio of the width to thickness (W/h) for the aluminium beams used in the experiment is 15.6, hence the finite width correction factor for the experimental beams $(W/h = 15.6)$ is obtained by a spline interpolation using the functions provided for discrete values of W/h in Eqn. [A.1] in Appendix A. The correction factor, $f(\gamma)$, thus obtained for $W/h = 15.6$ is presented in Eqn. [A.3] and the corresponding $g(\gamma)$ is presented in Eqn. [A.4].

113

The crack lengths and the crack locations obtained by solution of the inverse problem for the seven cases of the beam with centre crack damage using normalised curvatures of the undamaged beam obtained using modeshapes from *FEA* is presented in Table 6.3. The actual values of crack location and the crack size in the beams are also listed. The right hand side columns present the normalised discrepancies in each case. It may be noted that the normalised discrepancy is calculated as explained in Section 5.5.1.

Table 6.3: Predictions for crack size and location using inverse algorithm for beams with centre cracks

Damage case	Crack location, x_c/L			Crack size, γ		
	Actual	Predicted	Normalised Discrepancy (per cent)	Actual	Predicted	Normalised Discrepancy (per cent)
1	0.17	0.164	0.3	0.1	0.137	3.7
2	0.17	0.156	1.1	0.2	0.258	5.8
3	0.17	0.163	0.4	0.4	0.440	4.0
4	0.25	0.275	2.5	0.4	0.400	0.0
5	0.33	0.322	1.2	0.4	0.408	0.8
6	0.42	0.411	0.5	0.2	0.254	5.4
7	0.42	0.419	0.2	0.4	0.410	1.0

From Table 6.3, it can be seen that the normalised discrepancy in predictions of the crack locations is of the order of 1%, except in damage case 4 where it is 2.5%. The maximum normalised discrepancy in predictions of the crack length is 5.8% for case2. Curiously, the prediction for the crack length is spot on for case4, the damage case in which the location has the highest discrepancy. There does not seem to be any particular correlation between the magnitude of normalised discrepancy in crack location or size. In general, the normalised discrepancies in the predictions, using the developed theory, are significantly higher for frequency changes obtained from experiments than those obtained using frequency changes obtained from *FEA*. This may be attributed to the scatter in the experimental results and perhaps, variations in beam geometries and crack sizes in the real situation.

The beam deflections for determining the normalised curvatures of the undamaged beam above were obtained from a *FE* model with 14400 elements (240 elements along the length and 60 elements along the width). The deflections were extracted from *FE* at 100 points along the beam length. To analyse the effect of

mesh size and the discretisation of the deflection on the accuracy of the results, deflection data from the *FE* models with different mesh sizes and discretisation levels were employed in the inverse algorithm. The mesh densities employed were very fine mesh (14400 elements), fine mesh (4800 elements), coarse mesh (2400 elements) and very coarse mesh (400 elements). The modeshape deflections were extracted from 100 points, 20 points and 10 points along the length of the beam. The discrepancies in predictions of crack location and crack size obtained with the normalised curvatures from these 12 cases are presented Figs. 6.7(a) and 6.7(b) respectively, for the damage case 1 ($x_c = 0.17L, b = 0.1W$).
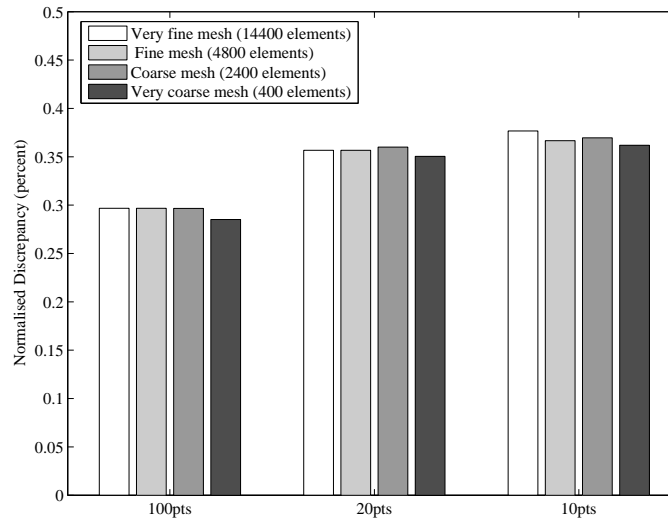
(a) Comparison of normalised discrepancy in locating the crack
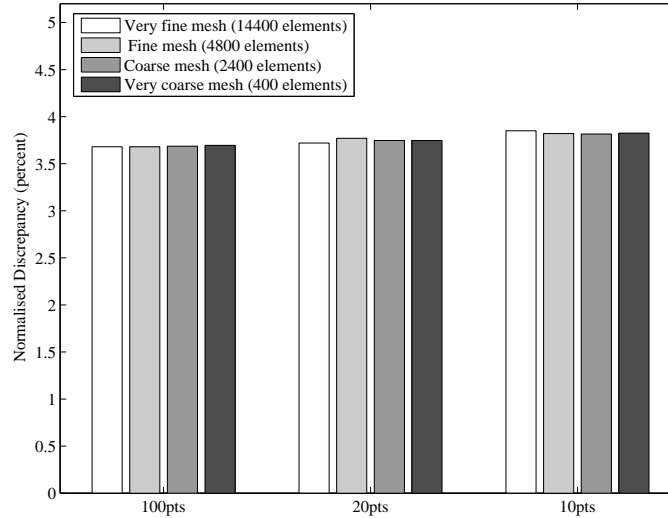
(b) Comparison of normalised discrepancy in determining the size of a crack

Figure 6.7: Comparison of normalised discrepancy in determining the location and size of a centre crack: Damage case 1

From these figures, it can be seen that (a) the size of the mesh has virtually no effect on the accuracy of either predictions, (b) the number of points over which the deflections were extracted has virtually no effect on the accuracy in predicting the damage size (Fig. 6.7(b)), but seems to have some influence on the accuracy of prediction of the location (the discrepancy with deflections extracted from 100 points is of the order of 0.3% for all four mesh sizes compared to a discrepancy of about 0.35% for all mesh sizes with a lower number of discretisation). The effects of mesh size and discretisation were similar in the remaining damage cases; the results for these are shown in Appendix E.1.

Figs. 6.8(a) and 6.8(b), respectively, compare the normalised discrepancies in crack location and crack size, predicted using modeshapes from four different sources, *viz.*

1. modeshapes of undamaged beam obtained from *ANSYS*
2. modeshapes of undamaged beam extracted from experiments
3. modeshapes of damaged beam (case 1) extracted from experiments
4. modeshapes of damaged beam (case 4) extracted from experiments

It can be seen that the discrepancies in the predictions of the crack location are lower when the curvatures are obtained from *FEA* than when the data is obtained from measurements. However, in the case of crack size, the discrepancies in the predictions using *FEA* data seem to be of the same order as those obtained with data from experiments. It is highly encouraging to note that the maximum normalised discrepancy in the predictions using experimental data is of the order of 6% for crack location and even lower in the case of crack size except for case 6 using modeshapes measured from the undamaged beam. Further, it is significant that the discrepancies are of the same order of magnitude in all cases of experimental measurements (within 6%), whether the modeshapes are measured on the undamaged beam or on any of the damaged beams.
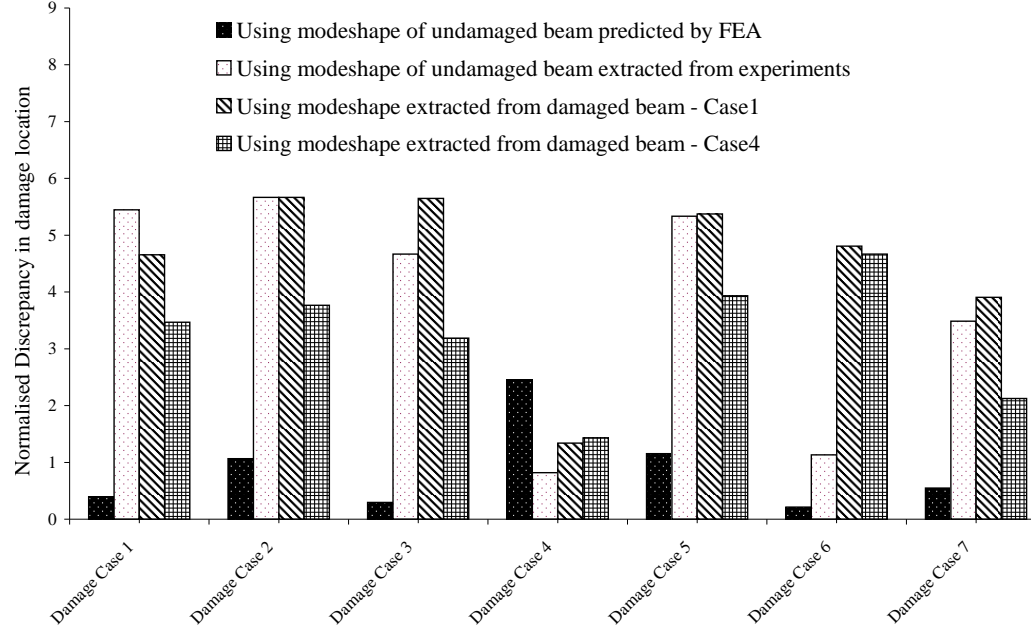
(a) Discrepancy between theory and prediction in crack location
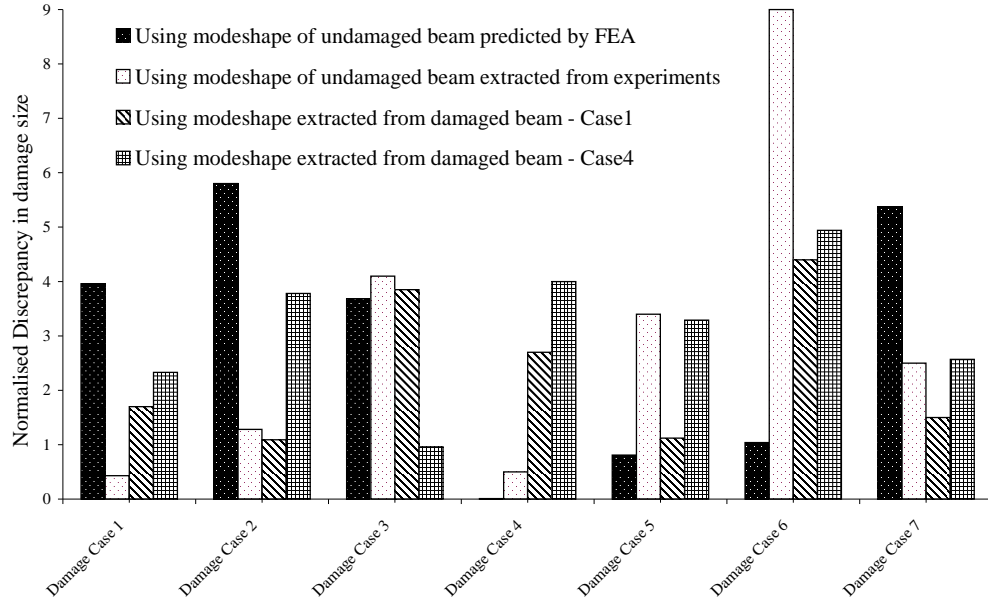
(b) Discrepancy between theory and prediction in crack size

Figure 6.8: Comparison of predictions using modeshapes from different sources (centre cracks)

6.5.2   Edge cracks

The crack lengths and the crack locations obtained by solution of the inverse problem, for the ten cases of steel cantilever beams with edge crack damage, using normalised curvatures of the undamaged beam obtained from *FEM* is presented in Table 6.4. The crack lengths were calculated using Eqn. [4.21] wherein, $g(a/h)$, the integral of the form factor $f(a/h)$ is obtained from Eqn. [4.23]. Table 6.4 also lists the actual values of crack location and the crack size and the normalised discrepancies in each case.

Table 6.4: Predictions for crack size and location using inverse algorithm for beams with edge cracks

Damage case	Crack location, x_c/L			Crack size, γ		
	Actual	Predicted	Normalised Discrepancy (per cent)	Actual	Predicted	Normalised Discrepancy (per cent)
1	0.05	0.065	1.5	0.08	0.110	3.0
2	0.05	0.076	2.6	0.16	0.168	0.8
3	0.05	0.078	2.8	0.24	0.209	3.2
4	0.05	0.085	3.5	0.32	0.283	3.7
5	0.25	0.272	2.2	0.16	0.197	3.7
6	0.25	0.265	1.5	0.24	0.267	2.7
7	0.25	0.280	3.0	0.32	0.316	0.4
8	0.50	0.421	7.9	0.16	0.181	2.1
9	0.50	0.428	7.2	0.24	0.242	0.2
10	0.50	0.422	7.8	0.32	0.334	1.4

From Table 6.4 for edge cracks, it can be seen that the damage sizes are predicted with an accuracy of over 96% in all ten cases and locations are predicted to within 3.5% for the first seven cases. However, the normalised discrepancies in damage locations are much higher, of the order of 7.5% for damage cases 8, 9 and 10. This is because the crack is located at $x_c = 0.5L$ for cases 8, 9 and 10. It was already observed in Section 6.4 that a damage at the mid point of the beam theoretically has no effect on the frequency in the third mode (see Fig. 6.6(c)) as this location is a node for the third mode.

The beam deflections for determining the normalised curvatures of the undamaged beam, in the results above, were obtained from a *FE* model with 14400 elements (240 elements along the length and 60 elements along the width) and the

deflections were extracted from *FE* at 100 points along the beam length. Similar to the study conducted on centre cracks, the effect of mesh size and the discretisation of deflection extraction were investigated for edge cracks also. The normalised discrepancies in predictions of crack location and crack size obtained with the normalised curvatures with four different mesh sizes (400, 2400, 4800 and 14400 elements) and 3 different discretisation levels (10, 20 and 100 points along the length of the beam) are presented Figs. 6.9(a) and 6.9(b) respectively for the damage case 1 ($x_c = 0.05L, a = 0.08h$).
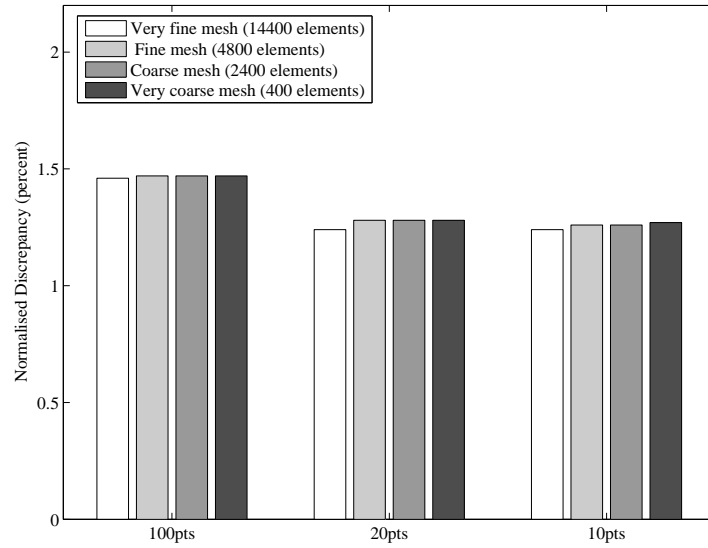
(a) Comparison of normalised discrepancy in locating the crack
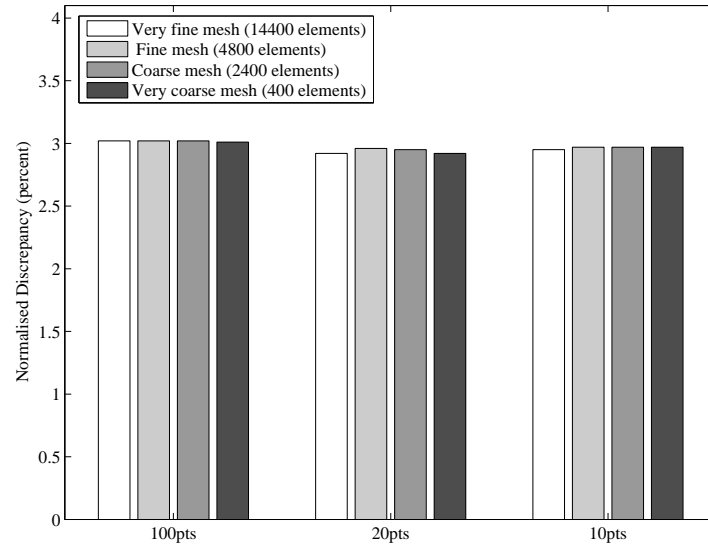
(b) Comparison of normalised discrepancy in determining the size of the crack

Figure 6.9: Comparison of normalised discrepancy in determining the location and size of edge cracks: Damage case 1

As before, it is seen that the mesh size has virtually no effect on the accuracy of the predictions of damage location or damage size and the number of points over which the deflections were extracted does not influence the accuracy of size predictions (See Fig. 6.9(b)). However, extraction of deflection data from 100 points appears to result in a greater inaccuracy (difference of the order of 0.2%) compared to extraction of data from 10 or 20 points only. Again, similar results were obtained for the remaining nine damage cases which are presented in Appendix E.2. These results as well as those presented earlier for centre cracks indicate that the accuracy of damage prediction using the energy method is more or less insensitive to mesh size and the number of points over which deflections are measured.

The errors obtained using modeshapes from four different sources were compared and the normalised discrepancies in crack location and crack size predicted are presented in Figs. 6.10(a) and 6.10(b) respectively, for the first seven cases of edge cracks. The four different sources are:

1. modeshape of undamaged beam obtained from ANSYS
2. modeshape of undamaged beam extracted from experiments
3. modeshape of damaged beam (case 1) extracted from experiments
4. modeshape of damaged beam (case 9) extracted from experiments

As opposed to the study in centre cracks, it can be seen that the normalised discrepancies in the predictions of the crack location are higher when the curvatures are obtained from *FEA* than when the data is obtained from measurements. However, in the case of determining crack size, there is no particular trend and the discrepancies in the predictions using modeshapes from different sources seem to be of the same order with a maximum normalised discrepancy of 7%. The maximum normalised discrepancy in prediction of location for these first seven damage cases is only 4%. It is remarkable that using modeshapes obtained from the damaged beams also yield similar results to those obtained with modeshapes from *FEA* and measurements on undamaged beams.
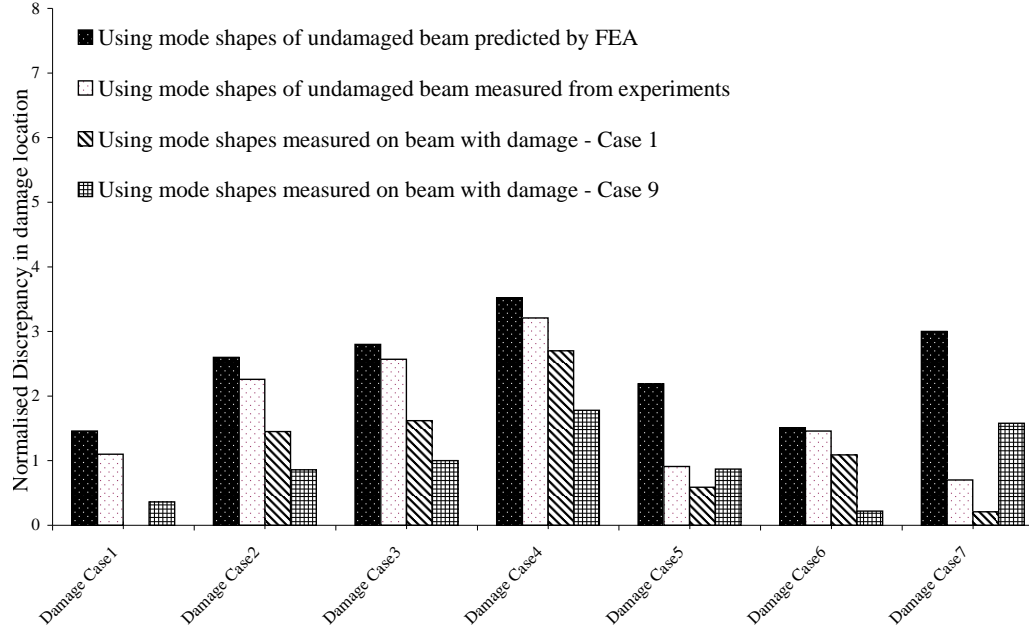
(a) Discrepancy between theory and prediction in crack location
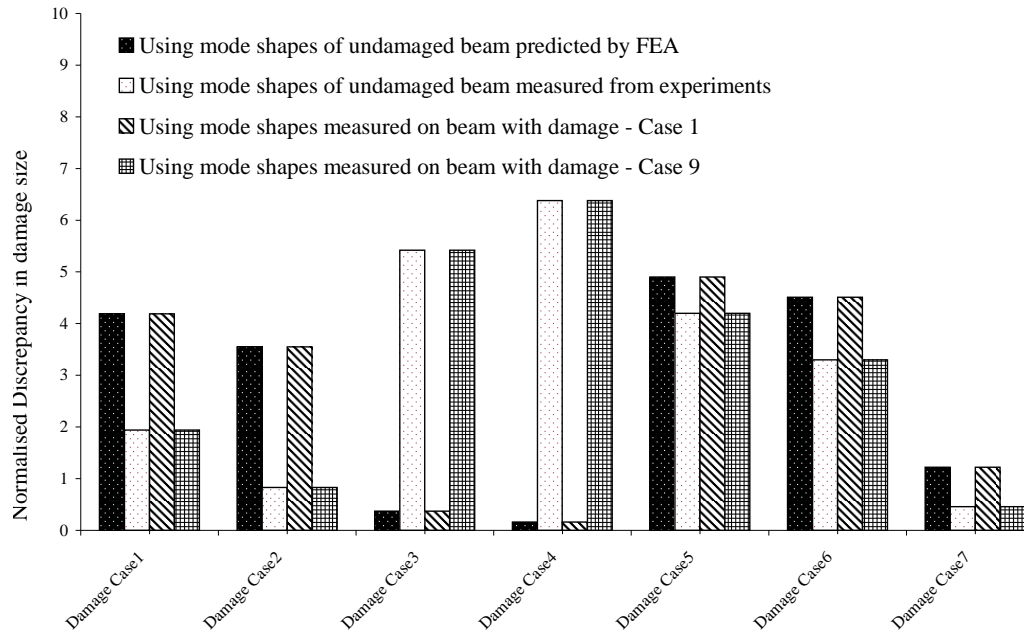
(b) Discrepancy between theory and prediction in crack size

Figure 6.10: Comparison of predictions using modeshapes from different sources (edge cracks)

The theory presented in Chapter 4 and the results in previous sections were obtained using the energy approach. The equilibrium technique based on the Euler-Bernoulli theory and crack-spring analogy has been implemented by several researchers [135, 136, 138, 140] using the natural frequency changes for edge crack detection in beams. The procedure for implementing the equilibrium technique is presented in detail in Appendix D. This procedure was employed to predict crack sizes and locations for the ten cases of edge cracks, listed in Table 6.2, to obtain a comparison of the accuracies obtained with the two techniques.

The normalised discrepancies in predictions of the crack location and size obtained with the equilibrium method and the present method using energy approach are presented in Figs. 6.11(a) & 6.11(b) respectively. It may be noted that, in general, the normalised discrepancies in determining the locations using the energy based technique are slightly higher (by $\approx 1\%$) than those obtained with the equilibrium method. However, the normalised discrepancies in estimation of crack sizes, using both methods are of the same order. It may also be noted that the normalised discrepancies in cracks locations for cases 8, 9 and 10 are high in both cases, due to the crack being located at the node of a mode, as mentioned previously. Thus the energy approach provides predictions which are nearly as good as the equilibrium method, for edge cracks, with the added advantage of versatility for application to centre cracks in beams and cracks in two dimensional cases.

The proposed method of damage detection using vibration parameters mainly relies on change in measured natural frequencies. It also needs the information of local change in curvature of undamaged structure to calculate the energy distribution. This can be calculated using modeshapes obtained theoretically, numerically or experimentally. It was shown that the modeshapes measured from the damaged structure can also be employed to detect damage accurately. This hybrid technique of using measured changes in natural frequencies and the measured modeshapes of undamaged or damaged structure can be reliably employed to detect damage in structures. The advantage of this hybrid technique is that theoretical or numerical modelling to extract modeshapes can be avoided.
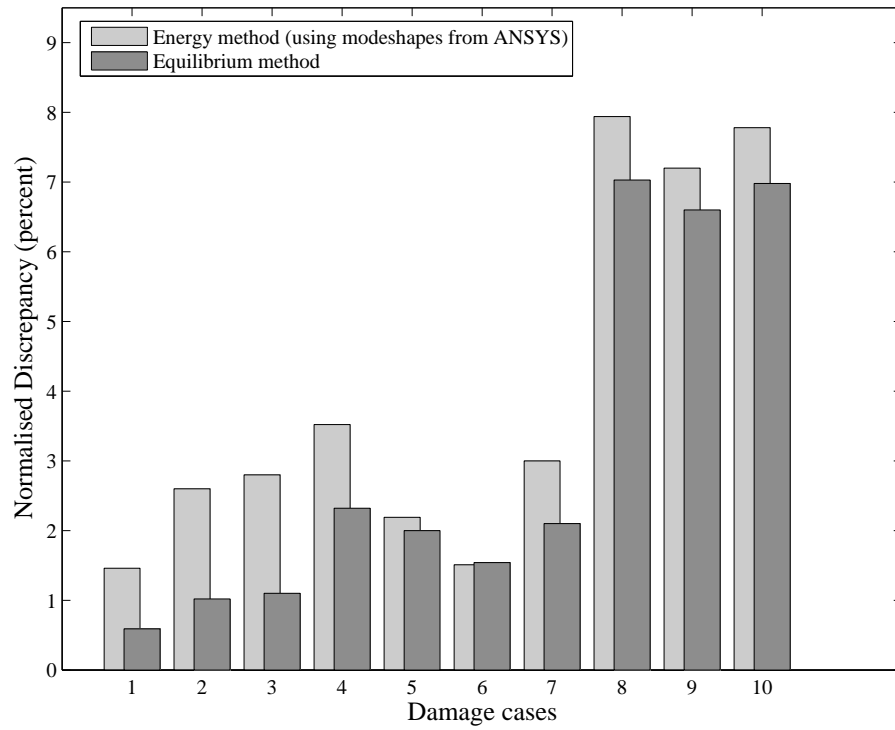
(a) Comparison of predicted crack locations
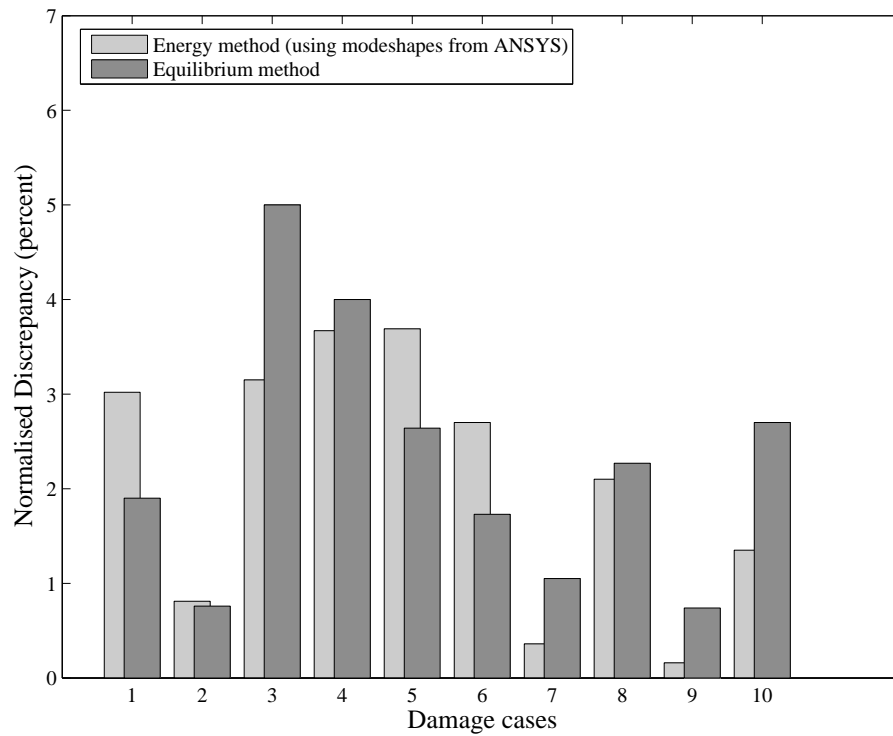
(b) Comparison of predicted crack lengths

Figure 6.11: Equilibrium method *vs* energy method (beam with edge crack)

6.6 Conclusion

In this chapter, the proposed damage detection methodology based on the energy approach was validated using data from experimental analysis conducted on cantilever beams with seven different cases of centre cracks and ten different cases of edge cracks. The predictions for the frequency changes from the theory (forward problem) were compared with the measured changes in frequency and found to be in good agreement. The applicability of the damage detection technique was assessed by comparing predictions of the damage location and size from the solution to the inverse problem using measured changes in frequencies to their actual values. Employing deflection data from *FEA* to determine the normalised curvature distributions, it was shown that the accuracy of the results is rather insensitive to mesh size and the number of finite points over which deflection measurements are taken.

Calculation of normalised curvatures from deflections measured from the undamaged and damaged beams for solution of the inverse algorithm also provided predictions for damage location and size within acceptable limits and comparable to those obtained using *FEA* data. This is significant in that it demonstrates that modeshapes measured on actual structures can be employed to provide predictions for crack size and location with reasonable accuracy. Further, it is seen that the results are equally good whether the measurements are taken from the damaged beam or the undamaged beam. This is highly encouraging since it provides assurance that, in applying this damage detection method to real situations, one need not necessarily resort to modeshape data from theory, numerical modelling or even measurements on the undamaged structure; measurements made on the damaged structure or a structure suspected of having damage would suffice. It is also remarkable that modeshapes measured on one damaged beam can not only be employed to estimate damage in the same beam but also to estimate damage in other beams with damages at different locations and different sizes. This indicates that the accuracy of the proposed method is rather insensitive to minor variations in modeshapes caused by damages as well as noise in the data. It is possible to employ a filtered and smoothed distribution of modeshape data obtained from measurements at discrete points for assessing the damage in the structure.

Traditional frequency based methods, such as the equilibrium method [142, 149] and the model updating technique [131,81], require the use of theoretical modelling or numerical analysis to assess the size and location of damage. On the other hand, methods employing modeshape measurements do not require the support of theoretical or numerical analysis, since the presence and severity of the damage are deduced directly from differences in the modeshapes of the damaged and undamaged structures. Modeshape methods, however, are highly sensitive to noise in the measurement data since the damage signature can often be drowned within the noise. The technique proposed herein is, in one sense, a hybrid between the traditional frequency based methods and the modeshape based methods, where, a combination of measurements of changes in frequency and measurements of modeshape data is employed to assess the damage. The advantage of this *hybrid technique* over the traditional frequency based methods is that theoretical and numerical modelling can be avoided. The advantage over modeshape methods is that it is insensitive to noise in the modeshape data since it is not dependent on differences in modeshapes.

In the next chapter, the sensitivity and the scope of the proposed damage detection technique is examined using the experimental results on beams with centre cracks.

Chapter 7

Sensitivity and probability of crack detection in beams with centre cracks

7.1 Introduction

In this chapter, an attempt is made to assess the sensitivity of the developed technique by estimating the probability of detection and determining the minimum size of the crack that can be detected in practice. The experimental data from the seven cases of cantilever beams with centre cracks presented in the previous chapter (Chapter 6) is employed for the analysis of probability of detection. The experimental data is used, in conjunction with results from *FEA*, to determine the minimum detectable crack size.

7.2 Statistical results from experimental data

The frequencies of the undamaged beams were calculated by averaging five measurements on each of the five beams without damage (25 trials). The frequencies of the damaged beams are average values of ten measurements for each damage case. The mean, minimum and maximum values and the standard deviations of the measured natural frequencies for modes 1, 2 and 3 are shown in Table 7.1 for the seven damage cases. Mean values are plotted graphically for modes 1, 2 and 3 respectively in Figs. 7.1(a), 7.1(b) and 7.1(c), along with scatter bars whose upper and lower intervals are equal to the standard deviations listed in Table 7.1. It can be seen that in most cases, the means of the frequencies of the damage cases are well below the scatter limits of the frequency of the undamaged beam. Even in cases

where there are exceptions in one mode, such as, damage case 6 in mode 1, there is a clear demarcation in the other modes, for the same case. Similarly, damage at the same location may generate a significant reduction in frequency in one mode (for example damage cases 3 and 4 in mode 1) but only smaller differences in the other modes.

Table 7.1: Statistical analysis of frequency measurements from experiments

	Mean	Minimum of trials	Maximum of trials	Standard Deviation
Undamaged beam				
Mode 1	7.151	7.098	7.202	0.030
Mode 2	45.074	45.033	45.108	0.021
Mode 3	126.468	126.346	126.564	0.067
Damage case 1 ($x_c/L = 0.167; \gamma = 0.1$)				
Mode 1	7.136	7.123	7.144	0.017
Mode 2	45.042	45.032	45.057	0.023
Mode 3	126.354	126.271	126.401	0.059
Damage case 2 ($x_c/L = 0.167; \gamma = 0.2$)				
Mode 1	7.117	7.093	7.140	0.013
Mode 2	45.025	45.000	45.039	0.012
Mode 3	126.350	126.281	126.365	0.025
Damage case 3 ($x_c/L = 0.167; \gamma = 0.4$)				
Mode 1	7.061	7.032	7.083	0.007
Mode 2	44.975	44.944	45.015	0.008
Mode 3	126.238	126.151	126.324	0.052
Damage case 4 ($x_c/L = 0.25; \gamma = 0.4$)				
Mode 1	7.081	7.047	7.117	0.027
Mode 2	45.009	44.989	45.064	0.028
Mode 3	125.386	125.348	125.508	0.063
Damage case 5 ($x_c/L = 0.33; \gamma = 0.4$)				
Mode 1	7.092	7.058	7.132	0.026
Mode 2	44.887	44.861	44.923	0.024
Mode 3	125.282	125.202	125.363	0.062
Damage case 6 ($x_c/L = 0.41; \gamma = 0.2$)				
Mode 1	7.137	7.124	7.148	0.010
Mode 2	44.926	44.895	44.938	0.016
Mode 3	126.198	126.106	126.240	0.046
Damage case 7 ($x_c/L = 0.41; \gamma = 0.4$)				
Mode 1	7.108	7.086	7.144	0.018
Mode 2	44.737	44.702	44.768	0.022
Mode 3	126.128	126.022	126.226	0.068
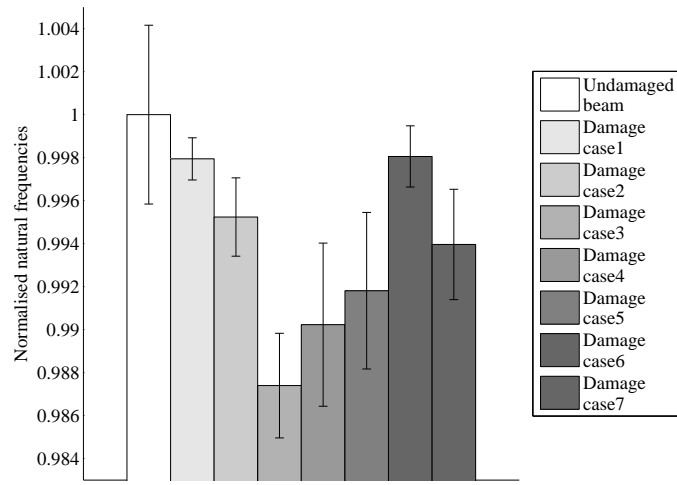
(a) Mode 1
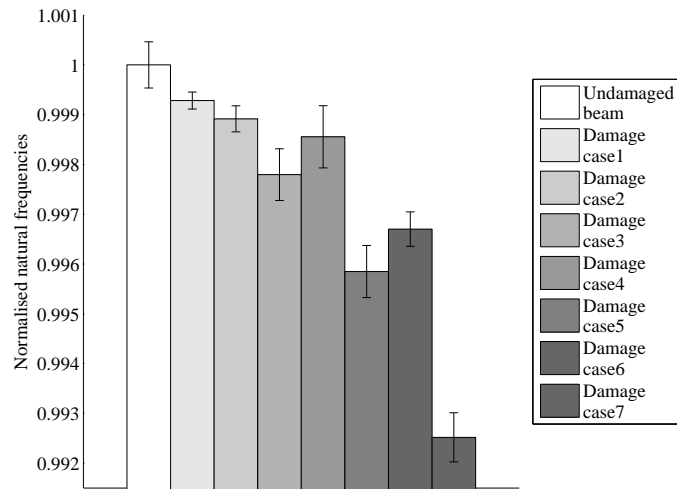
(b) Mode 2
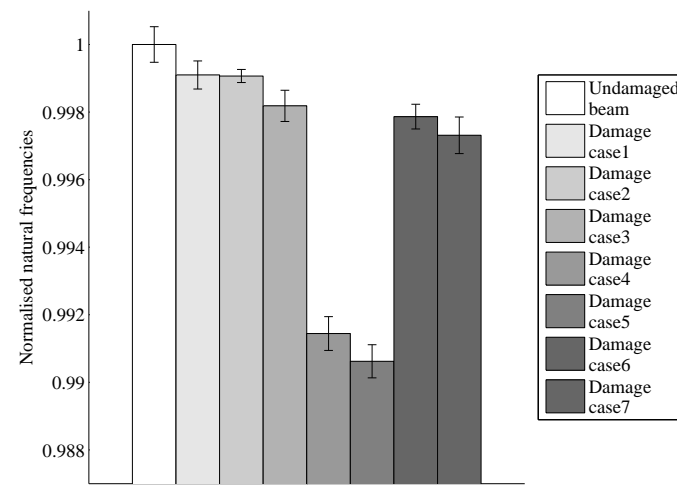
(c) Mode 3

Figure 7.1: Deviation of frequency measurements in mode1

7.3   Test of statistical significance

Tests of statistical significance are performed to determine whether two groups of data belong to the same normal distribution or not. If it is statistically established that the data sets of frequencies of the damaged and undamaged beams are significantly different, we may conclude that this difference is caused by the damage since the only difference between the two sets of samples tested is the presence of a damage. We may then be confident that these differences in frequencies are indicative of the presence of the damage and may therefore be used to locate and assess the size of the damage using the methodology developed.

A test of statistical significance of the measured frequencies of the undamaged beam and the seven damage cases was performed using the one-way ANalysis Of VAriance *(ANOVA)* [191]. In the one-way ANOVA, the F values and the *F-crit* values are calculated for each data set to be compared. If the value of F is greater than that of *F-crit*, then the two data sets belong to different parent populations; if not, they belong to the same parent population i.e., the influence of the damage is not significant. The F and *F-crit* values obtained by comparing each set of ten frequencies for each of the damaged cases with the set of 25 measurements of frequencies of the undamaged beams, using the statistical toolpack in *MS-Excel*, are presented in Table 7.2. Note that, a value of F higher than *F-crit* indicates that the two sets of data belong to different groups, i.e., the difference in the frequency caused by the damage is significant. It can be seen that, except for mode 1 in two cases (case 1 and case 6), all values of F are much higher than the values of *F-crit* indicating that the damage has caused a significant difference in the natural frequencies. Even for damage cases 1 and 6, the F values in modes 2 and 3 are much higher than the corresponding *F-crit* values. Therefore, even for damage cases 1 and 6, the statistically significant changes in the second and third natural frequencies assure the presence of a crack. Noting that the smallest crack size simulated in the experiments is 10% of the width, the results in Table 7.2 indicate that the centre crack of atleast 10% of the width will produce statistically significant frequency changes which may be employed for damage detection.

Table 7.2: ANOVA applied to natural frequencies of undamaged and damaged beams

	Damage cases	1	2	3	4	5	6	7
Mode 1	F	*2.4*	12.0	65.3	41.3	29.6	*2.1*	18.1
	F-crit	4.1	4.1	4.1	4.1	4.1	4.1	4.1
Mode 2	F	22.3	47.9	151.0	56.7	531.4	411.2	1791.4
	F-crit	4.1	4.1	4.1	4.1	4.1	4.1	4.1
Mode 3	F	23.3	29.3	90.5	1936.5	2350.4	136.5	182.9
	F-crit	4.1	4.1	4.1	4.1	4.1	4.1	4.1

7.4 Probability of frequency change caused by the damage - forward problem

The measurement of frequencies of the damaged and undamaged beams are expected to follow normal distribution. From the frequency distribution of the undamaged beam, we can determine the "90/95" lower limit i.e., the lower limit for the undamaged beam's natural frequency, such that 90% of the measurements lie above it with a confidence level of 95% using equations from statistics [192]. This value may be considered to be the practical lower limit of all measurements of the undamaged beam's natural frequency. Similarly, we can determine the "90/95" upper limit for the damage beam from its distribution which represents the practical upper limit of the frequency measurements made on the damaged beam.

In some cases, the natural frequency distributions of the undamaged and damaged beams are well differentiated with a large separation between the 90/95 lower limit of the undamaged beam and the 90/95 upper limit of the damaged beam as shown schematically in Fig. 7.2(a). Such a good separation in the measured frequency distributions provides us with a high certainty of the existence of damage. In other cases, the frequency distributions of the damaged and undamaged beams may overlap i.e., the 90/95 upper limit of the damaged beam will have a higher value than the 90/95 lower limit of the undamaged beam, as shown in Fig. 7.2(b). In this case, even though the mean values are distinct, there is much less certainty regarding the presence of the damage. Some of the experimental results obtained, e.g. damage cases 1 and 6 in mode 1 (see Fig. 7.1(a)), fall into this category.
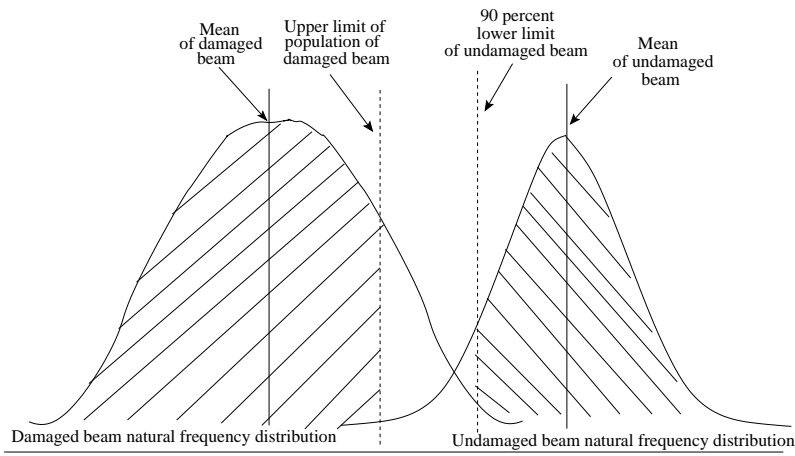
(a) Well-separated distributions of measured frequencies of damaged and undamaged beams
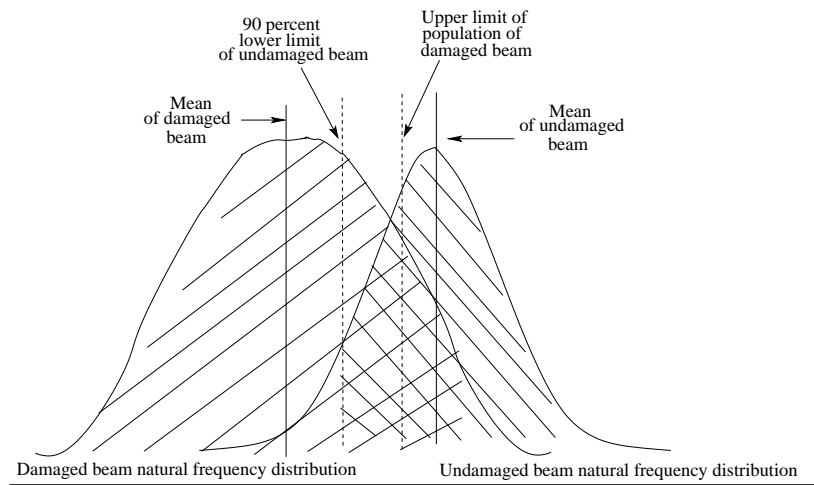
(b) Overlapping distributions of measured frequencies of damaged and undamaged beams
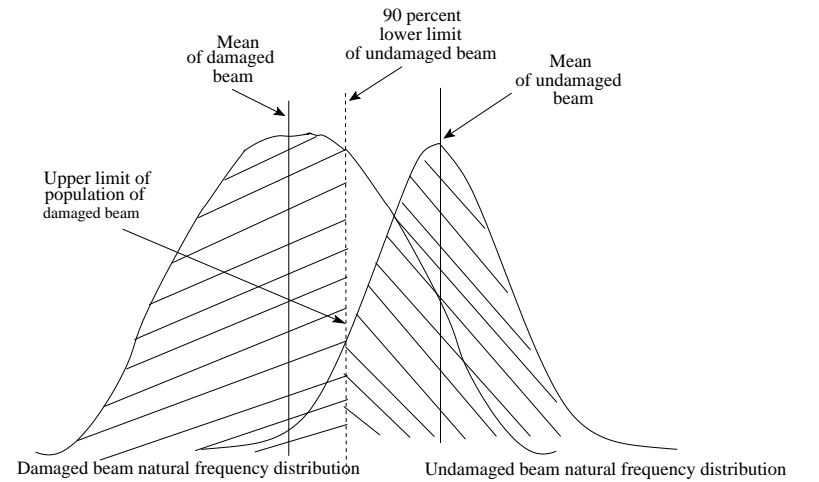
(c) Probability of frequency change due to damage

Figure 7.2: Representation of natural frequencies extracted from experiments as normal distribution

Instead of the 90/95 upper limit of the damaged beam, we can estimate the actual percentile population, "x", of the frequency measurements of a damaged beam that lies below the 90/95 lower frequency limit of the undamaged beam with a 95% confidence level, to give us "x/95" upper limit for that damage case, as illustrated in Fig. 7.2(c). The actual percentile populations of the damaged beam frequencies that lie below the 90/95 lower limit are calculated in this manner and shown in Table 7.3 for the three modes. It may be noted that the values in Table 7.3 may be considered as the probability with which a damage of a certain size at a given location will produce a change in frequency below the 90/95 limit of the undamaged frequency, in any given mode. Considering case 1, we can see that even though only 1% of the frequencies measured on the damaged beam in mode 1 will lie below the 90/95 lower limit, in modes 2 and 3, the probabilities of damaged frequencies falling below the practical minimum frequency of the undamaged beam are, respectively, 82% and 65%. The probability that atleast one frequency change will be caused by a particular damage may, therefore, be taken to be the maximum of percentile values for the three modes listed in Table 7.3, e.g., 82% for damage case 1.

Table 7.3: Percentile population of frequency measurements below 90/95 lower limit of the undamaged beam frequency

Damage case	Population below 90/95 of undamaged beam (%)		
	Mode1	Mode2	Mode3
1	1	82.2	65.1
2	51	92.6	90.8
3	98.4	97.8	95.3
4	78.6	79.7	100.0
5	70.2	100.0	100.0
6	2.6	100.0	99.7
7	61.3	100.0	99.2

7.5 Probability of crack detection from frequency change - inverse problem

The maximum percentile value in each row of Table 7.3 indicates the probability of reduction in frequency below the minimum value expected (90/95 lower limit) for the undamaged beam for that particular damage. But, the converse is not true, i.e., if the frequency falls below the minimum expected for the undamaged beam, we cannot say that the maximum percentile value in any row indicates the probability of the existence of a damage of that type in the beam. However, since the 90/95 lower limit is practically the lowest measurement that we will get for the frequency of the undamaged beam, any measurement below this value can be considered to indicate the presence of some damage. Table 7.4 lists the 90/95 lower limits i.e., the minimum values above which 90% of the frequency measurements on the undamaged beam are expected to lie for the three modes with a 95% confidence level. The values in the fourth column ($\mu - f_L$) thus represent the maximum drop in frequency from the mean of the undamaged beam that may be expected due to the scatter in the measurement. Any drop in frequency higher than that listed in the 4th column, in any of the three modes, indicates the presence of a damage with 90% probability and 95% confidence.

Table 7.4: Minimum changes in frequency for detection of crack with 90% probability and 95% confidence level

Mode	Mean frequency, μ	90/95 lower limit frequency, f_L	$\mu - f_L$	$\frac{\mu - f_L}{\mu}(\%)$
1	7.151	7.124	0.0267	0.37
2	45.074	45.056	0.0188	0.04
3	126.468	126.408	0.0598	0.05

7.6 Minimum detectable crack size - cantilever beams with centre cracks

The minimum frequency changes for 90/95 crack detection (with 90% probability with 95% confidence) listed in Table 7.4 can be used to determine the *Minimum Detectable Crack size (MDC)*. For this, we need to establish the relationship between crack sizes and frequency changes. This is achieved for cantilever beams with centre cracks using *FEA*.

The beam modelled in the *FEA* had dimensions of length $L = 850mm$, width $W = 100mm$ and thickness $h = 6.4mm$. This is a scaled version of the beam used in the experiments ($L = 600mm$, $W = 50mm$ and $h = 3.2mm$) with the same material properties (aluminium alloy). The scaling was done so as to obtain frequencies of the same order as those measured for the experimental beam (Mode1 $\approx$ 7Hz, mode2 $\approx$ 45Hz, mode3 $\approx$ 125Hz), using the fact that the frequencies are proportional to W, h and L^2. A scaled version of the beam was modelled in *FEA* so that, the same number of elements with the same mesh distribution could be employed to model beams with small cracks ($\gamma = 2\%$) as well as beams with large cracks ($\gamma = 40\%$). Through-thickness cracks were modelled in the beam at four different locations (x_c/L = *10, 20, 30 and 40 percent of the beam length measured from the fixed end*) and with nine different sizes ($\gamma = b/W$ = *2, 4, 6, 8, 10, 20, 30, 40 and 50 percent of the width of the beam*). The frequencies obtained by modal analysis in *FE* for the undamaged beam and the above 36 damage cases of beams with centre cracks are tabulated in Table B.1 in Appendix B.

The changes in frequency are plotted against crack size for the four locations $x_c/L = 0.1, 0.2, 0.3$ and 0.4 in Figs 7.3(a), 7.3(b), 7.3(c) and 7.3(d) respectively for each of the three modes. As expected, the magnitude of the changes in frequency increases with increase in crack size. The minimum detectable crack size in each mode at each of the above four locations is obtained by identifying the value of the crack size which produces a change in frequency equal to the minimum frequency change for 90/95 crack detection listed in Table 7.4 for each mode. This is indicated in Figs. 7.4(a), 7.4(b), 7.4(c) and 7.4(d).

(a)

(b)

(c)

(d)
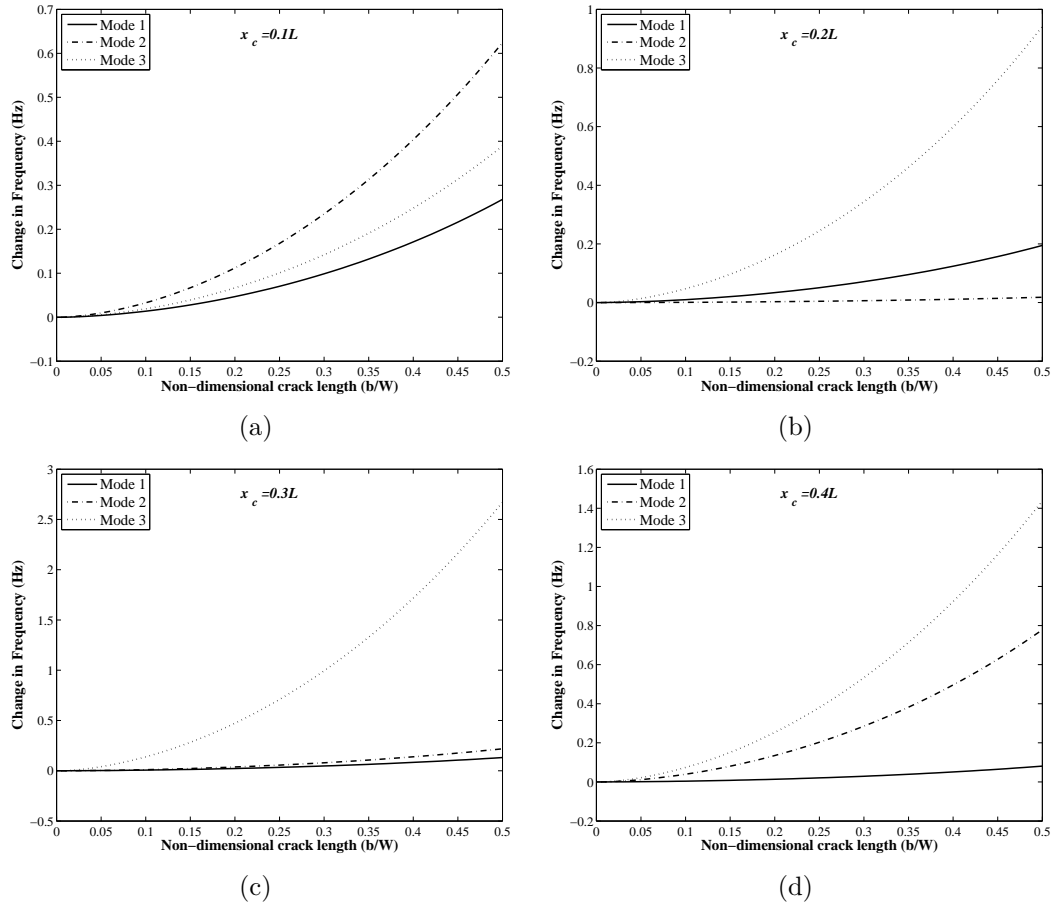
Figure 7.3: Plots of change in frequency with crack size (a) $x_c/L = 0.1$, (b) $x_c/L = 0.2$, (c) $x_c/L = 0.3$, (d) $x_c/L = 0.4$

Considering location $x_c = 0.1L$ shown in Fig. 7.4(a), it can be seen that the minimum detectable crack size (b/W), is about 0.146 in mode 1, 0.073 in mode 2 and 0.189 in mode 3. Observing frequency changes in all 3 modes, we could say that the *Minimum Detectable Crack size (MDC)* for this location is the minimum of these three values i.e., 0.073. This is because a crack with a size of $b = 0.073W$, will produce a significant reduction in frequency, below the minimum frequency of the undamaged beam represented by the 90/95 lower limit in one mode (mode 2) indicating the presence of the damage with 90% probability and 95% confidence. It is to be noted that the mode in which the detectable crack size is a minimum, does not always correspond to the mode in which the 90/95 frequency change has a minimum. For example, in Fig. 7.4(b), mode 2 has the minimum frequency change (0.0188) while the *MDC* $(b/W = 0.114)$ is in mode 3. The minimum detectable crack size of all three modes are listed in Table 7.5 for the four crack locations. It is thus seen that the *MDC* for the centre crack in a cantilever beam is dependent on
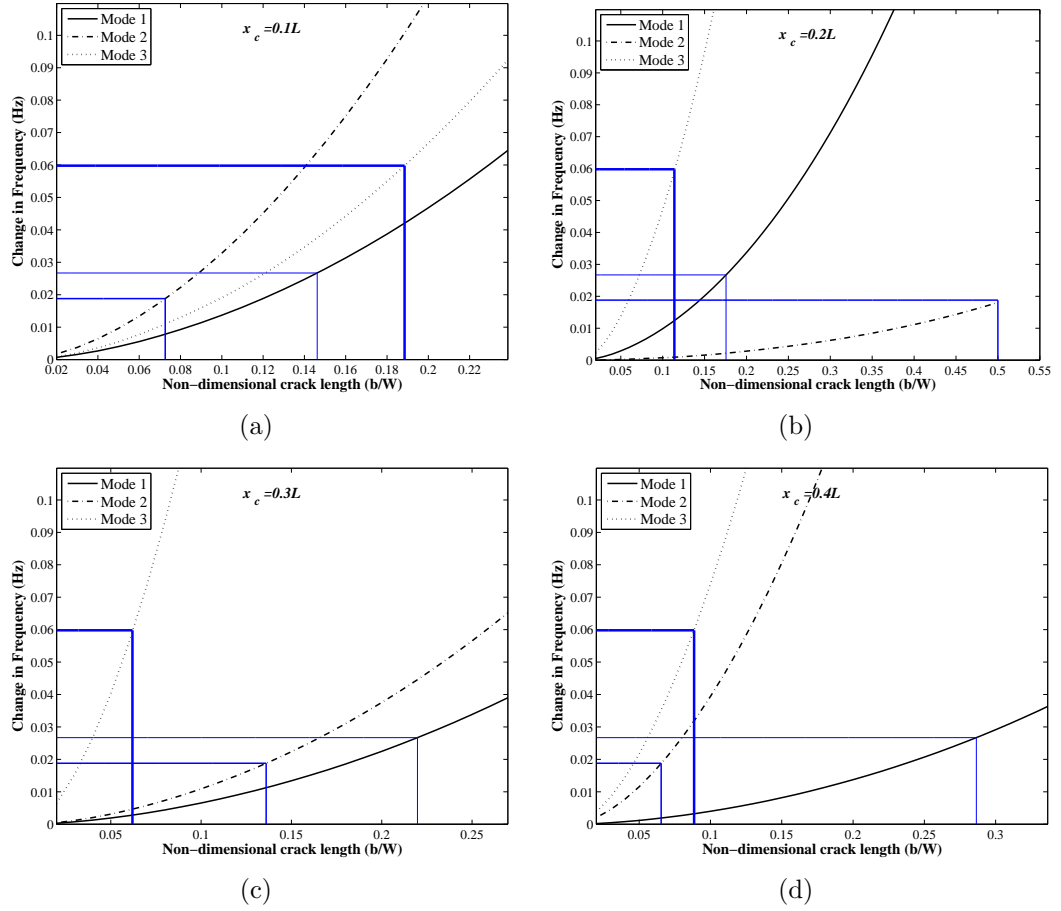
Figure 7.4: Identification of minimum detectable crack size (a) $x_c/L = 0.1$, (b) $x_c/L = 0.2$, (c) $x_c/L = 0.3$, (d) $x_c/L = 0.4$

the crack location. At a distance of 20% from the fixed end of the cantilever beam, the *MDC* is about 11% of the beam width, whereas, at distances of 30% and 40%, cracks of about 6% to 6.5% of the beam width can be detected. This is because the effect of the crack size on the frequency changes is location dependent. When the location of the damage is not known, one could extend the analysis to cover the whole beam so that crack detectability over the entire structure can be assessed. It should also be noted that, to detect a crack whose length is 7.3% the width of the plate located at 10% the length of the beam, a frequency change as small as 0.06Hz must be reliably measured. From Table 6.1, it can be seen that frequency change as small as 0.014Hz (damage case 6, mode1) can be measured in experiments and hence damage identification is quite feasible and reliable.

Table 7.5: Minimum detectable crack size

| | Minimum crack size detectable | | | |
	$x_c/L = 0.1$	$x_c/L = 0.2$	$x_c/L = 0.3$	$x_c/L = 0.4$
Mode 1	0.146	0.176	0.220	0.287
Mode 2	0.073	0.500	0.136	0.065
Mode 3	0.189	0.114	0.062	0.089
MDC	*0.073*	*0.114*	*0.062*	*0.065*

7.7   Conclusion

In the preceding sections, a statistical analysis of experimental measurements on cantilever beams with centre cracks was conducted. First, a test of significance was carried out for the seven damage cases to establish that the reductions in frequencies due to the presence of damage were statistically significant.

Assuming normal distribution, for each damage case, the probability of reduction in frequency to a level below the practical minimum frequency of undamaged beam was established for each mode to study the forward problem. The minimum frequency changes in each mode required to establish the presence of a crack with 90% probability and 95% confidence level was also calculated. These values of frequency changes for 90/95 crack detection are employed together with plots of frequency changes from *FEA vs* normalised crack size to determine the minimum detectable crack sizes for four different crack locations. The best value for the minimum crack size that can be detected was about 6.2%, at 30% of the beam length. This is very high when we note that the maximum percentage change in frequencies required for 90/95 crack detection is only 0.4% (mode 1) while the minimum is 0.04% (mode 2). Thus the minimum normalised detectable crack size is about 150 times the minimum normalised frequency change required to detect the crack. In other words, a crack size of 6% is required to produce a minimum frequency change of 0.04%, which is the least detectable. This is because the effect of a centre crack on the local stiffness is quite small and hence the change in natural frequencies is also small. For instance, a centre crack of size of 10% of the beam width produces only a 10% reduction in local stiffness. In comparison, an edge crack of depth equal to 10% the height of the beam will cause cause a 27% reduction in the local stiffness and hence is likely to cause a much higher change in frequency. The effect of crack

size on frequency change is also a function of boundary condition and the aspect ratio of the beam.

It may, however, be noted that even when the measured frequency changes are within the scatter limits of the frequencies of the undamaged beam, the inverse algorithm with the energy approach can be employed to provide estimates of the damage size and location, as was demonstrated with the *FEA*. Thus, even though the certainty of the presence of the damage is lower (than 90/95), we can still obtain fairly accurate assessment of the damage location and size by using the proposed methodology.

In the next two chapters, the application of the crack detection methodology for plates is validated using *FEA* and *EMA*.

Chapter 8

Validation of analytical model for plates using *FEA*

8.1 Introduction

The theory derived in Chapter 4 and the methodology for solution to the inverse problem is validated for the case of rectangular plates, using *FEA*. In the two dimensional case of a plate, the crack location has two variables x_c and y_c. In general, these co-ordinates, the crack size (b/W) and the crack orientation (ϕ) are the four unknowns to be determined. The validation is first performed for the special case of crack running parallel to the edge of the plate, where the number of unknowns is reduced to three, ϕ being known. Then the algorithm is extended to solve the general case where the crack orientation is also an unknown.

In Section 4.6.2, four different techniques were proposed to solve the inverse problem in plates; Least Square *(LS)* technique, Sequential Quadratic Programming *(SQP)*, Genetic Algorithm *(GA)* and a combination of the last two. All these techniques are implemented for detecting cracks for the special case, where the orientation of the crack is known a priori. For solving the general case of finding all four crack parameters, only *SQP* is used, as it was found to be most efficient of the four techniques.

8.2 Description of Finite Element Modelling

FEA was conducted using ANSYS Version 11 on a rectangular plate, simply supported on all four edges, made of steel ($Young's\ Modulus = 192.28 GPa; density = 7808.4 Kg/m^3$). The dimensions of the plate were: length=150mm, width=100mm and thickness=5mm. A preliminary study was conducted to compare the accuracies obtained with two different shell elements, viz. SHELL63 and SHELL93. The natural frequencies for the first ten modes predicted with these two types of elements is listed in Table 8.1, along with the frequencies predicted by Plate theory [186, 155]. The percentage deviations of the results obtained with the two SHELL elements from the theory are presented in the columns on the right. It can be seen that SHELL63 provides much closer agreement with the theoretical frequencies than SHELL93. This is contrary to the results obtained for beams, wherein, SHELL93 provided results closer to the theory (See Table 5.3 in Section 5.2). Hence SHELL63 was used for all further modelling on plates.

Table 8.1: Comparison of frequencies predicted by SHELL63 and SHELL93 with theory

Mode	Theory* (Hz)	Frequencies from FEA (Hz)		%change compared to theory	
		SHELL93	SHELL63	SHELL93	SHELL63
1	1721.76	1712.46	1721.47	0.54	0.02
2	3310.96	3277.31	3310.33	1.02	0.02
3	5297.32	5212.46	5296.60	1.60	0.01
4	5957.47	5852.43	5958.34	1.76	0.01
5	6885.98	6744.19	6884.77	2.06	0.02
6	9537.32	9265.65	9531.63	2.85	0.06
7	9667.22	9390.76	9665.36	2.86	0.02
8	11256.35	10884.15	11254.66	3.30	0.01
9	12845.48	12364.07	12841.69	3.74	0.03
10	13242.76	12731.95	13237.04	3.86	0.04

A convergence analysis was conducted using different mesh densities. The Root Mean Square (RMS) values of the differences between natural frequencies of successive models ($i - 1$ and i), obtained with Eqn. [5.2], for the first 6 modes, are plotted in Fig. 8.1. The RMS error is below 0.05% for the model with 1944 elements. This was considered sufficient accuracy keeping in mind that the computational time increases exponentially with the number of elements. Hence, all further modelling was conducted with 1944 elements over the entire plate.
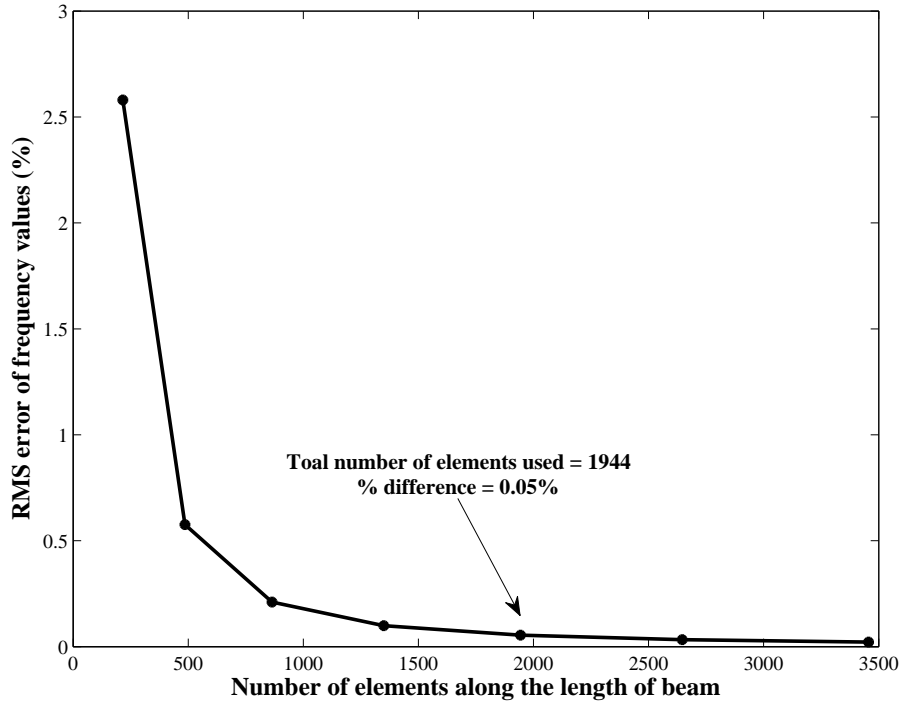
Figure 8.1: Convergence analysis for plates

8.3 Validation of Eqn. [4.18] for plates

As in the case with beams, the linearity between the normalised frequency change and the normalised curvature at the damage location, given by Eqn. [4.18], is verified here for the case of plates with parallel cracks ($\phi = 90°$). The normalised modal frequency change ($\Delta\omega/\omega$), obtained from *FEA*, is plotted against the square of the normalised curvature (χ_c^2/χ_{RMS}^2), for a crack of $b = 0.2W$ located at $x_c = 0.3L$ and $y_c = 0.3W$, in Fig. 8.2(a) for the first three modes and in Fig. 8.2(b) for the first six modes (the numerical labels indicate mode numbers). Since this relationship is supposed to be linear (and the gradient equal to DI), the equations and the r-square values of the linear regression lines fitted to the data points are also shown in the Figs. 8.2(a) and 8.2(b). It can be seen that the linearity is much better when using only three modes (which are sufficient to assess the damage in this case, since the angle is already known).
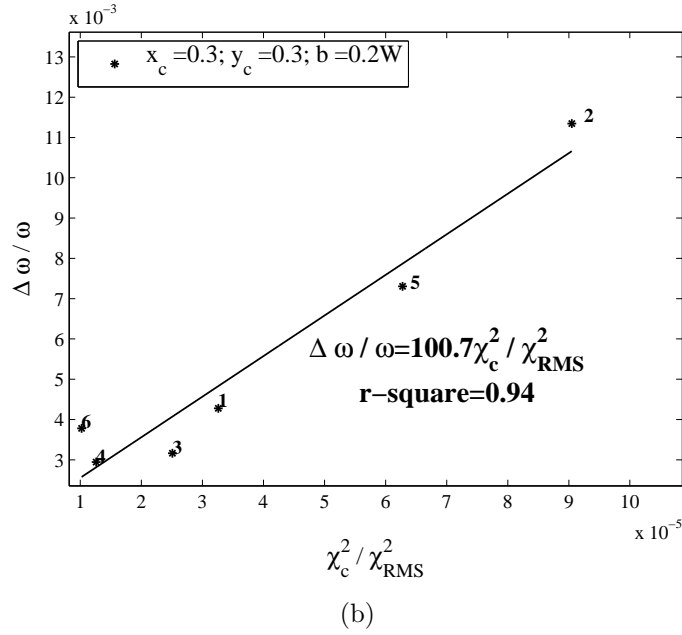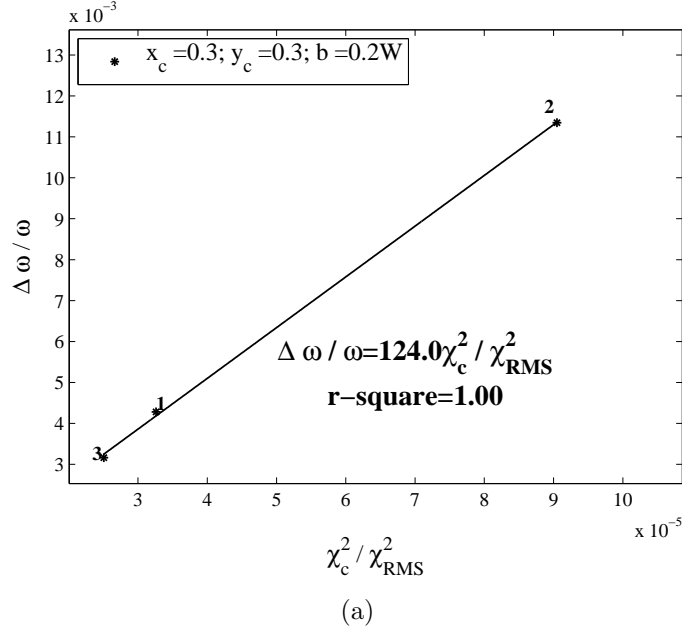
(a)

(b)

Figure 8.2: Variation of normalised change in frequency with normalised curvature (a) using 3 modes (b) using 6 modes

FEA was performed with the same damage location (x_c, y_c) for 20 parallel cracks with lengths (b/W) ranging from 0.02 to 0.4 and the $\Delta\omega/\omega$ was plotted against χ_c^2/χ_{RMS}^2 to determine the r-square values in a similar manner. Fig. 8.3 shows the plot of r-square values obtained with the first three modes as a function of the crack size. It is clear that the r-square value decreases with increasing crack size even when the number of modes is restricted to three.
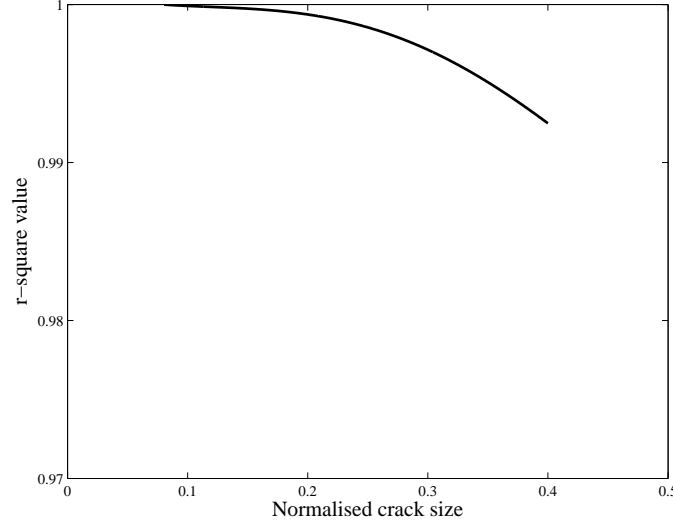

Figure 8.3: Effect of crack size on linearity of frequency change - curvature relationship

Fig. 8.4 shows the plot of r-square values obtained as a function of both crack size and number of modes. From the surface plot in Fig. 8.4, it can be observed that the r-square value is close to 1 and is independent of the number of modes for small crack sizes. The drop in linearity is small (r-square value of over 0.99) even for large cracks when using only the lower order modes. However, the linearity degrades rapidly with r-square values dropping exponentially when the crack size and the number of modes increase simultaneously. It can be seen that, for crack sizes over $b/W = 0.28$ and number of modes above 6, the r-square value is below 0.5. Based on this, we can conclude that, the use of only the lower order modes is likely to provide better accuracy in detecting and assessing the size of the damage.

It was considered that the drop in linearity in the relationship between $\Delta\omega/\omega$ and χ_c^2/χ_{RMS}^2 with increasing crack size and increasing number of modes could be attributed to the variation of the magnitude of curvature across the length of the crack. It may be noted that this variation would be higher for higher modes because
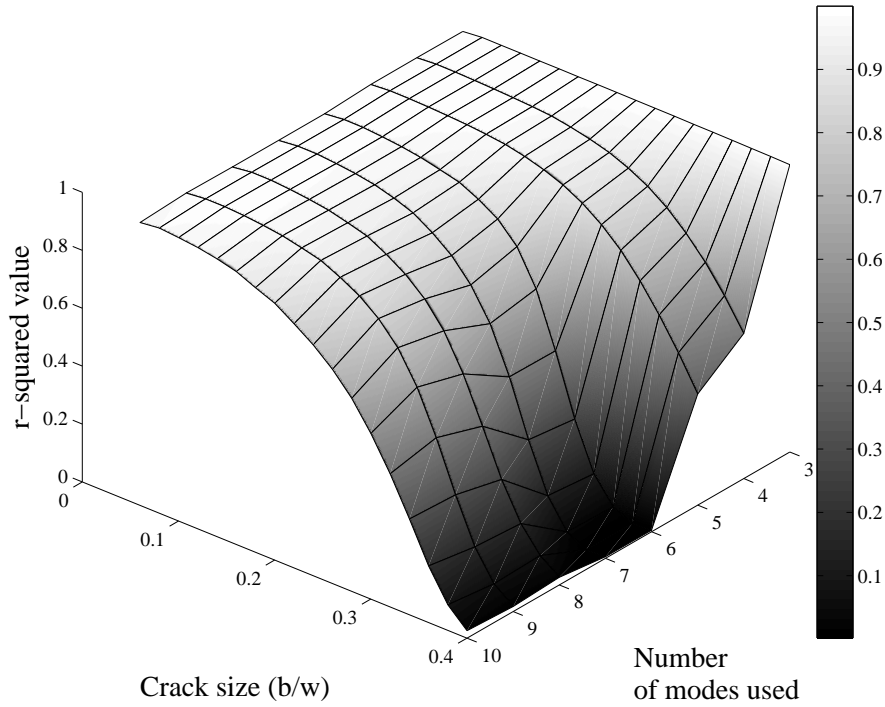
Figure 8.4: Effect of crack size and number of modes on linearity of frequency change - curvature relationship

of the number of half waves across the width of the plate. In the theory developed in Section 4.5, the change in frequency is obtained as a function of the curvature at the location of the crack which is taken to be the midpoint of the crack. While this approximation would be valid for small cracks, for large cracks and for large variations in curvature across the crack length, this may give rise to errors. This possibility was investigated by using a modified form of Eqn. [4.18], wherein instead of using a constant value of the curvature at the midpoint of the crack, the energy stored in the crack is calculated taking into account the variation in curvature using its mean value across the crack length. The mean value is obtained by integrating the curvature along the crack length and dividing by the crack length as shown in the numerator of Eqn. [8.1].

$$\left[\frac{\Delta\omega}{\omega}\right]_n = DI \left[\frac{\frac{1}{b}\int\limits_{-b/2}^{b/2}\chi_c^2 db}{\chi_{RMS}^2}\right]_n \tag{8.1}$$

However, the use of Eqn. [8.1] above provided only a marginal improvement in the linearity between frequency change and curvature relationship with large cracks and higher modes. Hence the reason for the non-linearity should be sought elsewhere. It is well known that errors in frequency values extracted from numerical models increase with increasing mode numbers [187, 188, 189]. This is most likely the major cause for the observed non-linearity in the frequency change curvature relationship when higher modes are employed. It has been reported earlier that more accurate values for the frequencies of plates with cracks can be obtained by modelling them as breathing cracks and imposing contact non-linearity conditions between the crack faces [193]. In our numerical model, cracks were only modelled by unstitching the nodes along the length of the crack which would have resulted in slightly erroneous values for the frequencies of the damaged plate. This may also have contributed partially to the discrepancy between theoretical predictions and frequency changes obtained from *FEA*.

8.4 Validation of assessment methodology for cracks parallel to an edge

The methodology for solution to the inverse problem is first assessed by applying it to the special case of cracks running parallel to y-axis of the plate, i.e., $\phi = 90°$ (see Fig. 4.5 for definition of coordinate axis and orientation angle). The natural frequencies predicted by the *FEA* for the first three modes of undamaged case and the ten damage cases with cracks parallel to the y-axis are presented in Table 8.2, along with the normalised coordinates of the mid points of the crack locations ($\alpha_c = x_c/L$ and $\beta_c = y_c/W$) and the crack sizes ($\gamma = b/W$).

The solution to the inverse problem is obtained using the Least Square method, described in Section 4.6.2. The difference in natural frequencies and the curvature distributions using modeshapes from *FEA* are employed in Eqn. [4.18], to determine *DI* as a function of the x and y locations. Note that the term, χ_c, in the numerator on the *RHS* of Eqn. [4.18] is dependent on the coordinates at the crack location, given by Eqn. [4.34]. The *RMS* value of the distance, given by Eqn. [4.38], is then expressed as a function of x and y. The minimum value of the d_{RMS} is determined

Table 8.2: Natural frequencies (in Hz) predicted by *FEA* for undamaged and plates with damage

Damage	Crack location		Crack	Natural frequencies		
case	$\alpha_c = x_c/L$	$\beta_c = y_c/W$	length, γ	Mode1	Mode2	Mode3
Undamaged plate				1721.49	3310.40	5296.69
1	0.2	0.2	0.2	1719.33	3290.11	5286.49
2	0.2	0.3	0.3	1711.66	3226.18	5269.86
3	0.2	0.4	0.4	1695.27	3118.33	5271.86
4	0.3	0.2	0.2	1717.64	3290.31	5280.38
5	0.3	0.3	0.1	1719.67	3300.92	5292.44
6	0.3	0.3	0.3	1705.15	3229.21	5262.59
7	0.3	0.4	0.4	1681.86	3130.61	5268.47
8	0.4	0.2	0.2	1716.28	3301.87	5274.53
9	0.4	0.3	0.3	1700.07	3271.35	5248.10
10	0.4	0.4	0.4	1671.84	3207.97	5252.24

graphically to obtain estimates of x and y coordinates of the crack location and the corresponding value of *DI*.

The crack size is estimated from the calculated *DI* value using Eqn. [4.35], where the integral $g(\gamma)$ of the correction factor $f(\gamma)$ is determined from the polynomial for $f(\gamma)$ given by Boduroglu and Erdogan [172] for $W/h = 100/5 = 20$ (see Eqns. [A.1] and [A.2] in Appendix A). The coordinates for the crack location, x_c and y_c, and the corresponding crack size b/W predicted by the solution of the inverse problem are listed in Table 8.3 for the ten damage cases. The table also lists the actual values used in the *FEA* and the corresponding percentage deviations. As in the case with beams, the normalised discrepancies are calculated from the normalised values of the crack coordinates and crack size.

The maximum normalised discrepancy in predicting damage location is under 6% and the maximum normalised discrepancy in the damage size is under 9%. In general, the discrepancies in the predictions of both location and size increase with increasing crack size but do not have any discernible correlation with the crack location.

Table 8.3: Results from damage detection algorithm using distance (graphical) technique

Damage Case	Actual crack parameters			Predicted crack parameters			Normalised discrepancy		
	α_c	β_c	γ	α_c	β_c	γ	α_c	β_c	γ
1	0.2	0.2	0.2	0.22	0.18	0.17	1.7	2.0	3.0
2	0.2	0.3	0.3	0.23	0.28	0.25	3.0	2.0	5.2
3	0.2	0.4	0.4	0.25	0.38	0.31	5.3	2.5	8.6
4	0.3	0.2	0.2	0.31	0.21	0.15	0.7	1.0	4.8
5	0.3	0.3	0.1	0.31	0.30	0.07	0.7	0.0	3.0
6	0.3	0.3	0.3	0.31	0.32	0.23	1.0	1.5	6.8
7	0.3	0.4	0.4	0.32	0.40	0.32	1.7	0.5	8.2
8	0.4	0.2	0.2	0.40	0.21	0.16	0.3	0.5	4.5
9	0.4	0.3	0.3	0.39	0.30	0.24	1.3	0.0	6.3
10	0.4	0.4	0.4	0.38	0.38	0.33	2.0	2.0	7.1

8.4.1 Influence of modeshape resolutions on accuracy of predictions

The estimation of crack parameters using Eqn. [4.18], requires the determination of curvatures at every point on the surface of the plate. These curvatures are calculated from the values of the plate deflections extracted from *FEA* using the Finite Difference *(FD)* approximations [168] given below.

$$
\begin{aligned}
\left(\frac{d^2\psi}{dx^2}\right)_{@ \ (i,j)} &= \frac{\psi_{i+1,j} + \psi_{i-1,j} - 2\psi_{i,j}}{\Delta x^2} \\
\left(\frac{d^2\psi}{dy^2}\right)_{@ \ (i,j)} &= \frac{\psi_{i,j+1} + \psi_{i,j-1} - 2\psi_{i,j}}{\Delta y^2} \\
\left(\frac{d^2\psi}{dxdy}\right)_{@ \ (i,j)} &= \frac{\psi_{i+1,j+1} - \psi_{i-1,j+1} + \psi_{i-1,j-1} - \psi_{i+1,j-1}}{4\Delta x\Delta y}
\end{aligned}
\tag{8.2}
$$

where ψ is the modeshape deflection of the plate and Δx and Δy are distances between nodes of the *FD* mesh in the x and y directions respectively.

The accuracy of *FD* approximations is known to be a function of the intervals Δx and Δy over which they are calculated, in other words, the number of points over which the deflection data is available. To reduce the interval size for the *FD* calculations, the modeshape deflections obtained from *FEA* over a discrete number of points were first interpolated using an in-built function *interp2* in *MATLAB*, so that deflection values were available over a greater number of points. A study was

conducted to investigate the effect of the discretisation interval and the *FD* mesh resolution on the accuracy of the damage detection algorithm. A separate *FEM* for the undamaged beam was created for this purpose with 150 elements along the length and 100 elements along the width. This provided a maximum of 15,251 points over the entire plate at which deflection values were available. The effect of discretisation interval was studied by choosing 4 smaller sets of data points from the total available to be input into the interpolation algorithm in each case, *viz.* 600, 2400, 5400 and 9600 points. To investigate the effect of the *FD* mesh resolution, the data from each of the above sets was interpolated to higher number of points to provide finer *FD* meshes. Five different levels of *FD* mesh sizes were chosen, *viz.* 1mm, 0.5mm, 0.25mm, 0.1mm and 0.05mm using interpolated values over 15,000, 60,000, 240,000, 960,000 and 6,000,000 points respectively. The curvatures of the undamaged plate obtained using the above discretisation levels and *FD* mesh sizes were employed in the inverse algorithm to estimate the x and y locations as well as the damage size for one particular damage case (case 8 in Table 8.2). The percentage difference between the predicted and actual values of x_c, y_c and b/W for the twenty different combinations of *FE* data discretisation and *FE* mesh sizes listed above are plotted respectively in Figs. 8.5, 8.6 and 8.7.
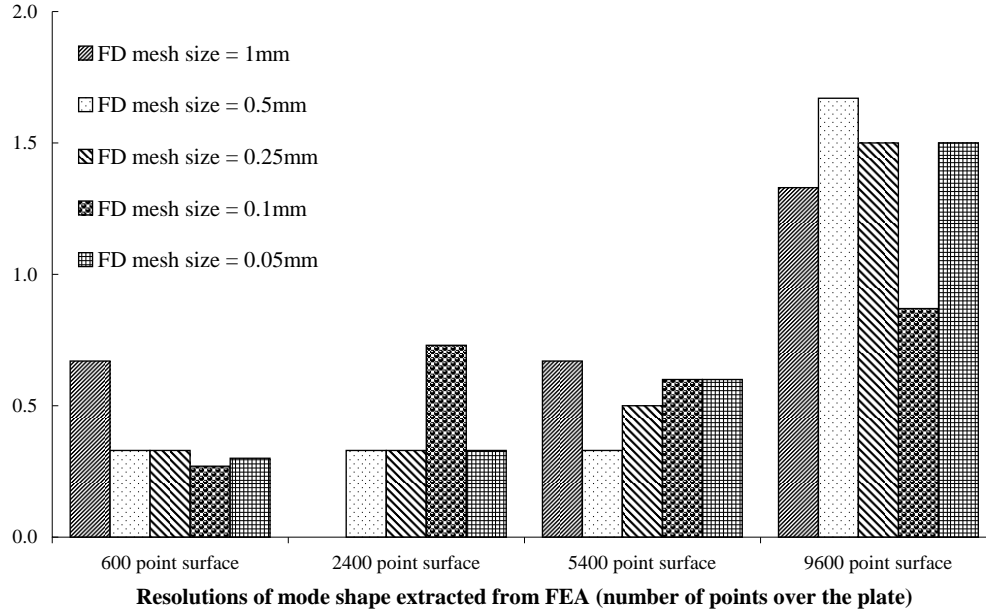
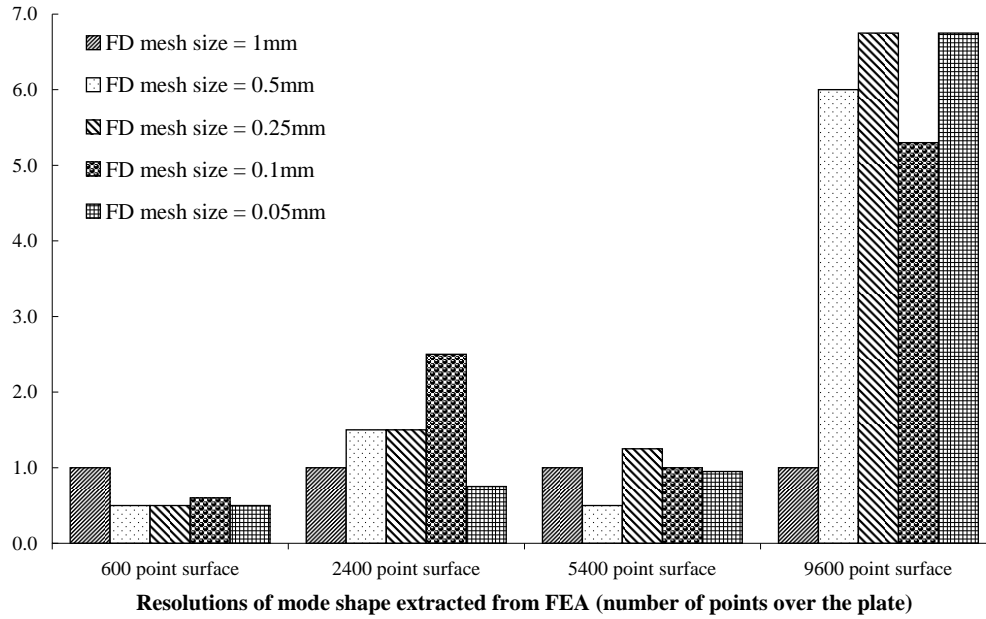Figure 8.5: Comparison of normalised discrepancies obtained in location of damage (x-coordinate)

Figure 8.6: Comparison of normalised discrepancies obtained in location of damage (y-coordinate)

The number of points at which the deflection data from *FE* was employed in the interpolation algorithm is shown along x-axis in the three figures. It can be seen that when data was extracted over 600, 2400 and 5400 points from FE, there was
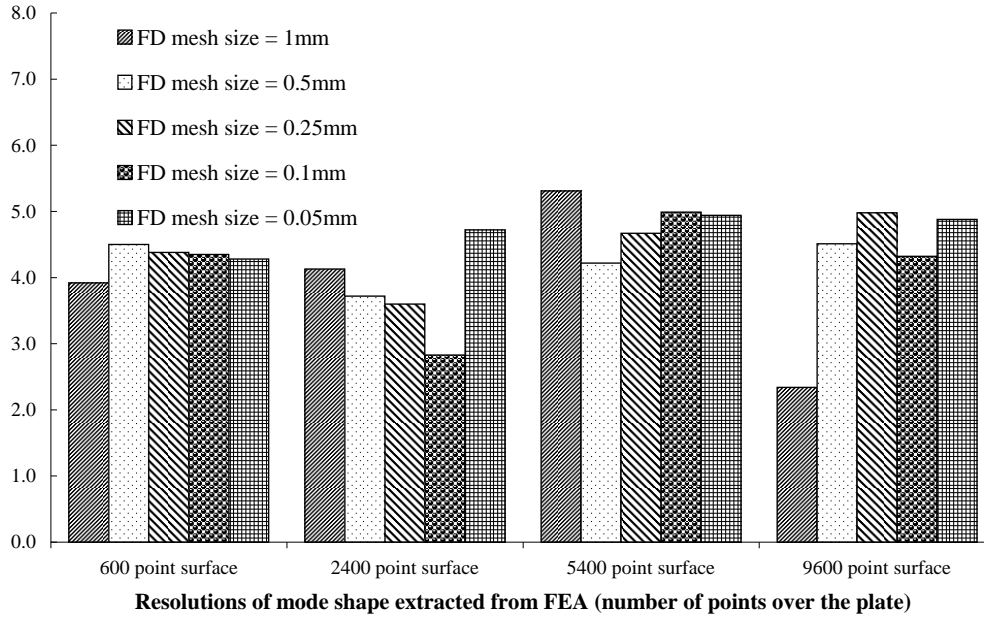
151

Figure 8.7: Comparison of normalised discrepancies obtained in damage size

not much variation in the normalised discrepancies in the three damage parameters irrespective of the *FD* mesh resolution. When deflection data was extracted over 9600 points from *FEA*, there is a significant increase in the normalised discrepancies of the estimated crack locations, which is contrary to expectations. This appears to be due to high frequency perturbations arising out of extracting modeshapes from *FEA* using PATH functions in *ANSYS* and amplification of this high frequency noise due to the differentiation. It is also clear from Figs. 8.5, 8.6 and 8.7 that the *FD* mesh resolution has negligible effect on the accuracy of estimation of any of the damage parameters. Hence it is concluded using a lower number of points of extraction of data from *FEA* (600 points) and using a coarse mesh of 1mm for *FD* calculations provided best accuracy while minimising the computation time.

8.5   Comparison of results using minimisation techniques with *LS* method

The solution to the inverse algorithm for determining the crack location and size for cracks with known orientation, presented in Section 8.4 above, were obtained using the *LS* technique. However, in the case of a crack oriented at an unknown angle,

it is more efficient to implement a minimisation algorithm for solving the inverse problem. This is done by minimising the objective function given in Eqn. [4.40] using three different techniques, *viz.* Sequential Quadratic Programming *(SQP)*, Genetic Algorithm *(GA)* and combination of the two as described in Section 4.6.2.

SQP and *GA* start with a random solution consisting of initial estimates of the unknown parameters and march towards the actual solution using gradient information and population based approach respectively. For this, it is essential to have a continuous objective function based on continuous deflection data, the latter is obtained by employing the spline-fit function *csape* and *fnder* in *MATLAB* within the minimisation technique. For both the techniques, we have to provide the bounds of the domain within which the search is to be carried out.

The bounds for the normalised x and y locations are given as 0 *to* $0.5L$ and 0 *to* $0.5W$, taking advantage of the symmetry of the simply supported plate. The bounds for the normalised crack length are also chosen as 0 *to* $0.5W$. The *SQP* algorithm suffers from the disadvantage that the solution may get stuck on local minima. Hence we cannot be sure that the solution represents the true solution. To overcome this, the optimisation algorithm is iterated for 20 times using different random starting points (random multi-start). The values for the 20 random starting points, within the bounds of the search domain, were generated using a pseudo-random number generator in *MATLAB*. The minimisation using *SQP* is performed using an in-built *MATLAB* function, *fmincon*.

Population based techniques, including *GA*, are computationally more expensive compared to gradient based methods. However, they do not depend on the starting point; instead, they search the whole search space with a number of sets of random variables to find the actual solution. The candidate solutions for the population is generated and their objective function values are calculated. The best solution, which yields the least objective function, is selected and perturbed to find if there exists an even better solution in its neighbourhood. This step is continued until the objective functions of the two best solutions do not experience significant changes in subsequent generations, at which point the algorithm is terminated. An optimum population size of 200 and 100 generations was chosen by trial and error.

Because SQP may get stuck to local optima and because evolutionary techniques are computationally expensive a combination of SQP and GA was also trialled to examine whether it provides a better efficiency. In this case, the solution starts with the GA using a bigger population size (250 candidate solutions) and after 20 generations, it switches to SQP to home-in on the final solution. The results in terms of the coordinates x_c and y_c and the damage size b/W obtained with the SQP, the GA and the combination of the two are presented in Figs. 8.8, 8.9 and 8.10 for the ten damage cases listed in Table 8.3, along with the results from LS technique for comparison.
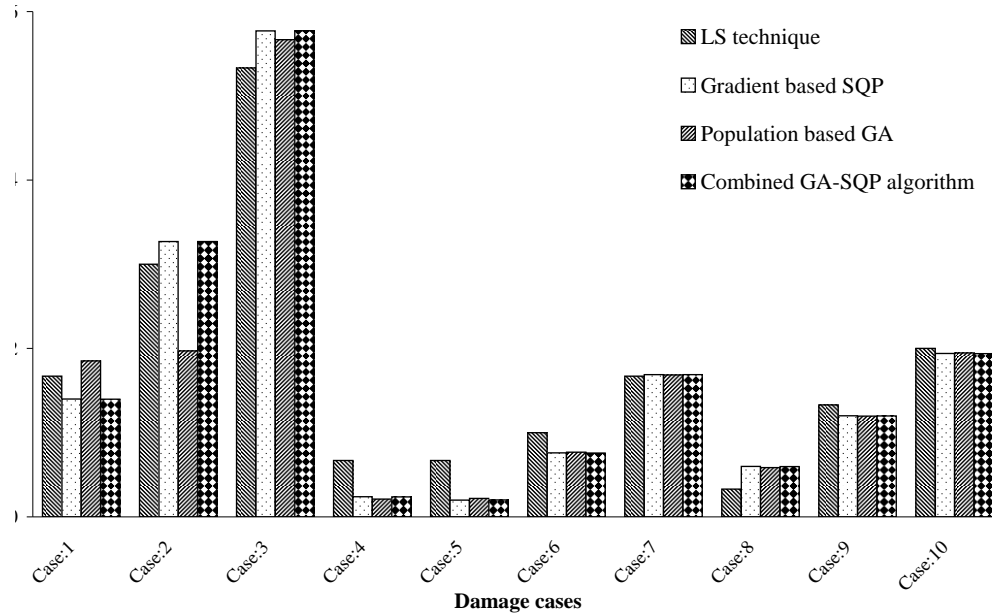

Figure 8.8: Comparison of normalised discrepancies obtained in location of damage (x-coordinate)

From these figures, it is clear that all four techniques yield similar results (within $\approx 1\%$ variation)in determining the location of the crack. Some solvers yield better results than others in some cases but this is not consistent in all damage cases. The three minimisation techniques determine the crack sizes with similar accuracies but are consistently better than the LS technique (by about 3%).
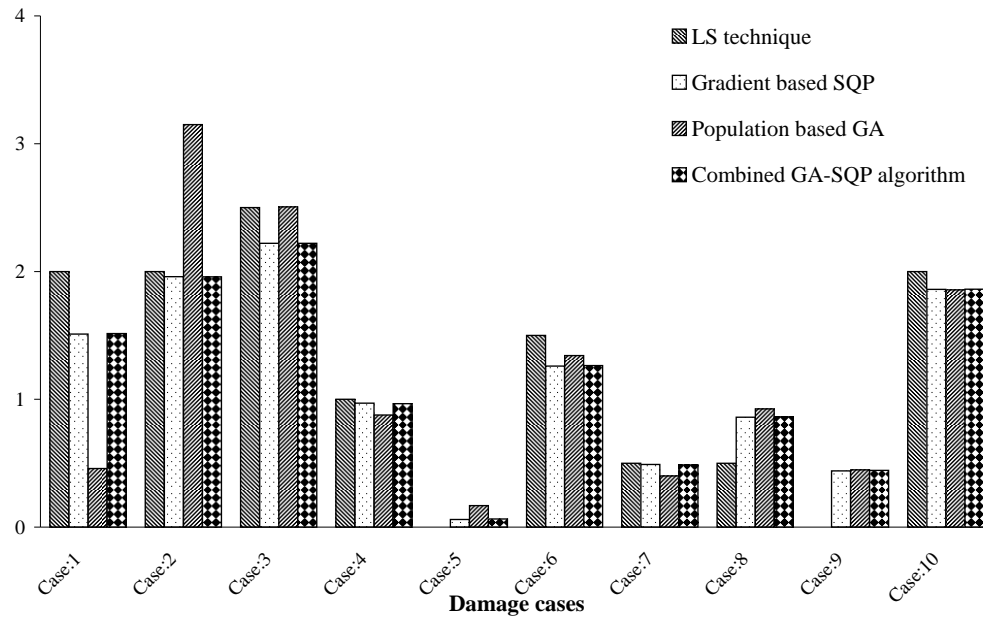
Figure 8.9: Comparison of normalised discrepancies obtained in location of damage (y-coordinate)
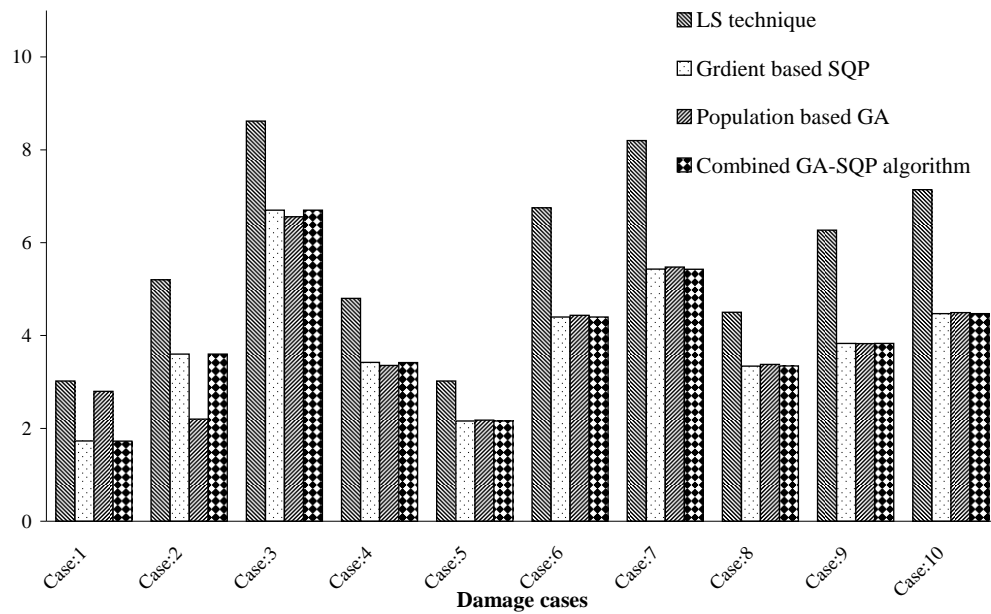

Figure 8.10: Comparison of normalised discrepancies obtained in damage size

8.5.1 Comparison of efficiencies of minimisation algorithms

In the previous section, it was seen that all the four solvers yielded comparable results except that the *LS* technique produced 3% greater normalised discrepancies in predicting the damage size. This suggests that better results can be obtained by using minimisation algorithms. A further attempt was made to determine which of the three minimisation algorithms, *viz. SQP*, *GA* and the combination of the two, is more efficient. Efficiency of a minimisation algorithm may be defined in terms of the time required to reduce the error in the objective function below a certain set level or in terms of the error in the value of the objective function after each technique has been run for a set period of time. Keeping both the error value and time factor in mind, a comparison is made in this section between the three techniques.

The value of the objective function when the three algorithms were terminated for the ten damage cases is shown in Table 8.4. The results of the *SQP* are the best of the solutions obtained with twenty runs starting with random initial estimates. In general *SQP* took about 10 minutes to complete the twenty iterations. The *GA* was set to run for 100 generations with a population size of 200 in each generation which took about 25 minutes to complete. The combined *GA-SQP* approach, started with the *GA*, with a population size of 250 *evolved* over 20 generations, and then switched to *SQP* which was set to run only once to obtain the final solution. The combined *GA-SQP* approach took approximately 15 minutes for each run.

Table 8.4: Comparison of objective function values

Damage cases	Objective function values ($X10^{-6}$)		
	SQP(best of 20 solutions)	GA	Combined *GA-SQP* algorithm
1	**0.015**	41.9	0.113
2	**0.036**	364.5	0.220
3	**0.067**	211.3	0.401
4	**0.005**	11.1	0.011
5	**0.001**	7.3	0.002
6	**0.030**	46.1	0.071
7	0.153	90.2	**0.110**
8	**0.004**	9.8	0.005
9	**0.012**	8.0	0.025
10	**0.065**	38.2	0.136

In Table 8.4, the minimum value of the objective function given by the three algorithms is highlighted in bold for each damage case. It is very clear that the errors in the GA are a few orders of magnitude (100 to 10,000) higher than the errors in the other two cases. The reason for the greater errors is due to its slow rate of convergence. Fig. 8.11(a) and 8.11(b) respectively show the progress of the convergence of the GA solution for the first 50 generations and the subsequent 50 generations. Note that, the scale of the objective function of the y-axis is different in Figs. 8.11(a) and 8.11(b). As seen in Fig. 8.11(a), the errors in the objective function drops rapidly in the first 15 to 20 generations from about $4X10^4$ to below 100. The rate of convergence in very slow for the next 70 iterations after which it again drops steeply to below 50 (see Fig. 8.11(b)). It is very likely that the GA permitted to run another 100 or 200 generations, will converge to a solution with errors of the same order as SQP and the combined algorithms. However, this would take 40 to 50 minutes more to provide a solution with the same accuracy as the other techniques.
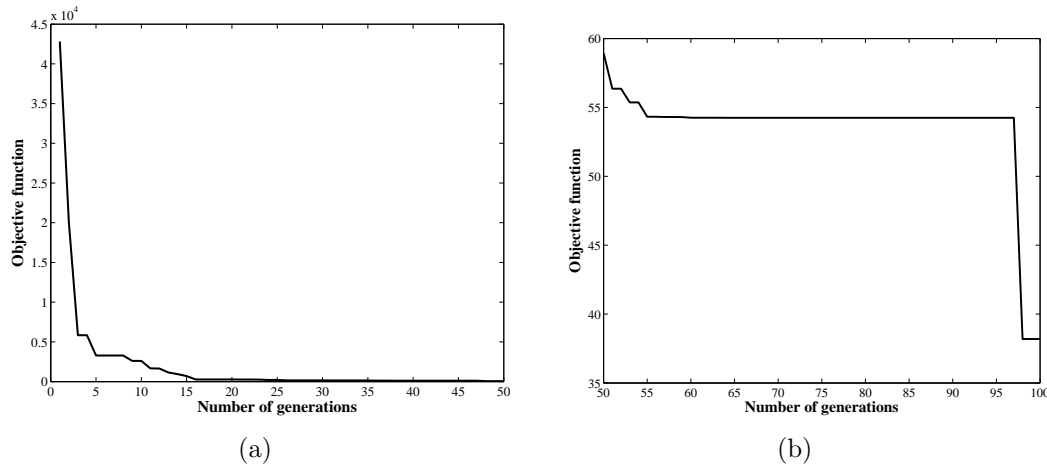

$$(a) \qquad\qquad\qquad (b)$$

Figure 8.11: Progress of convergence of the GA solution (a) for the first 50 iterations (b) for the next 50 generations

The difference in the errors from the SQP and the combined GA-SQP is small, however it is seen that SQP on its own provides better solutions in nine out of the ten cases (see Table 8.4). Only in case 7, the combined algorithm has offered a lower error. Therefore it was decided that stand-alone SQP will be employed for the solution of the inverse algorithm for the general case of the four variables.

8.6 Validation of detection algorithm for cracks with general orientation

As observed from the comparison of three minimisation algorithms applied to the three variable problem in Section 8.5, it was found that the SQP technique is the best for solution of the inverse problem. Hence, the general case of crack with an unknown orientation, wherein we now have four variables x_c, y_c, ϕ and γ to be estimated, the SQP algorithm is employed for the solution of the inverse problem. Ten different cases of simply-supported plates with cracks were modelled in $ANSYS$ using the same material properties ($Young's\ Modulus = 192.28GPa;\ density = 7808.4Kg/m^3$) and same dimensions ($L = 150mm,\ W = 100mm,\ h = 5mm$) as before. The normalised x and y coordinates ($\alpha_c = x_c/L,\ \beta_c = y_c/W$), the crack orientation (ϕ) and the normalised crack length ($\gamma = b/W$) for the ten cases modelled are listed in Table 8.5 along with the natural frequencies in the first 6 modes extracted from $ANSYS$. Note that in all cases, irrespective of the orientation of the crack, the crack length is normalised to the shorter side of the plate ($W = 100mm$). The frequencies of the undamaged plate are also listed in the table. Four of the ten cases (cases 1 and 2, and 9 and 10) have cracks parallel to the edges of the plate; however, their orientations are treated as unknown similar to the other cases, thus making the inverse problem a case of four variables.

Table 8.5: Crack parameters and natural frequencies of simply-supported plates with cracks of general orientation

Damage case	Normalised crack location $\alpha_c = x_c/L$	$\beta_c = y_c/W$	Orientation,ϕ (in degrees)	Normalised crack length, $\gamma = b/W$	Extracted natural frequencies Mode1	Mode2	Mode3	Mode4	Mode5	Mode6
Undamaged plate					1721.5	3310.4	5296.7	5958.5	6885.1	9532.3
1	0.25	0.25	90	0.05	1721.2	3308.5	5295.8	5956.3	6881.0	9528.0
2	0.25	0.25	90	0.10	1720.4	3302.4	5293.0	5948.9	6868.9	9514.1
3	0.25	0.30	60	0.15	1714.6	3289.6	5286.1	5944.3	6844.3	9484.6
4	0.25	0.30	60	0.20	1709.3	3273.9	5277.7	5932.0	6815.8	9449.0
5	0.35	0.25	30	0.05	1720.4	3310.0	5291.1	5957.9	6880.2	9532.0
6	0.35	0.25	30	0.10	1717.1	3308.8	5273.6	5955.8	6865.0	9530.8
7	0.40	0.25	30	0.05	1720.4	3310.3	5290.2	5956.9	6882.4	9529.2
8	0.40	0.25	30	0.10	1717.0	3310.1	5270.3	5951.8	6874.4	9518.8
9	0.25	0.40	0	0.15	1712.1	3292.5	5280.4	5947.8	6854.9	9516.2
10	0.25	0.40	0	0.20	1704.8	3279.0	5266.1	5939.9	6828.9	9500.6

The computed change in frequencies are employed along with the curvatures of the undamaged plate, to predict the x and y coordinates, size and orientation of the crack, using the *SQP* minimisation technique. The predicted damage parameters are presented in Table 8.6, for the ten cases along with their percentage variations from the actual values. Note that, in keeping with our previous practice, the errors in crack sizes and locations are calculated from their normalised values. The value of ϕ is also normalised by dividing it by 90° (the maximum value possible) for determining the normalised discrepancy in estimation of orientation of the crack, as explained in Section 5.5.1.

Table 8.6: Results from damage detection algorithm using *SQP* implemented on plates containing cracks oriented at different angles

Damage cases	Predicted crack parameters				Normalised Discrepancy			
	α_c	β_c	ϕ	γ	α_c	β_c	ϕ	γ
1	0.250	0.249	0.9	0.035	0.0	0.1	1.0	1.5
2	0.247	0.254	1.0	0.077	0.3	0.4	1.1	2.3
3	0.248	0.306	31.6	0.123	0.2	0.6	1.7	2.7
4	0.246	0.310	32.3	0.168	0.4	1.0	2.6	3.2
5	0.353	0.255	60.6	0.035	0.3	0.5	0.6	1.5
6	0.353	0.255	60.5	0.078	0.3	0.5	0.5	2.2
7	0.402	0.255	61.7	0.035	0.2	0.5	1.9	1.5
8	0.403	0.253	60.8	0.078	0.3	0.3	0.9	2.2
9	0.251	0.395	88.5	0.124	0.1	0.5	1.7	2.6
10	0.251	0.391	87.6	0.171	0.1	0.9	2.7	2.9

As seen from Table 8.6, the normalised discrepancy in crack location is <1% in all cases and the normalised discrepancy in the crack orientation is less than 3%. Also, the discrepancies in all four crack parameters are less (maximum $\sim 1.5\%$ in determining crack length) for damage cases 1 and 5 where the cracks are small ($\gamma = 5\%$ *of the plate width)* compared to the other cases. The maximum normalised discrepancy ($\sim 3\%$) is observed when crack length is 20% of the plate width (cases 4 and 10). Thus the trend of increasing normalised discrepancy with increasing crack size appears to be retained. The discrepancies in the predictions of the damage parameters for the four variable cases listed in Table 8.6 are of the same order as that obtained with the *SQP* algorithm, for the three variable cases of parallel cracks, shown in Figs. 8.8, 8.9 and 8.10 for cracks of comparable sizes.

The results in Fig. 8.4 (in Section 8.3) indicate that the magnitude of discrepancies increase with increasing number of modes employed in the damage detection algorithm. It was therefore concluded that lesser number of modes will provide greater accuracy. However, in implementing the SQP algorithm for the general case using only 4 modes (the minimum required for the solution for four variables), it was found that the solution often converged to other minima in the vicinity of the actual solution. The same was found to occur even when 5 modes were employed. When six modes were employed, the majority of the twenty iterations with random start points employed in the SQP algorithm converged to the actual solution providing the best accuracy. Thus, employment of six modes is a practical compromise between the occurrence of multiple minima with less number of modes and higher magnitudes of discrepancies in prediction with larger number of modes.

The ten results presented in this section were a few cases selected at random to investigate the applicability of the damage detection algorithm for the four variable case. Before conducting experiments, a study is conducted to establish the robustness of this vibration based damage detection technique by modelling cracks with a wider range of parameters. The results of this study are presented below.

8.6.1 Robustness analysis

For the robustness analysis, 9 crack locations (3 values for x_c and 3 for y_c), 4 orientations and 6 different crack sizes, totalling 216 damage cases were selected as shown in Table 8.7. The plate dimensions, boundary conditions and material properties are the same as used above. The inverse algorithm using SQP technique was employed to predict the four crack parameters in all 216 cases.

Table 8.7: Crack parameters used for analysis

| α_c	β_c	ϕ_c	γ_c
0.25	0.25	0	0.05
0.35	0.3	30	0.1
0.4	0.4	60	0.15
		90	0.2
			0.25
			0.3

The normalised discrepancies of the predicted values of the x and y coordinates, the crack orientation and the crack length for the 9 crack locations are plotted against the crack length for $\phi = 0°$, $30°$, $60°$ *and* $90°$ in Figs. F.1, F.2, F.3 and F.4 in Appendix F. It is apparent that the normalised discrepancies increase with increasing crack length, but no particular correlation between the errors and the locations of the crack is evident. The maximum normalised discrepancies in x_c, y_c, γ and ϕ are plotted against the crack orientation, ϕ, for crack lengths (b/W) equal to 0.1, 0.15 and 0.2, in Figs. 8.12(a), 8.12(b), 8.12(c) and 8.12(d) respectively. It is clear from these figures that the magnitudes of the normalised discrepancies increase with increasing crack size as expected, but it also appears that the discrepancies increase as ϕ increases from 0° to 90°, i.e., as the crack orientation moves from being parallel to the long side of the plate to being parallel to the short side. This may partly be an artefact resulting from the crack sizes being normalised with respect to the shorter edge of the plate. For the plate considered here, a crack of length 15mm $(\gamma = b/W = 0.15)$ will occupy 15% of the length of the short side of the plate if running parallel to it $(\phi = 90°)$, whereas it will occupy only 10% of the longer edge of the plate if oriented parallel to it $(\phi = 0°)$. Hence, the latter should have discrepancies of the same magnitude as a crack with $b/W = 0.1$ and $\phi = 90°$. While this is so in some cases, the increase in the magnitude of normalised discrepancies as the crack orientation passes over 45° is unexpected.
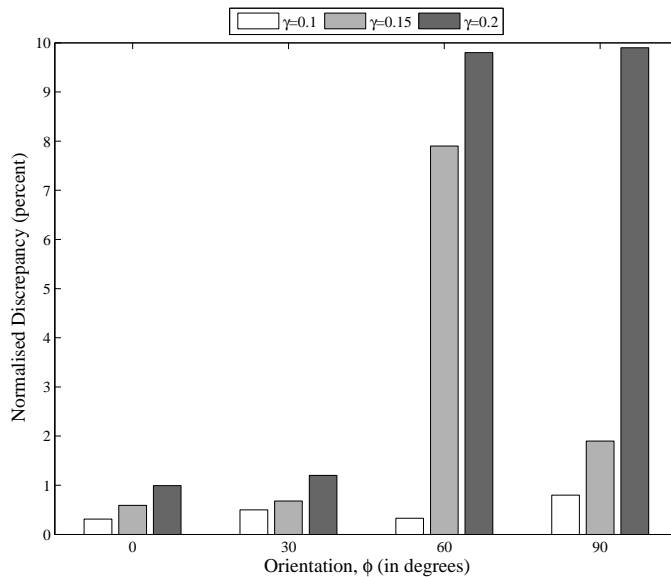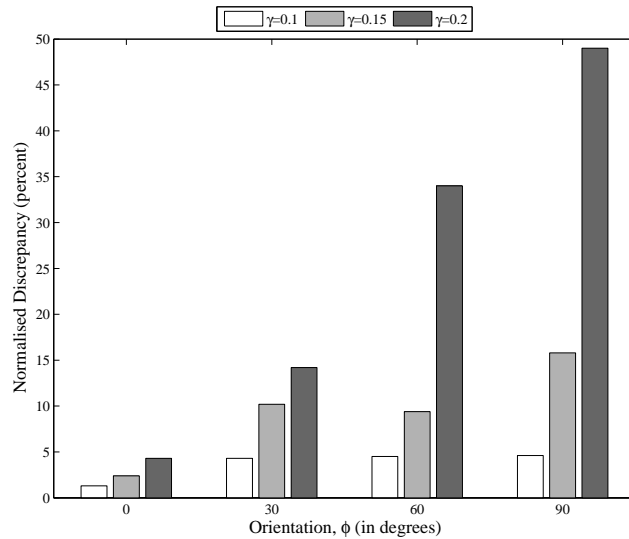

(a) Normalised discrepancies in estimating x coordinate of the crack
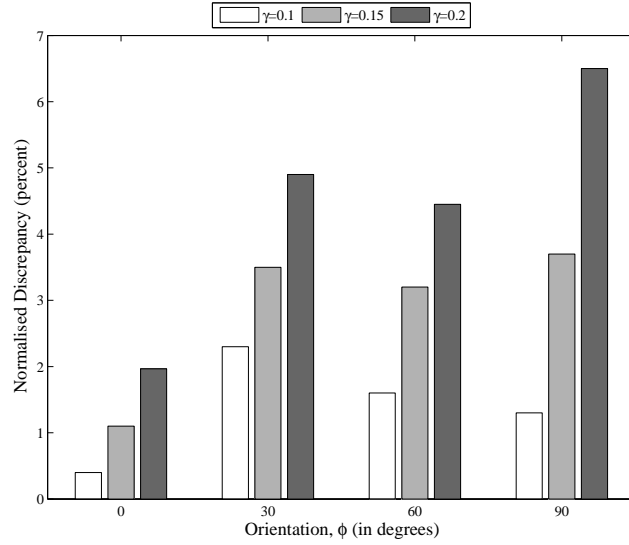
(b) Normalised discrepancies in estimating y coordinate of the crack
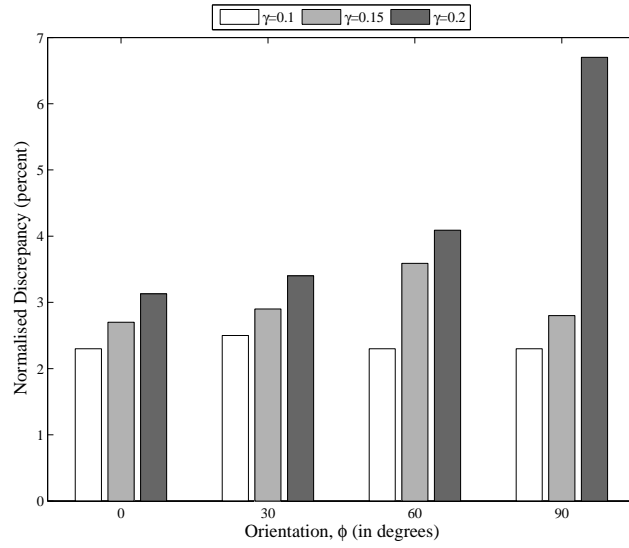
(c) Normalised discrepancies in estimating crack size

(d) Normalised discrepancies in estimating crack orientation

Figure 8.12: Maximum normalised discrepancies in crack parameters as a function of crack orientation, ϕ

163

8.7   Effect of finite widths of cracks

In the *FE* modelling presented in the previous sections, cracks were simulated by unstitching the nodes along their length thus having zero widths. This may be considered to be a good approximation of cracks in real structures generated by fatigue. However, for the experimental validation described in Chapter 9, the cracks were simulated by creating rectangular slots in the plates using a wire-cut *EDM* process. The wire-cut *EDM* process produced rectangular slots with finite widths ranging from 0.33mm to 1mm (see Section 9.3). Hence an analysis is conducted here to determine the effect of finite widths of cracks represented by rectangular slots.

Through-thickness cracks of different widths were incorporated in the *FE* model of the simply supported rectangular plate described in Section 8.2. All the cracks were positioned at the same location ($x_c/L = 0.3$, $y_c/W = 0.3$), had the same orientation, $\phi = 90°$ (parallel to the shorter edge of the plate) and the same crack size, $b/W = 0.1$ as in damage case 5 (Table 8.2). Seven cracks of finite slot widths ranging from 0.5mm to 3.5mm with 0.5mm increments were modelled using rectangular slots. A crack of zero width was modelled by unstitching the nodes along the crack length as described earlier. The frequencies obtained from *FEA* of these plates with cracks were employed in the inverse algorithm using the *SQP* minimisation technique for estimating all four crack parameters. The normalised discrepancies between the predictions from the damage assessment methodology and the actual crack parameters modelled are shown in Table 8.8 for the eight cases of crack widths ranging from zero to 3.5mm.

It can be seen that the crack locations are predicted accurately with discrepancies < 2.5% and are more or less independent of the width of the crack. The crack modelled with zero width has 2.2% discrepancy in the predicted crack size and under 5.6% discrepancy in crack orientation. However, the discrepancies in predicted crack size as well as crack orientations increase with increasing crack widths. It can, therefore, be inferred that modelling the cracks as rectangular slots of finite width either in numerical simulation or in experiments has a detrimental effect on the accuracy of the predictions and the normalised discrepancies increase with increasing width of the slots.

Table 8.8: Results obtained from modelling cracks as *EDM* slots (FEA)

	Normalised discrepancy			
	α_c	β_c	ϕ	γ
Zero width crack	1.29	0.7	5.53	2.15
Slot width=0.5mm	1.81	0.61	7.76	3.48
Slot width=1mm	1.89	0.61	8.18	3.85
Slot width=1.5mm	2.03	0.63	8.74	4.13
Slot width=2mm	2.1	0.65	9.55	4.39
Slot width=2.5mm	2.17	0.74	10.09	4.62
Slot width=3mm	2.27	0.7	10.96	4.86
Slot width=3.5mm	2.35	0.75	11.93	5.07

Actual crack parameters:
$\alpha_c = 0.3$, $\beta_c = 0.3$, $\phi = 90°$, $\gamma = 0.1$

8.8 Conclusion

In this chapter, the damage detection methodology was validated using numerical simulation on plates with cracks. Three different minimisation techniques for solving the inverse algorithm, *SQP*, *GA* and combination of the two, were compared with the least square method employed previously for beams and were seen to be better. Amongst the three, the *SQP* method comprising 20 iterations starting from 20 random initial estimates was found to be the most efficient in terms of accuracy over computational time. A study of the linearity between the frequency change and normalised curvature showed that the use of higher modes leads to greater discrepancy for larger cracks. However, using the minimum number of modes required for the algorithm leads to multiple minima. The use of six modal values for predicting the four unknown variables for the case of crack oriented in a general direction in the plate was found to give the best compromise in terms of accuracy and reliable convergence to the global minimum.

A parametric study of 216 models were conducted to investigate the robustness of the damage detection methodology. It is clear from the results that the algorithm predicts the damage size and location with less than 5% normalised discrepancy for crack sizes below $0.15W$ and the crack orientation under 15%. Noting that cracks in structural components with sizes over $b/W = 0.15$ will normally be visible to the naked eye and will not require the use of damage detection technique, the high accuracy of the proposed method for detecting small cracks is very encouraging. It

should be observed that accuracy in estimation of crack orientation is not critical as long as the crack location and size can be predicted accurately.

In the next chapter, the efficacy of the damage detection technique for plates is investigated experimentally.

CHAPTER 9

Application of damage detection methodology to plates - Experimental validation

9.1 Introduction

This chapter presents the practical implementation of the damage detection methodology to two dimensional structures (plates). Experimental Modal Analysis *(EMA)* is conducted on aluminium alloy plates with asymmetric boundary conditions, *viz.* simply supported along two adjacent edges and free along the other two edges *(SS-SS-F-F)*. Through-thickness cracks were machined into the plates at different locations using a wire-cut *Electric Discharge Machining (EDM)* process. Fourteen damage cases were examined and their natural frequencies in the first eight modes measured experimentally. The undamaged *SS-SS-F-F* plate was modelled numerically to extract the natural frequencies and modeshapes. Modeshapes extracted from both numerical analysis and experiments are employed in the solution to the inverse problem to predict the locations, sizes and orientations of the cracks. The damage parameters predicted by theory are compared to the actual parameters of the cracks in the specimens tested. An analysis is conducted to examine the sensitivity of the proposed technique and to establish the *Minimum Detectable Crack (MDC)* size in plates.

9.2   Finite Element Modelling

In the numerical simulation described in the previous chapter (Chapter 8), the plates were modelled with simple support boundary conditions on all sides. For the experimental validation here, the plates were tested in *SS-SS-F-F* conditions. For the purpose of comparison with the experimental data and the predictions by the proposed theory, the undamaged *SS-SS-F-F* plate was also modelled in *FEA*. The natural frequencies for the first eight modes of the undamaged plate obtained from numerical modelling are presented in Table 9.2 in the following section. The modeshapes of the undamaged plate in the first eight modes were also extracted from *FEA* for subsequent use in the damage detection algorithm, and are shown in Figs. 9.1(a) - 9.1(h).

9.3   Experiments - Groundwork

EMA was conducted on plates made of aluminium alloy *(Al 7075-T6)*. The plates for the different damage cases were cut from the same sheet. The average thickness of the whole sheet, measured at various points, was 3.18mm. The plates were 449mm long and 299mm wide. Two thin strips of width 50mm and lengths 220mm and 195mm were cut from the same sheet to determine its material properties. The Young's Modulus was obtained by measuring strains in bending, in a manner similar to that described for beams in Section 6.2. The average Young's Modulus was $67.96GPa$ and the density $2759.95Kg/m^3$.

The plates tested were simply supported along two adjacent edges while the other two were free *(SS-SS-F-F* boundary condition*)*. A schematic of the plate with its boundary conditions is shown in Fig. 9.2. Simulating simply-supported boundary conditions can be easily accomplished in beams using knife-edge supports but knife edge support alone on one side of the plate will constrain movement in the direction perpendicular to that edge to have a constant slope. Whereas, a proper simple-support along the edge of a plate should constrain only the deflection and curvature to zero but allow rotation in the perpendicular direction to vary along the edge (allowing for twist to be non-zero along that edge). This cannot be accomplished with a knife-edge support. Some researchers have used test rigs where the plate
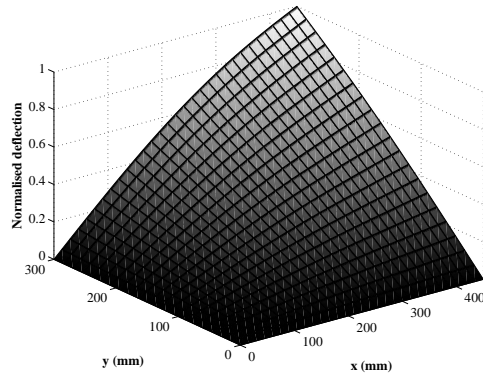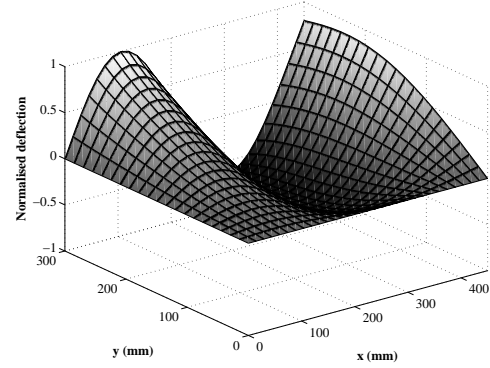
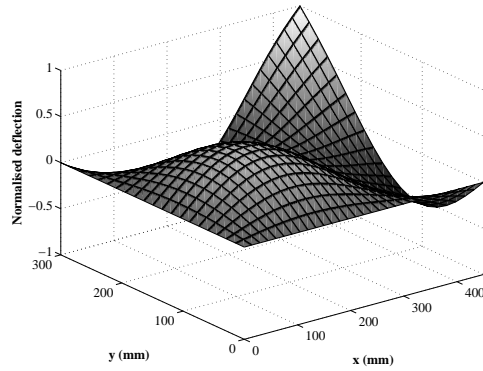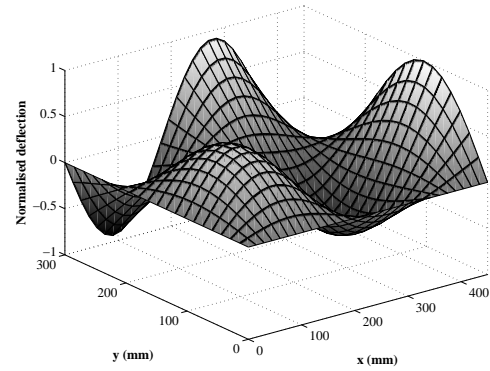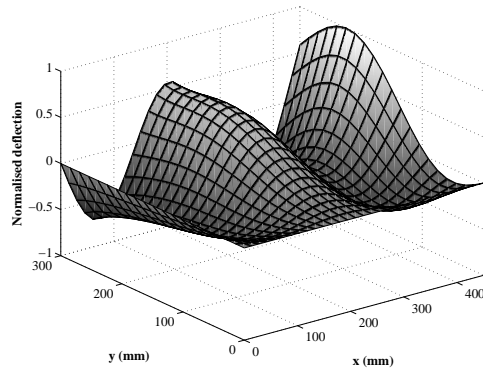(a) Mode1   (b) Mode2
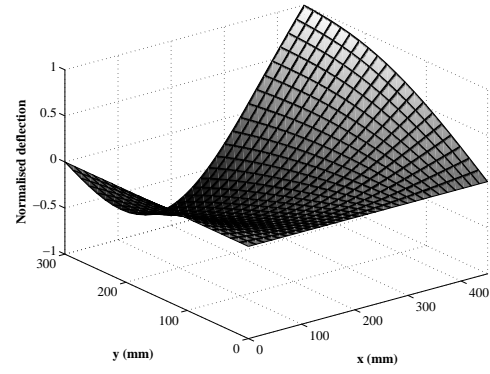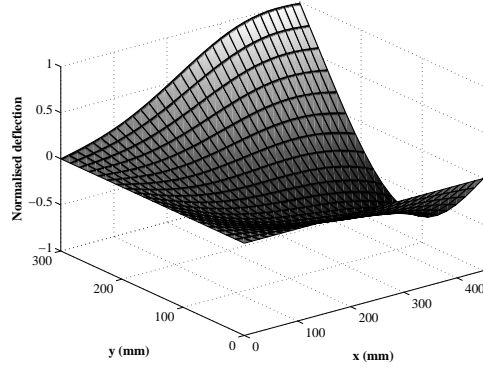
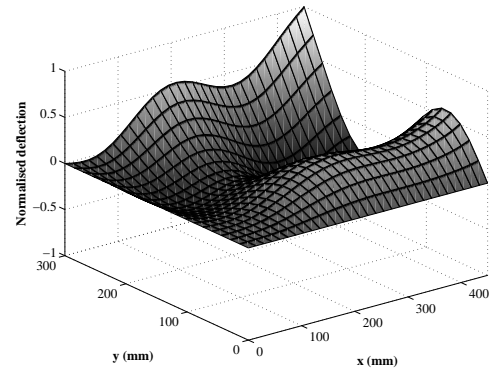(c) Mode3   (d) Mode4

(e) Mode5   (f) Mode6

(g) Mode7   (h) Mode8

Figure 9.1: Modeshapes of *SS-SS-F-F* plate extracted from *FEA*

169

edges are inserted into sand [194, 195]. One major disadvantage of this technique is that the sealing of the sand between the rig and the plate makes the repeatability of *exactly* the same boundary conditions difficult to achieve. In such cases, it is also difficult to measure the effective dimensions of the plate.
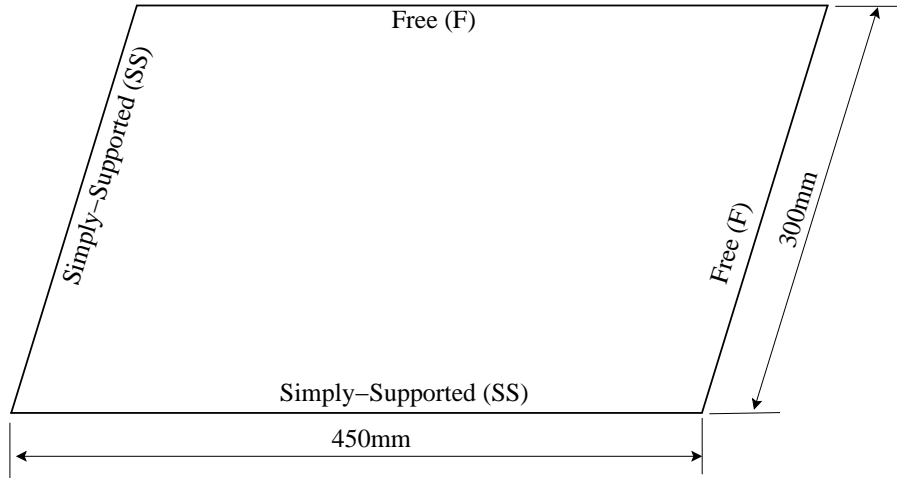

Figure 9.2: Schematic of the plate and boundary conditions
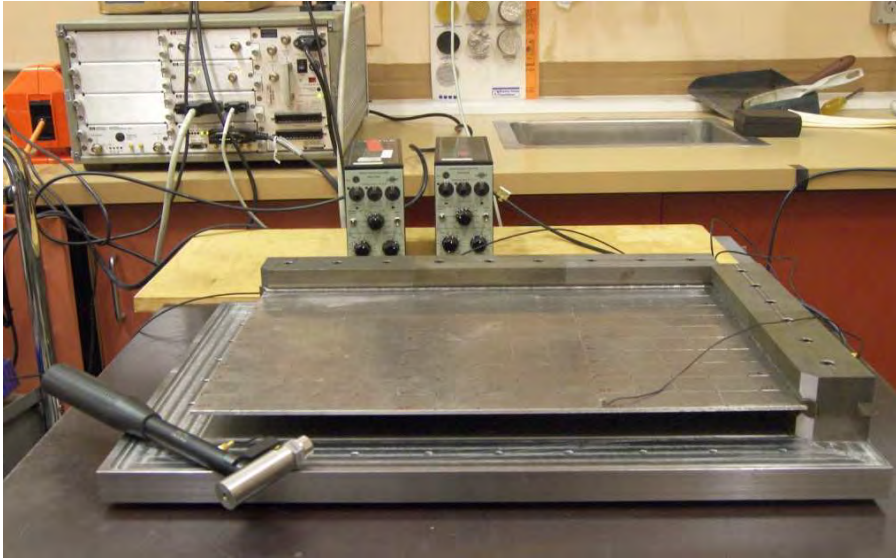
Figure 9.3: Experimental set-up showing test rig and plate

In the present study, simple support allowing for variation of slope along the supported edge is implemented using short cylindrical buttons as reported in [196]. A special test rig was designed and manufactured to provide simple support along two edges in this manner as shown in the photograph in Fig. 9.3. A schematic of the mechanism to provide simple support along the edge is shown in Fig. 9.4. The edge of the plate was fitted tightly into the rectangular slots in cylindrical buttons

(approximately 13mm diameter and 6 mm long), component 2 in Fig. 9.4. Fig. 9.4(b) schematically shows the possible rotation of the plate normal to the supported edge within individual buttons. About 75 cylindrical buttons were employed along the long edge and around 50 along the shorter simply-supported edge. When the plate bends in vibration, the deflection along the supported edges of the plate will remain zero but allow for varying gradients perpendicular to the edges. Detailed drawings of the test rig are shown in Appendix G.
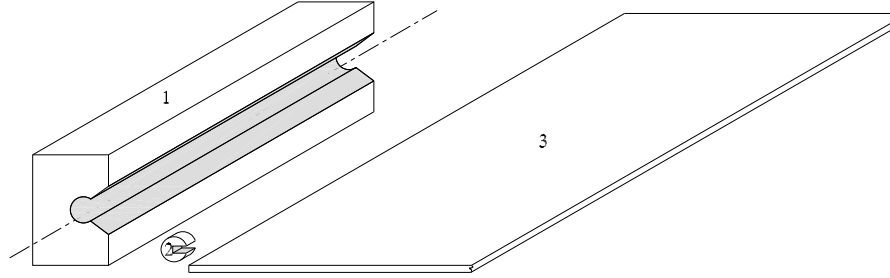
(a)
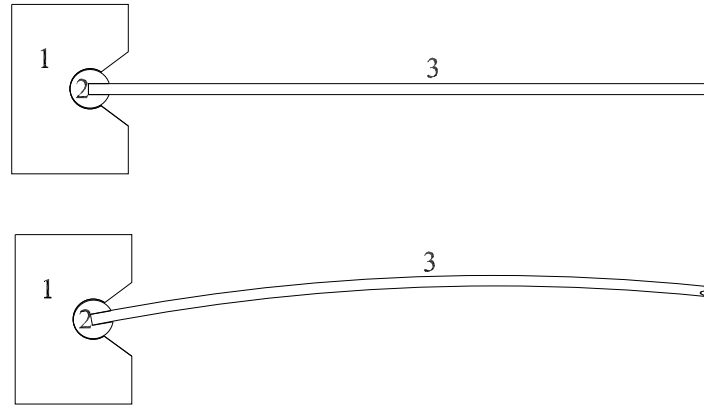
(b)

Figure 9.4: Schematic of mechanism for simple support (1. Sleeve, 2. Cylindrical button, 3. Test plate)

EMA was conducted on five rectangular plates containing through thickness cracks representing fourteen different damage cases. The locations, orientations and sizes of the cracks for these fourteen cases are listed in Table 9.1. α_c and β_c are the normalised crack coordinates ($\alpha_c = x_c/L$; $\beta_c = y_c/W$) and γ is the normalised crack size ($\gamma = b/W$). *EMA* was conducted on the plates before introducing damage to measure the actual frequencies of the undamaged structure. Subsequently,

rectangular slots were machined in the five plates using wire-cut *EDM* process to represent through-thickness cracks at the damage locations. Initially a 1 mm diameter hole was drilled at the location of the mid-point of the crack and a 0.25mm dia. wire was introduced into this hole for the *EDM* process to create rectangular slots (see Fig. 9.5) representing cracks with predetermined lengths corresponding to the initial lengths (cases 1, 3, 5, 13 and 14) for each location and orientation in Table 9.1. The slots created by the 0.25mm dia. wire had widths between 0.33mm and 0.4mm.

Table 9.1: Damage cases employed for experimentation on plates

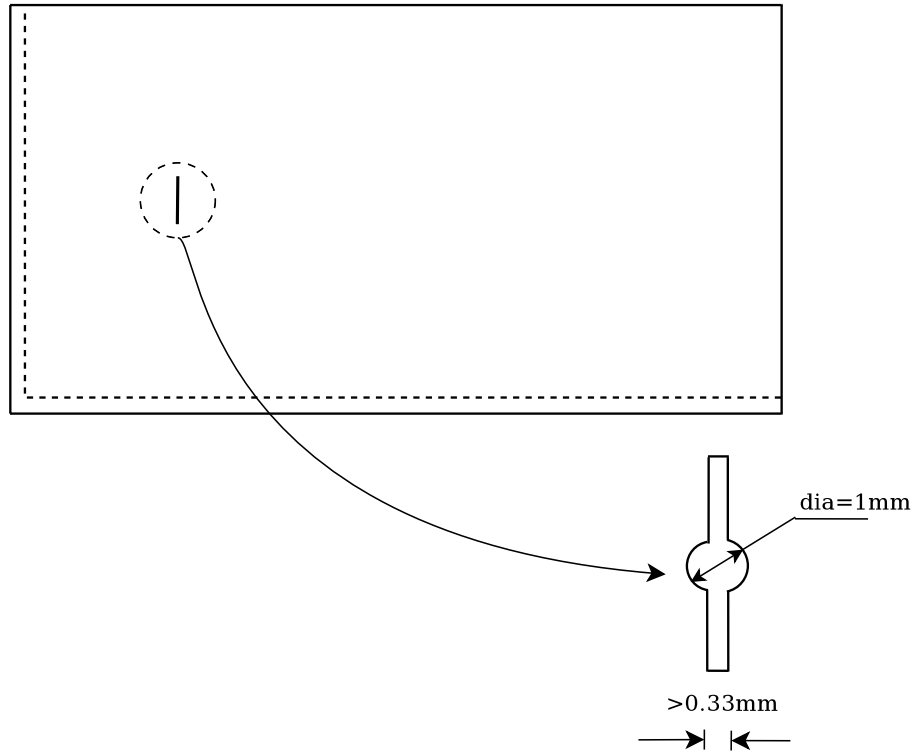| Damage case	Crack parameters			
	Location		Orientation,	Normalised
	α_c	β_c	ϕ (degrees)	length, γ
1	0.3	0.3	90	0.07
2	0.3	0.3	90	0.1
3	0.3	0.3	90	0.15
4	0.3	0.3	90	0.2
5	0.3	0.3	60	0.07
6	0.3	0.3	60	0.1
7	0.3	0.3	60	0.15
8	0.3	0.3	60	0.2
9	0.3	0.3	30	0.07
10	0.3	0.3	30	0.1
11	0.3	0.3	30	0.15
12	0.3	0.3	30	0.2
13	0.2	0.6	60	0.1
14	0.5	0.4	60	0.1

Figure 9.5: Simulation of cracks using wire-cut *EDM* process

For extraction of the natural frequencies, the plates were excited using an impact hammer (*B&K*8202) at one location and the accelerations were measured using a *B&K*4374 miniature accelerometer at another location. The locations of the excitation and the measurement point were selected on the basis of modal analysis using numerical modelling so as to avoid nodal points of deflection. From the modeshapes extracted from *FEA* described in the previous section, it was determined that both the corner between the free edges and a point 150mm along longer free edge, as shown in Fig. 9.6, had non-zero deflections for the first ten modes of vibration. Hence one of these points (the inner point) was chosen as point of excitation and the other (the corner point) as the point of measurement.

The natural frequencies of the undamaged plate extracted from experiments for the first eight modes are compared with those obtained from vibration theory [186] and *FE* Modelling using *ANSYS* in Table 9.2. The experimental values presented in the table are averages of 5 measurements on each of the five undamaged plates. It can be seen from the table that the agreement between measurements and predictions by *FEA* and theory are quite good with differences of less than 2.4% in the former and less than 4.1% in the latter case.
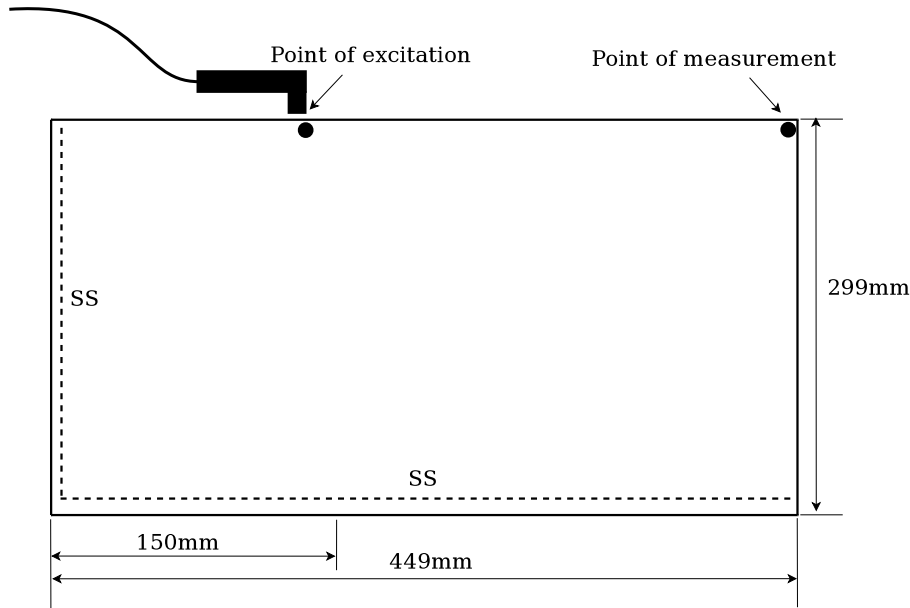
Figure 9.6: Experimental set-up showing points of excitation and response measurement

Table 9.2: Comparison of natural frequencies of undamaged *SS-SS-F-F plate*

Mode	Natural frequencies (Hz)			Difference between measurements and *FEA* (%)	Difference between measurements and theory (%)
	Measurements	FEA	Theory		
1	18.94	18.78	19.18	0.81	1.29
2	78.98	80.88	82.21	2.42	4.09
3	139.68	142.41	143.96	1.96	3.06
4	210.21	209.28	211.78	0.44	0.75
5	228.87	230.1	232.35	0.54	1.52
6	380.06	375.37	379.33	1.23	0.19
7	418.68	411.49	419.61	1.72	0.22
8	439.71	438.59	439.85	0.26	0.03

Once the natural frequencies of the undamaged plates were extracted, through-thickness cracks were introduced in the 5 plates as described above and *EMA* was conducted to determine the natural frequencies in the damaged state. The length of the cracks in three of the plates (cases 1, 5 and 9) were progressively increased to obtain cracks of increasing sizes for the remaining damage cases. The progressive increment of the length of the rectangular slots to represent cracks with larger sizes sometimes resulted in an increase in the slot width, in some cases upto a maximum of 1mm due to machining limitations. The measured frequencies in the first eight modes for the fourteen damage cases are tabulated in Table 9.3.

Table 9.3: Natural frequencies of undamaged plate and all damage cases

Damage case	Mode1	Mode2	Mode3	Mode4	Mode5	Mode6	Mode7	Mode8
UC	18.94	78.98	139.68	210.21	228.87	380.06	418.68	439.71
1	18.66	78.72	139.52	209.80	226.29	376.73	418.10	439.11
2	18.46	78.51	139.39	209.56	224.98	374.67	417.93	439.00
3	18.38	78.40	139.15	208.89	222.71	371.59	417.73	438.44
4	18.24	78.14	138.90	208.47	219.69	367.65	417.08	437.82
5	18.62	78.75	139.44	209.98	226.03	376.52	418.12	439.44
6	18.54	78.65	139.35	209.81	224.85	374.64	417.82	439.34
7	18.47	78.56	139.25	209.66	223.28	373.01	417.54	439.13
8	18.35	78.40	139.02	209.31	220.20	369.61	416.74	438.70
9	18.77	78.72	139.22	209.88	225.39	376.69	418.03	438.73
10	18.65	78.67	139.01	209.79	223.87	375.35	417.75	438.40
11	18.56	78.54	138.72	209.68	222.15	374.25	417.43	437.86
12	18.46	78.45	138.29	209.52	219.60	372.96	416.29	437.32
13	18.76	78.80	139.00	208.80	226.40	378.62	413.93	438.00
14	18.73	78.51	138.96	209.45	226.90	377.92	416.66	437.95

UC→ Undamaged Case

9.4 Implementation of the damage detection algorithm

It was shown in Section 6.5 that one of the advantages of the proposed *hybrid* technique is that we require only the modeshapes of the undamaged (or the damaged) structure for implementation of the damage detection algorithm. Further, the modeshapes for this purpose could be extracted either from numerical modelling or from measurements on the structure. In the following subsections, the damage parameters are estimated from the measured changes in frequencies using modeshapes from *FEA* and modeshapes measured on the actual structure. It may be observed that only approximate solutions for the calculation of the analytical modeshapes for plates with *SS-SS-F-F* boundary conditions are available in literature [155], hence theoretical modeshapes were not employed for damage assessment. Note that the solution to the inverse problem is obtained using the *SQP* algorithm as it was seen to be the most efficient for minimisation (see Section 8.5).

9.4.1 Damage assessment using modeshapes from FEA

Normalised deflections were extracted from *FEA* over 600 points on the surface of the plate for the first eight modes as shown in Fig. 9.1(a) - 9.1(h). These were used to calculate the curvature terms as described in Section 8.5. In implementing

the *SQP*, the search space for the unknown variables has to be defined. In the damage detection of simply-supported plates using simulated data, in Chapter 8, quarter symmetry was employed for defining the search space for the locations. Since the modeshapes in the present case are not symmetrical due to the asymmetric boundary conditions, the computations are carried out over the whole plate. The range for the normalised x and y locations of the crack is 0 to 1, the range for orientation is 0° to 90° and that for normalised crack lengths is 0 to 0.5. The normalised x and y coordinates (α_c and β_c), crack orientation (ϕ) and the normalised crack size (γ) obtained from the inverse algorithm using modeshapes from *FEA* are shown in Table 9.4. The percentage differences between the predicted parameters and actual values are also shown. From the figures listed, it can be seen that the crack locations and sizes for the fourteen cases are determined reasonably accurately (within 9%). However, it may be observed that the normalised discrepancies in predicting the crack parameters using experimentally measured frequency changes (Table 9.4) are, in general, higher than the normalised discrepancies obtained in the solution of the inverse algorithm in the previous chapter using data from *FE* simulation for simply-supported plates (Table 8.6). This may partly be attributed to the inaccuracies in measurement of frequencies and perhaps partly to the more complex boundary conditions used in the experiments. In particular, the normalised discrepancies in the cracks sizes predicted in the experiments are higher than those in the numerical simulation. The finite widths of the rectangular slots simulating cracks in the experiment may have partly been responsible for this discrepancy since the crack sizes are determined from fracture mechanics theory which considers cracks to have sharp crack tips. The normalised discrepancy between the orientation of the crack and its actual value is higher in most cases, with a maximum of 35% in case 1. It was observed that normalised discrepancies in predictions of the crack orientations were also high in the previous chapter where data from numerical simulation was employed for damage assessment.

The results in the Table 9.4 were obtained using data from six modes, from mode 3 to mode 8. It was noted in the previous chapter that using six modes helps to avoid the occurrence of multiple minima while maintaining the discrepancies to a minimum. The results of the inverse algorithm obtained using modes 1 to 6, 2 to

Table 9.4: Normalised damage parameters predicted with measured frequencies from modes 3 to 8 and modeshapes from *FEA*

Damage	Predicted crack parameters				Normalised discrepancy			
cases	α_c	β_c	ϕ	γ	α_c	β_c	ϕ	γ
1	0.31	0.28	31.83	0.14	1.2	2.4	35.4	7.0
2	0.30	0.31	22.63	0.16	0.2	1.4	25.1	6.3
3	0.29	0.38	7.20	0.20	1.4	8.4	8.0	5.2
4	0.29	0.35	15.31	0.25	0.9	5.2	17.0	4.6
5	0.30	0.31	32.39	0.13	0.3	0.9	2.7	6.7
6	0.30	0.31	29.89	0.16	0.1	0.8	0.1	6.3
7	0.30	0.31	30.74	0.19	0.3	0.8	0.8	4.0
8	0.30	0.31	32.36	0.23	0.3	1.2	2.6	3.3
9	0.32	0.29	44.13	0.14	2.0	0.7	17.6	7.7
10	0.32	0.31	44.60	0.17	1.5	0.8	17.1	6.9
11	0.32	0.31	47.68	0.19	1.7	1.1	13.7	4.2
12	0.31	0.32	51.12	0.22	1.5	2.4	9.9	1.9
13	0.23	0.59	25.16	0.14	3.0	1.3	5.4	4.3
14	0.50	0.38	29.00	0.15	0.2	2.4	1.1	4.9

7, 1 to 8 and 2 to 8 are shown in Appendix H. The use of data from modes 1 and 2 provided highly inaccurate results (See Tables H.1, H.2, H.3 and H.4 in Appendix H) and much better accuracies were obtained for the majority of the cases when modes 3 to 8 were employed as shown above. This is possibly due to the noise in the data and difficulty in measuring frequencies accurately in the lower order modes. It may be noted that the *SIF* for infinite plate (obtained from Zehnder and Hui [174, 175]) is employed for the determination of the crack lengths.

9.4.2 Damage assessment using modeshapes from experiments

In this section, modeshapes measured experimentally are employed for damage assessment from the measured changes in frequencies. The modeshapes were measured at 150 points on the surface of the plate and the data was smoothed using spline interpolation for implementation in the *SQP* minimisation technique for solution of the inverse problem. The modeshapes measured from the undamaged plate as well as three of the damaged plates *(Damage cases 8, 12 and 14)* are employed separately in order to verify whether measurements made on the damaged plate are as good as those from the undamaged plate in predicting the damage parameters.

The x and y coordinates of the damage location, crack size and crack orientation predicted using modeshapes from the undamaged plate and from damage cases 8, 12 and 14 are plotted along with the predictions using modeshapes from *ANSYS* in Figs. 9.7, 9.8, 9.9 and 9.10 respectively.
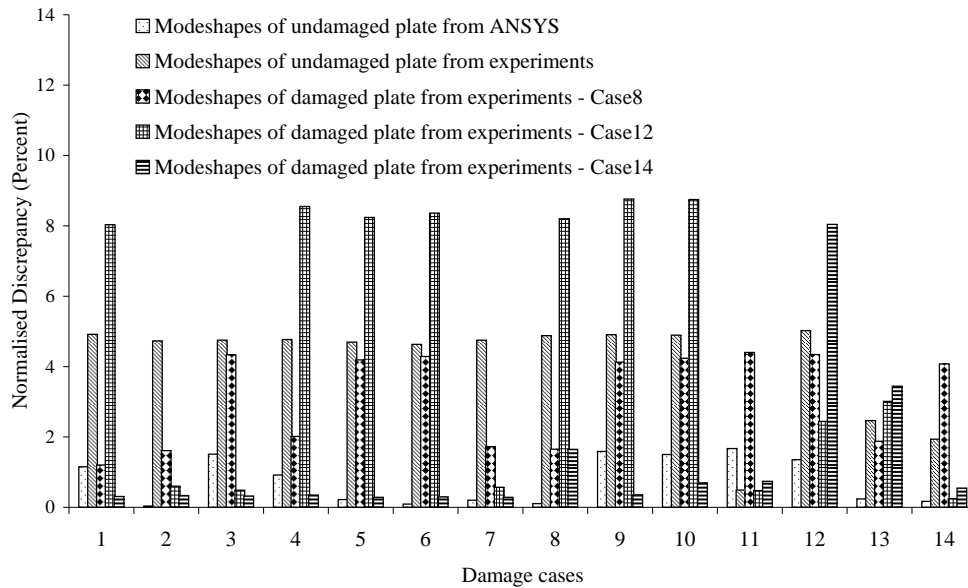
Figure 9.7: Normalised discrepancies in location of damage (x-coordinate) using modeshapes from experiments and *FEA*
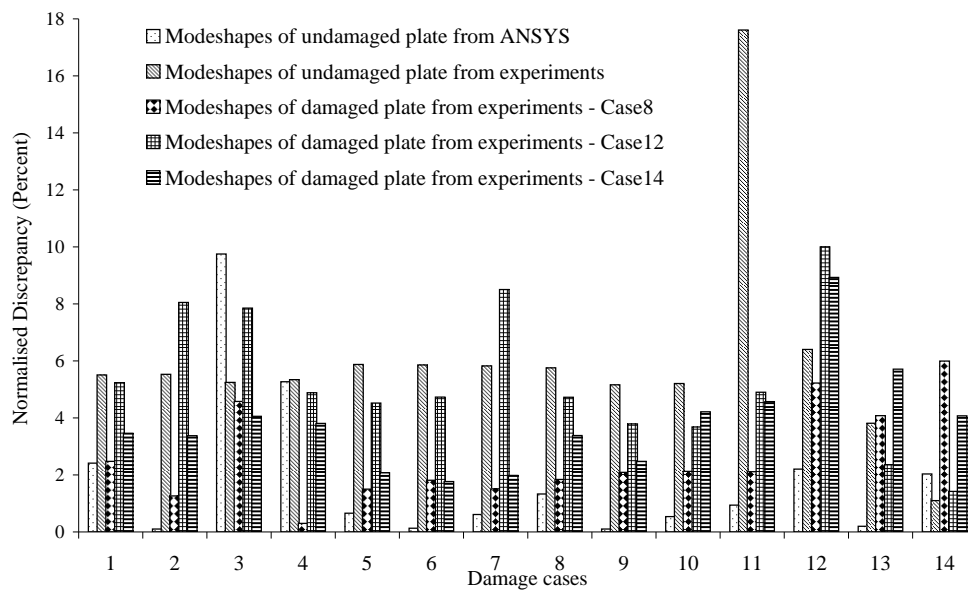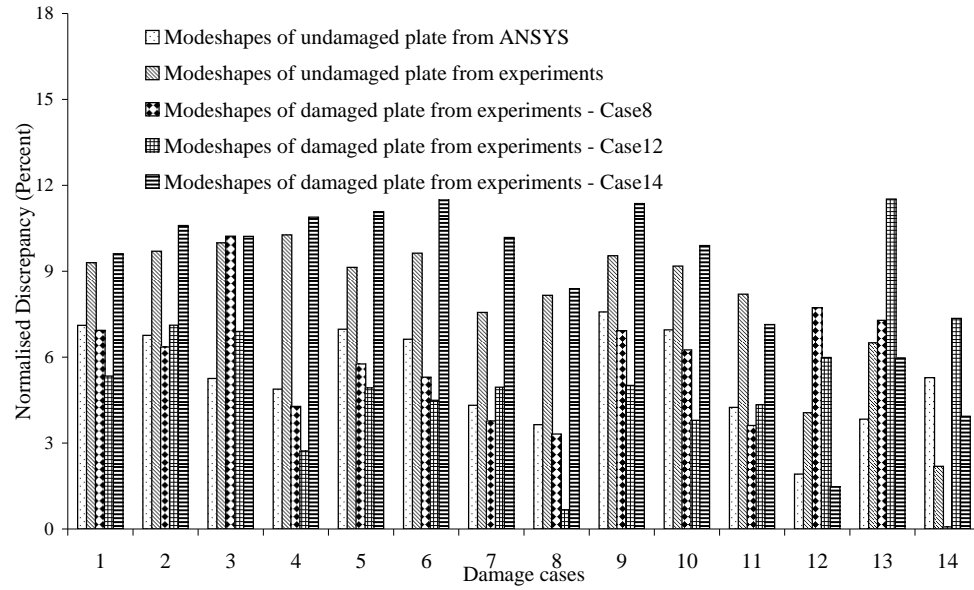

Figure 9.8: Normalised discrepancies in location of damage (y-coordinate) using modeshapes from experiments and *FEA*

Figure 9.9: Normalised discrepancies in determining crack length using modeshapes from experiments and *FEA*
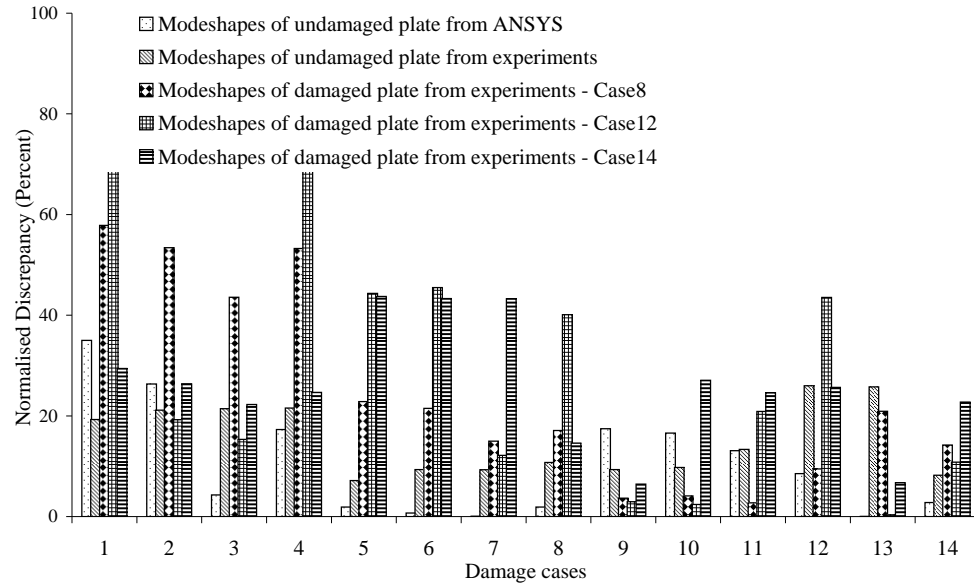
Figure 9.10: Normalised discrepancies in determining crack orientation using mode-shapes from experiments and *FEA*

From the plots, it can be seen that the modeshapes measured experimentally do not produce results as accurate as those obtained with modeshapes from *AN-SYS*. This is to be expected due to the noise that would be present in the measured data and inaccuracies arising from actual boundary conditions and limitations of the experimental set-up. However, the normalised discrepancies in the predictions obtained with measured modeshapes are still of the same order as those obtained with modeshapes from numerical modelling. Further, the predictions obtained with modeshapes from plates with damage are comparable to each other as well as those obtained with modeshapes measured on the undamaged plate. In fact, the worst discrepancy in damage location is obtained when modeshape measurements from the undamaged case is employed (Damage case 11 in Fig. 9.8). This may be the effect of the location of the damage. It is also to be noted that the assessment of the damage parameters obtained using measured frequency changes (with modeshapes from *FEA* or experiments) are prone to higher discrepancies than assessment made using natural frequencies from numerical simulations as in the previous chapter. This may be attributed partially to uncertainties in measurements and experimental procedures compared to numerical simulation but may also be partly due to the finite width of the slots representing cracks in the plates tested (see Section 8.7). In general, however, it may be concluded that measurements made on the actual structure can be successfully employed to predict the location and size of the damage with reasonable accuracy. The discrepancies in the predictions of the crack orientations are much higher than those of the other damage parameters in all cases whether modeshapes from experiments or *FEA* are employed. This again follows the trend that was seen in the numerical validation of the damage detection algorithm presented in the previous chapter.

9.5   Effect of scatter in the measurement of frequencies

The results presented above for the 14 damage cases show much higher normalised discrepancies in the damage parameters predicted by the inverse algorithm using measured frequency changes than in the case of numerical simulation. It was mentioned that the higher discrepancies could partly be attributed to the uncertainties in the measurement of the frequency values. Though great care was taken to ensure the repeatability of measurements by designing the special test rig, the frequency values of both the undamaged and damaged plates varied in each trial on the same plate. To take into account these variations, the frequencies were measured 5 times on each plate and the mean value was used in the damage detection algorithm. The dispersions of the measured natural frequencies are shown for the first eight modes in Figs. 9.11(a) -9.11(h) respectively. The mean frequency values for the undamaged plate and the 14 damage cases are plotted in the figures along with scatter bars of magnitude equal to the standard deviations above and below.

(a) Mode 1

(b) Mode 2

(c) Mode 3

(d) Mode 4

(e) Mode 5   (f) Mode 6

(g) Mode 7   (h) Mode 8
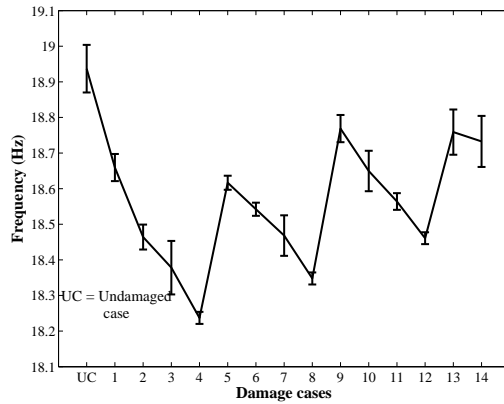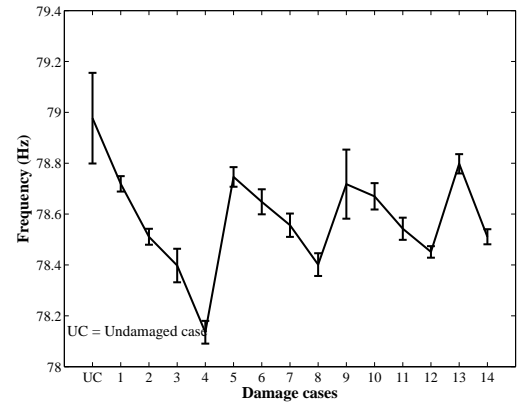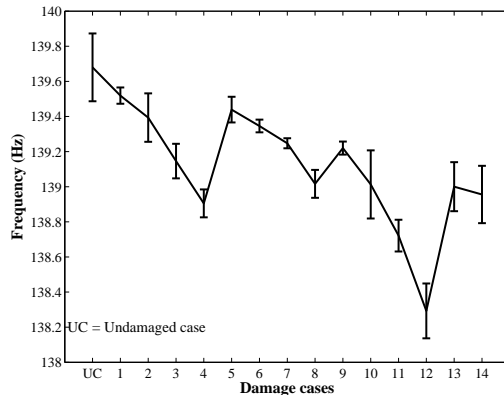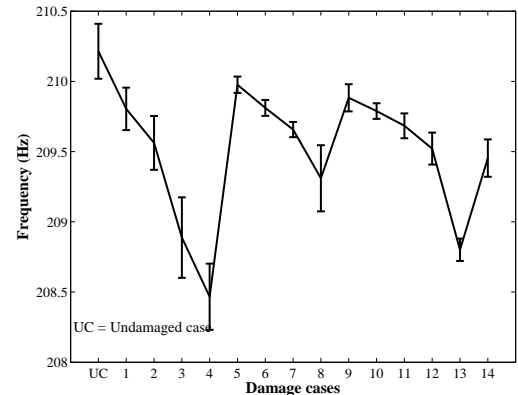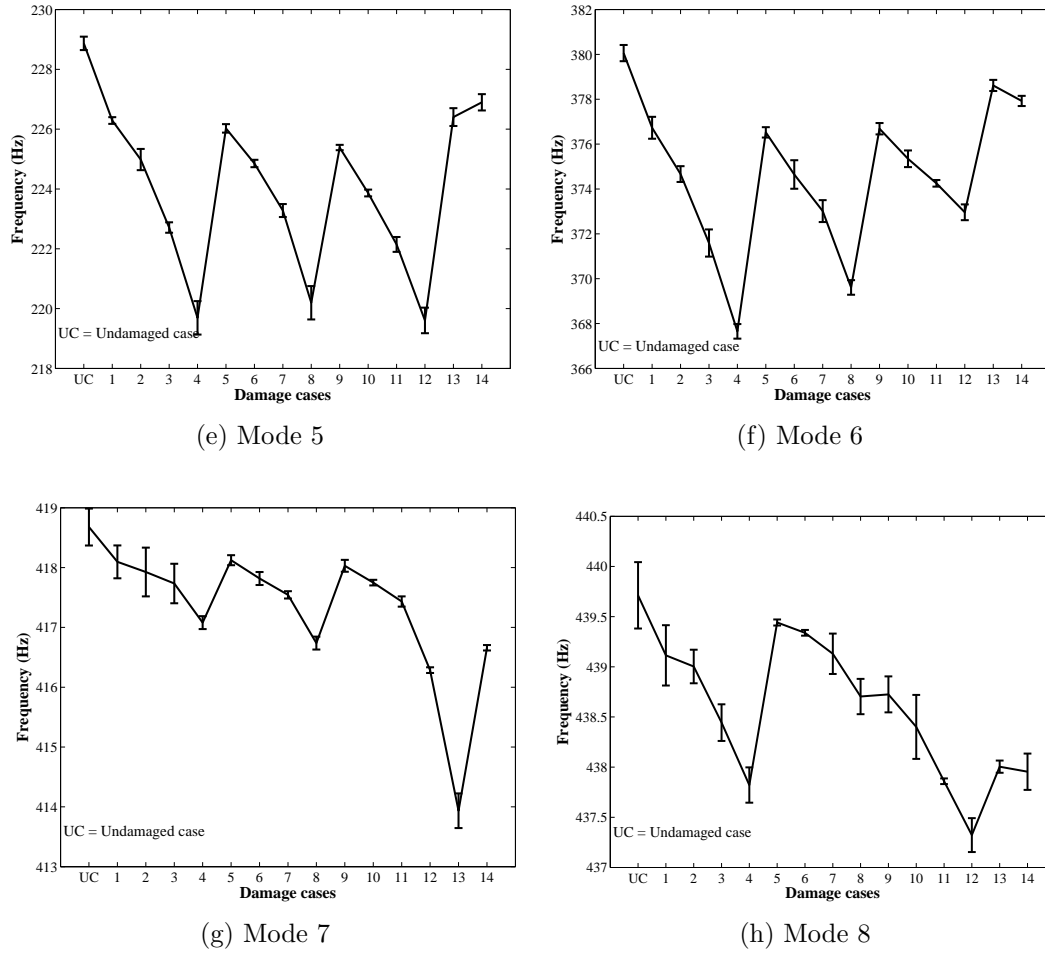
Figure 9.11: Scatter in the measurement of natural frequencies for all damage cases

It may be observed that the scatter in the frequency values of the undamaged plate are higher. This is possibly due to the fact that these values were obtained from 5 trials on 5 different plates. In most cases, the frequencies of the damaged plate are separated from the deviations of the undamaged plate. Even in cases where the scatter bars of the natural frequencies of the damaged plates overlap with those from either the undamaged plate or other damage cases, the discrepancies in the predictions of the crack location are small (see Table 9.4). This is perhaps because variations in the natural frequencies of one of the modes are compensated for by the more accurate extraction of the frequencies in other modes. With such variations in the natural frequencies, cracks as small as 7% of the plate width were still detected with reasonable accuracy. Since no smaller cracks were employed in the experimentation, a sensitivity analysis is performed to determine the *Minimum Detectable Crack size (MDC)*, similar to that conducted for cracks in beams (Section 7.6), which is described below.

9.6 Sensitivity Analysis

The sensitivity of the damage detection algorithm for plates is assessed in a manner similar to that conducted for beams by first performing a statistical analysis to determine the "90/95" probability of crack detection. The 90/95 lower limits are then used in the plots of frequency changes *vs* crack size obtained from *FEA* to determine the minimum detectable crack size.

9.6.1 90/95 probability of crack detection for plates

As explained in Section 7.5, from the normal distributions of the frequency measurements of the undamaged plates, we can determine the minimum crack size above which 90% of the frequency measurements on the undamaged plate are expected to fall with 95% confidence level. The 90/95 lower limits determined in this manner from the measured frequencies of the undamaged plates are listed in Table 9.5 for the first eight modes. The differences between the mean values and 90/95 lower limits and their percentage values are also shown. As in the case of beams, when a frequency lower than the 90/95 lower limit is measured in any mode on a plate, we can consider this to indicate the existence of a crack with 90% probability and 95% confidence.

Table 9.5: Minimum changes in frequency for detection of crack with 90% probability and 95% confidence level

Mode	Mean frequency, μ	90/95 lower limit frequency, f_L	$\mu - f_L$	$\frac{\mu - f_L}{\mu}(\%)$
1	18.94	18.87	0.07	0.37
2	78.98	78.82	0.16	0.20
3	139.68	139.47	0.21	0.15
4	210.21	209.99	0.23	0.11
5	228.87	228.68	0.19	0.08
6	380.06	379.73	0.32	0.09
7	418.68	418.39	0.29	0.07
8	439.71	439.41	0.30	0.07

9.6.2 Minimum detectable crack size (MDC) for plates

The dependency of the change in frequencies due to damage on crack parameters was established for three different damage locations and three different crack orientations

183

providing a total of nine cases as listed in Table 9.6. Plates with cracks of varying sizes ranging from $b/W = 2.5\%$ to $b/W = 27.5\%$ were modelled in *ANSYS* for the nine damage cases and their frequencies determined by numerical modal analysis. The changes in frequencies between the damaged and undamaged plates in the first eight modes are plotted for damage cases 1 to 9 in Figs. 9.12(a) - 9.12(i) respectively.

Table 9.6: Damage cases used to find *MDC*

Damage cases	α_c	β_c	ϕ
1	0.3	0.3	90
2	0.3	0.3	60
3	0.3	0.3	30
4	0.2	0.6	90
5	0.2	0.6	60
6	0.2	0.6	30
7	0.5	0.4	90
8	0.5	0.4	60
9	0.5	0.4	30

$2.5\% \leq \gamma \leq 27.5\%$

Noting that the difference between the mean and the 90/95 lower limit listed in column 4 of Table 9.5 is the minimum change in frequency required to be recorded for a reliable indication of the presence of damage, these values are employed in the above plots to calculate the minimum size of the crack that can be detected in each mode for each damage case. These are shown in Figs. 9.13(a) - 9.13(i) respectively for damage cases 1 to 9. Each vertical line in Figs. 9.13(a) - 9.13(i) represents the value of the minimum detectable crack size in a particular mode for that damage case. These are listed in Table 9.7. The minimum of the values listed in each column in Table 9.7 represents the actual *Minimum Detectable Crack size (MDC)* for that damage case. These are listed in the last row in the table. The *MDC* is 4.7% of the width for damage case 4 and 8% for damage case 8. It may be noted that as in the case of beams, the *MDC* is a function of crack location and orientation as well as the boundary conditions of the plate. Again, as in the case of beams, the *MDC* arises out of different modes for different damage cases. Hence it is useful to look for changes in frequencies in as many different modes as possible when inspecting for damage.

Table 9.7: Minimum detectable crack size

	Minimum crack size detectable (normalised)								
	Case 1	Case 2	Case 3	Case 4	Case 5	Case 6	Case 7	Case 8	Case 9
Mode1	0.300	0.195	0.199	0.300	0.185	0.196	0.300	0.192	0.199
Mode2	0.158	0.155	0.222	0.109	0.097	0.138	0.126	0.235	0.300
Mode3	0.206	0.146	0.106	0.224	0.300	0.300	0.160	0.125	0.077
Mode4	0.195	0.300	0.252	0.059	0.066	0.118	0.105	0.080	0.084
Mode5	*0.057*	*0.054*	*0.049*	0.076	0.111	0.108	0.100	0.088	*0.069*
Mode6	0.064	0.071	0.076	0.113	0.119	0.114	0.096	0.109	0.116
Mode7	0.237	0.244	0.300	*0.048*	*0.063*	0.121	*0.063*	*0.082*	0.145
Mode8	0.223	0.171	0.111	0.088	0.080	*0.077*	0.107	0.134	0.127
MDC	*0.057*	*0.054*	*0.049*	*0.048*	*0.063*	*0.077*	*0.063*	*0.080*	*0.069*

9.7 Conclusion

In the preceding sections it was demonstrated that the proposed damage detection methodology based on frequency measurements can be successfully employed to detect cracks in plates. The practical application of the method was experimentally validated for 14 different damage cases in *SS-SS-F-F* plates with crack sizes ranging from 7% to 20% of the width of the plate. It was shown that using the *SQP* technique for the solution of the inverse algorithm, the damage location and size can be estimated with reasonable accuracy although not to the same degree as that obtained in numerical simulation. The discrepancies in predictions of the crack orientations are larger but it may be considered that accurate determination of crack orientation is not as critical as determination of crack location and size. A significant contribution in this chapter is the demonstration that modeshapes measured experimentally either on the damaged or undamaged structure can be successfully employed for the estimation of the damage parameters. This eliminates the need to resort to theoretical analysis or numerical modelling for application of this damage detection method. A statistical analysis based on the measured natural frequencies was performed to determine the 90/95 lower limits in each mode which were employed together with *FE* data to determine the minimum detectable crack size. Note that the magnitudes of the *MDC*s are dependant on the scatter in the measured frequency values. For the *SS-SS-F-F* plate, the lowest value of the *MDC* was found to be 4.8% and the highest was 8%.
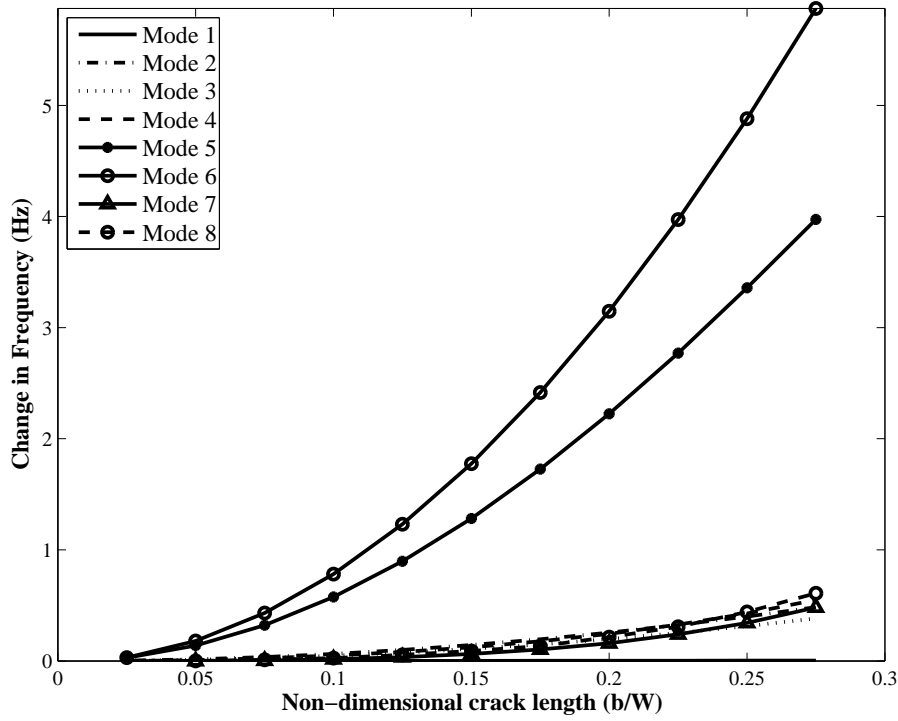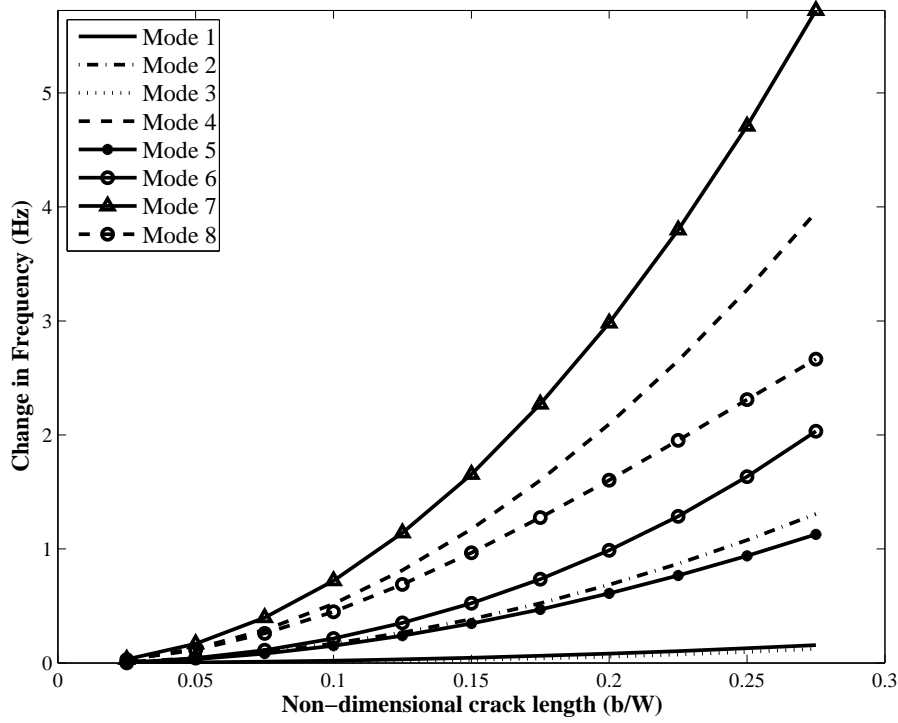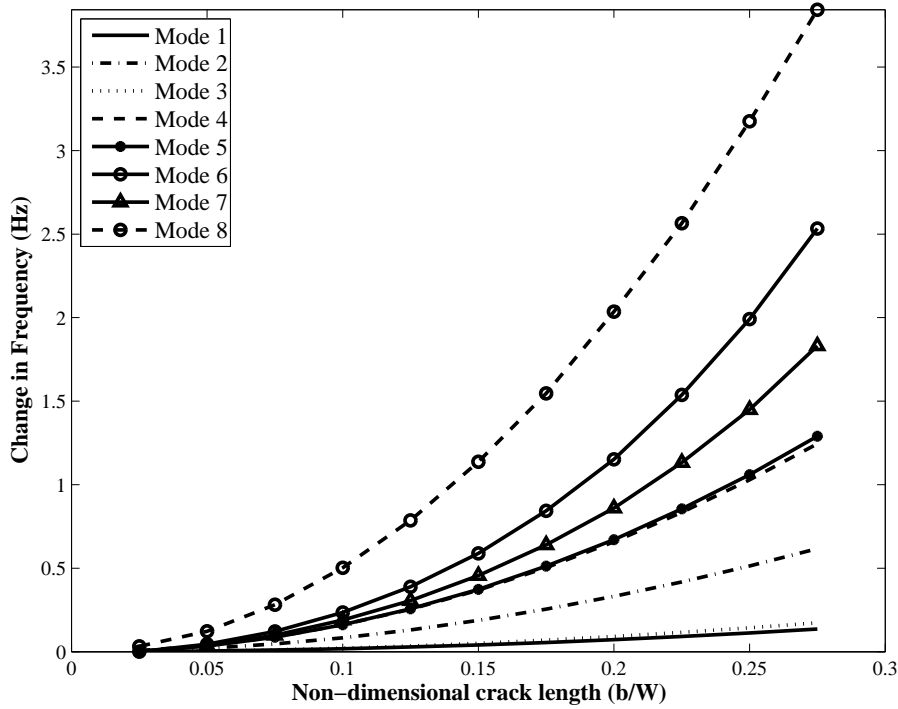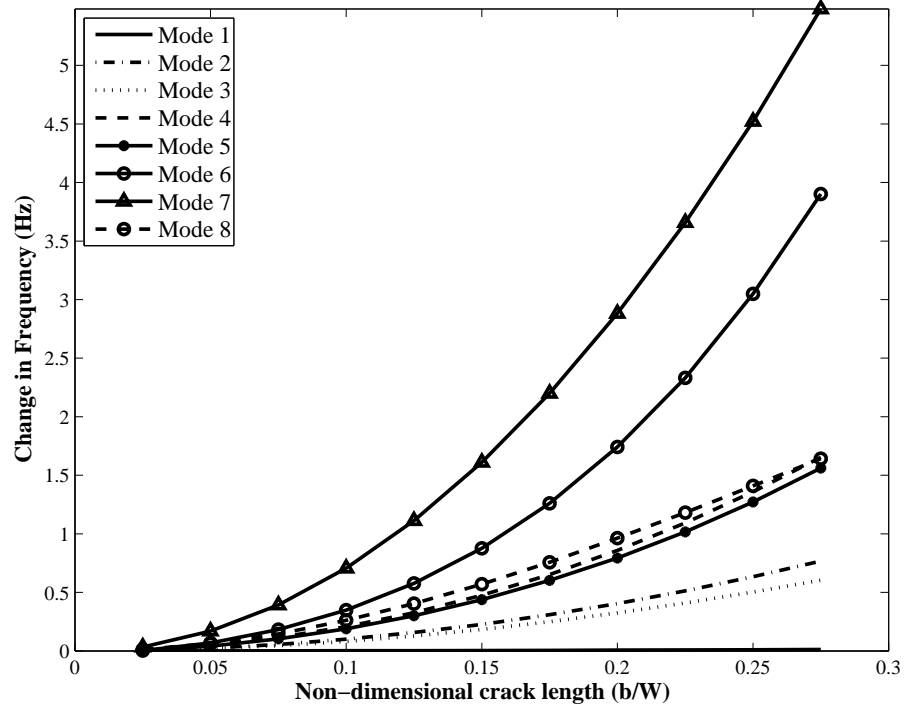
(a) Damage case1
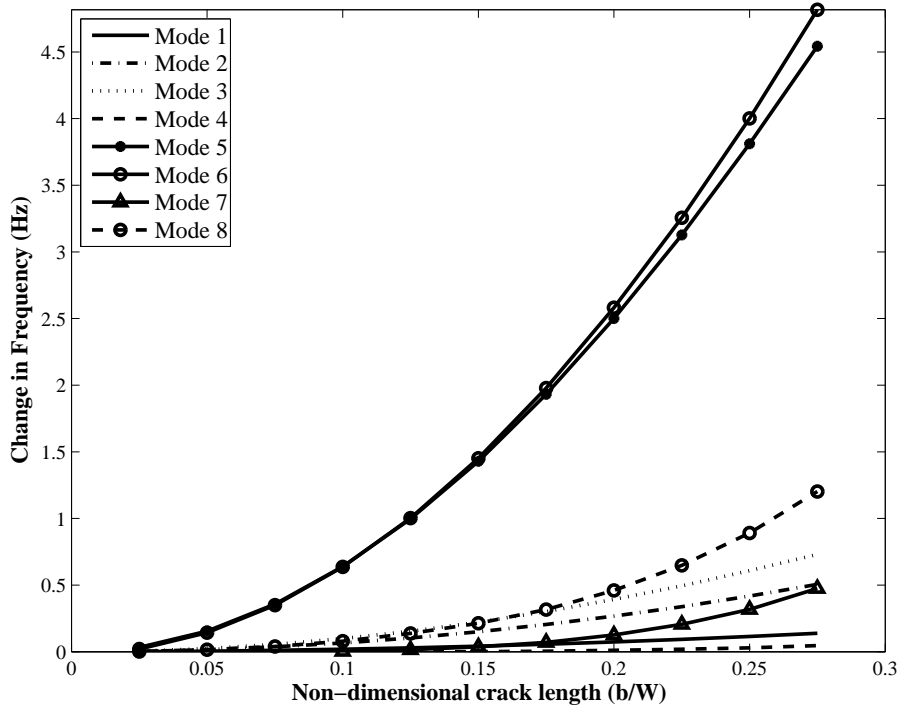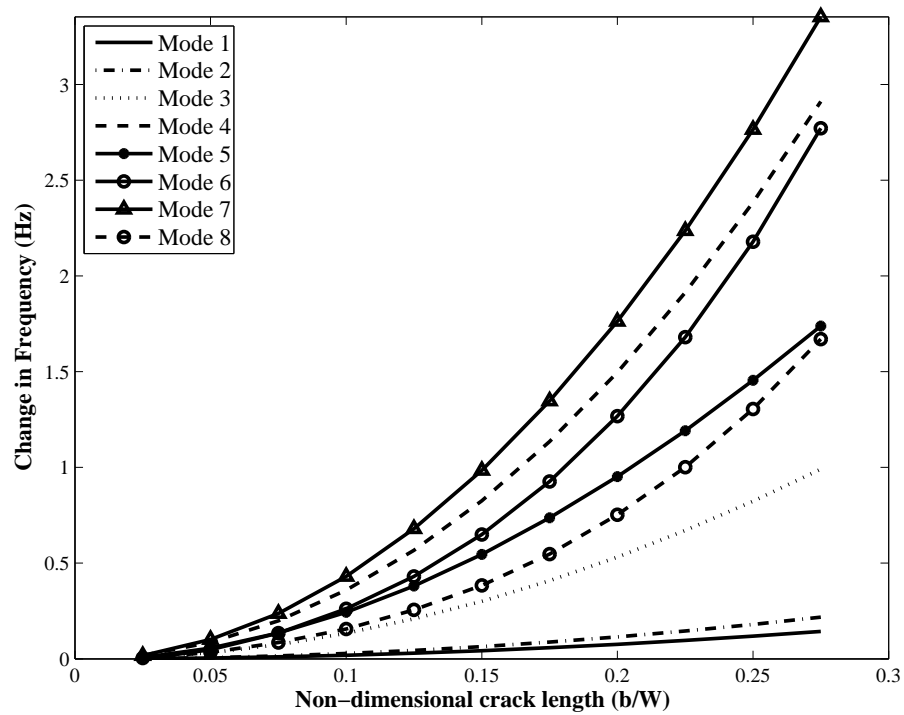

(b) Damage case2

(c) Damage case3

(d) Damage case4

187

(e) Damage case5

(f) Damage case6

(g) Damage case7
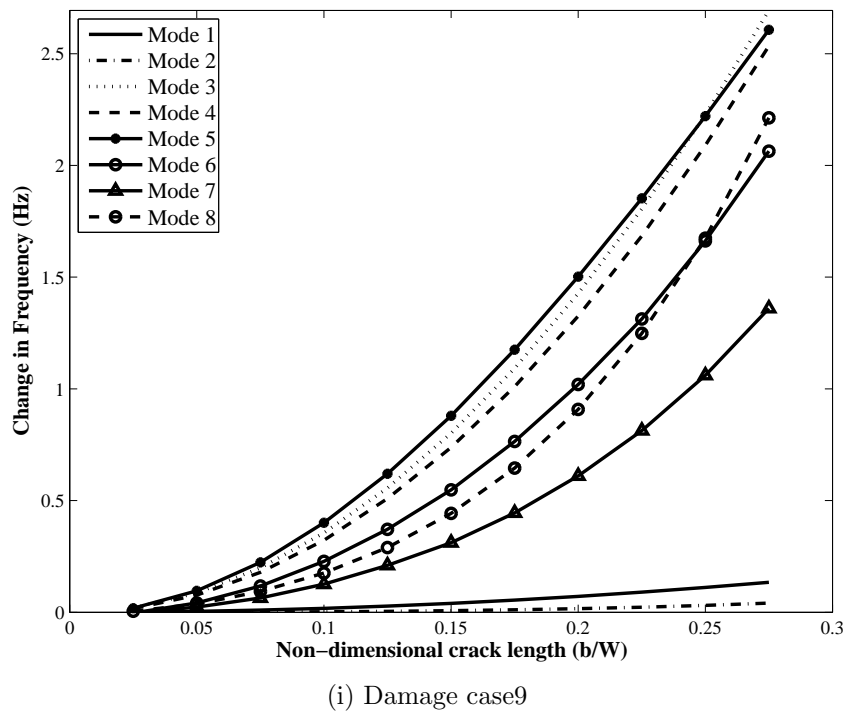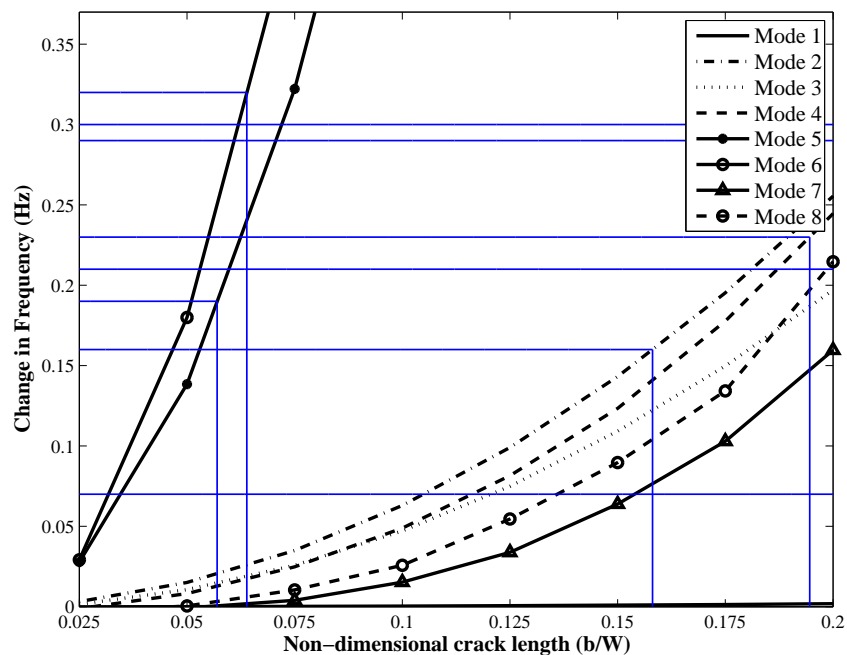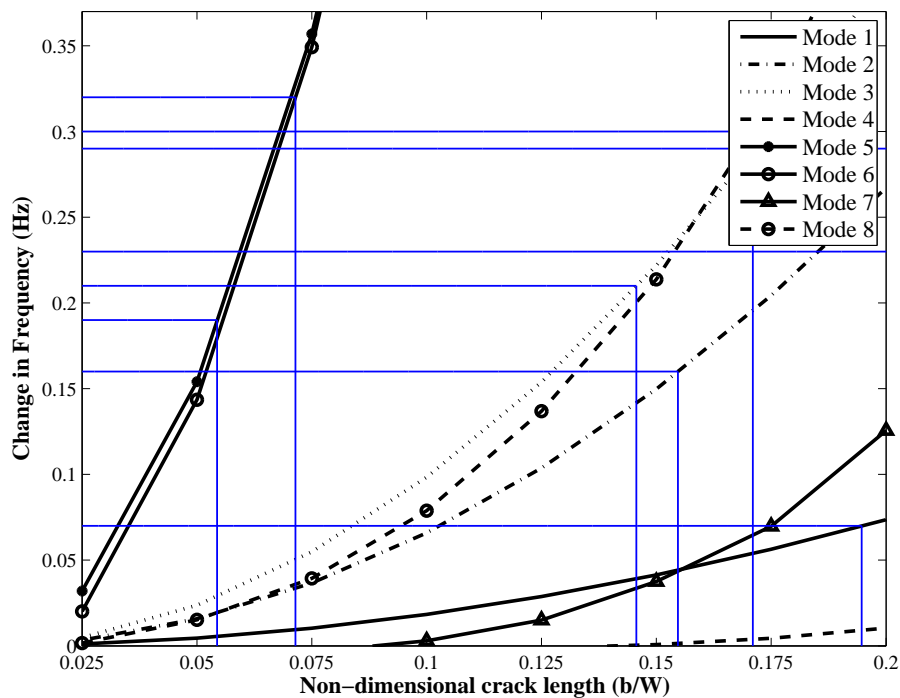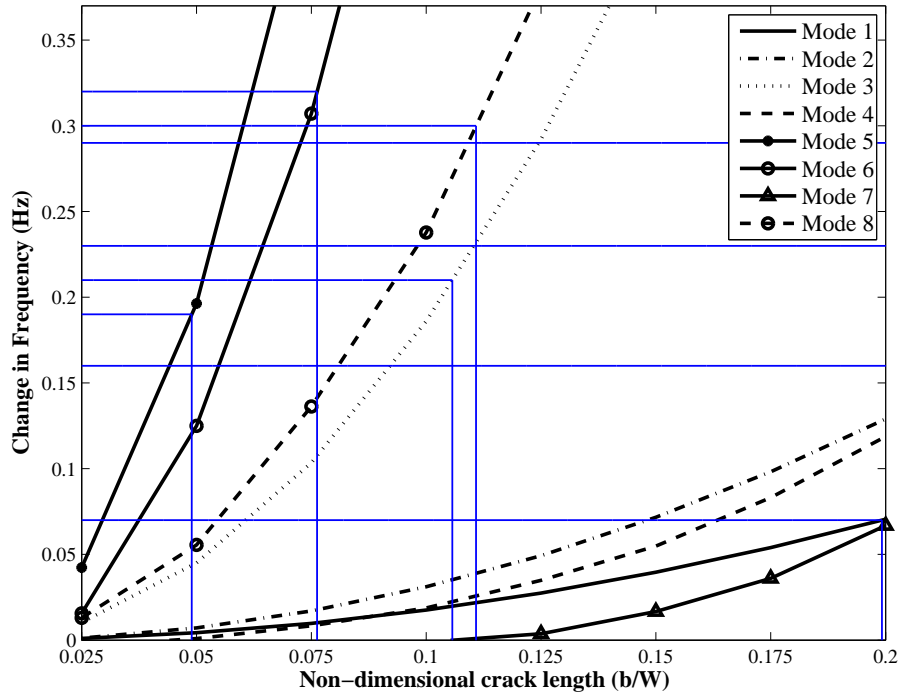

(h) Damage case8

189

(i) Damage case9

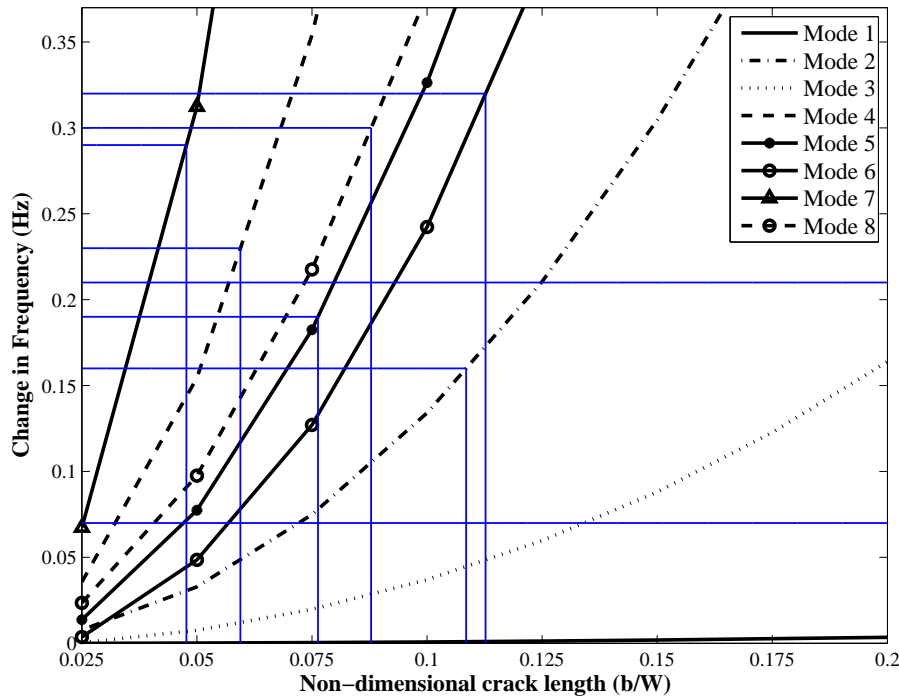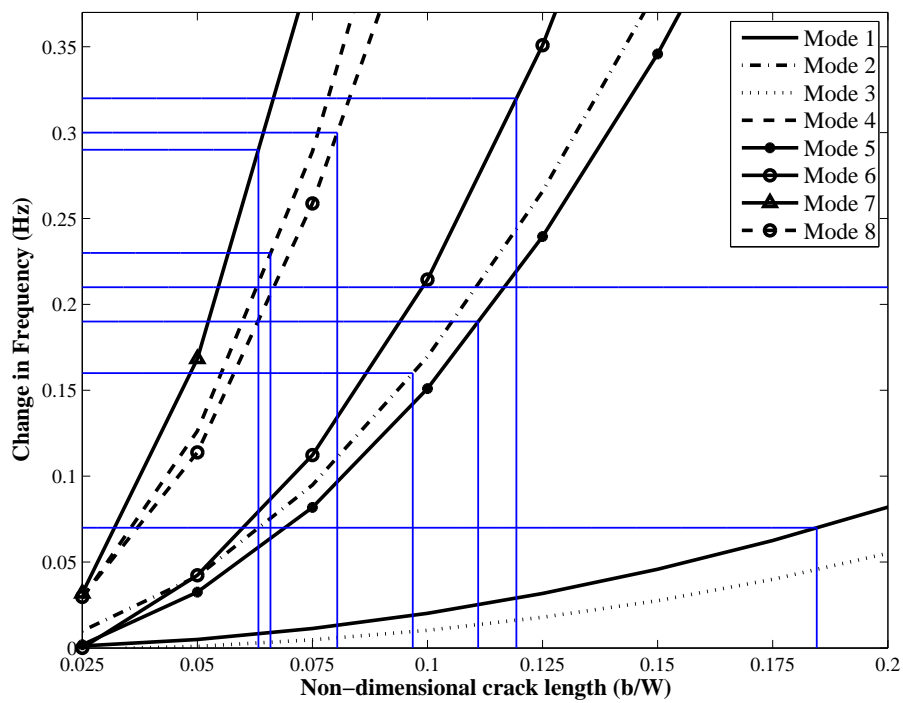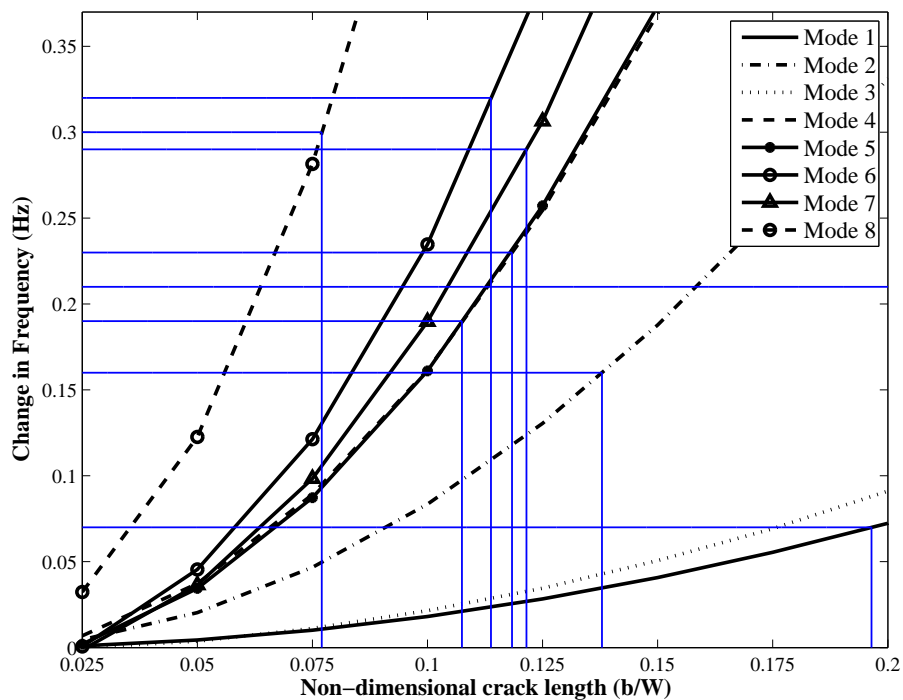Figure 9.12: Variation of natural frequencies in all 9 damage cases for first 8 modes

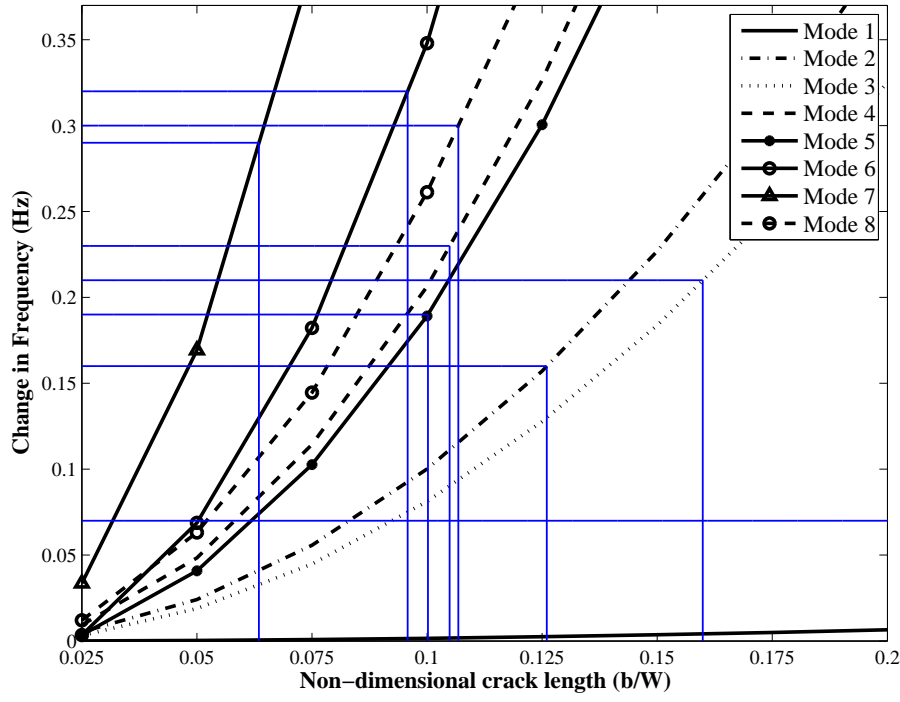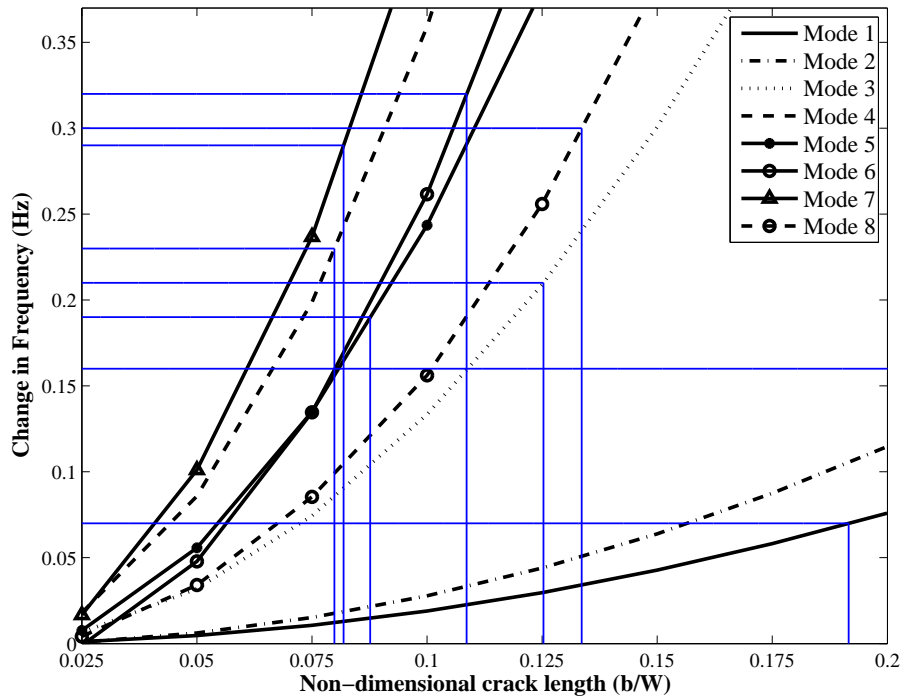(a) Damage case1

(b) Damage case2

191

(c) Damage case3

(d) Damage case4

(e) Damage case5

(f) Damage case6

193

(g) Damage case7

(h) Damage case8

(i) Damage case9
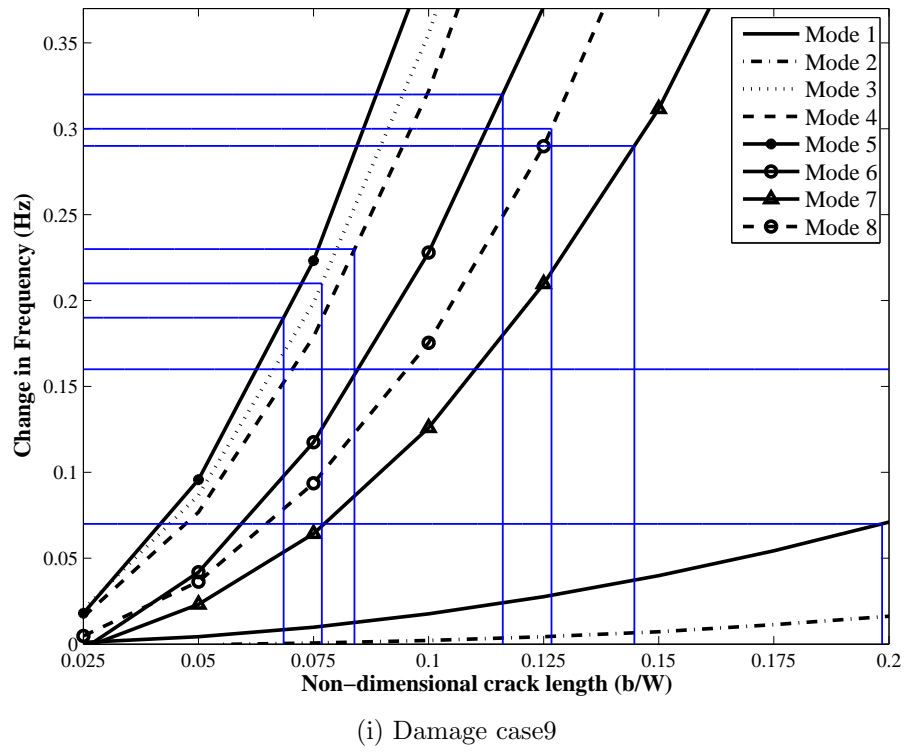
Figure 9.13: Finding *MDC* using deviations from measured natural frequencies

Chapter 10

Conclusions and recommendations

10.1 Conclusions

The core of this thesis is the development and validation of a vibration based damage detection technique, especially for application to plate structures. The motivation for this study is the development of techniques that can eventually be used for Structural Health Monitoring *(SHM)* in aircraft maintenance. An overview of potential *SHM* techniques was presented in Chapter 2 along with a detailed review of literature relating to techniques of vibration based damage detection. Two such techniques were identified as prospective candidates for investigation in this thesis: modeshape based techniques and methods based on frequency measurement. Analytical approaches for damage detection using frequency measurements have hitherto been restricted to beams containing edge cracks; methods for detection of damage in plates have until now mostly relied upon numerical simulation and model updating.

In Chapter 3, a preliminary study was carried out to assess the performance of modeshape based techniques in comparison to frequency measurements. Modeshapes of beams obtained from numerical modelling and measurements from experiments were implemented in a variety of modeshape based techniques. While curvature based techniques using modeshapes from numerical modelling showed promising results, they performed poorly with experimentally measured modeshapes. The measured modeshape data was noisy and the damage signatures, which depended on the difference in deflections or curvatures of the damaged and undamaged beams,

were drowned in the noise. Extraction of modeshapes using better sensing techniques could have helped overcome this limitation. On the other hand, natural frequencies from the beams could be extracted accurately with good repeatability. Hence damage detection based on frequency measurements was pursued.

Existing frequency based techniques using analytical models are limited to beams mostly containing edge cracks. In the present work, the energy approach was extended to cover the case of beams with centre cracks employing mode I *Stress Intensity Factor* solutions from fracture mechanics theory to relate the energy stored in the crack directly to the crack size and thus avoiding the spring analogy. Further, the theoretical formulation was extended to the two dimensional case of plates containing through-thickness cracks. It is shown that, in all cases, the effect of damage in a structure can be expressed in terms of Eqn. [4.18]. This equation relates the change in frequency in any mode to the square of the curvature at the location of damage normalised with respect to the average (*RMS* value) curvature of the structure in that mode. The constant of proportionality is the damage index factor whose relation to the crack size can be determined from fracture mechanics theory. Another significant contribution of this thesis is the identification of the fact that modeshapes determined from numerical modelling or from actual measurements can be employed in the energy formulation to determine the crack parameters from frequency measurements. Note that this *hybrid* approach does not depend on differences in measured modeshapes of the damaged and undamaged structures, but only uses either the modeshape deflections of the undamaged structure or those of the damaged structure in conjunction with measured frequency changes. Hence it is not susceptible to noise in the modeshape measurements which can be filtered out to provide smooth data.

In Chapters 5 and 6, the theory using the energy formulation was validated for beams with edge cracks as well as centre cracks using numerical data obtained from finite element simulation and experimental data measured on actual beam samples respectively. Further it was shown that the crack sizes and locations can be successfully determined from measured changes in frequencies by solving the inverse problem using either a graphical solution or a least square technique.

In Chapter 7, a statistical analysis was conducted on experimental data on beams with centre cracks to determine the 90/95 probability of crack detection in each mode. This was combined with a database of change in frequencies with crack size obtained with *FEA* for centre cracks to determine minimum detectable crack size. The minimum detectable crack size is a function of the crack location and ranges from about 6.5% to 11.5% of the beam width for centre cracks in cantilever beams.

The theoretical model using energy formulation for through thickness cracks in plates was validated using numerical data from *FEA* and experiments on plates with simulated cracks in Chapters 8 and 9 respectively. In the case of plates, there are four crack parameters to be determined, *viz.* the two coordinates of the crack location, crack orientation and crack size, making the inverse problem more complex. A comparison of different numerical approaches including the least square method, the gradient based minimisation technique *Sequential Quadratic Programming (SQP)*, the population based *Genetic Algorithm* and the combination of the latter two, revealed that *SQP* method is the most efficient. It is to be noted that while crack locations and sizes could be determined with reasonable accuracy, large discrepancies were observed in the predicted values of crack orientation. Chapter 9 concludes with a statistical analysis of the experimental data determining the 90/95 probability of crack detection and the minimum detectable crack size for through-thickness cracks in *SS-SS-F-F* plates which again is a function of crack location.

In conclusion, it is believed that this thesis has contributed to the advancement of frequency measurement based damage detection technique for Structural Health Monitoring of plates and plate-like structures. Indeed, there is a large amount of further research which remains to be undertaken. Some recommendations are given below.

10.2   Recommendations for future work

- In the present study experimental modal analysis was performed only on plates with *SS-SS-F-F* boundary condition to validate the theory and illustrate the application of the proposed damage detection methodology. The statistical

analysis determining the 90/95 probability for crack detection and the minimum detectable crack size was also restricted to plates with this boundary condition. It is recommended that similar numerical and experimental studies be conducted on plates with other boundary conditions such as those with simple supports on all edges, built-in edges and combinations of the two.

- In the theory developed, the energy stored in the crack is calculated from fracture mechanics principles using only the mode I *Stress Intensity Factor (SIF)* solutions i.e., it was tacitly assumed that contributions from modes II and III could be neglected. It is possible that propagation of through-thickness cracks of general orientations in plates may also be driven by loading in modes II and III i.e., by in-plane and out of plane shear stresses. In fact, it is possible that the large discrepancies in the predictions of the crack orientations, ϕ, in Chapters 8 and 9, were caused by the omission of fracture modes other than mode I in the energy formulation. It is recommended that the effects of modes II and III be included in the theory and numerical and experimental studies be conducted to assess their significance.

- Metallic skin panels on aircraft fuselage and wing structures usually have stiffeners running in orthogonal directions. While the principle of change in frequencies due to damage being proportional to the normalised energy stored in the damage may hold good, its application to built-up structures consisting of panels with stiffeners is likely to be quite complex. Measurements made on an individual panel are likely to be influenced by lower frequencies of the global modes over the whole structure as well as higher frequencies of local mode. A crack in an individual panel is unlikely to influence the frequencies of local modes in other panels and will have only a marginal effect on the frequencies of the global mode. This may necessitate instrumenting all panels that are suspected of being prone to damage and the use of filtering techniques to extract individual local frequencies for inspecting individual panels. It is also to be noted that damage in built-up skin structures may also include cracks along rivet holes, loosened fasteners as well as cracking or buckling of

the stiffeners. It is recommended that some of these complexities of built-up structures be investigated numerically and experimentally.

- It is believed that Eqn. [4.18] is not necessarily restricted to one or two dimensional structures but may also hold good to thick three dimensional shapes. One may therefore also investigate the application of the proposed frequency based damage detection to structural health monitoring of thick structures, eg. wing spars and landing gear struts.

- A major area of research that remains to be done is to extend the proposed frequency based technique to damage detection in composites. The theory will remain the same, however the curvature terms on the *RHS* of Eqn. [4.18] will have to be modified to take into account the anisotropic nature of composites. Further, more serious damage in laminated composites is in the form of delaminations, hence the relationship between damage index parameter and the damage size (delamination area) will have to be developed using *SIF* for inter laminar cracks. It is suspected that the *SIF* in mode II may also play a significant role in this case.

- In the last two decades vibration based methods have been increasingly used for monitoring damage in bridges. Many of the techniques currently employed are frequency based, but rely on model updating. The applicability of the method proposed in this thesis to civil engineering structures such as bridges is another avenue of investigation that may be pursued.

References

[1] S. S. Kessler, M. S. Spearing and C. Soutis, "Damage detection in composite materials using lamb wave methods", *Smart Materials and Structures*, vol. 11, no. 2, pp. 269–278, 2002.

[2] K. Worden and J. M. Dulieu-Barton, "An overview of intelligent fault detection in systems and structures", *Structural Health Monitoring*, vol. 3, no. 1, pp. 85–98, 2004.

[3] C. E. Davis, "Strain survey of an F/A-18 stabilator spindle using high density bragg grating arrays", Technical Report. DSTO-TN-0615, DSTO Platforms Sciences Laboratory, Fishermans Bend, Victoria, Australia, 2005.

[4] G. Wehrle, P. Nohama, H. J. Kalinowski, P. I. Torres and L. C. G. Valente, "A fibre optic bragg grating strain sensor for monitoring ventilatory movements", *Measurement Science and Technology*, vol. 12, no. 7, pp. 805–809, 2001.

[5] X.-D. Wu, C. Schmidt-Hattenberger, K. Krger and J. Chen, "Temperature-controlled fiber bragg grating dynamic strain detection system", *Sensors and Actuators A: Physical*, vol. 119, no. 1, pp. 68 – 74, 2005.

[6] P. Moyo, J. M. W. Brownjohn, R. Suresh and S. C. Tjin, "Development of fiber bragg grating sensors for monitoring civil infrastructure", *Engineering Structures*, vol. 27, no. 12, pp. 1828 – 1834, 2005. SEMC 2004 Structural Health Monitoring, Damage Detection and Long-Term Performance.

[7] C. E. Davis, H. C. H. Li, A. F. Dethlefsen, A. Thompson and P. R. Stoddart, "A low-cost and temperature-insensitive fibre bragg grating sensor for monitoring localized strain concentrations", *Measurement Science and Technology*, vol. 20, no. 2, p. 025201025207, 2009.

[8] H. C. H. Li, I. Herszberg, C. E. Davis and P. R. Stoddart, "Composite scarf repair monitoring using fiber bragg grating sensors", *proceedings of Society of Photo-optical Instrumentation Engineers (SPIE), Sensors and Smart Structures Technologies for Civil, Mechanical, and Aerospace Systems*, vol. 6529, no. 1, pp. 65291Z.1–65291Z.7, 2007.

[9] R. M. Measures, N. D. W. Glossop, J. Lymer, M. Leblanc, J. West, S. Dubois, W. Tsaw and R. C. Tennyson, "Structurally integrated fiber optic damage assessment system for composite materials", *Applied optics*, vol. 28, no. 13, pp. 2626–2633, 1989.

[10] B. Lee, "Review of the present status of optical fiber sensors", *Optical Fiber Technology*, vol. 9, no. 2, pp. 57–79, 2003.

[11] Y. J. Rao, "Recent progress in applications of in-fibre bragg grating sensors", *Optics and Lasers in Engineering*, vol. 31, no. 4, pp. 297–324, 1999.

[12] T. D. Dudderar, B. R. Peters and J. A. Gilbert, "Fiber optic sensor systems for ultrasonic NDE: State-of-the-art and future potential", *proceedings of IEEE Ultrasonics Symposium*, vol. 2, pp. 1181–1190, 1989.

[13] J. R. Casas and P. J. S. Cruz, "Fiber optic sensors for bridge monitoring", *Journal of Bridge engineering*, vol. 8, no. 6, pp. 362–373, 2003.

[14] M. Majumder, T. Gangopadhyay, A. Chakraborty, K. Dasgupta and D. K. Bhattacharya, "Fibre bragg gratings in structural health monitoring - Present status and applications", *Sensors and Actuators A: Physical*, vol. 147, no. 1, pp. 150–164, 2008.

[15] P. Rossi and F. Le Maou, "Device for the detection and location of cracks in concrete using fibre optics", *Engineering Fracture Mechanics*, vol. 35, no. 1-3, pp. 303–311, 1990.

[16] G. Kawiecki, "Modal damping measurement for damage detection", *Smart Materials and Structures*, vol. 10, no. 3, pp. 466–471, 2001.

[17] D. I. H. Vallen, "AE testing fundamentals, equipment, applications", *e-Journal of Nondestructive Testing*, vol. 7, no. 9, 2002.

[18] T. Jayakumar, K. H. J. Buschow, W. C. Robert, C. F. Merton, I. Bernard, J. K. Edward, M. Subhash and V. Patrick, "NDT techniques: Acoustic emission", in *Encyclopedia of Materials: Science and Technology*, pp. 6001–6003,

Oxford: Elsevier, 2001.

[19] M. Shiwa, T. Kishi, K. H. J. Buschow, W. C. Robert, C. F. Merton, I. Bernard, J. K. Edward, M. Subhash and V. Patrick, "NDT-based assessment of damage: An overview", in *Encyclopedia of Materials: Science and Technology*, pp. 1–8, Oxford: Elsevier, 2001.

[20] K. V. Steiner, R. F. Eduljee, X. Huang and J. W. Gillespie, "Ultrasonic NDE techniques for the evaluation of matrix cracking in composite laminates", *Composites Science and Technology*, vol. 53, no. 2, pp. 193–198, 1995.

[21] H. Dunegan and D. Harris, "Acoustic emission - A new nondestructive testing tool", *Ultrasonics*, vol. 7, no. 3, pp. 160–166, 1969.

[22] I. A. Viktorov, *Rayleigh and Lamb waves - Physical theory and applciations*. Plenum press, NY, 1967.

[23] A. Raghavan and E. S. C. Carlos, "Review of guided-wave structural health monitoring", *The Shock and Vibration Digest*, vol. 39, no. 2, pp. 91–114, 2007.

[24] A. Raghavan and E. S. C. Carlos, "Lamb-wave based structural health monitoring", in *Damage Prognosis - for Aerospace, Civil and Mechanical Systems*, John Wiley & sons, Ltd., 2005.

[25] Z. Su, L. Ye and Y. Lu, "Guided lamb waves for identification of damage in composite structures: A review", *Journal of Sound and Vibration*, vol. 295, no. 3-5, pp. 753–780, 2006.

[26] J.-B. Ihn and F.-K. Chang, "Detection and monitoring of hidden fatigue crack growth using a built-in piezoelectric sensor/actuator network: I - Diagnosis", *Smart Materials and Structures*, vol. 13, pp. 315–423, 2004.

[27] V. Giurgiutiu and A. N. Zagrai, "Characterization of piezoelectric active wafer sensors", *Journal of Intelligent Material Systems and Structures*, vol. 11, p. 959975, 2000.

[28] P. Wilcox, "Omni-directional guided wave transducer arrays for the rapid inspection of large areas of plate structures", *IEEE Transactions on Ultrasonics, Ferroelectrics, and Frequency control*, vol. 50, no. 6, p. 699709, 2003.

[29] V. Giurgiutiu and J. Bao, "Embedded-ultrasonics structural radar for in situ structural health monitoring of thin-wall structures", *Structural Health Monitoring*, vol. 3, pp. 121–140, 2004.

[30] A. S. Purekar, D. J. Pines, S. Sundararaman and D. E. Adams, "Directional piezoelectric phased array filters for detecting damage in isotropic plates", *Smart Materials and Structures*, vol. 13, no. 4, pp. 838–850, 2004.

[31] E. V. Malyarenko and M. K. Hinders, "Fan beam and double crosshole lamb wave tomography for mapping flaws in aging aircraft structures", *The Journal of the Acoustical Society of America*, vol. 108, no. 4, pp. 1631–1639, 2000.

[32] E. V. Malyarenko and M. K. Hinders, "Ultrasonic lamb wave diffraction tomography", *Ultrasonics*, vol. 39, no. 4, pp. 269 – 281, 2001.

[33] E. J. Michaels and E. T. Michaels, "Guided wave signal processing and image fusion for in situ damage localization in plates", *Wave Motion*, vol. 44, no. 6, pp. 482–492, 2007.

[34] Y.-H. Kim, D.-H. Kim, J.-H. Han and C.-G. Kim, "Damage assessment in layered composites using spectral analysis and lamb wave", *Composites Part B: Engineering*, vol. 38, no. 7-8, pp. 800–809, 2007.

[35] S. S. Kessler, *Piezoelectric based in-situ damage detection of composite materials for structural health monitoring systems.* Phd thesis, Massachusetts Institute of Technology, 2002.

[36] B. C. Lee and W. J. Staszewski, "Lamb wave propagation modelling for damage detection: I - Two-dimensional analysis", *Smart Materials and Structures*, vol. 16, no. 2, pp. 249–259, 2007.

[37] B. C. Lee and W. J. Staszewski, "Lamb wave propagation modelling for damage detection: II - Damage monitoring strategy", *Smart Materials and Structures*, vol. 16, no. 2, pp. 260–274, 2007.

[38] Y. L. Koh, W. K. Chiu and N. Rajic, "Effects of local stiffness changes and delamination on lamb wave transmission using surface-mounted piezoelectric transducers", *Composite Structures*, vol. 57, no. 1-4, pp. 437 – 443, 2002.

[39] Y. L. Koh, W. K. Chiu and N. Rajic, "Integrity assessment of composite repair patch using propagating lamb waves", *Composite Structures*, vol. 58, no. 3, pp. 363 – 371, 2002.

[40] S. Yuan, L. Wang and G. Peng, "Neural network method based on a new damage signature for structural health monitoring", *Thin-Walled Structures*, vol. 43, no. 4, pp. 553–563, 2005.

[41] Z. Su and L. Ye, "Lamb wave-based quantitative identification of delamination in CF/EP composite structures using artificial neural algorithm", *Composite Structures*, vol. 66, no. 1-4, pp. 627–637, 2004.

[42] Z. Su and L. Ye, "Lamb wave propogation based damage identification for quasi-isotropic CF/EP composite laminates using artificial neural algorithm: Part I - Methodology and database development", *Journal of Intelligent Matrial Systems and Structures*, vol. 16, no. 2, pp. 97–111, 2005.

[43] Z. Su and L. Ye, "Lamb wave propagation based damage identification for quasi-isotropic CF/EP composite laminates using artificial neural algorithm: Part II - Implementation and validation", *Journal of Intelligent Material Systems and Structures*, vol. 16, no. 2, pp. 113–125, 2005.

[44] S. Hall and M. Vellacott, "Safe and economic management of widespread fatigue damage (WFD) using prognostic/diagnostic health and usage monitoring", *proceedings of 5th DSTO International Conference on Health & Usage Monitoring*, 2007.

[45] M. Wishaw and D. P. Barton, "Comparative vacuum monitoring: A new method of in-situ real-time crack detection and monitoring", September, 2001 2001.

[46] D. Roach, K. Rackow and W. De Long, "Living infrastructure concepts: Part II - Smart structures, In-situ distributed health monitoring sensors", Technical report., Sandia National Laboratories, 2007.

[47] G. Park, H. Cudney and D. J. Inman, "An integrated health monitoring technique using structural impedance sensors", *Journal of Intelligent Material Systems and Structures*, vol. 11, no. 6, pp. 448–455, 2000.

[48] F. P. Sun, Z. Chaudhry, C. Liang and C. A. Rogers, "Truss structure integrity identification using PZT sensor-actuator", *Journal of Intelligent Material Systems and Structures*, vol. 6, pp. 134–139, 1995.

[49] G. Park, H. Sohn, C. R. Farrar and D. J. Inman, "Overview of piezoelectric impedance-based health monitoring and path forward", *The Shock and Vibration Digest*, vol. 35, no. 6, pp. 451–463, 2003.

[50] Z. Chaudhry, T. Joseph, F. P. Sun and C. A. Rogers, "Local-area health monitoring of aircraft via piezoelectric actuator/sensor patches", *proceedings*

of Society of Photo-optical Instrumentation Engineers (SPIE), Smart Structures and Materials, vol. 2443, pp. 268–276, 1995.

[51] G. L. Andrew, M. E. Richard, S. T. Jerzy and B. Y. George, "Damage assessment of aerospace structural components by impedance based health monitoring", Technical report., National Aeronautics and Space Administration, John H. Glenn Research Center at Lewis Field, 2005.

[52] V. Giurgiutiu, A. Zagrai and J. Bao, "Damage identification in aging aircraft structures with piezoelectric wafer active sensors", *Journal of Intelligent Material Systems and Structures*, vol. 15, no. 9-10, pp. 673–687, 2004.

[53] V. Lopes Jr, G. Park, H. Cudney and D. J. Inman, "Smart structure health monitoring using artificial Neural Network", *proceedings of 2nd International workshop on Structural Health Monitoring*, 8-10 September, 1999.

[54] J. Xu, Y. Yang and C. K. Soh, "Electromechanical impedance-based structural health monitoring with evolutionary programming", *Journal of Aerospace Engineering*, vol. 17, no. 4, pp. 182–193, 2004.

[55] Y. Zou, L. Tong and G. P. Steven, "Vibration-based model-dependent damage (delamination) identification and health monitoring for composite structures - a review", *Journal of Sound and Vibration*, vol. 230, no. 2, pp. 357–378, 2000.

[56] S. W. Doebling, C. R. Farrar and M. B. Prime, "A summary review of vibration-based damage identification methods", *The Shock and Vibration Digest*, vol. 30, no. 2, pp. 91–105, 1998.

[57] S. W. Doebling, C. R. Farrar and R. S. Goodman, "Effects of measurement statistics on the detection of damage in the alamosa canyon bridge", 1997.

[58] H. Sohn, C. R. Farrar, M. Hemez, D. Shunk, W. Stinemates and R. Nadler, "A review of structural health monitoring literature: 1996-2001", Technical report., Los Alamos National Laboratory report, 2003.

[59] E. P. Carden and P. Fanning, "Vibration based condition monitoring: A review", *Journal of Structural Health monitoring*, vol. 3, no. 4, pp. 355–377, 2004.

[60] A. D. Dimarogonas, "Vibration of cracked structures: A state of the art review", *Engineering Fracture Mechanics*, vol. 55, no. 5, pp. 831–857, 1996.

[61] D. Montalvao, N. M. Maia and A. M. R. Ribeiro, "A review of vibration-based structural health monitoring with special emphasis on composite materials", *The Shock and Vibration Digest*, vol. 38, no. 4, pp. 295–324, 2006.

[62] C. Modena, D. Sonda and D. Zonta, "Damage localization in reinforced concrete structures by using damping measurements", *Key engineering materials*, vol. 167-168, pp. 132–141, 1999.

[63] D. Zonta, *Structural damage detection and localization by using vibrational measurements*. Phd thesis, The University of Bologna, 2000.

[64] O. S. Salawu, "Detection of structural damage through changes in frequency: A review", *Engineering Structures*, vol. 19, no. 9, pp. 718–723, 1997.

[65] T. Wolff and M. Richardson, "Fault detection in structures from changes in their modal parameters", *proceedings of 7th International Modal Analysis Conference*, pp. 87–94, 1989.

[66] R. J. Allemang and D. L. Brown, "A correlation coefficient for modal vector analysis", *proceedings of 1st International Modal Analysis Conference*, pp. 110–116, 1982.

[67] S. Moore, Z. Biaobiao, J. Lai and K. Shankar, "Model updating and determination of structural dynamic properties in the presence of a second surce of excitation", *proceedings of 3rd International conference on Health and Usage Monitoring Systems (HUMS) conference*, 2003.

[68] A. K. Pandey, M. Biswas and M. M. Samman, "Damage detection from changes in curvature mode shapes", *Journal of Sound and Vibration*, vol. 145, no. 2, pp. 321–332, 1991.

[69] N. Stubbs, J.-T. Kim and C. R. Farrar, "Field verification of a nondestructive damage localization and severity estimation algorithm", *proceedings of the 13th International Modal Analysis Conference*, vol. 2460, pp. 210–218, 1995.

[70] M. M. Abdel Wahab and G. De Roeck, "Damage detection in bridges using modal curvatures: Application to a real damage scenario", *Journal of Sound and Vibration*, vol. 226, no. 2, pp. 217–235, 1999.

[71] A. Dutta and T. S., "Damage detection in bridges using accurate modal parameters", *Finite Elements in Analysis and Design*, vol. 40, no. 3, pp. 287–304, 2004.

[72] W. Lestari and P. Qiao, "Damage detection of fiber-reinforced polymer honeycomb sandwich beams", *Composite Structures*, vol. 67, no. 3, pp. 365–373, 2005.

[73] C. S. Hamey, W. Lastari, P. Qiao and G. Song, "Experimental damage identification of carbon/epoxy composite beams using curvature mode shapes", *Journal of Structural Health Monitoring*, vol. 3, no. 4, pp. 333–353, 2004.

[74] S. Choi and N. Stubbs, "Nondestructive damage detection algorithms for 2-D plates", *proceedings of Society of Photo-optical Instrumentation Engineers (SPIE), Smart Structures and Materials*, pp. 193–204, 1997.

[75] P. Cornwell, S. W. Doebling and C. R. Farrar, "Application of the strain energy damage detection method to plate-like structures", *Journal of Sound and Vibration*, vol. 224, no. 2, pp. 359–374, 1999.

[76] S. Park, Y. Kim and N. Stubbs, "Nondestructive damage detection in large structures via vibration monitoring", *Electronic Journal of Structural Engineering*, vol. 2, pp. 59–75, 2002.

[77] J.-T. Kim, Y.-S. Ryu, H.-M. Cho and N. Stubbs, "Damage identification in beam-type structures: Frequency-based method vs mode-shape-based method", *Engineering Structures*, vol. 25, no. 1, pp. 57–67, 2003.

[78] D. A. Jauregui and C. R. Farrar, "Comparison of damage identification algorithms on experimental modal data from a bridge", *In proceedings of the 14th International Modal Analysis Conference*, pp. 1423–1429, 1996.

[79] C. R. Farrar and D. A. Jauregui, "Comparative study of damage identification algorithms applied to a bridge: I - Experiment", *Smart materials and structures*, vol. 7, no. 5, pp. 704–719, 1998.

[80] P. J. Cornwell, M. Kam, B. Carlson, B. Hoerst, S. W. Doebing and C. R. Farrar, "Comparative study of vibration-based damage identification algorithms", *proceedings of the 16th International Modal Analysis Conference*, 1998. MS P-946, Los Alamos National Laboratory, Los Alamos, NM 87545, USA.

[81] D. C. Zimmerman and M. Kaouk, "Structural damage detection using a minimum rank update theory", *ASME Transactions - Journal of Vibration and Acoustics*, vol. 116, no. 2, pp. 222–231, 1994.

[82] G. M. Owolabi, A. S. J. Swamidas and R. Seshadri, "Crack detection in beams using changes in frequencies and amplitudes of frequency response functions", *Journal of Sound and Vibration*, vol. 265, pp. 1–22, 2003.

[83] I. C. Davis and A. L. Wicks, "Sources of frf variation in damage detection", *Society of Photo-Optical Instrumentation Engineers Journal*, vol. 4753, no. 2, pp. 1618–1623, 2002.

[84] I. Herszberg, H. C. H. Li, F. Dharmawan, A. P. Mouritz, M. Nguyen and J. Bayandor, "Damage assessment and monitoring of composite ship joints", *Composite Structures*, vol. 67, no. 2, pp. 205 – 216, 2005.

[85] H. Sohn, C. R. Farrar, N. F. Hunter and K. Worden, "Structural health monitoring using statistical pattern recognition techniques", *Journal of Dynamic Systems, Measurement, and Control*, vol. 123, no. 4, pp. 706–711, 2001.

[86] H. Sohn and C. R. Farrar, "Damage diagnosis using time series analysis of vibration signals", *Smart Materials and Structures*, vol. 10, no. 3, pp. 446–451, 2001.

[87] H. Sohn, K. Worden and C. R. Farrar, "Statistical damage classification under changing environmental and operational conditions", *Journal of Intelligent Material Systems and Structures*, vol. 13, no. 9, pp. 561–574, 2002.

[88] K. K. Nair, A. S. Kiremidjian and K. H. Law, "Time series-based damage detection and localization algorithm with application to the asce benchmark structure", *Journal of Sound and Vibration*, vol. 291, no. 1-2, pp. 349–368, 2006.

[89] C. Shane and R. Jha, "Structural health monitoring of a composite wing model using proper orthogonal decomposition", *proceedings of 48th AIAA/ ASME/ ASCE/ AHS/ ASC Structures, Structural Dynamics, and Materials Conference*, 2007. (AIAA 2007-1726).

[90] L. Garibaldi, S. Marchesiello and D. J. Gorman, "Bridge dynamics misinterpretations due to low spatial resolution and closeness of frequencies", *proceedings of the International Conference on Damage Assessment of Structures (DAMAS 99)*, pp. 411–422, 1999.

[91] L. Garibaldi, E. Giorcelli, S. Marchesiello and M. Ruzzene, "CVA-BR against ARMAV: Comparison over real data from an ambient noise excited bridge",

proceedings of the International Conference on Damage Assessment of Structures (DAMAS 99), pp. 423–432, 1999.

[92] M. Abe, Y. Fujino, T. Y. Kajimura, M. Yanagihara and M. Sato, "Monitoring of a long span suspension bridge by ambient vibration measurement", 1999.

[93] S. R. Ibrahim and E. C. Mikulcik, "A method for the direct determination of vibration parameters from free responses", *Shock and Vibration Bulletin*, vol. 47, no. 4, pp. 183–198, 1977.

[94] W. Vill, "Theorie et applications de la notion de signal analytique", *Cables et Transmission*, vol. 2a, pp. 61–74, 1947.

[95] Z. K. Peng and F. L. Chu, "Application of the wavelet transform in machine condition monitoring and fault diagnostics: A review with bibliography", *Mechanical Systems and Signal Processing*, vol. 18, no. 2, pp. 199–221, 2004.

[96] K. A. Al-Nefaie, *New method for structural damage identification using experimental modal analysis.* PhD thesis, Department of Mechanical, Materials and Aerospace Engineering, University of Central Florida, 2000.

[97] J. Lin and L. Qu, "Feature extraction based on morlet wavelet and its application for mechanical fault diagnosis", *Journal of Sound and Vibration*, vol. 234, no. 1, pp. 135–148, 2000.

[98] B. Liu and S. F. Ling, "On the selection of informative wavelets for machinery diagnosis", *Mechanical Systems and Signal Processing*, vol. 13, no. 1, pp. 145–162, 1999.

[99] A. Chukwujekwu Okafor and A. Dutta, "Structural damage detection in beams by wavelet transforms", *Smart Materials and Structures*, vol. 9, no. 6, pp. 906–917, 2000.

[100] G. Yan, L. Zhou Lily and F. G. Yuan, "Wavelet-based built-in damage detection and identification for composites", *proceedings of Society of Photo-optical Instrumentation Engineers (SPIE), The International Society for Optical Engineering*, pp. 324–334, 2005.

[101] C. Biemans, W. J. Staszewski, C. Boller and G. R. Tomlinson, "Crack detection in metallic structures using piezoceramic sensors", *proceedings of International Conference on Damage Assessment of Structures, DAMAS 99*, pp. 112–121, 1999.

[102] H. Melhem and H. Kim, "Damage detection in concrete by fourier and wavelet analyses", *Journal of Engineering Mechanics*, vol. 129, no. 5, pp. 571–577, 2003.

[103] H. Kim and H. Melhem, "Damage detection of structures by wavelet analysis", *Engineering Structures*, vol. 26, no. 3, pp. 347–362, 2004.

[104] D.-U. Sung, C.-G. Kim and C.-S. Hong, "Monitoring of impact damages in composite laminates using wavelet transform", *Composites Part B: Engineering*, vol. 33, no. 1, pp. 35–43, 2002.

[105] Y. J. Yan and L. H. Yam, "Online detection of crack damage in composite plates using embedded piezoelectric actuators/sensors and wavelet analysis", *Composite Structures*, vol. 58, no. 1, pp. 29–38, 2002.

[106] L. H. Yam, Y. J. Yan and J. S. Jiang, "Vibration-based damage detection for composite structures using wavelet transform and Neural Network identification", *Composite Structures*, vol. 60, no. 4, pp. 403–412, 2003.

[107] M. Akgun and F. D. Ju, "Diagnosis of multiple cracks on a beam structure", *International Journal of Analytical and Experimental Modal Analysis*, vol. 2, no. 4, pp. 149–154, 1987.

[108] D.-Y. Song, N. Takeda and A. Kitano, "Correlation between mechanical damage behavior and electrical resistance change in CFRP composites as a health monitoring sensor", *Materials Science and Engineering: A*, vol. 456, pp. 286–291, 2007.

[109] J. K. Vandiver, "Detection of structural failure on fixed platforms by measurement of dynamic response", *Journal of Petroleum Technology*, pp. 305–310, 1977.

[110] M. M. Abdel Wahab, "Effect of modal curvatures on damage detection using model updating", *Mechanical Systems and Signal Processing*, vol. 15, no. 2, pp. 439–445, 2001.

[111] C.-P. Fritzen, D. Jennewein and T. Kiefer, "Damage detection based on model updating methods", *Mechanical Systems and Signal Processing*, vol. 12, no. 1, pp. 163–186, 1998.

[112] J. E. Mottershead and M. I. Friswell, *Finite element model updating in structural dynamics*. Dordrecht, Netherlands: Kluwer Academic Publishers, 1995.

[113] P. Cawley and R. D. Adams, "Location of defects in structures from measurements of natural frequencies", *Journal of strain analysis*, vol. 14, no. 2, pp. 49–57, 1979.

[114] Z. Y. Shi, S. S. Law and L. M. Zhang, "Structural damage localization from modal strain energy change", *Journal of Sound and Vibration*, vol. 218, no. 5, pp. 825–844, 1998.

[115] J. E. Mottershead and M. I. Friswell, "Model updating in structural dynamics: A survey", *Journal of Sound and Vibration*, vol. 167, no. 2, pp. 347–375, 1993.

[116] Y.-S. Lee and M.-J. Chung, "A study on crack detection using eigenfrequency test data", *Computers & Structures*, vol. 77, no. 3, pp. 327–342, 2000.

[117] J. K. Sinha and M. I. Friswell, "The use of model updating for reliable finite element modelling and fault diagnosis of structural components used in nuclear plants", *Nuclear Engineering and Design*, vol. 223, no. 1, pp. 11–23, 2003.

[118] J. M. W. Brownjohn, P.-Q. Xia, H. Hao and Y. Xia, "Civil structure condition assessment by fe model updating: Methodology and case studies", *Finite Elements in Analysis and Design*, vol. 37, no. 10, pp. 761–775, 2001.

[119] M. I. Friswell and J. E. T. Penny, "Crack modeling for structural health monitoring", *Structural Health Monitoring*, vol. 1, no. 2, pp. 139–148, 2002.

[120] S. Christides and A. D. S. Barr, "One-dimensional theory of cracked bernoulli-euler beams", *International Journal of Mechanical Sciences*, vol. 26, no. 11-12, pp. 639–648, 1984.

[121] Z. Y. Shi, S. S. Law and L. M. Zhang, "Damage localization by directly using incomplete mode shapes", *Journal of Engineering Mechanics*, vol. 126, no. 6, pp. 656–660, 2000.

[122] A. Messina, E. J. Williams and T. Contursi, "Structural damage detection by a sensitivity and statistical-based method", *Journal of Sound and Vibration*, vol. 216, no. 5, pp. 791–808, 1998.

[123] W.-X. Ren and G. D. Roeck, "Structural damage identification using modal data I: Simulation verification", *Journal of Structural Engineering*, vol. 128, no. 1, pp. 87–95, 2002.

[124] W.-X. Ren and G. D. Roeck, "Structural damage identification using modal data II: Test verification", *Journal of Structural Engineering*, vol. 128, no. 1, pp. 96–104, 2002.

[125] S. Keye, "Improving the performance of model-based damage detection methods through the use of an updated analytical model", *Aerospace Science and Technology*, vol. 10, no. 3, pp. 199–206, 2006.

[126] J. R. Wu and Q. S. Li, "Structural parameter identification and damage detection for a steel structure using a two-stage finite element model updating method", *Journal of Constructional Steel Research*, vol. 62, no. 3, pp. 231–239, 2006.

[127] N. T. Khiem and T. V. Lien, "Multi-crack detection for beam by the natural frequencies", *Journal of Sound and Vibration*, vol. 273, no. 1-2, pp. 175–184, 2004.

[128] M. Krawczuk, "Natural vibrations of rectangular plates with a through crack", *Archive of Applied Mechanics (Ingenieur Archiv)*, vol. 63, no. 7, pp. 491–504, 1993.

[129] H. Hao and Y. Xia, "Vibration-based damage detection of structures by genetic algorithm", *Journal of Computing in Civil Engineering*, vol. 16, no. 3, pp. 222–229, 2002.

[130] M. I. Friswell and J. E. T. Penny, "Is damage location using vibration measurements practical?", *Euromech 365 International Workshop: DAMAS 97, Structural Damage Assessment using Advanced Signal Processing Procedures*, 1997.

[131] M. I. Friswell, "Damage identification using inverse methods", *Transactions of the Royal Society of London, Series A, Mathematical, Physical and Engineering Sciences, Special Issue on Structural Health Monitoring*, vol. 365, no. 1851, pp. 393–410, 2006.

[132] T. G. Chondros and A. D. Dimarogonas, "Identification of cracks in welded joints of complex structures", *Journal of Sound and Vibration*, vol. 69, no. 4, pp. 531–538, 1980.

[133] R. D. Adams, P. Cawley, C. J. Pye and S. B., "A vibration technique for non-destructively assessing the integrity of structures", *Journal of Mechanical Engineering Science*, vol. 20, no. 2, pp. 93–100, 1978.

[134] T. G. Chondros, A. D. Dimarogonas and J. Yao, "A continuous cracked beam vibration theory", *Journal of Sound and Vibration*, vol. 215, no. 1, pp. 17–34, 1998.

[135] P. F. Rizos, N. Aspragathos and A. D. Dimarogonas, "Identification of crack location and magnitude in a cantilever beam from the vibration modes", *Journal of Sound and Vibration*, vol. 138, no. 3, pp. 381–388, 1990.

[136] W. M. Ostachowicz and M. Krawczuk, "Analysis of the effect of cracks on the natural frequencies of a cantilever beam", *Journal of Sound and Vibration*, vol. 150, no. 2, p. 191, 1991.

[137] R. Y. Liang, J. Hu and F. K. Choy, "Detection of cracks in beam structures using measurements of natural frequencies", *Journal of the Franklin Institute*, vol. 328, no. 4, p. 505, 1991.

[138] R. Y. Liang, J. Hu and F. K. Choy, "Theoretical study of crack-induced eigen-frequency changes on beam structures", *Journal of Engineering Mechanics*, vol. 118, no. 2, pp. 384–396, 1992.

[139] R. Y. Liang, J. Hu and F. K. Choy, "Quantitative NDE technique for assessing damages in beam structures", *Journal of Engineering Mechanics*, vol. 118, no. 7, pp. 1468–1487, 1992.

[140] B. P. Nandwana and S. K. Maiti, "Detection of the location and size of a crack in stepped cantilever beams based on measurements of natural frequencies", *Journal of Sound and Vibration*, vol. 203, no. 3, p. 435, 1997.

[141] D. P. Patil and S. K. Maiti, "Transverse vibration of slender beam of variable depth and constant width with and without crack", *proceedings of 8th International Congress on Sound and Vibration, Hong Kong, China*, pp. 1729–1736, 2001.

[142] B. P. Nandwana and S. K. Maiti, "Modelling of vibration of beam in presence of inclined edge or internal crack for its possible detection based on frequency measurements", *Engineering Fracture Mechanics*, vol. 58, no. 3, p. 193, 1997.

[143] S. P. Lele and S. K. Maiti, "Modelling of transverse vibration of short beams for crack detection and measurement of crack extension", *Journal of Sound and Vibration*, vol. 257, no. 3, pp. 559–583, 2002.

[144] J. A. Loya, L. Rubio and J. Fernandez-Saez, "Natural frequencies for bending vibrations of timoshenko cracked beams", *Journal of Sound and Vibration*, vol. 290, no. 3-5, pp. 640–653, 2006.

[145] E. J. Williams, A. Messina and B. S. Payne, "A frequency-change correlation approach to damage detection", *proceedings of 15th International Modal Analysis Conference*, vol. 3089, pp. 652–657, 1997.

[146] L. Rayleigh, "On the calculation of the frequency of vibration of a system in its gravest mode, with an example from hydrodynamics", *Philosophical Magazine*, vol. 47, no. 5, pp. 566–572, 1899.

[147] L. Rayleigh, "On the calculation of chandni's figures for a square plate", *Philosophical Magazine*, vol. 22, no. 6, pp. 225–229, 1911.

[148] P. Gudmundson, "Eigenfrequency changes of structures due to cracks, notches or other geometrical changes", *Journal of the Mechanics and Physics of Solids*, vol. 30, no. 5, pp. 339–353, 1982.

[149] J. Hu and R. Y. Liang, "An integrated approach to detection of cracks using vibration characteristics", *Journal of the Franklin Institute*, vol. 330, no. 5, pp. 841–853, 1993.

[150] D. P. Patil and S. K. Maiti, "Detection of multiple cracks using frequency measurements", *Engineering Fracture Mechanics*, vol. 70, no. 12, pp. 1553–1572, 2003.

[151] D. P. Patil and S. K. Maiti, "Modelling for crack detection in beams on elastic foundation", *proceedings of 7th Pan American Congress of Applied Mechanics, University de LaFrontera Temuco, Chile*, pp. 1–4, 2002.

[152] D. P. Patil and S. K. Maiti, "Experimental verification of a method of detection of multiple cracks in beams based on frequency measurements", *Journal of Sound and Vibration*, vol. 281, no. 1-2, pp. 439–451, 2005.

[153] D. P. Patil and S. K. Maiti, "Modelling of geometrically segmented beams to facilitate crack detection using frequency measurements", *proceedings of 18th*

References

Canadian Congress of Applied Mechanics, Memorial University of Newfoundland, Canada, vol. 1, 2001.

[154] A. W. Leissa, "The free vibration of rectangular plates", *Journal of Sound and Vibration*, vol. 31, no. 3, pp. 257–293, 1973.

[155] A. W. Leissa, "Vibration of plates", Technical report., National Aeronatics and Apace Administration, Washington, D.C., 1969.

[156] T. G. Chondros and A. D. Dimarogonas, "Identification of cracks in circular plates welded at the contour", *ASME Design Engineering Technical Conference*, 1979.

[157] N. K. Anifantis, R. L. Actis and A. D. Dimarogonas, "Vibration of cracked annular plates", *Engineering Fracture Mechanics*, vol. 49, no. 3, pp. 371–379, 1994.

[158] H. T. Banks and P. R. Emeric, "Detection of non-symmetrical damage in smart plate-like structure", *Journal of Intelligent Material Systems and Structures*, vol. 9, no. 10, pp. 818–828, 1998.

[159] C. C. Ma and C. H. Huang, "Experimental and numerical analysis of vibrating cracked plates at resonant frequencies", *Experimental Mechanics*, vol. 41, no. 1, pp. 8–18, 2001.

[160] R. Ganguli, "A fuzzy logic system for ground based structural health monitoring of a helicopter rotor using modal data", *Journal of Intelligent Material Systems and Structures*, vol. 12, no. 6, pp. 397–408, 2001.

[161] P. P. Pawar and R. Ganguli, "Genetic fuzzy system for damage detection in beams and helicopter rotor blades", *Computer Methods in Applied Mechanics and Engineering*, vol. 192, no. 16-18, pp. 2031–2057, 2003.

[162] R. R. K. Reddy and R. Ganguli, "Structural damage detection in a helicopter rotor blade using radial basis function Neural Networks", *Smart Structures and Materials*, vol. 12, no. 2, pp. 232–241, 2003.

[163] S. Suresh, S. N. Omkar, R. Ganguli and V. Mani, "Identification of crack location and depth in a centilever beam using a modular Neural Network approach", *Smart Materials and Structures*, vol. 13, no. 4, pp. 907–916, 2004.

[164] M. Krawczuk, W. Ostachowicz and G. Kawiecki, "Detection of delaminations in cantilevered beams using soft computing methods", *proceedings of the European COST F3 Conference on System Identification and Structural Health Monitoring*, pp. 243–252, 2000.

[165] T. M. Hatem, M. N. Abuelfoutouh and H. M. Negm, "Application of genetic algorithms and Neural Networks to health monitoring of composite structures", *proceedings of the 2nd European Workshop on Structural Health Monitoring*, pp. 616–623, 2004.

[166] A. S. Kobayashi, *Linear elastic fracture mechanics*, vol. 2. Netherlands: Elsevier science publishers, 1986.

[167] S. P. Timoshenko and S. Winowsky-Krieger, *Theory of plates and shells.* Newyork: McGraw-Hill, second ed., 1959.

[168] A. C. Ugural, *Stresses in plates and shells.* Singapore: McGraw-Hill Publishers, second ed., 1999.

[169] E. N. Dowling, *Mechanical behavior of materials: Engineering methods for deformation, fracture & fatigue.* NewJersy: Prentice Hall, second ed., 2006.

[170] C.-G. Gustafson, "Discussion: The stress intensity factors for cyclic reversed bending of a single edge cracked strip including crack surface interference, by P. C. Paris and H. Tada", *International Journal of Fracture*, vol. 12, no. 3, pp. 460–462, 1976.

[171] N. Anifantis and A. Dimarogonas, "Stability of columns with a single crack subjected to follower and vertical loads", *International Journal of Solids and Structures*, vol. 19, no. 4, pp. 281 – 291, 1983.

[172] H. Boduroglu and F. Erdogan, "Internal and edge cracks in plate of finite width under bending", *Journal of Applied Mechanics*, vol. 50, pp. 620–629, 1983.

[173] W. K. Wilson and D. G. Thompson, "On the finite element method for calculating stress intensity factors for cracked plates in bending", *Engineering fracture mechanics*, vol. 3, pp. 97–102, 1971.

[174] A. T. Zehnder and C. Y. Hui, "A theory for the fracture of thin plates subjected to bending and twisting moments", *International journal of Fracture*, vol. 61, pp. 211–229, 1993.

[175] A. T. Zehnder and C. Y. Hui, "Stress intensity factors for plate bending and shearing problems", *Journal of Applied Mechanics*, vol. 61, pp. 719–722, 1994.

[176] D. P. Rooke and D. J. Cartwright, *Compendium of stress intensity factors.* London: HMSO, 1976.

[177] A. D. Belegundu and T. R. Chandrupatla, *Optimization concepts and applications in engineering.* Singapore: Pearson Eucation Pte. Ltd., (Indian print), second ed., 2003.

[178] M. S. Gockenbach, "Introduction to sequential quadratic programming (lecture notes on numerical optimisation)", 2003.

[179] J. L. Hu, Z. Wu, H. McCann, L. E. Davis and C. G. Xie, "Sequential quadratic programming method for solution of electromagnetic inverse problems", *Antennas and Propagation, IEEE Transactions on*, vol. 53, no. 8, pp. 2680–2687, 2005.

[180] G. N. Vanderplaats, *Numerical optimization techniques for engineering design: With applications.* McGraw-Hill Inc.: New York, 1984.

[181] K. Deb, *Optimization for Engineering Design: Algorithms and Examples.* NewDelhi: Prentice Hall of India, 1995.

[182] K. Deb, *Multi-Objective optimization using evolutionary algorithms.* England: John Wiley and Sons Ltd., first ed., 2001.

[183] K. Deb and H.-G. Beyer, "Self-aadaptive genetic algorithms with simulated binary crossover", *Evolutionary computation*, vol. 9, no. 2, pp. 197–221, 2001.

[184] K. Deb, A. Pratap, S. Agarwal and T. A. Meyarivan, "A fast and elitist multiobjective genetic algorithm: NSGA-II", *Evolutionary Computation, IEEE Transactions on*, vol. 6, no. 2, pp. 182–197, 2002.

[185] D. J. Inman, *Engineering vibration.* Upper Saddle River, NJ: Prentice Hall, 2001.

[186] R. D. Blevins, *Formulas for Natural Frequency and Mode Shape.* New York: Van Nostrand Reinhold Company, 1979.

[187] Z. K. Kusculuoglu, B. Fallahi and T. J. Royston, "Finite element model of a beam with a piezoceramic patch actuator", *Journal of Sound and Vibration*, vol. 276, no. 1-2, pp. 27–44, 2004.

[188] R. I. Mackie, "Improving finite element predictions of modes of vibration", *International Journal for Numerical Methods in Engineering*, vol. 33, no. 2, pp. 333–344, 1992.

[189] J. Kim, V. V. Varadan and V. K. Varadan, "Finite element modelling of structures including piezoelectric active devices", *International Journal for Numerical Methods in Engineering*, vol. 40, no. 5, pp. 817–832, 1997.

[190] F. Beer and E. R. Johnston Jr, *Vector Mechanics for Engineers: Statics and Dynamics*. St. Paul: West Publishing Company, 1976.

[191] A. R. de Leon and Y. Zhu, "ANOVA extensions for mixed discrete and continuous data", *Computational Statistics Data Analysis*, vol. 52, no. 4, pp. 2218–2227, 2008.

[192] "The statistical analysis of data from normal distribution, with particular reference to small samples (Report no: ESDU 91041)", Technical report., ESDU - Engineering Sciences Data Unit, December, 1991.

[193] T. G. Chondros, A. D. Dimarogonas and J. Yao, "Vibration of a beam with a breathing crack", *Journal of Sound and Vibration*, vol. 239, no. 1, pp. 57 – 67, 2001.

[194] M. Amabili, "Theory and experiments for large-amplitude vibrations of rectangular plates with geometric imperfections", *Journal of Sound and Vibration*, vol. 291, no. 3-5, pp. 539–565, 2006.

[195] M. Amabili, "Nonlinear vibrations of rectangular plates with different boundary conditions: Theory and experiments", *Computers & Structures*, vol. 82, no. 31-32, pp. 2587–2605, 2004.

[196] L. Dietrich, W. Kawahara and A. Phillips, "An experimental study of plastic buckling of a simply supported plate under edge thrusts", *Acta Mechanica*, vol. 29, pp. 257–267, 1978.

[197] A. D. Dimarogonas and S. A. Paipetis, *Analytical methods in rotor dynamics*. London: Applied Science publishers, 1983.

Finite width correction factors for through thickness cracks and their integrals

A.1 Correction factors for through-thickness cracks in thick beams

The finite width correction factor for through-thickness cracks in beams or plates, $f(b/W)$ or $f(\gamma)$, in Eqn. [4.24], can be obtained from Boduroglu and Erdogan [172]. In case of thick plates, the $f(\gamma)$ is not just a function of normalised crack length (b/W), but also a function of width to thickness ratio (W/h). Boduroglu and Erdogan [172] derived the *SIF* for plates with 5 different width to thickness $(W/h = 4, 8, 12, 16 \text{ and } 20)$ ratios as

$$
\begin{aligned}
f(\gamma)_{W/h=4} &= 21.15\gamma^5 - 34.6\gamma^4 + 20.15\gamma^3 - 3.39\gamma^2 - 0.53\gamma + 1 \\
f(\gamma)_{W/h=8} &= 37.97\gamma^5 - 52.28\gamma^4 + 24.63\gamma^3 - 0.16\gamma^2 - 1.63\gamma + 1 \\
f(\gamma)_{W/h=12} &= 2.12\gamma^5 + 8.22\gamma^4 - 16.82\gamma^3 + 11.17\gamma^2 - 2.94\gamma + 1.01 \quad \text{(A.1)} \\
f(\gamma)_{W/h=16} &= 26.65\gamma^5 + 8.09\gamma^4 - 34.84\gamma^3 + 19.03\gamma^2 - 3.91\gamma + 1.01 \\
f(\gamma)_{W/h=20} &= -79.64\gamma^5 + 144.38\gamma^4 - 98.15\gamma^3 + 31.75\gamma^2 - 4.88\gamma + 1
\end{aligned}
$$

The integral $g(\gamma)$ of the finite width correction factor is obtained from Eqn. [4.26] as

$$
g(\gamma) = \frac{8}{b^2} \int\limits_{0}^{b/2} f(\zeta/W)^2 \zeta d\zeta
$$

The values of $g(\gamma)$ corresponding to the above equations for $f(\gamma)$ (in Eqn. [A.1]) are obtained as

$$
\begin{aligned}
g(\gamma)_{W/h=4} \;=\; & 74.55\gamma^{10} - 266.09\gamma^{9} + 409.85\gamma^{8} - 341.62\gamma^{7} + 154.48\gamma^{6} \\
& -16.49\gamma^{5} - 26.33\gamma^{4} + 17.56\gamma^{3} - 3.25\gamma^{2} - .7\gamma + 1 \\[4pt]
g(\gamma)_{W/h=8} \;=\; & 240.25\gamma^{10} - 790.76\gamma^{9} + 1030.12\gamma^{8} - 629.66\gamma^{7} + 125.32\gamma^{6} \\
& +72.86\gamma^{5} - 65.07\gamma^{4} + 19.97\gamma^{3} + 1.17\gamma^{2} - 2.18\gamma + 1.01 \\[4pt]
g(\gamma)_{W/h=12} \;=\; & .75\gamma^{10} + 6.34\gamma^{9} - .76\gamma^{8} - 50.92\gamma^{7} + 113.51\gamma^{6} \\
& -119.93\gamma^{5} + 80.06\gamma^{4} - 39.8\gamma^{3} + 15.55\gamma^{2} - 3.94\gamma + 1.01 \\[4pt]
g(\gamma)_{W/h=16} \;=\; & 118.4\gamma^{10} + 78.37\gamma^{9} - 358.4\gamma^{8} + 100.25\gamma^{7} + 328.3\gamma^{6} \\
& -381.71\gamma^{5} + 217.07\gamma^{4} - 87.61\gamma^{3} + 26.8\gamma^{2} - 5.25\gamma + 1.01 \\[4pt]
g(\gamma)_{W/h=20} \;=\; & 1057.06\gamma^{10} - 4181.16\gamma^{9} + 7295.82\gamma^{8} - 7422.32\gamma^{7} + 4894.94\gamma^{6} \\
& -2228.94\gamma^{5} + 751.84\gamma^{4} - 202.75\gamma^{3} + 43.79\gamma^{2} - 6.53\gamma + 1.01
\end{aligned}
\tag{A.2}
$$

A.2 Correction factor for beams used in Experiments

In experiments, for validation of the inverse problem of beams with centre cracks, their width to thickness ratio was 15.6 ($W/h = 15.6$). The correction factors were obtained by interpolating the above equations, which is shown below along with the function $g(\gamma)$.

$$
f(\gamma)_{W/h=15.6} \;=\; 25.68\gamma^{5} + 6.76\gamma^{4} - 32.71\gamma^{3} + 18.25\gamma^{2} - 3.83\gamma + 1
$$

$$
\tag{A.3}
$$

$$
\begin{aligned}
g(\gamma)_{W/h=15.6} \;=\; & 110.7\gamma^{10} + 63.8\gamma^{9} - 329.1\gamma^{8} + 110.2\gamma^{7} + 282.4\gamma^{6} - \\
& 343.3\gamma^{5} + 200\gamma^{4} - 82.5\gamma^{3} + 25.8\gamma^{2} - 5.1\gamma + 1
\end{aligned}
$$

$$
\tag{A.4}
$$

Comparison of graphical and numerical solution to the inverse problem for beams

Damage detection in beams is carried out by finding the point of intersection of the *DI vs* x_c curves. This section compares two different techniques for triangulating and finding the optimum crack parameters.

B.1 Natural frequency extraction

The natural frequencies of the uncracked beam and the beams containing through-thickness cracks were extracted from *FEA* and incorporated into the damage detection algorithm. The dimensions of the cantilever beam used in the simulation were $L = 850mm$, $W = 100mm$ and $h = 6.4mm$. The beam is made of aluminium alloy with a Young's Modulus of $69.6GPa$ and density of $2772Kg/m^3$. Through-thickness cracks were incorporated in the beams at four different locations with nine different crack sizes at each location. *SHELL93* elements were used to model the beams to facilitate modelling the through-thickness cracks. The natural frequencies extracted from the *FEM* for various damage cases, which were incorporated into the damage detection algorithm, are shown in Table B.1.

Table B.1: Natural frequencies and % change in natural
frequencies for beam damaged at different locations and
of different lengths

	$x_c/L\sharp$	$\gamma\sharp$	Natural frequencies (Hz) (Hz)			% change in frequencies compared to undamaged beam		
			Mode1	Mode2	Mode3	Mode1	Mode2	Mode3
		0.02	7.233	45.299	126.932	0.010	0.004	0.001
		0.04	7.231	45.295	126.929	0.036	0.014	0.003
		0.06	7.228	45.288	126.925	0.076	0.030	0.006
		0.08	7.224	45.279	126.92	0.127	0.049	0.010
	0.1	0.1	7.22	45.268	126.914	0.188	0.072	0.015
		0.2	7.186	45.189	126.866	0.647	0.247	0.053
		0.3	7.135	45.066	126.791	1.365	0.518	0.112
		0.4	7.062	44.897	126.685	2.367	0.891	0.195
Damaged		0.5	6.965	44.677	126.544	3.702	1.378	0.306
beam		0.02	7.233	45.301	126.931	0.007	0.000	0.002
		0.04	7.231	45.301	126.924	0.026	0.000	0.007
		0.06	7.229	45.301	126.914	0.055	0.001	0.015

Continued on next page. . .

	$x_c/L\sharp$	$\gamma\sharp$	Natural frequencies (Hz) (Hz)			% change in frequencies compared to undamaged beam		
			Mode1	Mode2	Mode3	Mode1	Mode2	Mode3
		0.08	7.227	45.31	126.901	0.091	0.001	0.025
	0.2	0.1	7.223	45.3	126.886	0.135	0.002	0.037
		0.2	7.12	45.298	126.77	0.466	0.006	0.128
		0.3	7.162	45.295	126.589	0.984	0.014	0.271
		0.4	7.109	45.29	126.334	1.713	0.025	0.472
		0.5	7.039	45.283	125.991	2.692	0.040	0.742
		0.02	7.233	45.301	126.926	0.004	0.001	0.005
		0.04	7.232	45.299	126.906	0.017	0.005	0.021
		0.06	7.231	45.297	126.877	0.036	0.010	0.044
		0.08	7.229	45.294	126.839	0.061	0.016	0.074
	0.3	0.1	7.227	45.29	126.794	0.090	0.024	0.109
		0.2	7.211	45.264	126.46	0.310	0.083	0.373
		0.3	7.186	45.222	125.938	0.658	0.176	0.783
		0.4	7.15	45.162	125.216	1.149	0.306	1.353
Damaged		0.5	7.102	45.082	124.262	1.814	0.483	2.104
beam		0.02	7.233	45.299	126.929	0.003	0.005	0.003

	$x_c/L\sharp$	$\gamma\sharp$	Natural frequencies (Hz) (Hz)			% change in frequencies compared to undamaged beam		
			Mode1	Mode2	Mode3	Mode1	Mode2	Mode3
		0.04	7.232	45.294	126.918	0.011	0.017	0.011
		0.06	7.232	45.285	126.903	0.022	0.036	0.024
		0.08	7.231	45.275	126.883	0.037	0.059	0.040
	0.4	0.1	7.229	45.262	126.859	0.055	0.087	0.058
		0.2	7.22	45.166	126.679	0.189	0.298	0.200
		0.3	7.204	45.016	126.399	0.402	0.630	0.421
		0.4	7.182	44.805	126.01	0.705	1.095	0.727
		0.5	7.152	44.523	125.495	1.118	1.718	1.132

$\sharp \Rightarrow x_c/L$ and $\gamma\ (= b/W)$ denote the location and size of crack respectively

B.2   Results from *graphical* and *least square (numerical)* methods

As explained in Section 4.6.1, the solution to the inverse problem in beams can be obtained using the graphical technique (also called as *centroid* method) or using the numerical *least square* method (also called the *distance* method). Both the methods are applied to the 36 damage cases shown in Table B.1 and the results are presented in the Figs. B.1 and B.2.

Figs. B.1(a) and B.1(b) show the normalised discrepancies in predicting the locations of cracks using the *centroid* method and the *least square* method respectively. It can be observed that the locations of cracks are predicted accurately ($< 1\%$) irrespective of the triangulation technique used. The normalised discrepancies in predicting the sizes of cracks using the two techniques are shown in Figs. B.2(a) and B.2(b). Again, it is seen that the crack sizes are predicted with a good accuracy ($< 0.8\%$) using either technique. Thus either methods can be applied to deduce the location and sizes of cracks in beams, with *least square* method having the added advantage that it can be extended to the solution of the inverse problem in plates which involves three or four crack variables.
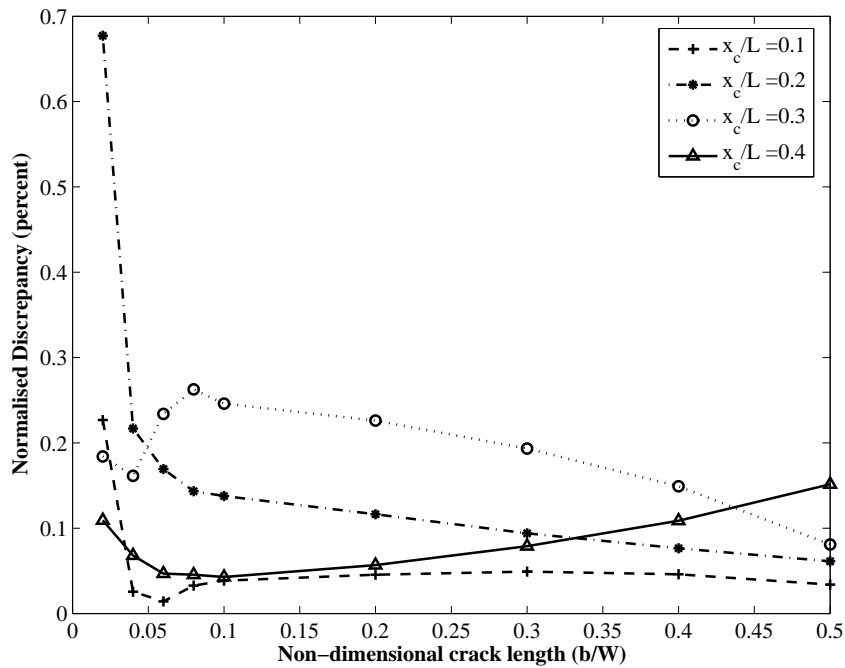
(a) *Centroid* method
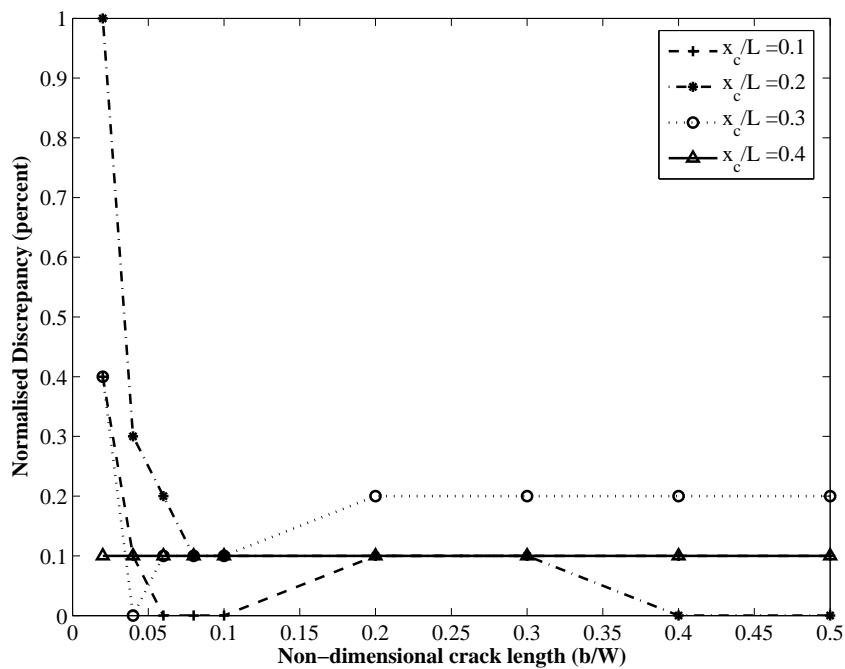
(b) *Least square* method

Figure B.1: Normalised discrepancy in locating cracks
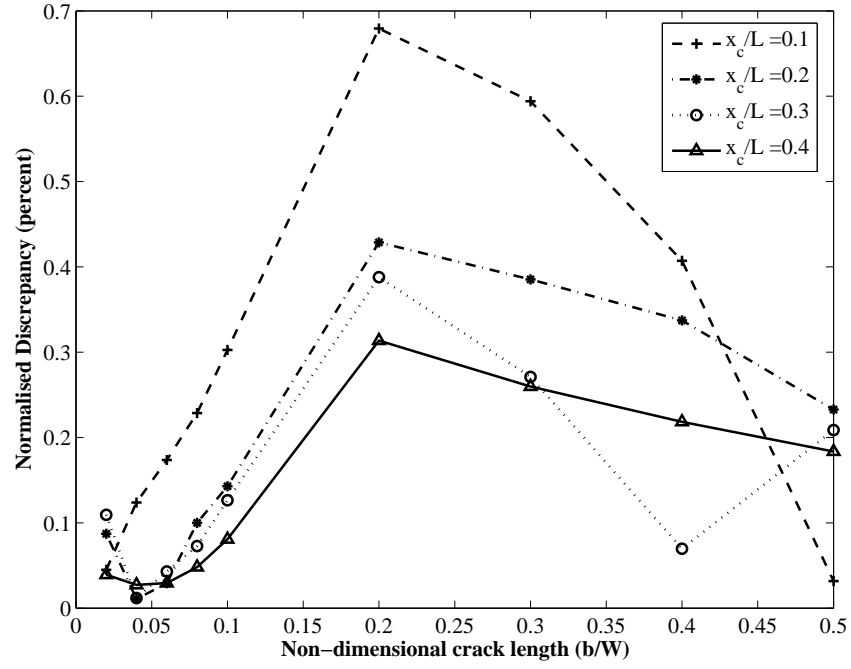
(a) *Centroid* method
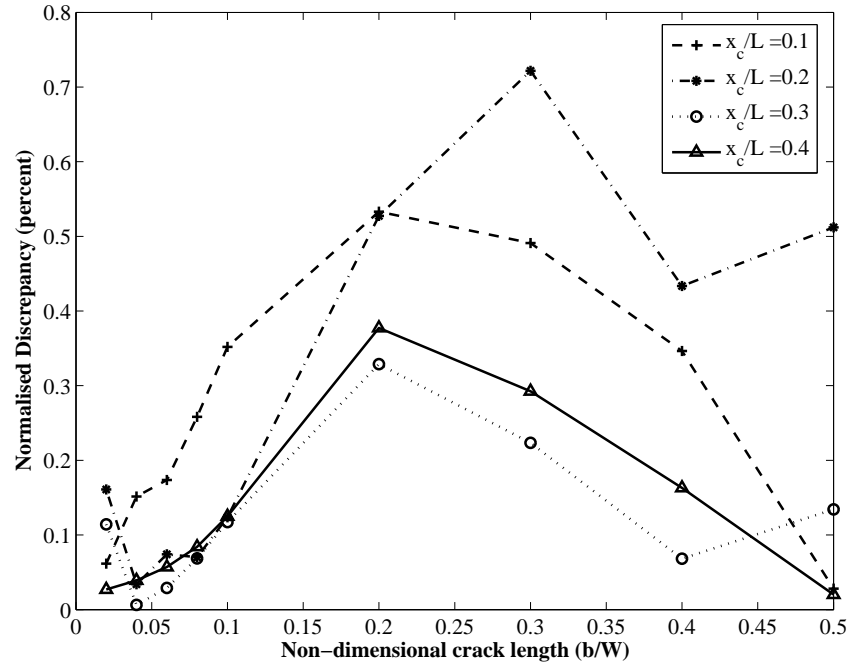
(b) *Least square* method

Figure B.2: Normalised discrepancy in determining sizes of cracks

Linearity of frequency change with square of normalised curvature

Eqn. [4.18] establishes that the normalised frequency change varies linearly with the square of the curvature at the damage location normalised with the average curvature of the structure (χ_c^2/χ_{RMS}^2). This is verified in Section 5.3 using natural frequencies and curvatures for the first ten modes of damage case 1 in Table 5.4 (Fig. 5.4). This section presents results from this analysis for the remaining nine damage cases in Table 5.4. (The numerical labels indicate mode numbers)
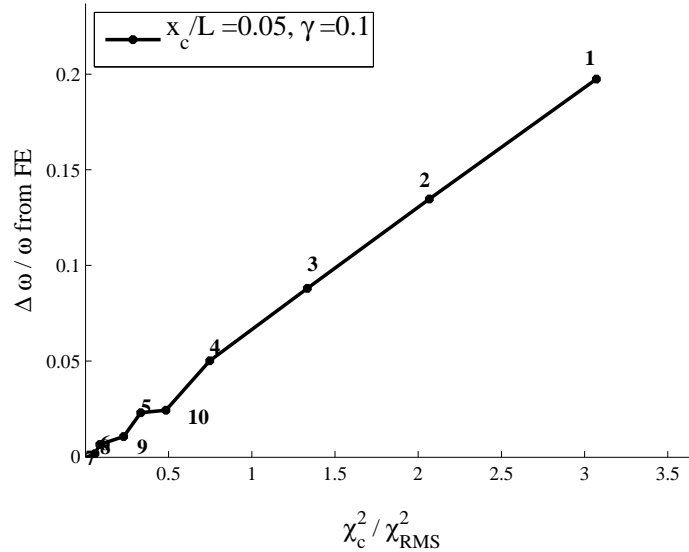
(a) Damage case 2
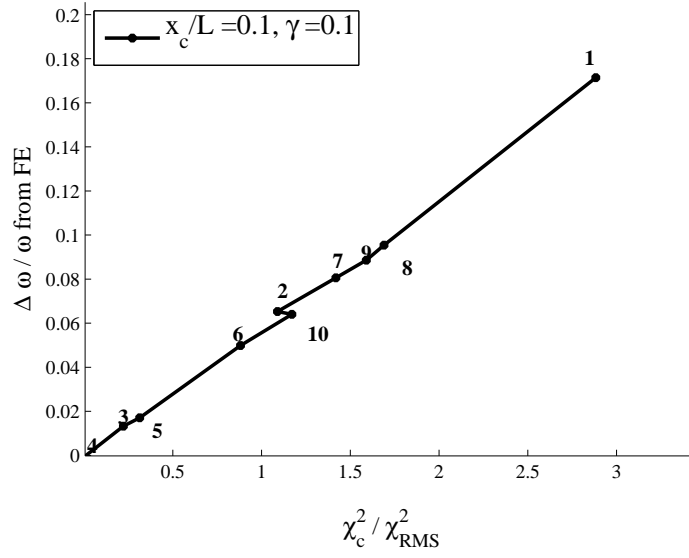
(b) Damage case 3
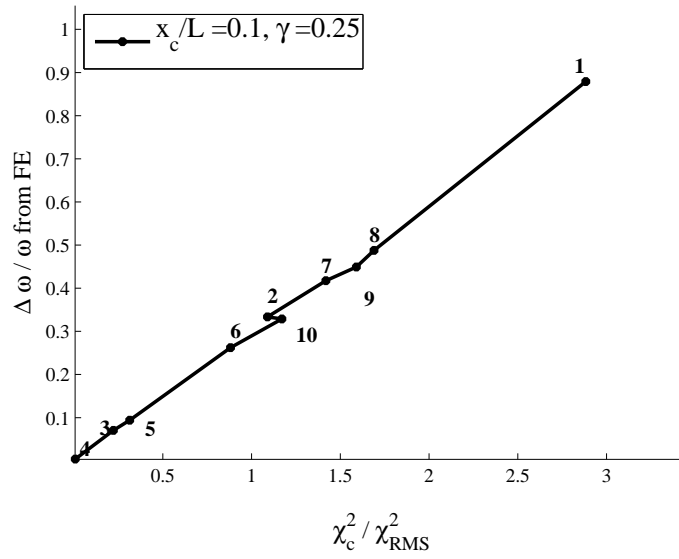
(c) Damage case 4
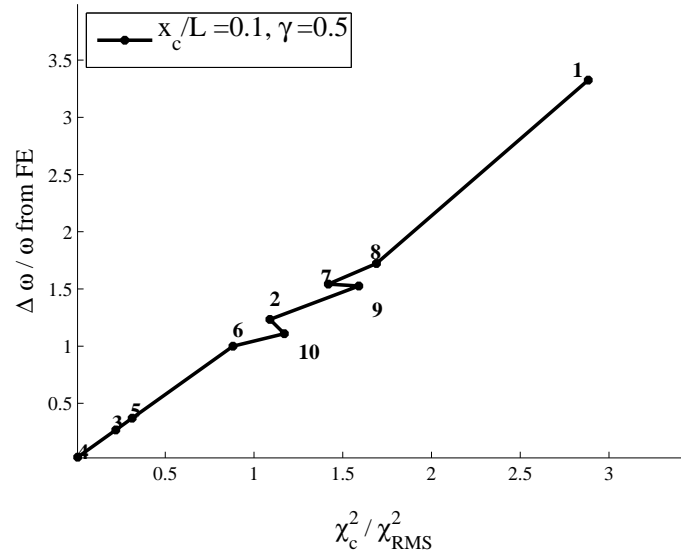
(d) Damage case 5
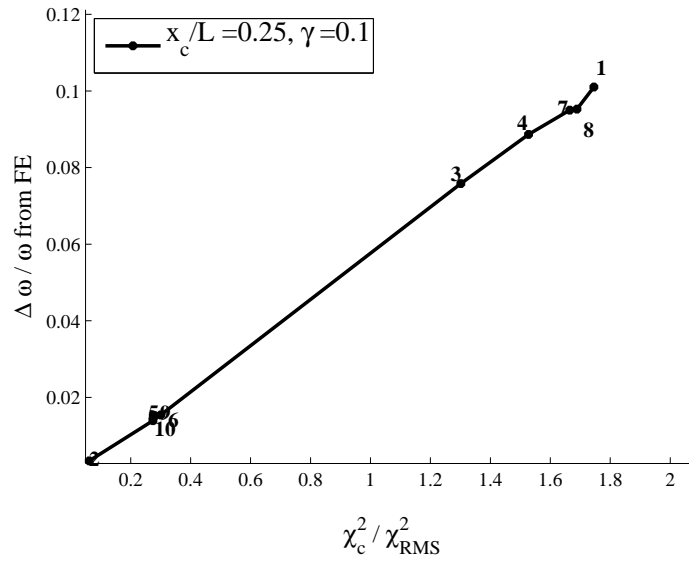
(e) Damage case 6
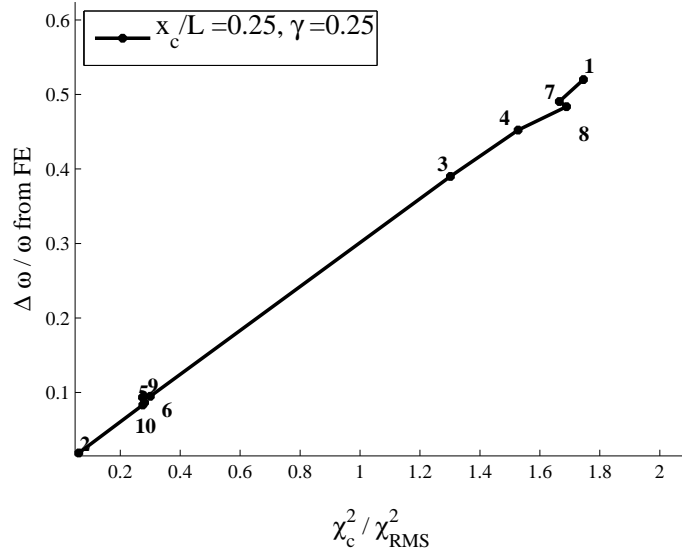
(f) Damage case 7

(g) Damage case 8
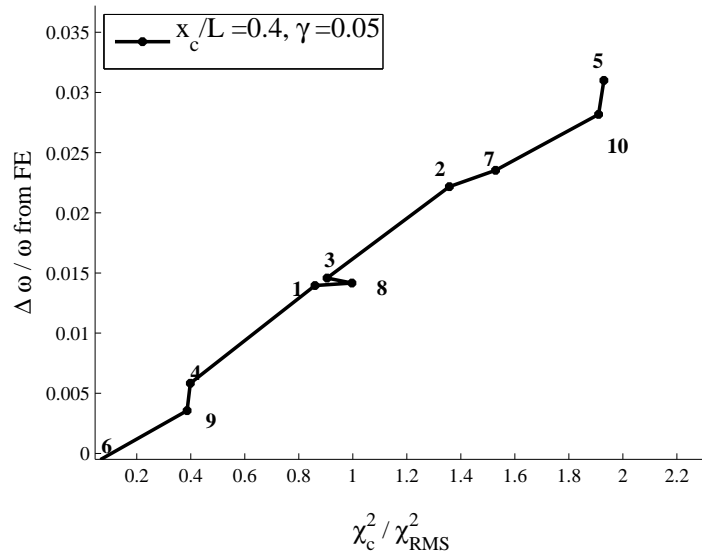
(h) Damage case 9

(i) Damage case 10
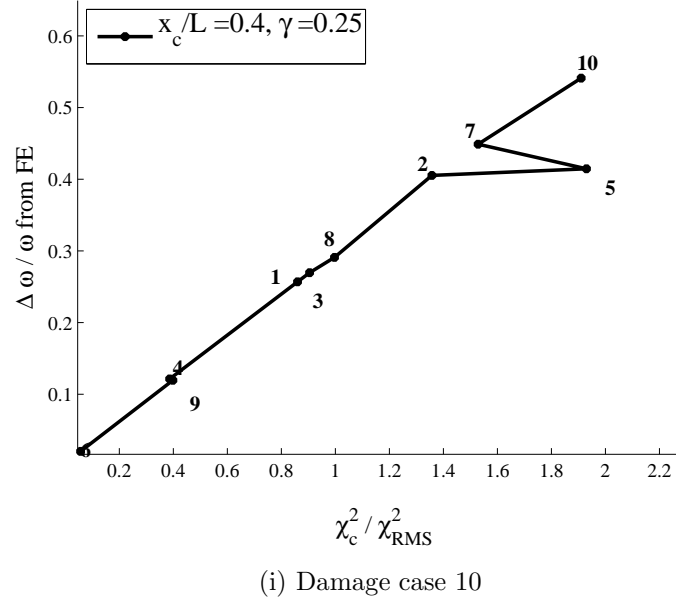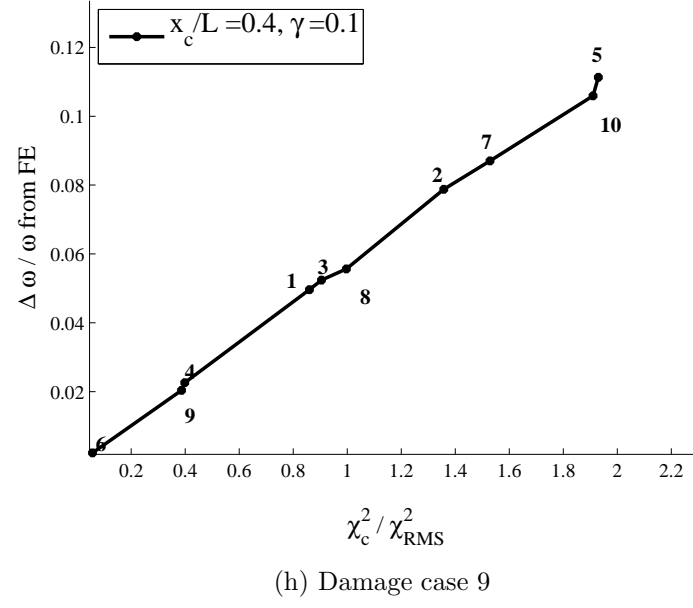
Figure C.1: Variation of normalised change in frequency with normalised curvature

Appendix D

Damage detection using equilibrium approach: Beams containing edge cracks

The theory for frequency changes due to edge cracks in beams using the force - equilibrium method [138,135,136,140] is presented below. Cracks can be represented as a rotational spring with stiffness, k_r, inversely proportional to its size. It is assumed that where there is a crack, the beam is segmented, but connected by the spring.

D.1 Determination of location of crack

The presence of crack causes a local reduction in stiffness and hence a discontinuity (sudden increase) in slope at the location of the crack. This local change in stiffness and variation in slope can be modelled by a rotational spring which replaces the beam material at the location of crack. The spring stiffness can be tailored so that its rotational deformation is same as the change in slope at the location of crack. Bigger the crack, greater is the change in slope, hence the spring has a lower stiffness. Based on this principle, a crack beam vibration theory is derived (equilibrium method).

According to Euler-Bernoulli vibration theory, the governing equation for transverse beam vibration is given as [185],

$$EI\frac{\partial^4 y}{\partial x^4} = -\rho A\frac{\partial^2 y}{\partial t^2} \tag{D.1}$$

The beam is segmented at the crack location, as shown in Fig. D.1. The deflection of the two segments, segment1 to the left and segment2 to the right of
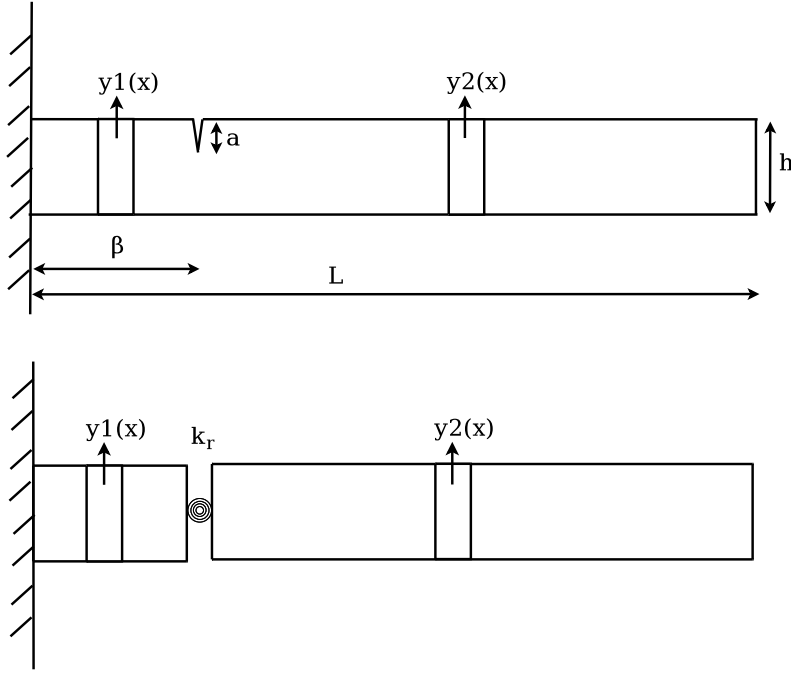
Figure D.1: Cantilever beam segmented along location of crack

the crack satisfying the governing differential equation can be assumed to be of the form

$$y_1(x) = a_1 sin\lambda x + a_2 cos\lambda x + a_3 sinh\lambda x + a_4 cosh\lambda x \qquad \text{(D.2)}$$

$$y_2(x) = b_1 sin\lambda x + b_2 cos\lambda x + b_3 sinh\lambda x + b_4 cosh\lambda x \qquad \text{(D.3)}$$

Here, y_1, y_2 are deflections along the beam of length L, λ is the normalised natural frequency of the damaged beam defined as $\lambda^4 = \frac{\omega^2}{c2}$, ω is the natural frequency of the damaged beam and $c = \sqrt{\frac{EI}{\rho A}}$. Here, E is the youngs modulus, I the second moment of area of the beam whose thickness and width are h and W respectively, ρ density and A the cross section area. The coefficients a_1 to a_4 and b_1 to b_4 are determined by substituting the eight boundary conditions, four for each segment of the beam.

The solutions for vibration of Euler-Bernoulli beam , with or without crack, depends on the boundary conditions. The characteristic equation of the damaged beam for solving the forward problem of extracting the natural frequencies of a cracked beam is derived for two different boundary conditions, fixed-free (cantilever) and simply supported boundary condition.

D.1.1 Fixed-free beams

For a fixed-free beam, the conditions of zero deflection and slope at the fixed end, vanishing shear force and bending moment at the free end [185] shown in Eqns.[D.4] [D.5], continuity in deflection, shear force and bending moments across the crack and discontinuity in gradient deflection across the crack, given by Eqn. [D.6] are substituted in Eqns. [D.2] and [D.3] to obtain characteristic equation for the damaged cantilever beam.

At fixed end,

$$
\begin{aligned}
\text{Deflection, } y_1 &= 0 \\
\text{Slope, } \frac{\partial y_1}{\partial x} &= 0
\end{aligned}
\tag{D.4}
$$

At free end,

$$
\begin{aligned}
\text{Bending moment, } EI\frac{\partial^2 y_2}{\partial x^2} &= 0 \\
\text{Shear force, } \frac{\partial}{\partial x}\left[EI\frac{\partial^2 y_2}{\partial x^2}\right] &= 0
\end{aligned}
\tag{D.5}
$$

At the crack location $(x = x_c)$,

$$
\begin{aligned}
\text{Deflection, } y_1 &= y_2 \\
\text{Bending moment, } EI\frac{\partial^2 y_1}{\partial x^2} &= EI\frac{\partial^2 y_2}{\partial x^2} \\
\text{Shear force, } \frac{\partial}{\partial x}\left[EI\frac{\partial^2 y_1}{\partial x^2}\right] &= \frac{\partial}{\partial x}\left[EI\frac{\partial^2 y_2}{\partial x^2}\right]
\end{aligned}
\tag{D.6}
$$

$$
\begin{aligned}
Slope, \frac{\partial y_2}{\partial x} &= \frac{\partial y_1}{\partial x} + \theta_{crack} \\
\text{but, } \theta_{crack} &= \frac{M}{k_r} = \frac{EI\frac{\partial^2 y_1}{\partial x^2}}{k_r} \\
\text{Hence, slope } \frac{\partial y_2}{\partial x} &= \frac{\partial y_1}{\partial x} + \frac{EI}{k_r}\frac{\partial^2 y_1}{\partial x^2}
\end{aligned}
\tag{D.7}
$$

Introducing a non-dimensional parameter for location along the beam length defined as $\beta = x/L$

$$\text{Slope } \frac{\partial y_2}{\partial \beta} \quad = \quad \frac{\partial y_1}{\partial \beta} + \frac{1}{K}\frac{\partial^2 y_1}{\partial \beta^2} \tag{D.8}$$

$$\text{where, } K \quad = \quad \frac{k_r L}{EI} \tag{D.9}$$

The characteristic equation obtained substituting these boundary conditions in Eqns. [D.2] and [D.3] is shown in Eqn. [D.11]. This characteristic equation can be rewritten as

$$\lambda \Delta_1 + K \Delta_2 = 0 \tag{D.10}$$

$$|\Delta| = \begin{vmatrix} 1 & 1 & 0 & 0 & 0 & 0 & 0 & 0 \\ 0 & 0 & 1 & 1 & 0 & 0 & 0 & 0 \\ 0 & 0 & 0 & 0 & -\cos\lambda & \cosh\lambda & -\sin\lambda & \sinh\lambda \\ 0 & 0 & 0 & 0 & \sin\lambda & \sinh\lambda & -\cos\lambda & \cosh\lambda \\ \cos\alpha & \cosh\alpha & \sin\alpha & \sinh\alpha & -\cos\alpha & -\cosh\alpha & -\sin\alpha & -\sinh\alpha \\ -\cos\alpha & \cosh\alpha & -\sin\alpha & \sinh\alpha & \cos\alpha & -\cosh\alpha & \sin\alpha & -\sinh\alpha \\ \sin\alpha & \sinh\alpha & -\cos\alpha & \cosh\alpha & -\sin\alpha & -\sinh\alpha & \cos\alpha & -\cosh\alpha \\ -\frac{K}{\lambda}\sin\alpha - \cos\alpha & \frac{K}{\lambda}\sinh\alpha + \cosh\alpha & \frac{K}{\lambda}\cos\alpha - \sin\alpha & \frac{K}{\lambda}\cosh\alpha + \sinh\alpha & \frac{K}{\lambda}\sin\alpha & -\frac{K}{\lambda}\sinh\alpha & -\frac{K}{\lambda}\cos\alpha & -\frac{K}{\lambda}\cosh\alpha \end{vmatrix} = 0 \qquad \text{(D.11)}$$

where $\alpha = \lambda\beta$

Δ_1 and Δ_2 for cantilever beams are given as

$$|\Delta_1| = \begin{vmatrix} 1 & 1 & 0 & 0 & 0 & 0 & 0 & 0 \\ 0 & 0 & 1 & 1 & 0 & 0 & 0 & 0 \\ 0 & 0 & 0 & 0 & -cos\lambda & cosh\lambda & -sin\lambda & sinh\lambda \\ 0 & 0 & 0 & 0 & sin\lambda & sinh\lambda & -cos\lambda & cosh\lambda \\ cos\alpha & cosh\alpha & sin\alpha & sinh\alpha & -cos\alpha & -cosh\alpha & -sin\alpha & -sinh\alpha \\ -cos\alpha & cosh\alpha & -sin\alpha & sinh\alpha & cos\alpha & -cosh\alpha & sin\alpha & -sinh\alpha \\ sin\alpha & sinh\alpha & -cos\alpha & cosh\alpha & -sin\alpha & -sinh\alpha & cos\alpha & -cosh\alpha \\ -sin\alpha & sinh\alpha & cos\alpha & cosh\alpha & sin\alpha & -sinh\alpha & -cos\alpha & -cosh\alpha \end{vmatrix}$$

(D.12)

$$|\Delta_2| = \begin{vmatrix} 1 & 1 & 0 & 0 & 0 & 0 & 0 & 0 \\ 0 & 0 & 1 & 1 & 0 & 0 & 0 & 0 \\ 0 & 0 & 0 & 0 & -cos\lambda & cosh\lambda & -sin\lambda & sinh\lambda \\ 0 & 0 & 0 & 0 & sin\lambda & sinh\lambda & -cos\lambda & cosh\lambda \\ cos\alpha & cosh\alpha & sin\alpha & sinh\alpha & -cos\alpha & -cosh\alpha & -sin\alpha & -sinh\alpha \\ -cos\alpha & cosh\alpha & -sin\alpha & sinh\alpha & cos\alpha & -cosh\alpha & sin\alpha & -sinh\alpha \\ sin\alpha & sinh\alpha & -cos\alpha & cosh\alpha & -sin\alpha & -sinh\alpha & cos\alpha & -cosh\alpha \\ -cos\alpha & cosh\alpha & -sin\alpha & sinh\alpha & 0 & 0 & 0 & 0 \end{vmatrix}$$

(D.13)

D.1.2 Simply-supported beam

This approach of modelling crack as a rotational spring is also implemented for simply supported beams containing edge crack. Here the boundary condition will remain the same at the location of crack. As far as the boundary conditions at the two ends of the beam, the deflection and bending moment at both the ends are zero, as shown in Eqns. [D.14 & D.15].

At near end of a simply supported beam,

$$
\begin{aligned}
\text{Deflection, } y_1 &= 0 \\
\text{Bending moment, } EI\frac{\partial y_1''}{\partial x} &= 0
\end{aligned}
\tag{D.14}
$$

At farther end of a simply supported beam,

$$
\begin{aligned}
\text{Deflection, } y_2 &= 0 \\
\text{Bending moment, } EI\frac{\partial y_2''}{\partial x} &= 0
\end{aligned}
\tag{D.15}
$$

These four equations for the end conditions (Eqns. [D.14 & D.15]) together with the boundary conditions at the location of crack, as in Eqns. [D.6 & D.8], are substituted in Eqns. [D.2 & D.3]. A characteristic equation is thus obtained to find natural frequency of a simply supported beam containing edge crack, as shown in Eqn. [D.16].

This equation can be used to calculate the damaged beams natural frequencies, if the damage parameters are known. It can also be seen that the characteristic equation obtained for simply supported beam is different from that of fixed-free beam. Thus it can be stated that the characteristic equations of damaged beams are highly dependent on the boundary conditions. Eqn. [D.16] can also be rewritten as in Eqn. [D.10], but here, $\Delta 1$ and $\Delta 2$ are derived as presented in Eqns. [D.17] and [D.18].

$$|\Delta| = \begin{vmatrix} 1 & 0 & 1 & 0 & 0 & 0 & 0 & 0 \\[6pt] 1 & 0 & -1 & 0 & 0 & 0 & 0 & 0 \\[6pt] \cosh\alpha & \sinh\alpha & \cos\alpha & \sin\alpha & -\cosh\alpha & -\sinh\alpha & -\cos\alpha & -\sin\alpha \\[6pt] \sinh\alpha & \cosh\alpha & \sin\alpha & -\cos\alpha & -\sinh\alpha & -\cosh\alpha & -\sin\alpha & \cos\alpha \\[6pt] \cosh\alpha & \sinh\alpha & -\cos\alpha & -\sin\alpha & -\cosh\alpha & -\sinh\alpha & \cos\alpha & \sin\alpha \\[6pt] 0 & 0 & 0 & 0 & \cosh\lambda & \sinh\lambda & \cos\lambda & \sin\lambda \\[6pt] 0 & 0 & 0 & 0 & \cosh\lambda & \sinh\lambda & -\cos\lambda & -\sin\lambda \\[6pt] \frac{K}{\lambda}\sin\alpha+\cosh\alpha & \frac{K}{\lambda}\cosh\alpha+\sinh\alpha & -\frac{K}{\lambda}\sin\alpha-\cos\alpha & \frac{K}{\lambda}\cos\alpha-\sin\alpha & -\frac{K}{\lambda}\sinh\alpha & -\frac{K}{\lambda}\cosh\alpha & \frac{K}{\lambda}\sin\alpha & -\frac{K}{\lambda}\cos\alpha \end{vmatrix} = 0 \qquad \text{(D.16)}$$

where $\alpha = \lambda\beta$

$$|\Delta_1| = \begin{vmatrix} sinh\alpha & sin\alpha & -cosh\alpha & -sinh\alpha & -cos\alpha & -sin\alpha \\ cosh\alpha & -cos\alpha & -sinh\alpha & -cosh\alpha & -sin\alpha & cos\alpha \\ sinh\alpha & -sin\alpha & -cosh\alpha & -sinh\alpha & cos\alpha & sin\alpha \\ 0 & 0 & cosh\lambda & sinh\lambda & cos\lambda & sin\lambda \\ 0 & 0 & cosh\lambda & sinh\lambda & -cos\lambda & -sin\lambda \\ cosh\alpha & cos\alpha & -sinh\alpha & -cosh\alpha & sin\alpha & -cos\alpha \end{vmatrix}$$

(D.17)

$$|\Delta_2| = \begin{vmatrix} sinh\alpha & sin\alpha & -cosh\alpha & -sinh\alpha & -cos\alpha & -sin\alpha \\ cosh\alpha & -cos\alpha & -sinh\alpha & -cosh\alpha & -sin\alpha & cos\alpha \\ sinh\alpha & -sin\alpha & -cosh\alpha & -sinh\alpha & cos\alpha & sin\alpha \\ 0 & 0 & cosh\lambda & sinh\lambda & cos\lambda & sin\lambda \\ o & 0 & cosh\lambda & sinh\lambda & -cos\lambda & -sin\lambda \\ sinh\alpha & -sin\alpha & 0 & 0 & 0 & 0 \end{vmatrix}$$

(D.18)

Eqn. [D.10] is used to solve the forward problem of detecting natural frequencies and Eqns. [D.12] and [D.13] or [D.17] and [D.18] are used depending on the beams boundary condition. The same equations can be used to find the location and size of crack in terms of the non-dimensional spring stiffness, K using the graphical technique explained in Section 4.6.1.

D.1.3 Correction factor for equilibrium method

In equilibrium technique, the decrease in frequencies calculated from Eqn. [D.10] is only a shift from the theoretical weighted frequencies obtained from Euler - Bernoulli beam vibration theory. Hence solving inverse problem of identifying the crack location and size using this technique does not only rely on the damaged beams natural frequencies, but inherently it also relies on the fact that measured natural frequencies of the undamaged beam are the same as those calculated from theory. In cases where the measured and theoretical natural frequencies of undamaged beam are not same, the measured natural frequencies of the damaged beam cannot be used directly in the damage detection algorithm and a correction factor is introduced. If non-dimensional natural frequencies measured from experiments on undamaged and damaged beam are λ_{UE} and λ_{DE} respectively, and those of undamaged beam calculated from theory are λ_{UT}, percentage differences between theoretical and experimental undamaged frequencies (λ_{UT} and λ_{UE}) is calculated and the same differences are incorporated to the cracked beams natural frequencies [140, 142].

$$\lambda_{DT} = \frac{\lambda_{UT}}{\lambda_{UE}} \lambda_{DE} \tag{D.19}$$

D.2 Determination of crack length

Stiffness of the spring, which is used to represent the crack, is analytically modelled such that it is proportional to the extent of damage. To quantitatively represent the extent of damage, a relation between the spring stiffness and crack length for beams with part thickness through width cracks (edge cracks), vibrating transversely has been derived by a few researchers [136, 135, 197] using the *Stress Intensity Factor (SIF)* for that crack configuration. They related the energy stored in the spring to the strain energy release which is a function of *SIF*.

If K_I is the *SIF* and A the area of the crack along the cross section of the beam, then the change in elastic deformation energy due to the crack, as given by Kobayashi [166], is

$$\Delta U = \frac{1}{E} \int^A K_I^2 dA \tag{D.20}$$

where, $K_I = \sigma \sqrt{\pi a} f(a/h)$, a is crack length and h is thickness of the beam. $f(a/h)$ is the correction factor and can be obtained from standard fracture mechanics handbook [176] as

$$f(a/h) = 1.13 - 1.374(a/h) + 5.74(a/h)^2 - 4.46(a/h)^3.$$

If M is the bending moment at the location of the crack then gross stress, $\sigma = 6M/Wh^2$ where W is the width of the beam. Also, if θ is the additional bending due to the presence of the crack, represented here as a rotational spring with stiffness is k_r, then the energy stored in the crack is given by,

$$\Delta U = \frac{1}{2} M\theta$$

Since $\theta = \frac{M}{k_r}$,

$$\Delta U = \frac{1}{2} \frac{M^2}{k_r} \tag{D.21}$$

Relating Eqns. [D.21] and [D.20], Ostcahowicz and Krawczuk [136] derived the relation between the non-dimensional spring stiffness (K) and thickness normalised crack length (a/h) as

$$K = \frac{L}{6\pi h g(a/h)} \tag{D.22}$$

where,

$$g(a/h) = 0.64(a/h)^2 - 1.035(a/h)^3 + 3.72(a/h)^4 -$$

$$5.18(a/h)^5 + 7.55(a/h)^6 - 7.33(a/h)^7 + 2.5(a/h)^8$$

Appendix E

Effect of modeshape resolution and mesh density on accuracy of crack detection

E.1 Beams containing though-thickness centre cracks

In Section 6.5.1, for validation of inverse problem from the experimental data, modeshapes extracted form *FEA* were used to calculate the curvatures. These modeshapes can be obtained with different resolutions and modelled with different mesh densities. While Section 6.5.1 presents prediction results of damage case 1 using 12 different modeshapes obtained from *FEA*, comparison of prediction of normalised discrepancies in the remaining 6 damage cases are presented here.
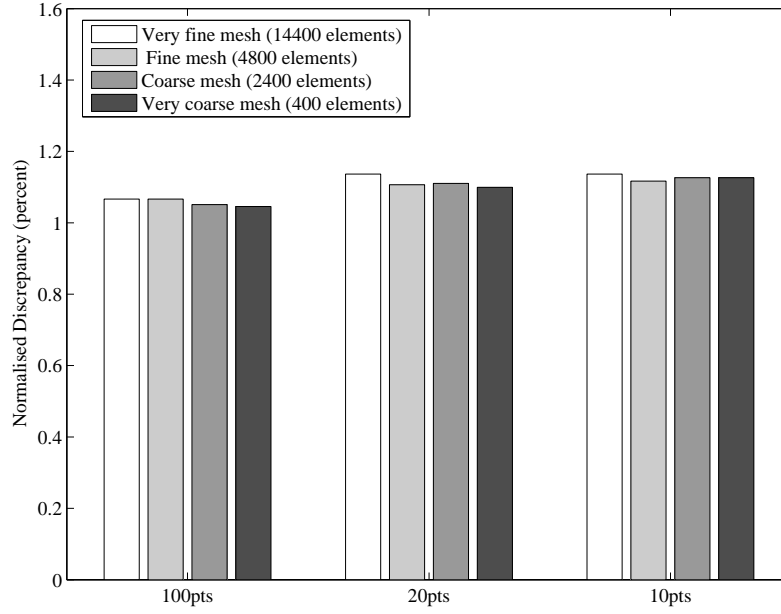
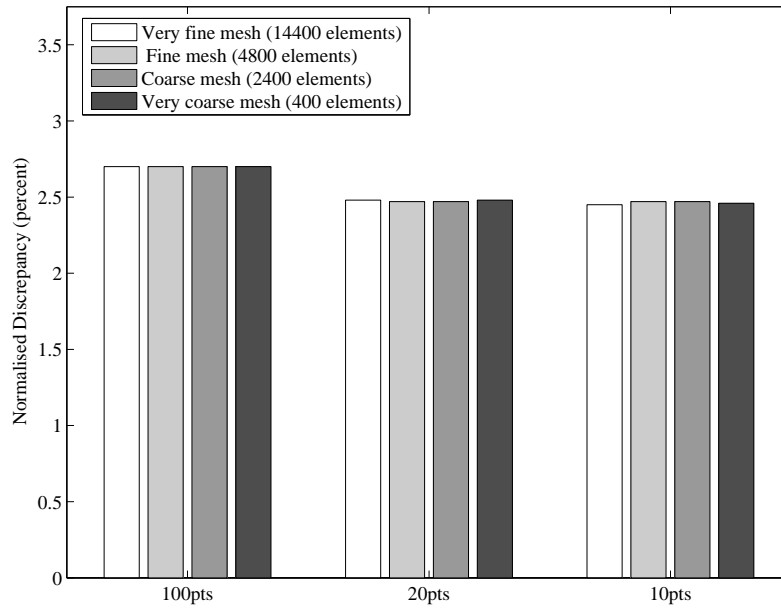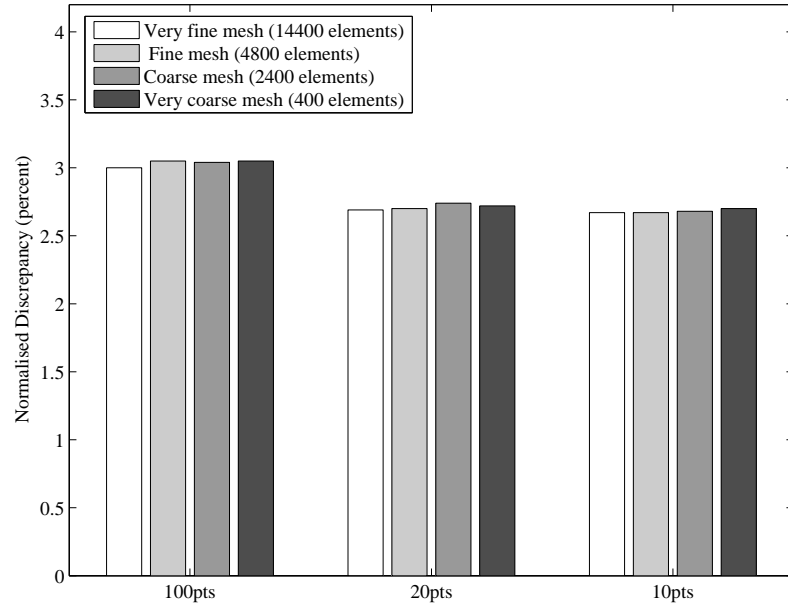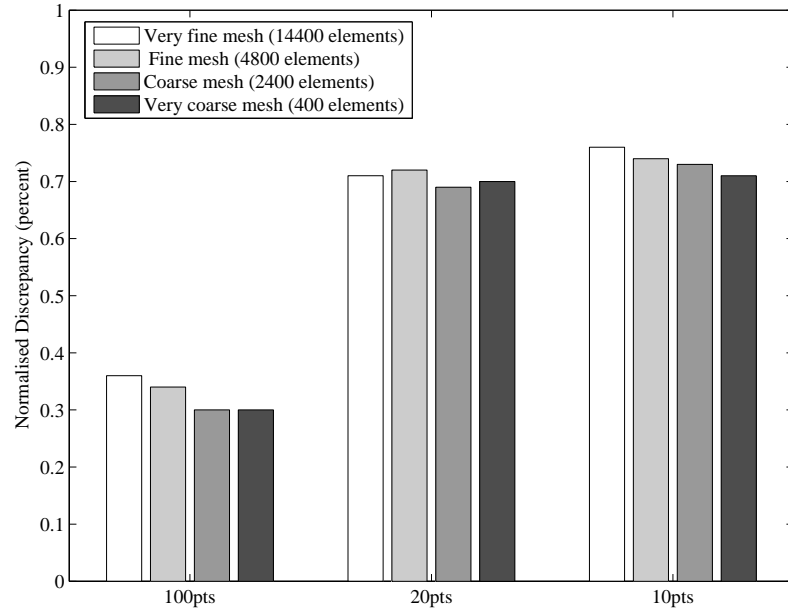(a) Comparison of normalised discrepancy in locating the crack
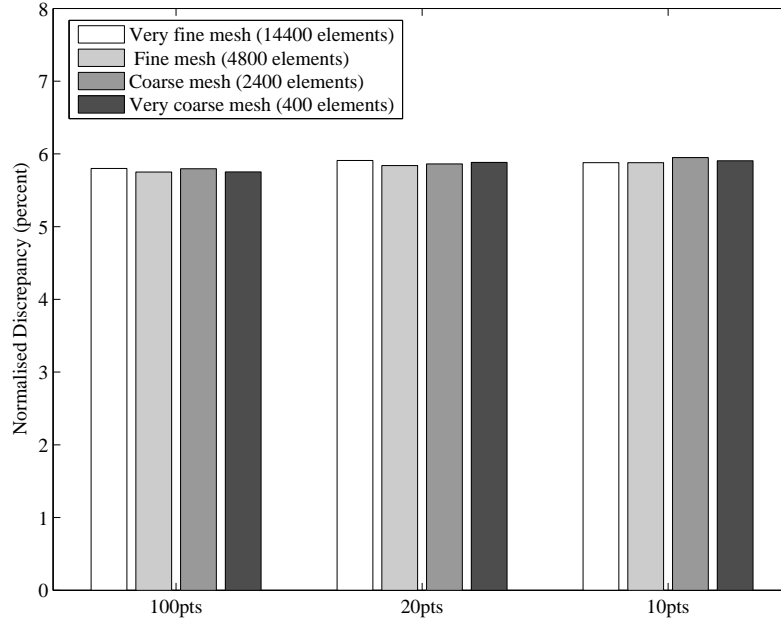
(b) Comparison of normalised discrepancy in determining the size of crack

Figure E.1: Comparison of normalised discrepancy in determining the location and size of centre crack : Damage case 2
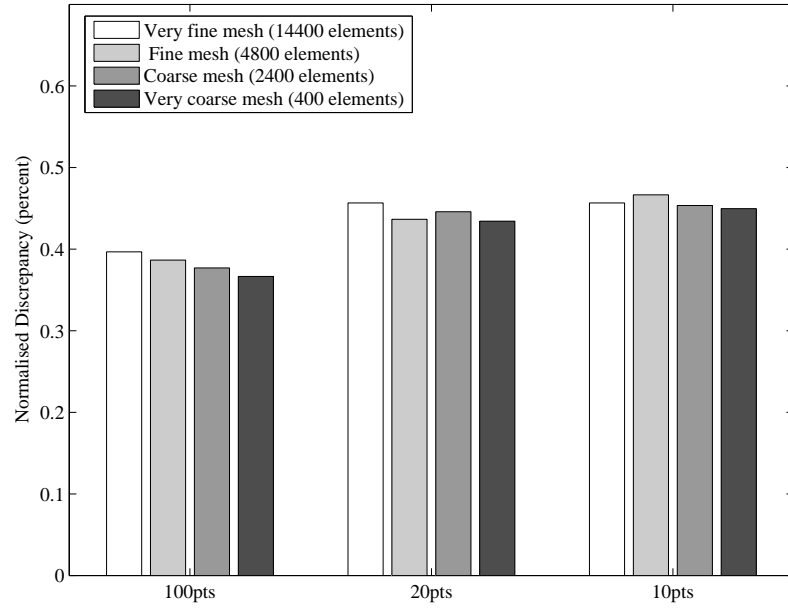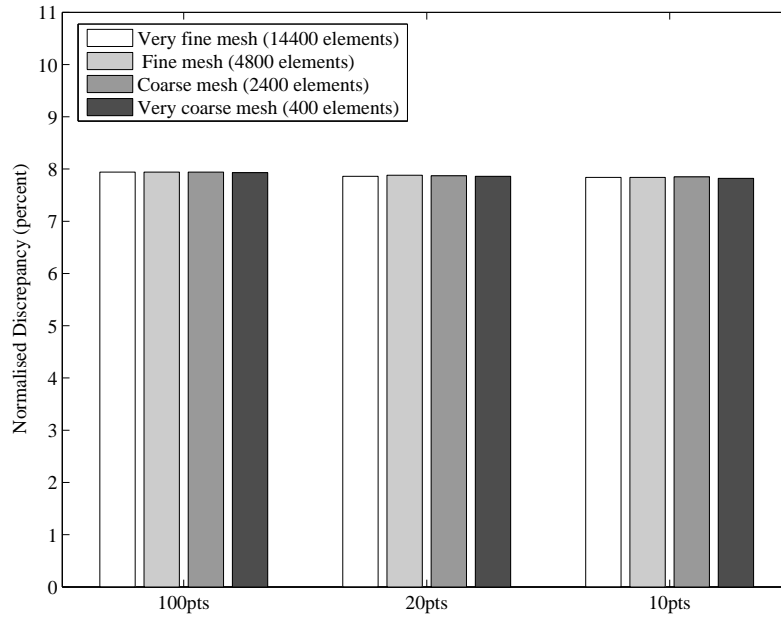
(a) Comparison of normalised discrepancy in locating the crack
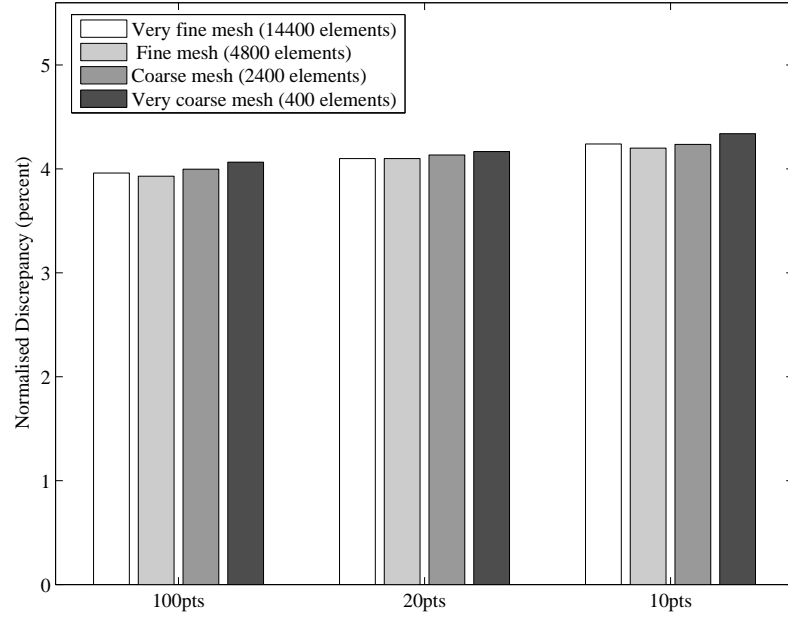
(b) Comparison of normalised discrepancy in determining the size of crack

Figure E.2: Comparison of normalised discrepancy in determining the location and size of centre crack : Damage case 3
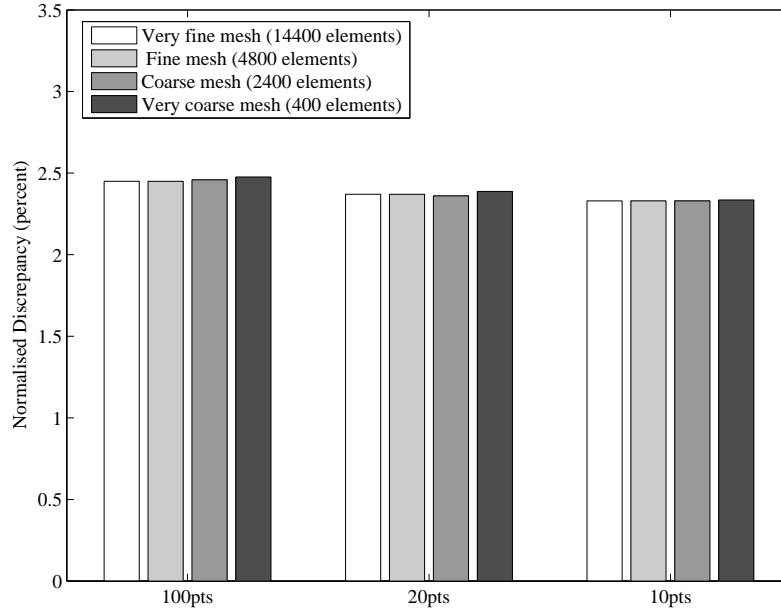
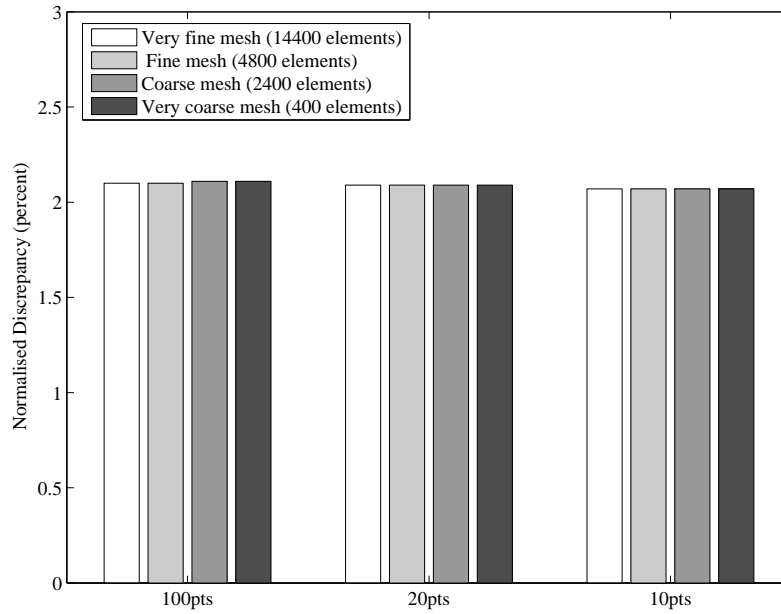(a) Comparison of normalised discrepancy in locating the crack
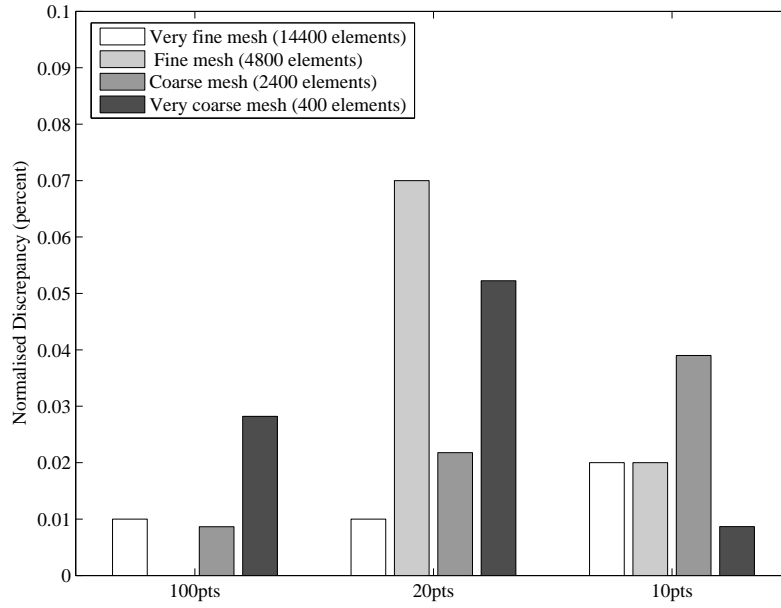
(b) Comparison of normalised discrepancy in determining the size of crack

Figure E.3: Comparison of normalised discrepancy in determining the location and size of centre crack : Damage case 4
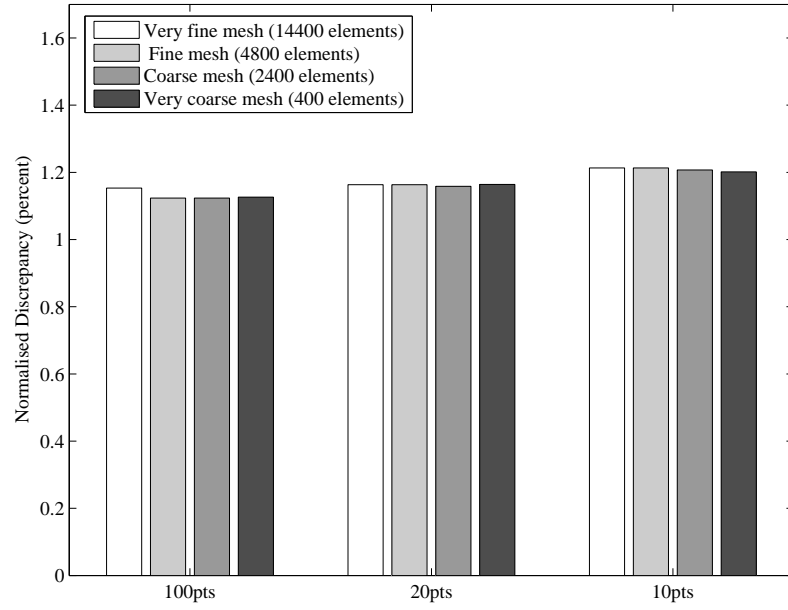
(a) Comparison of normalised discrepancy in locating the crack
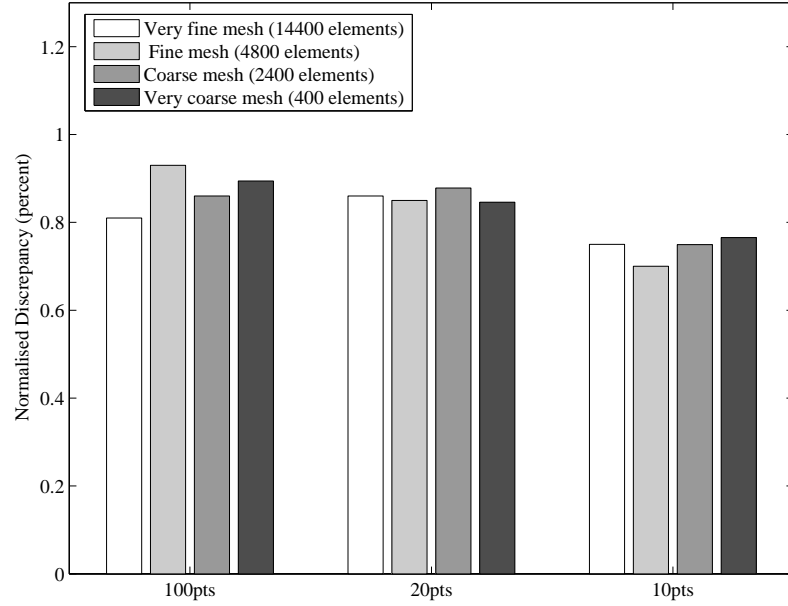
(b) Comparison of normalised discrepancy in determining the size of crack

Figure E.4: Comparison of normalised discrepancy in determining the location and size of centre crack : Damage case 5
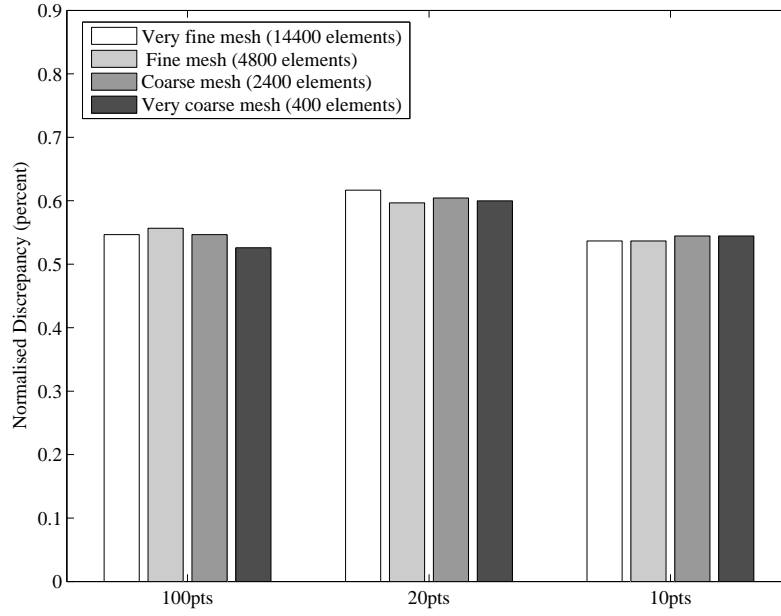
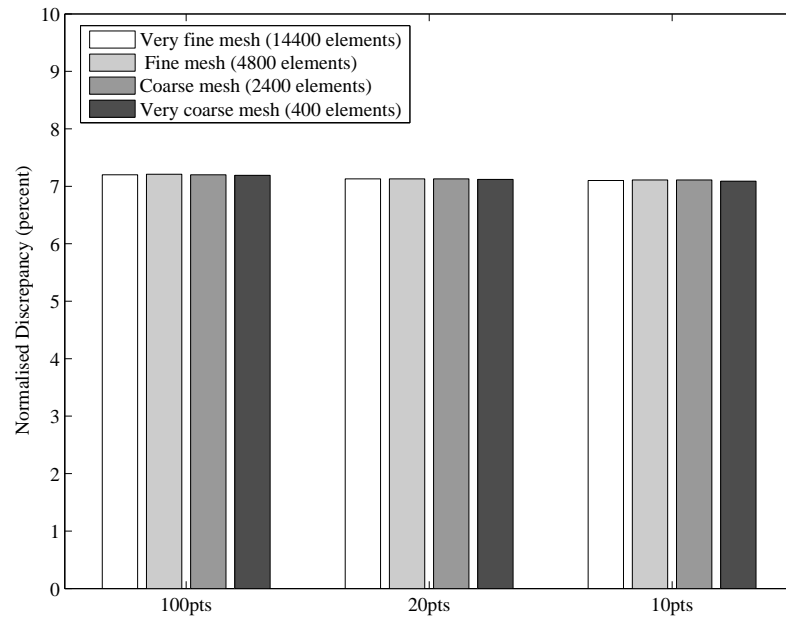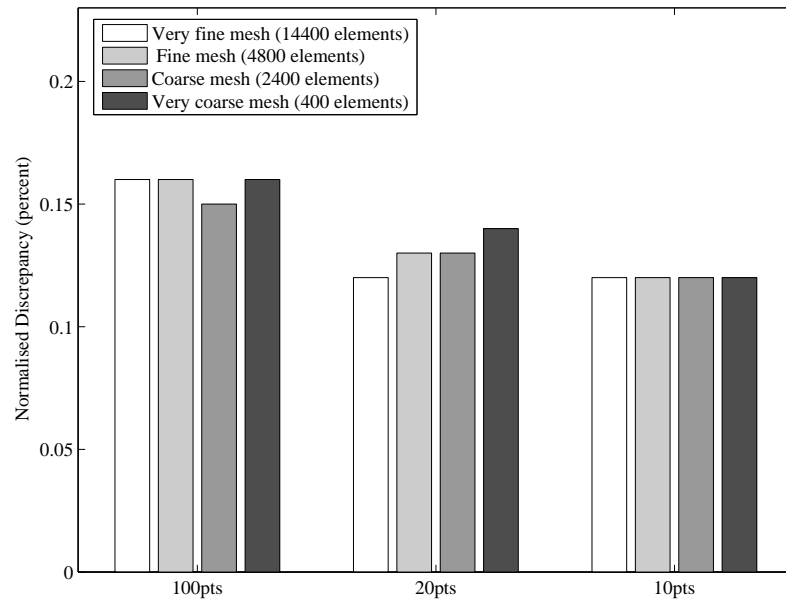(a) Comparison of normalised discrepancy in locating the crack
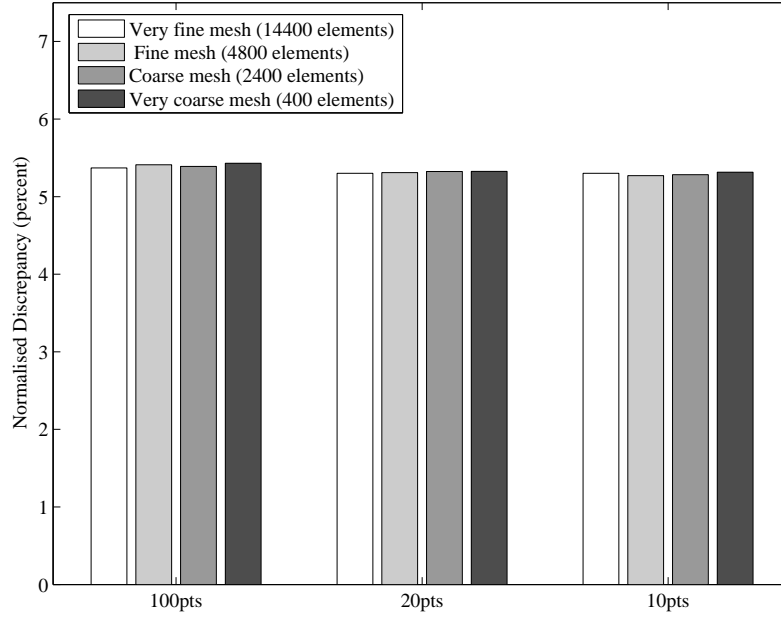
(b) Comparison of normalised discrepancy in determining the size of crack

Figure E.5: Comparison of normalised discrepancy in determining the location and size of centre crack : Damage case 6
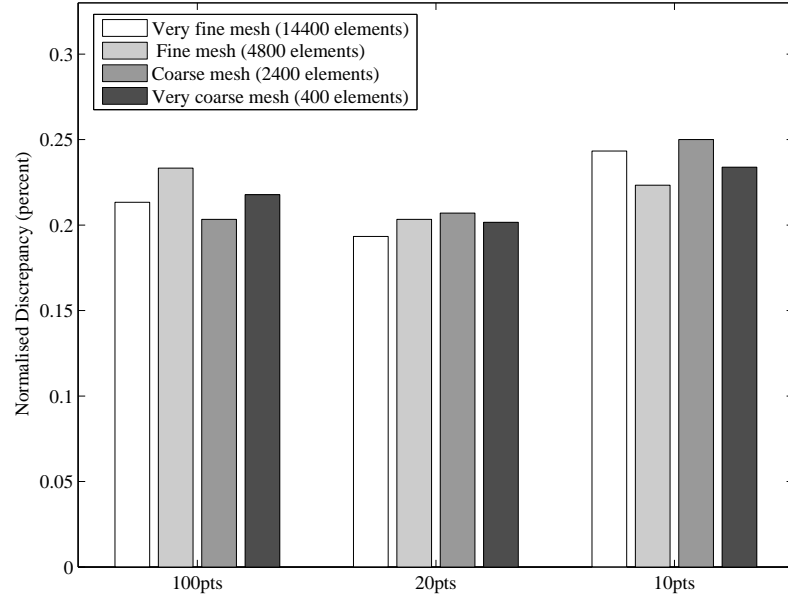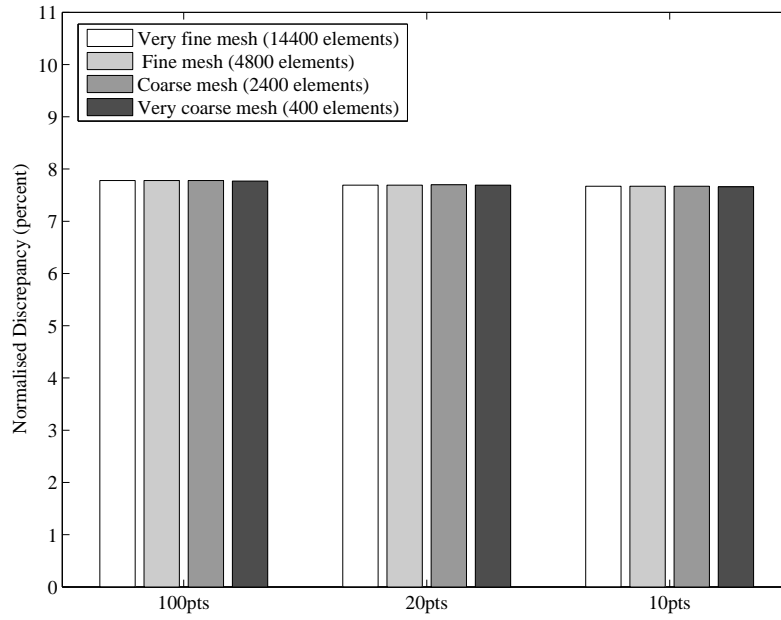
(a) Comparison of normalised discrepancy in locating the crack
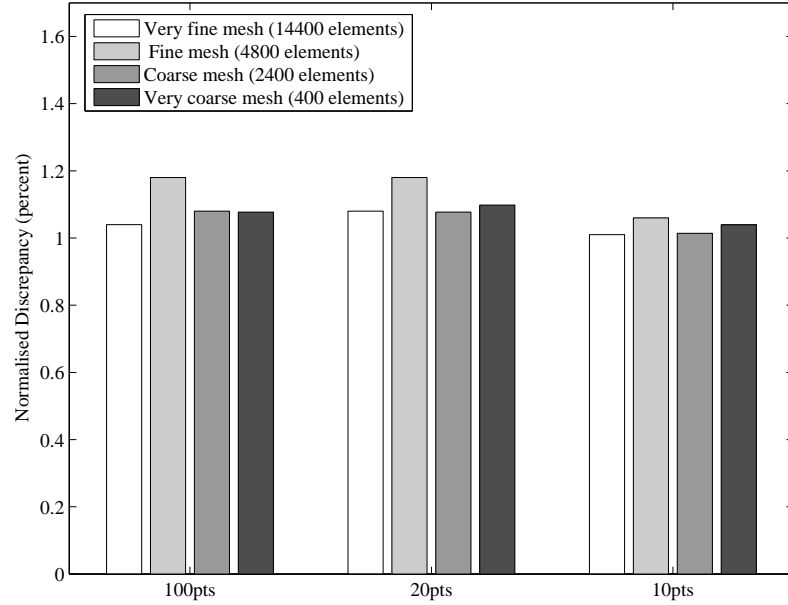
(b) Comparison of normalised discrepancy in determining the size of crack

Figure E.6: Comparison of normalised discrepancy in determining the location and size of centre crack : Damage case 7

E.2 Beams containing edge (part-through) cracks

This section presents results obtained from using the 12 different modeshapes to locate and characterise edge cracks from the experimental data. Section 6.5.2 presented comparison of normalised discrepancies for damage case 1, while the discrepancies in the remaining 9 damage cases are presented here.
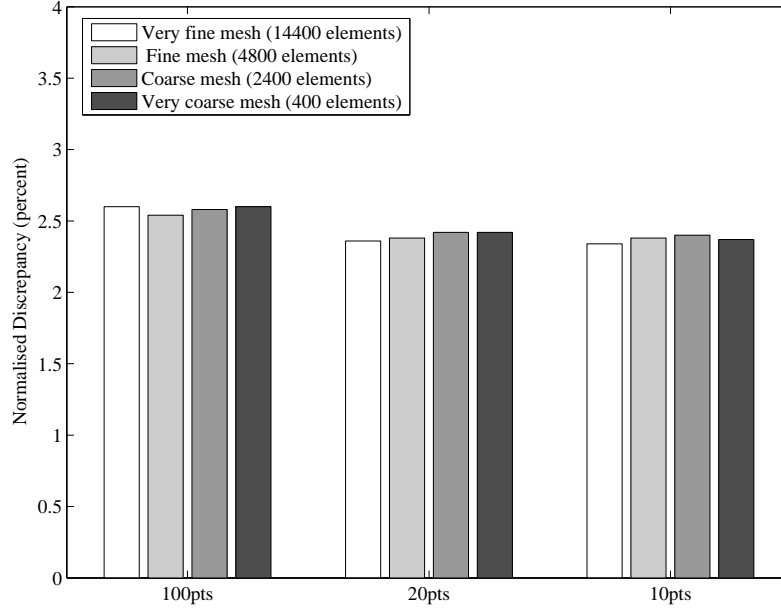
(a) Comparison of normalised discrepancy in locating the crack
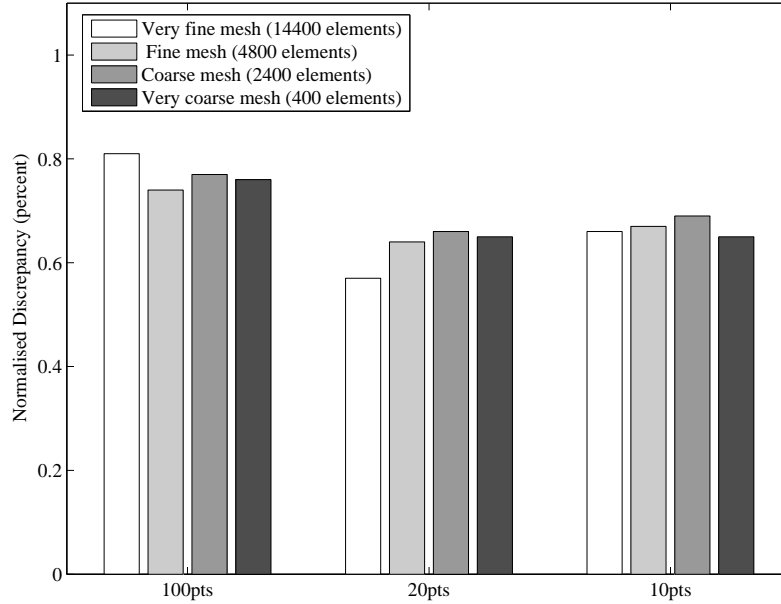
(b) Comparison of normalised discrepancy in determining the size of crack

Figure E.7: Comparison of normalised discrepancy in determining the location and size of edge crack : Damage case 2
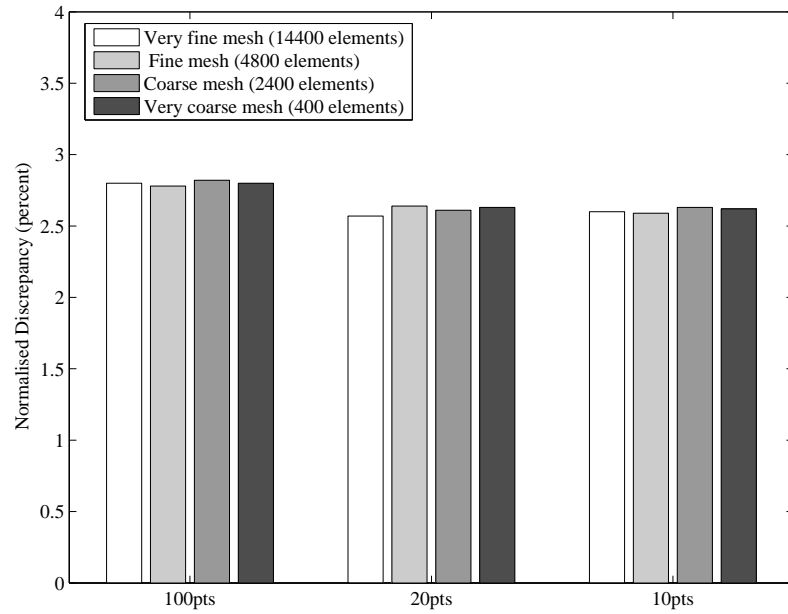
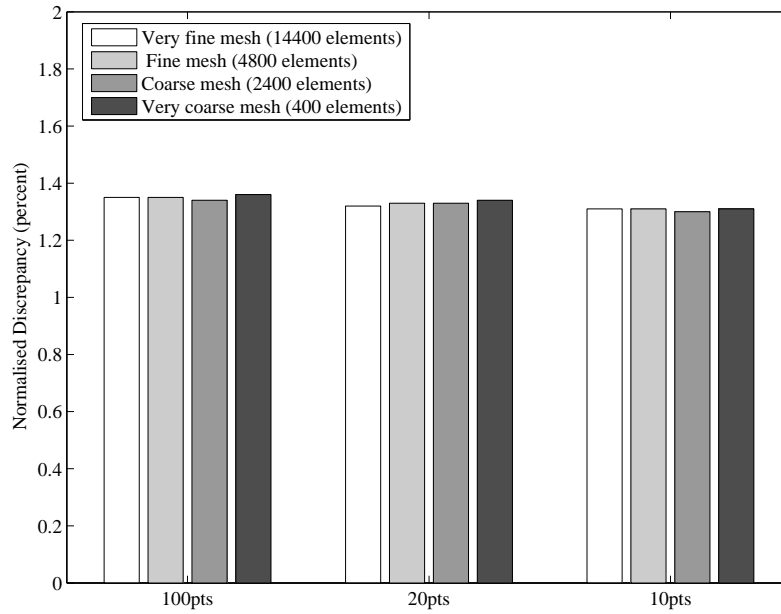(a) Comparison of normalised discrepancy in locating the crack
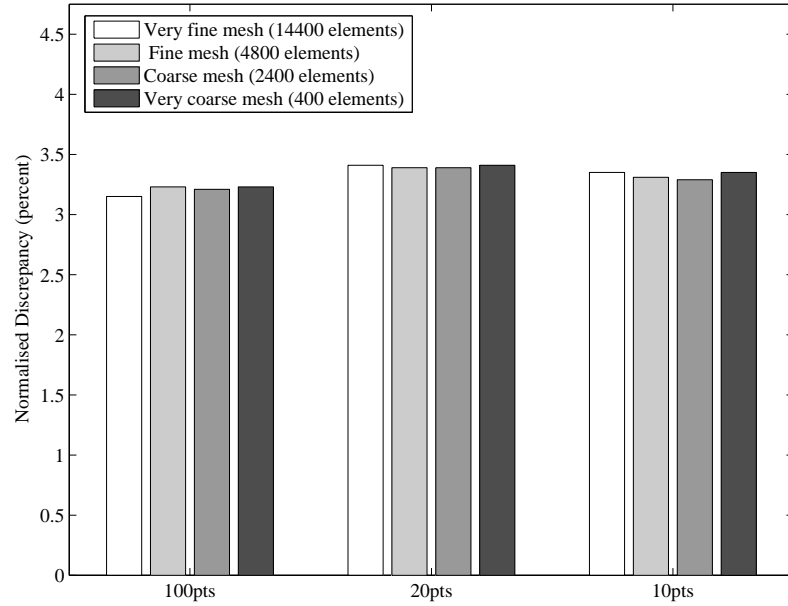
(b) Comparison of normalised discrepancy in determining the size of crack

Figure E.8: Comparison of normalised discrepancy in determining the location and size of edge crack : Damage case 3
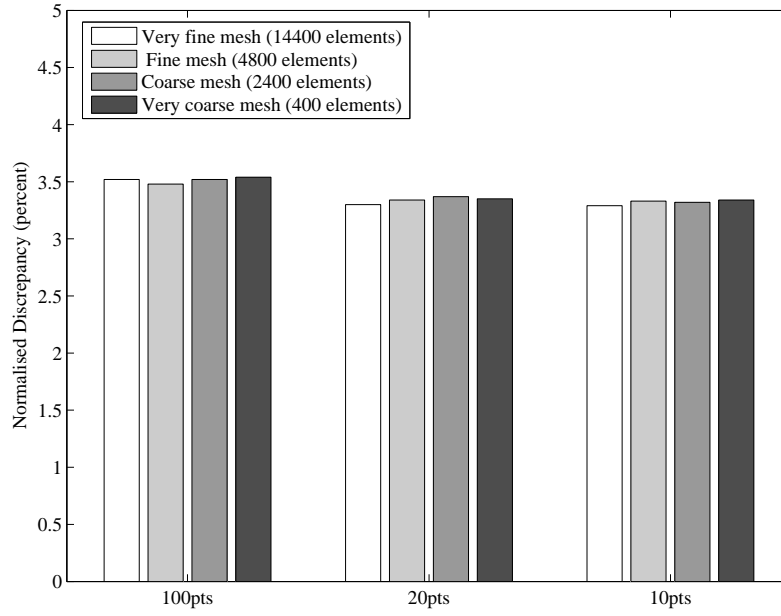
(a) Comparison of normalised discrepancy in locating the crack
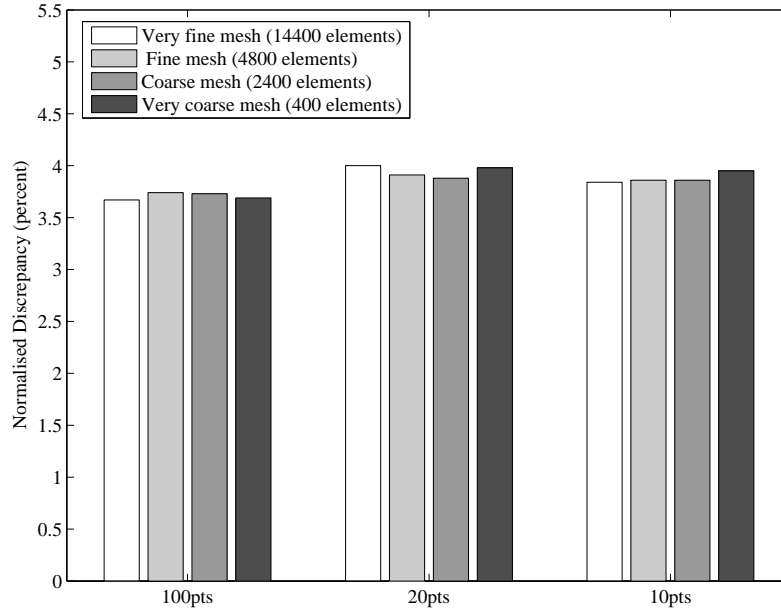
(b) Comparison of normalised discrepancy in determining the size of crack

Figure E.9: Comparison of normalised discrepancy in determining the location and size of edge crack : Damage case 4
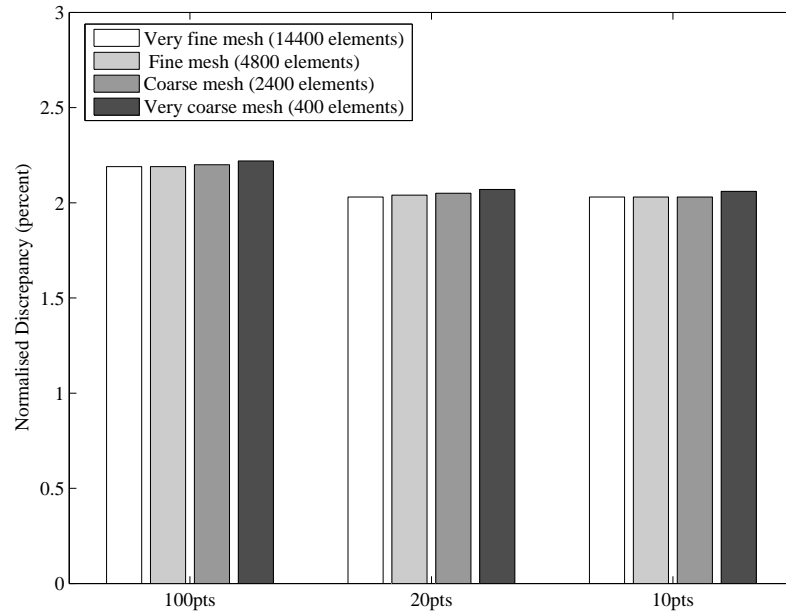
(a) Comparison of normalised discrepancy in locating the crack
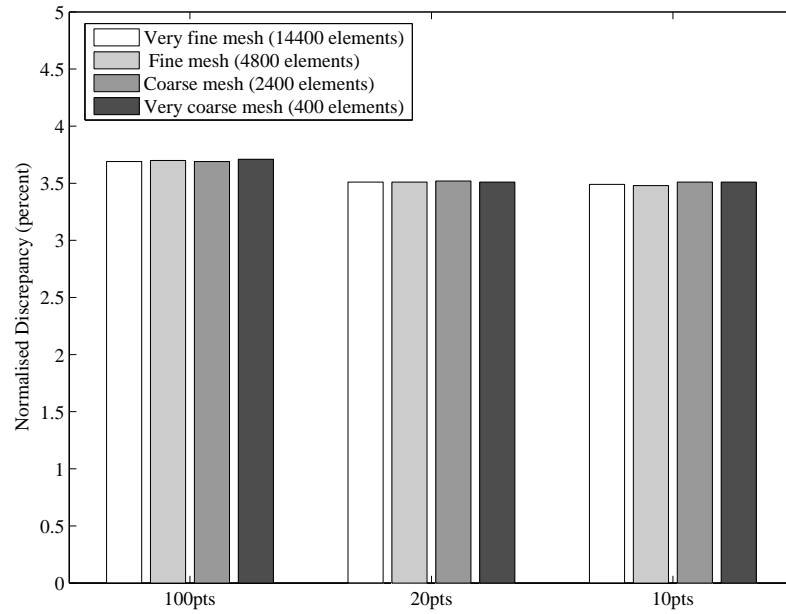
(b) Comparison of normalised discrepancy in determining the size of crack

Figure E.10: Comparison of normalised discrepancy in determining the location and size of edge crack : Damage case 5
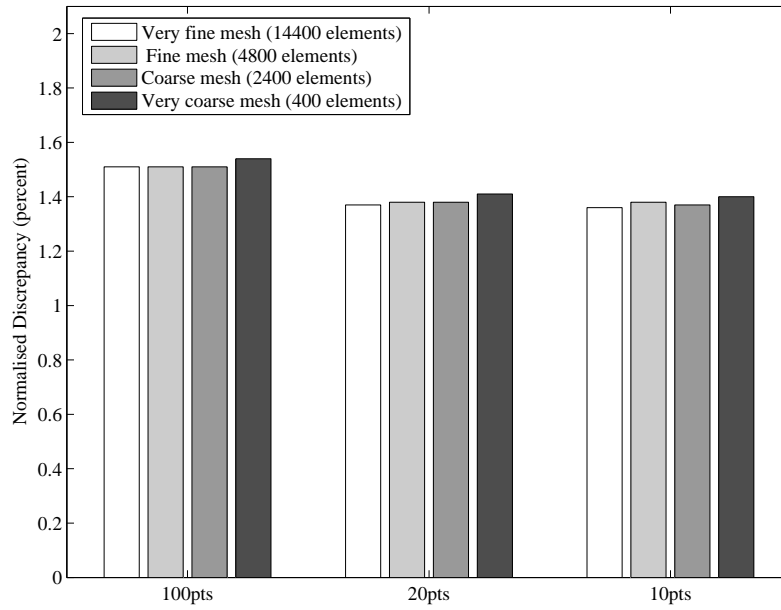
(a) Comparison of normalised discrepancy in locating the crack

(b) Comparison of normalised discrepancy in determining the size of crack

Figure E.11: Comparison of normalised discrepancy in determining the location and size of edge crack : Damage case 6

(a) Comparison of normalised discrepancy in locating the crack

(b) Comparison of normalised discrepancy in determining the size of crack

Figure E.12: Comparison of normalised discrepancy in determining the location and size of edge crack : Damage case 7

(a) Comparison of normalised discrepancy in locating the crack

(b) Comparison of normalised discrepancy in determining the size of crack

Figure E.13: Comparison of normalised discrepancy in determining the location and size of edge crack : Damage case 8

(a) Comparison of normalised discrepancy in locating the crack

(b) Comparison of normalised discrepancy in determining the size of crack

Figure E.14: Comparison of normalised discrepancy in determining the location and size of edge crack : Damage case 9

(a) Comparison of normalised discrepancy in locating the crack

(b) Comparison of normalised discrepancy in determining the size of crack

Figure E.15: Comparison of normalised discrepancy in determining the location and size of edge crack : Damage case 10

Results from Robustness analysis

Section 8.6 in Chapter 8 presents results from the inverse problem using SQP technique for plates containing cracks with unknown orientation. A robustness analysis was conducted which showed that the normalised discrepancies in estimating the crack parameters increased with increasing crack size. This section presents the normalised discrepancies in estimating the normalised x and y coordinates, orientation and size of the crack for the 216 different damage cases listed in Table 8.7 as a function of the crack size.
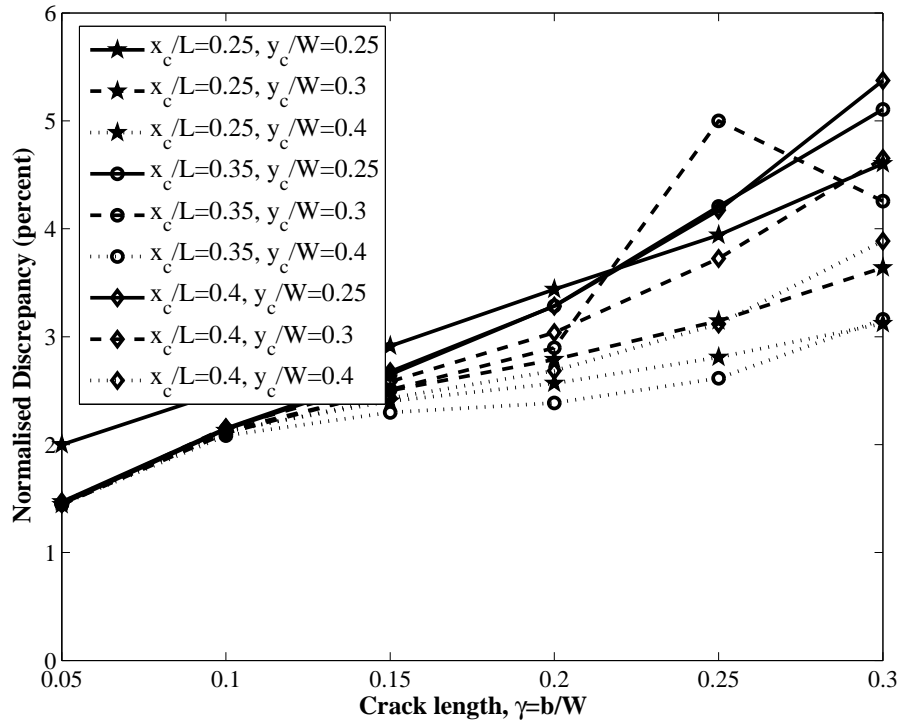
F.1 Damage cases with orientation $\phi = 0°$
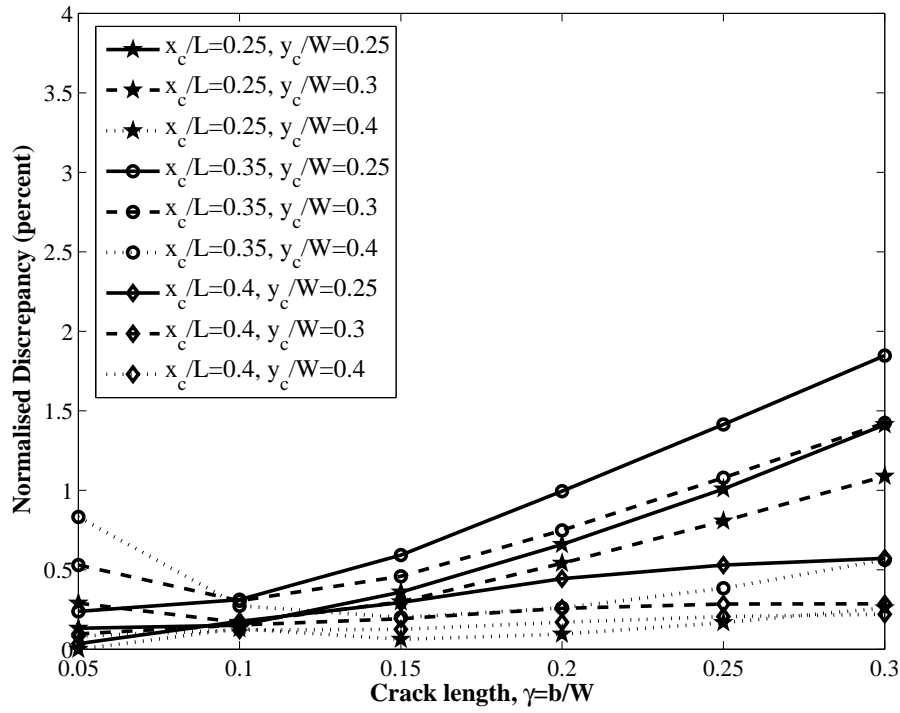
(a) Normalised discrepancy in predicting the x-coordinate of location of crack
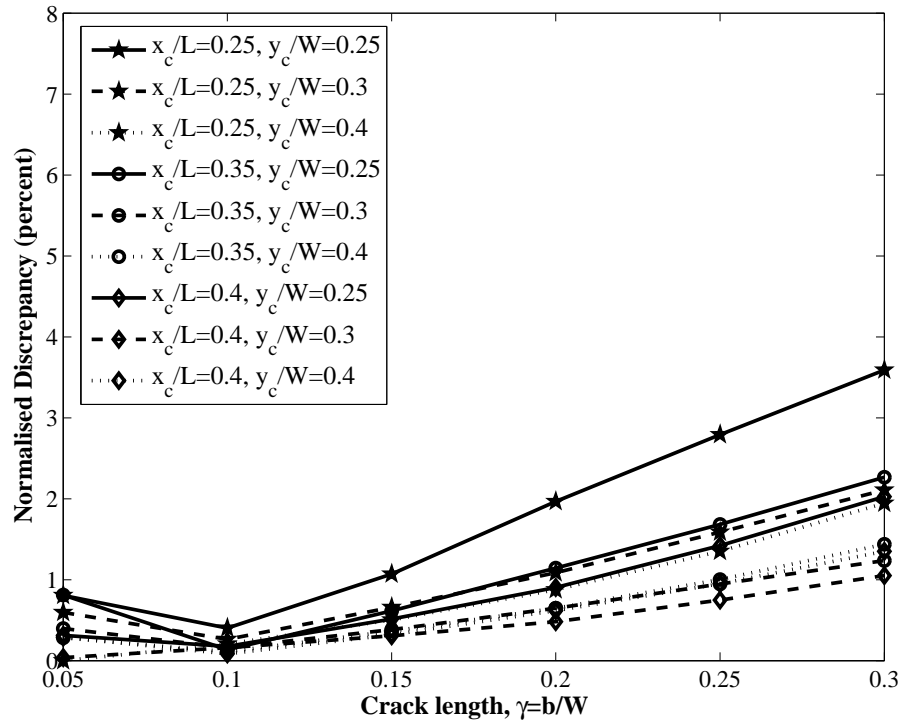
(b) Normalised discrepancy in predicting the y-coordinate of location of crack
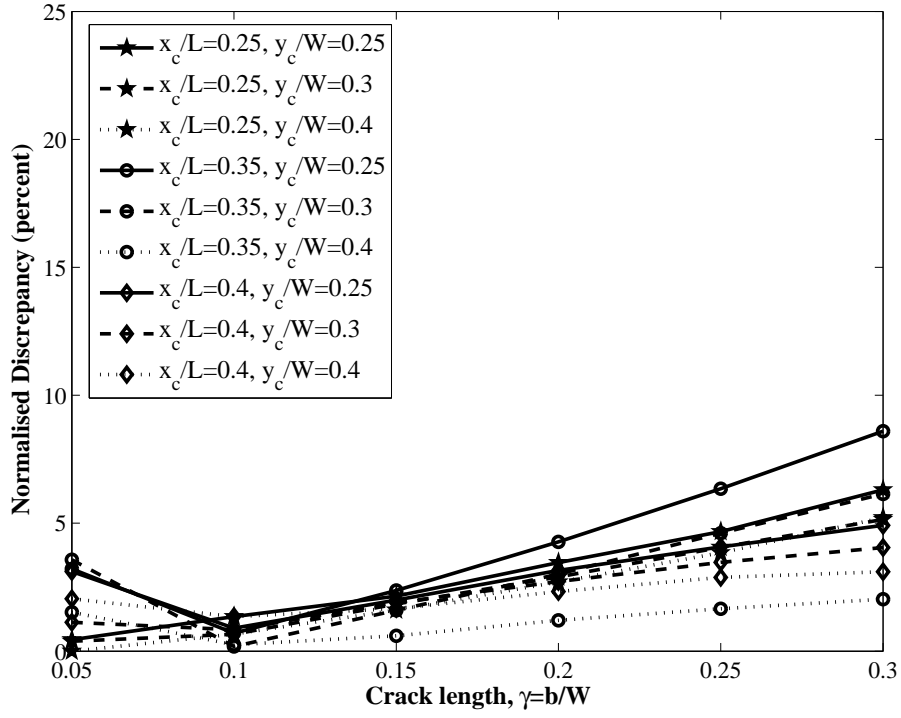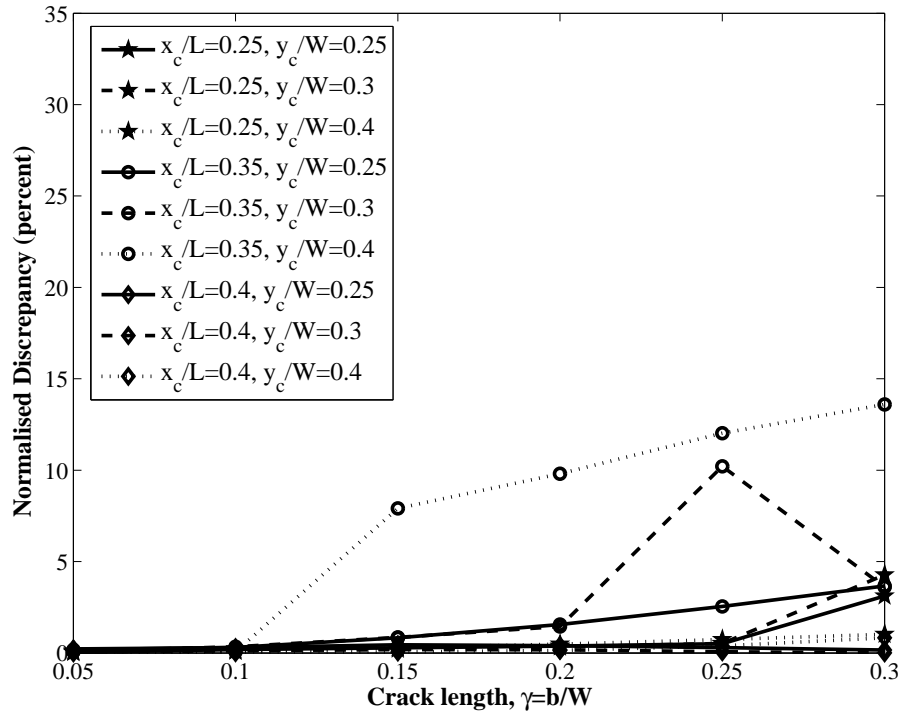
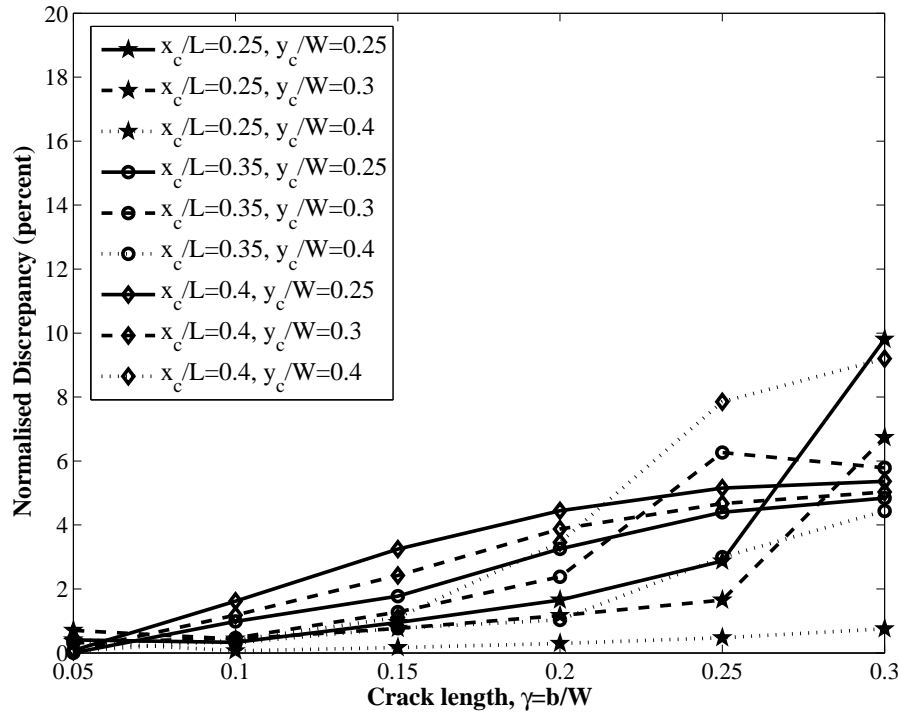(c) Normalised discrepancy in predicting the orientation of crack
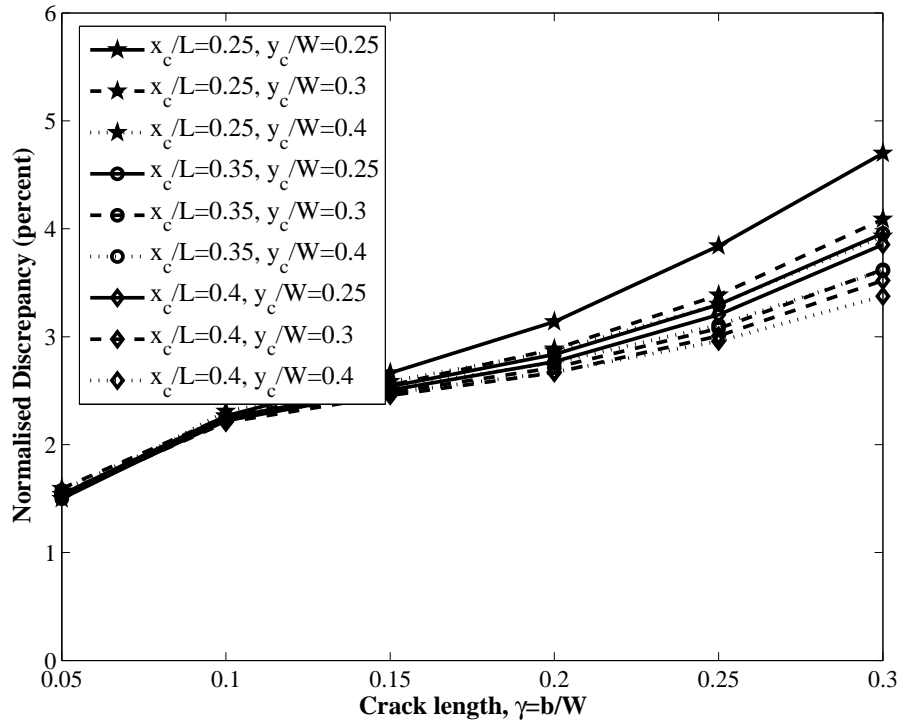
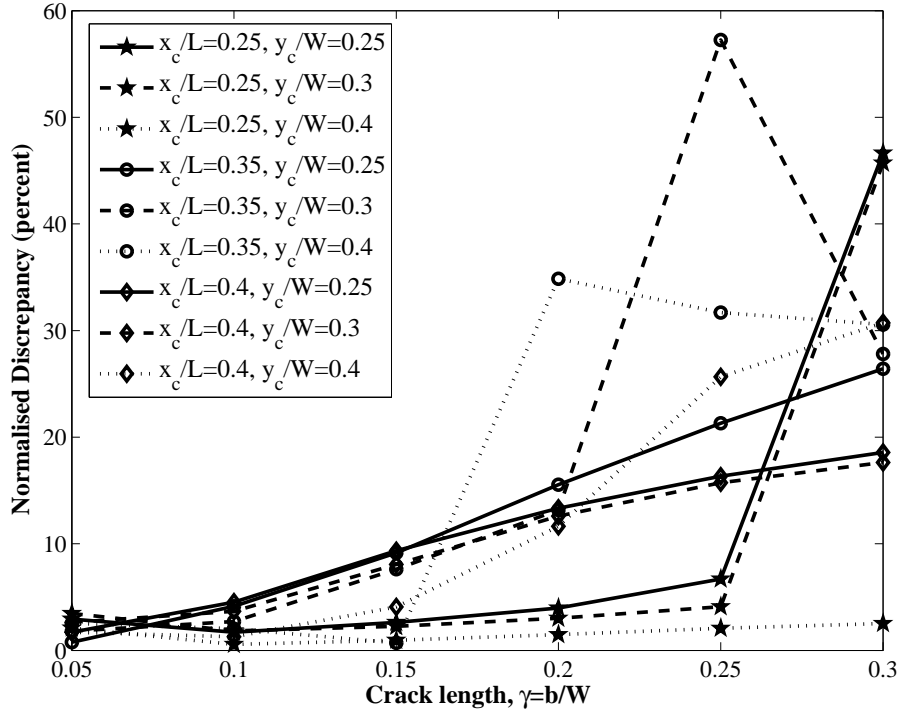(d) Normalised discrepancy in predicting the size of crack

Figure F.1: Normalised discrepancies in predicting the crack parameters for damage cases where $\phi = 0°$

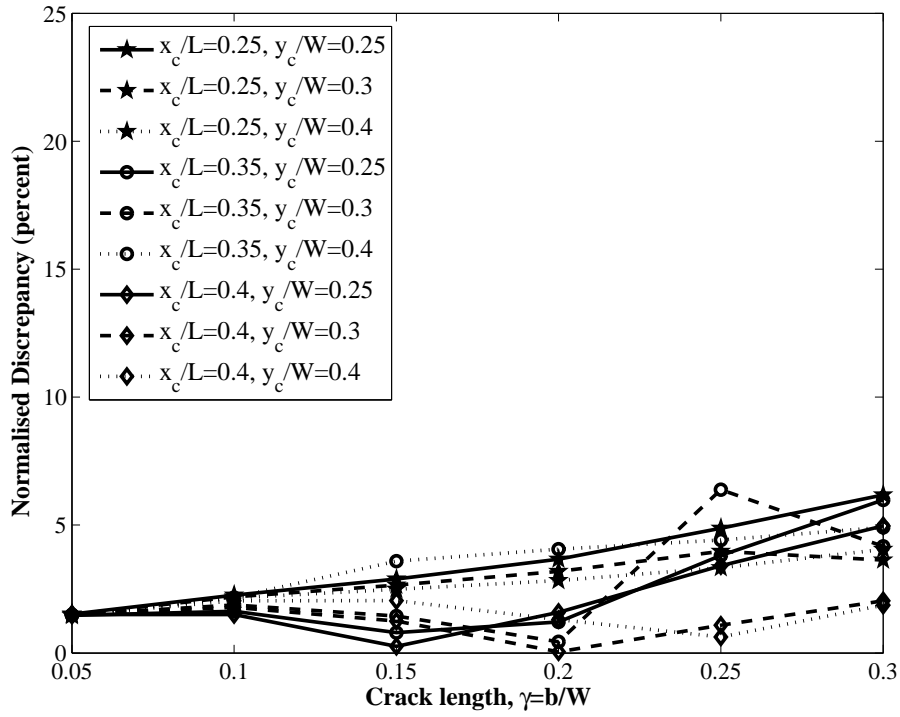## F.2   Damage cases with orientation $\phi = 30°$
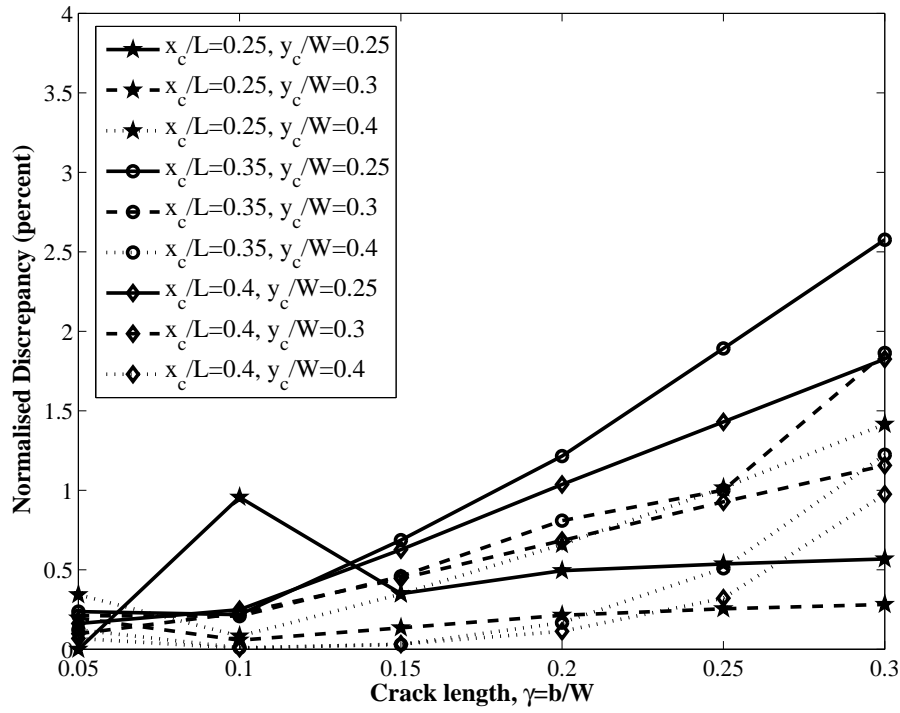
(a) Normalised discrepancy in predicting the x-coordinate of location of crack
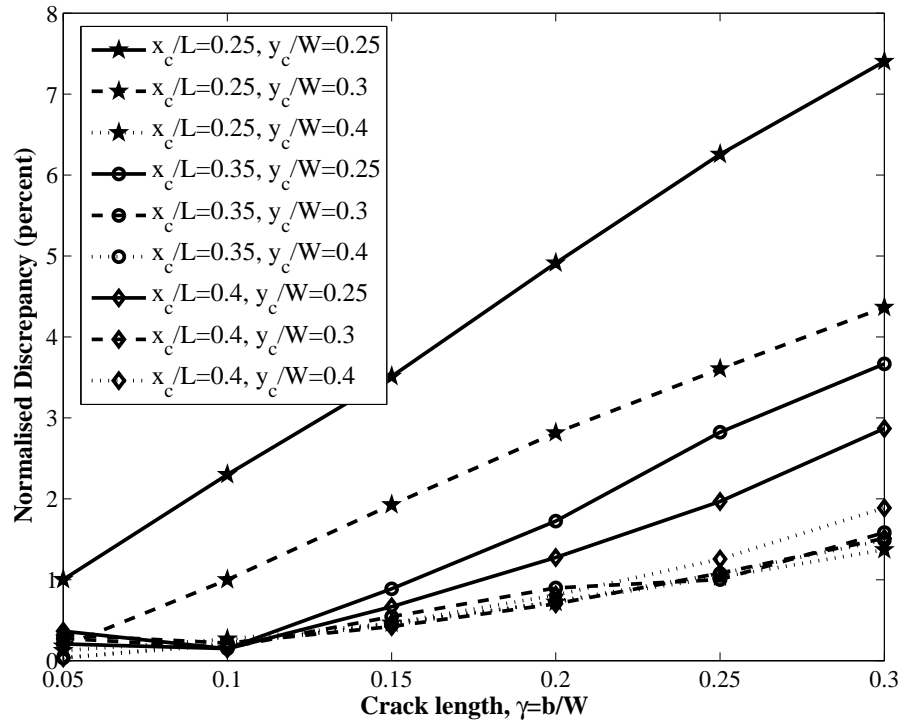
(b) Normalised discrepancy in predicting the y-coordinate of location of crack
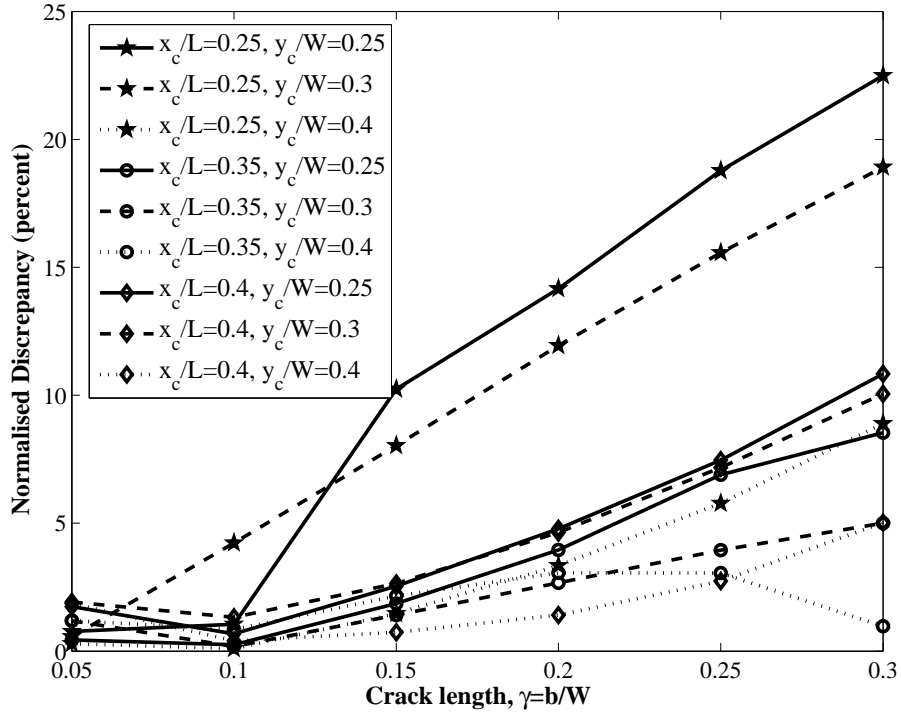
(c) Normalised discrepancy in predicting the orientation of crack

(d) Normalised discrepancy in predicting the size of crack

Figure F.2: Normalised discrepancies in predicting the crack parameters for damage cases where $\phi = 30°$

F.3   Damage cases with orientation $\phi = 60°$

(a) Normalised discrepancy in predicting the x-coordinate of location of crack

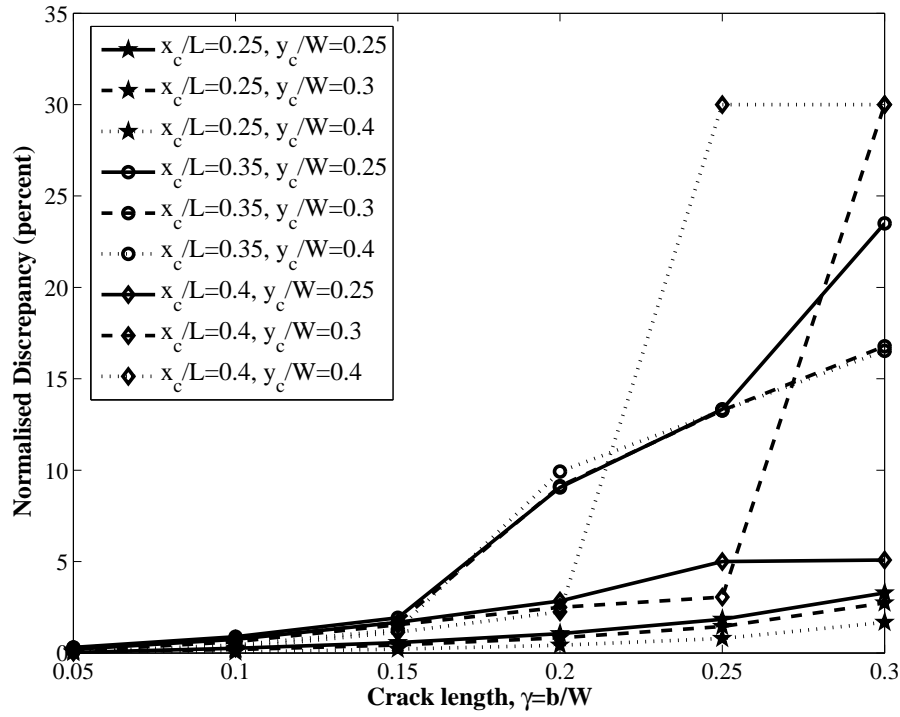(b) Normalised discrepancy in predicting the y-coordinate of location of crack

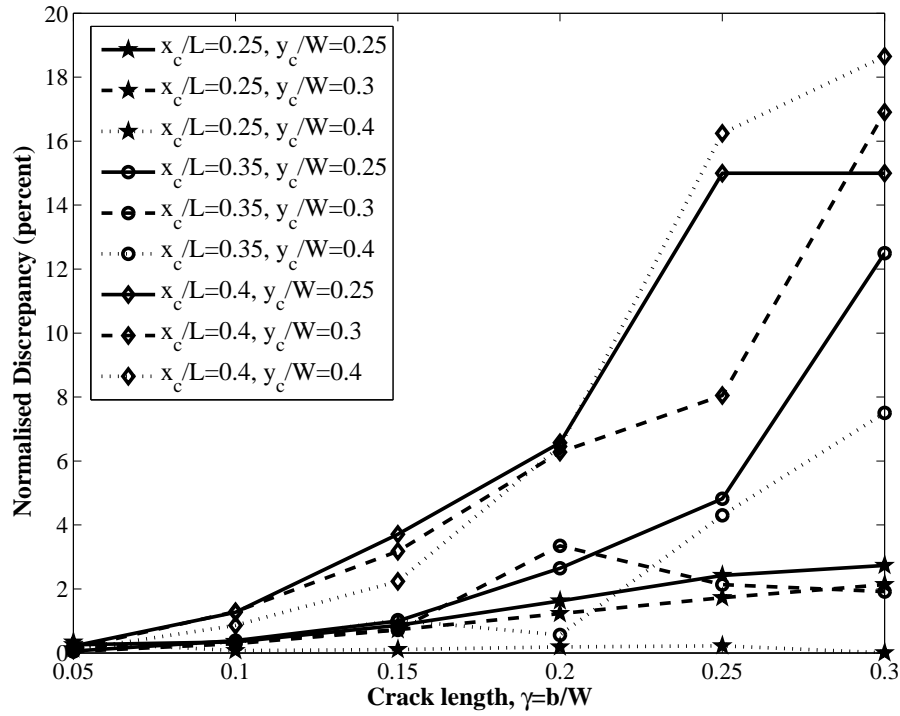(c) Normalised discrepancy in predicting the orientation of crack

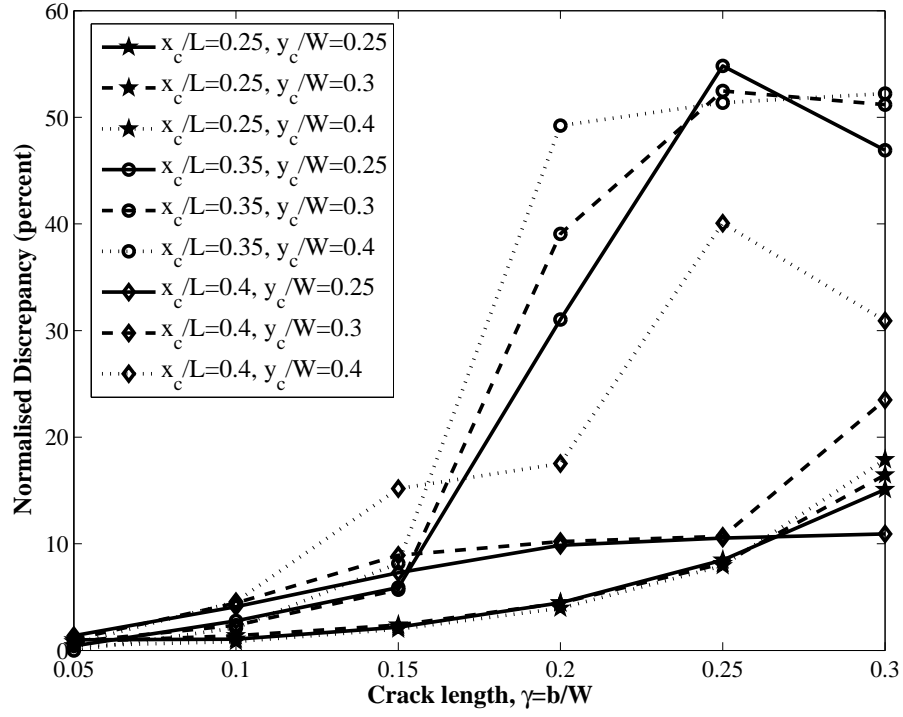(d) Normalised discrepancy in predicting the size of crack

Figure F.3: Normalised discrepancies in predicting the crack parameters for damage cases where $\phi = 60°$

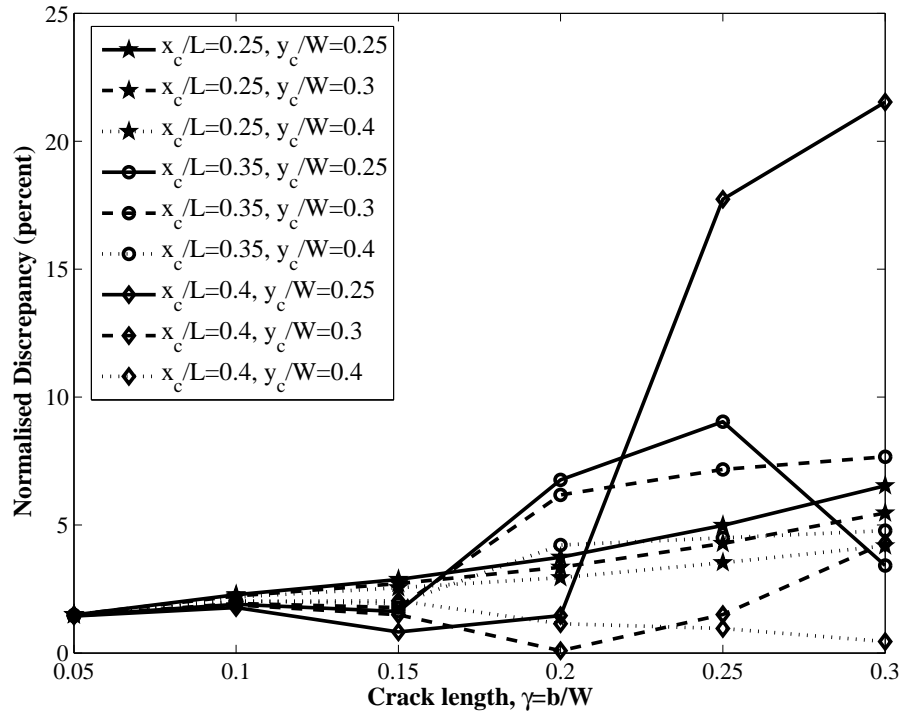## F.4   Damage cases with orientation $\phi = 90°$

(a) Normalised discrepancy in predicting the x-coordinate of location of crack

(b) Normalised discrepancy in predicting the y-coordinate of location of crack

(c) Normalised discrepancy in predicting the orientation of crack

(d) Normalised discrepancy in predicting the size of crack

Figure F.4: Normalised discrepancies in predicting the crack parameters for damage cases where $\phi = 90°$

Appendix G

Experimental test rig - Design drawings

To study the practical applicability of the proposed vibration based damage detection method to plates, *Experimental Modal Analysis* was conducted on plates with two edges simply-supported and the other two edges free, *SS-SS-F-F* boundary condition. A test-rig was specially designed for this purpose and manufactured in the school's workshop. This section presents detailed drawing of the experimental set-up constructed and employed in the tests on plates.
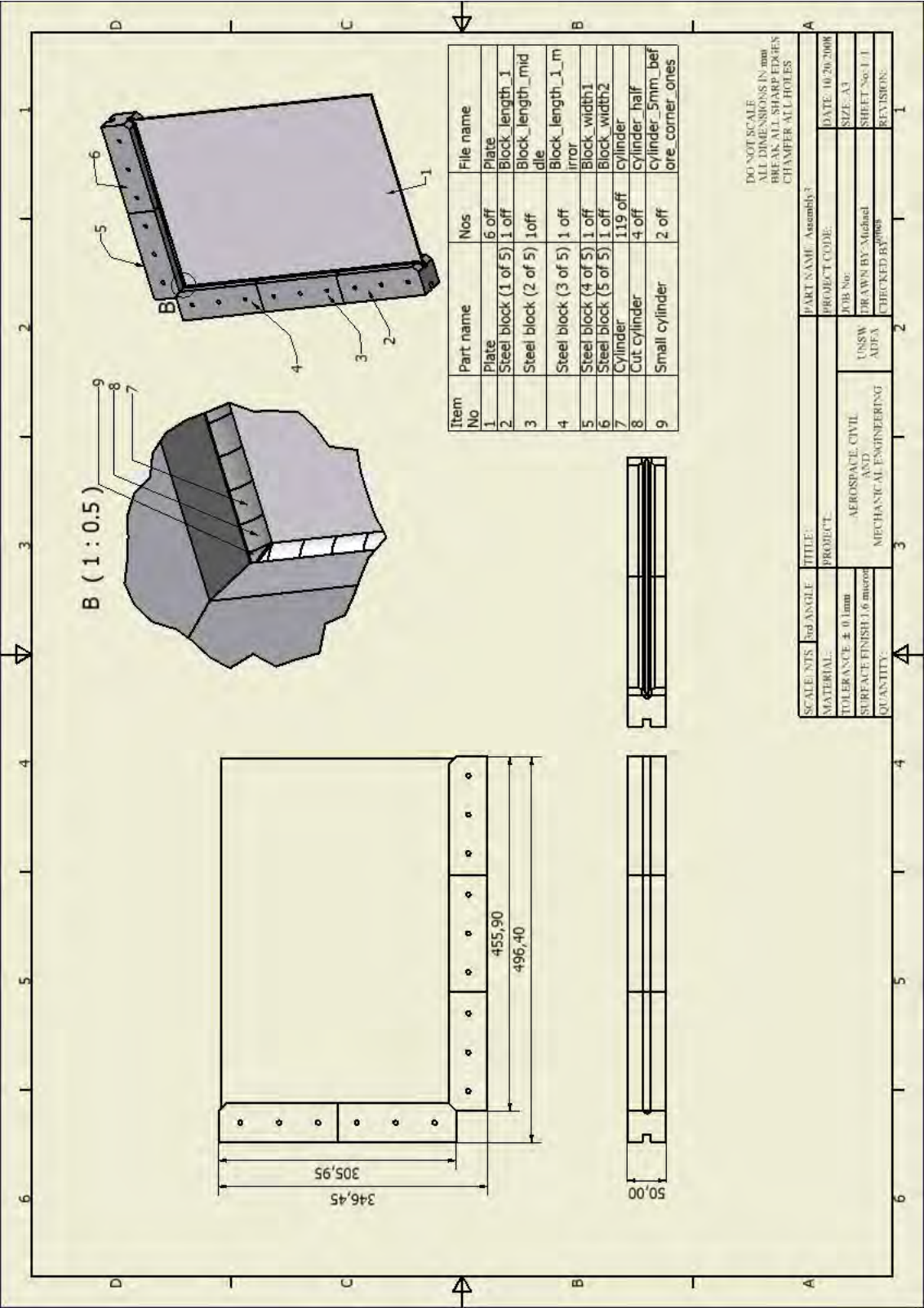
Figure G.1: Assembly

Figure G.2: Part drawings for test rig

Figure G.3: Part drawings for test rig

Figure G.4: Part drawings for test rig

Figure G.5: Part drawings for test rig

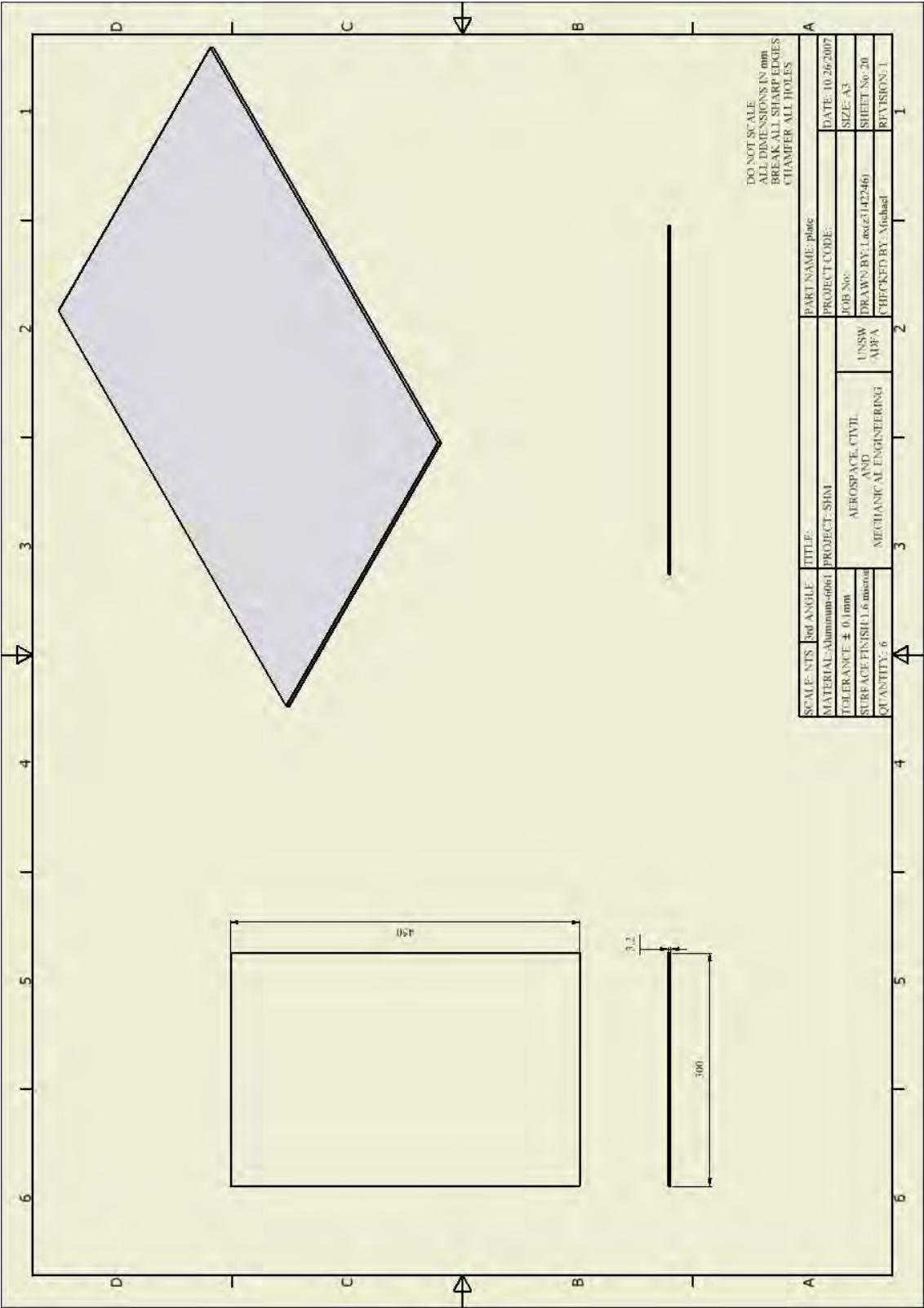Figure G.6: Part drawings for test rig
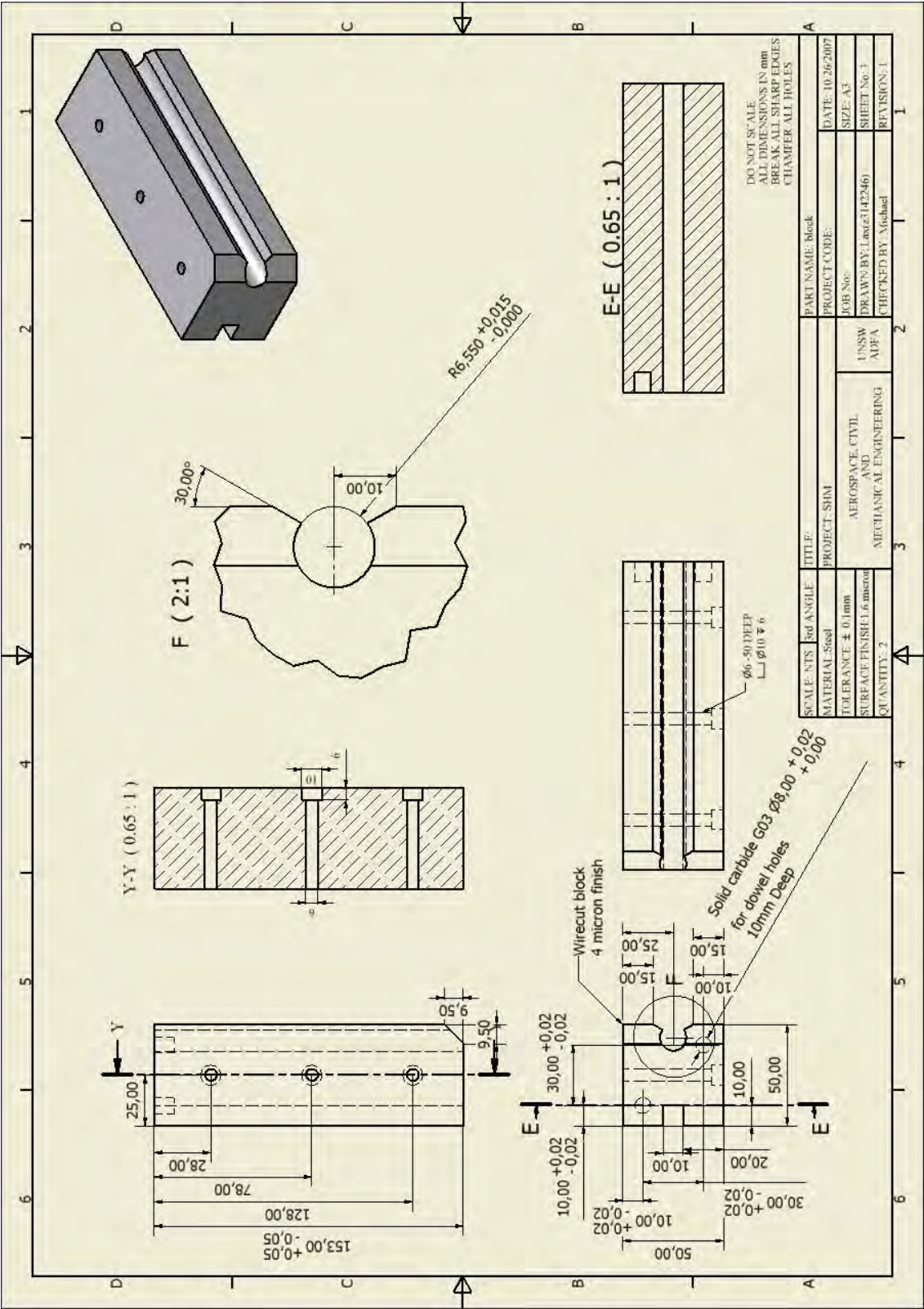
Figure G.7: Part drawings for test rig
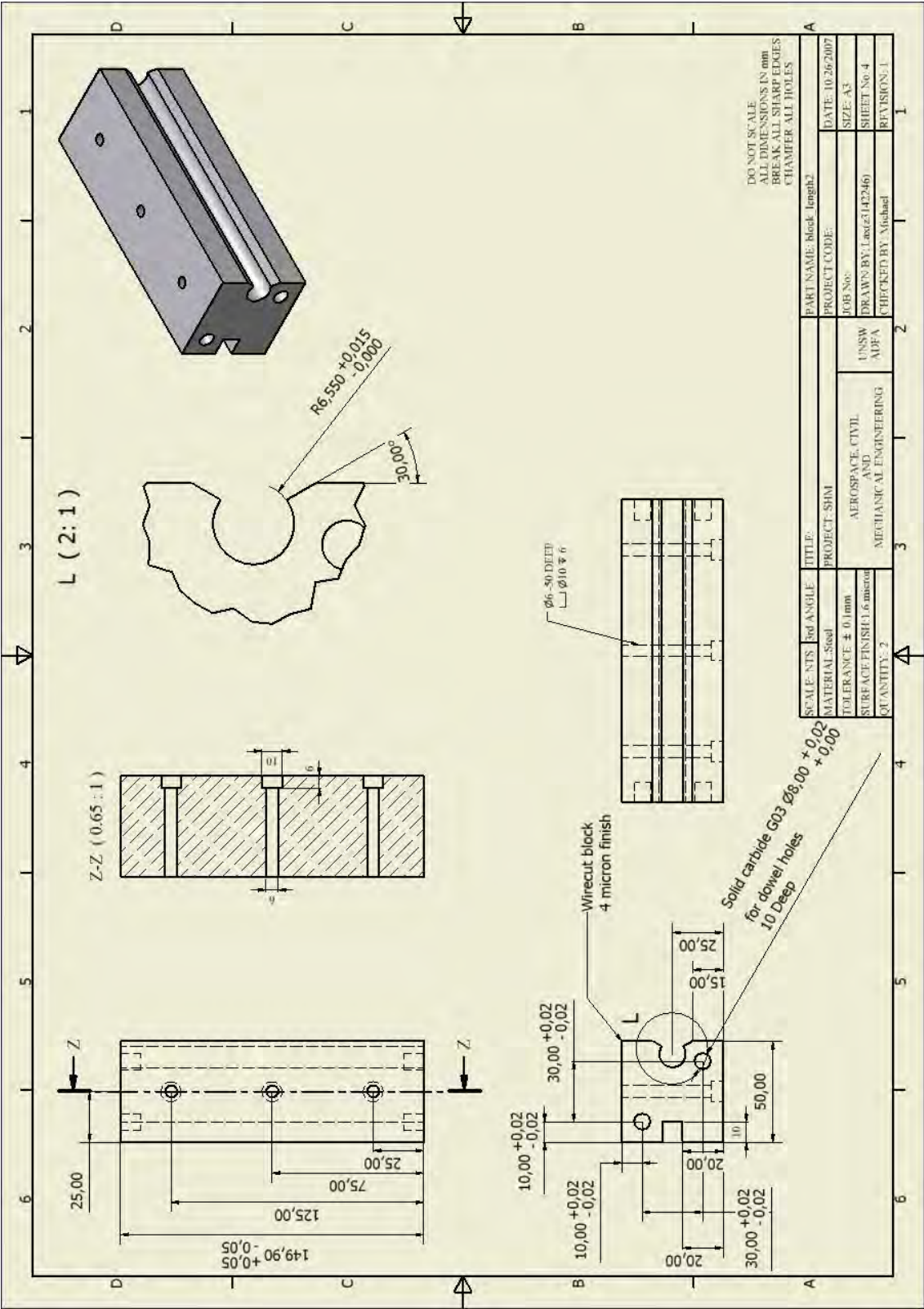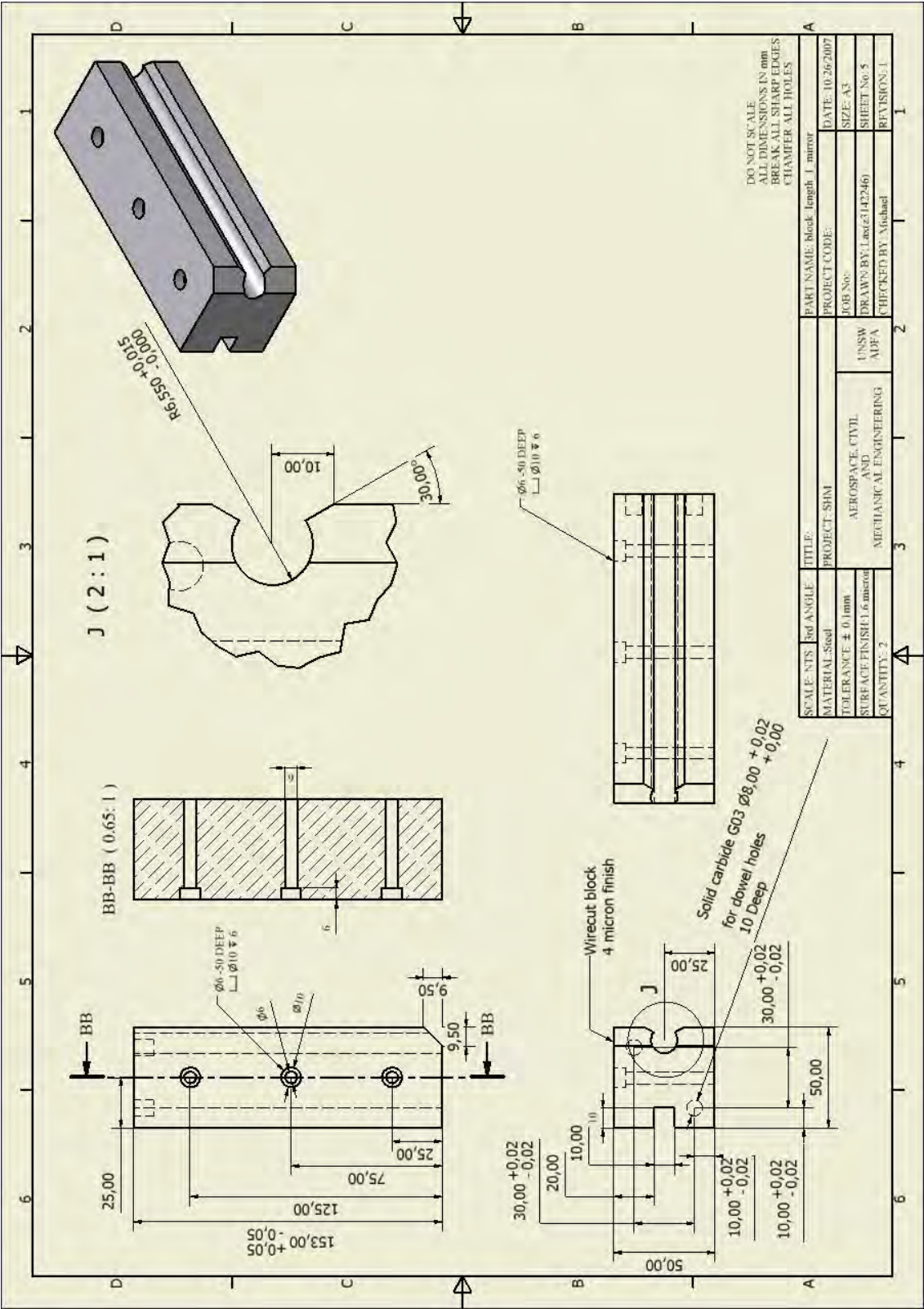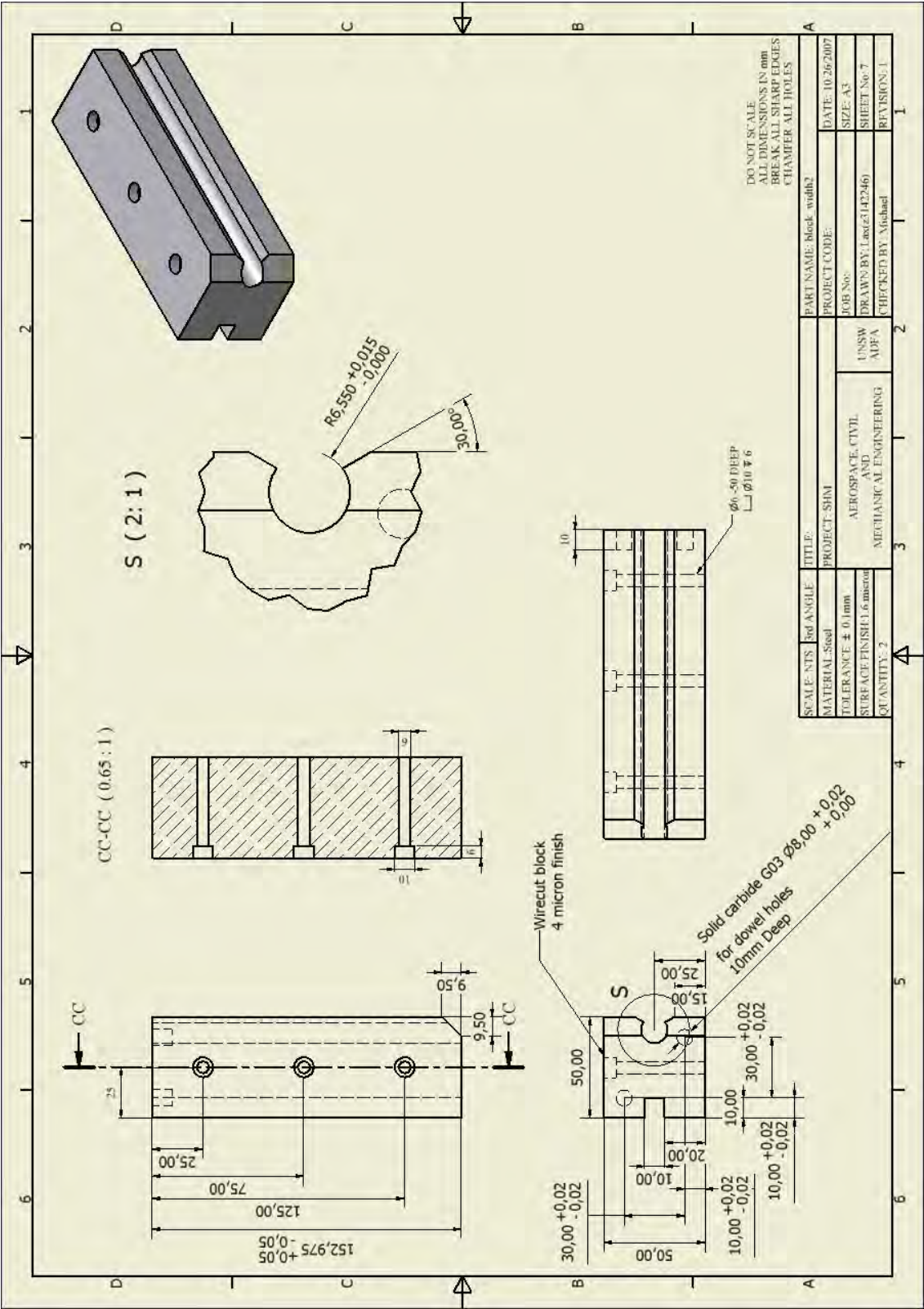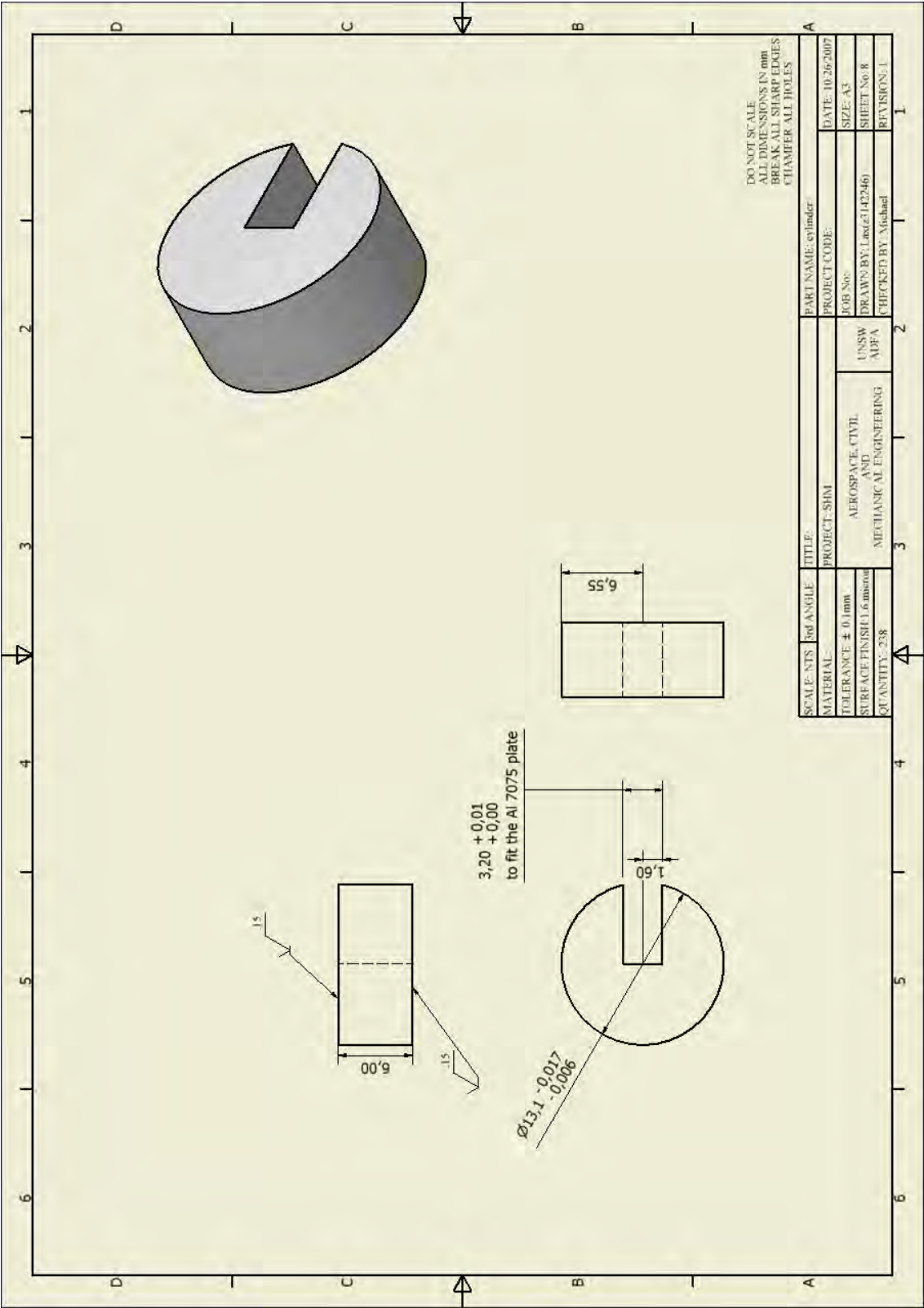
Figure G.8: Part drawings for test rig
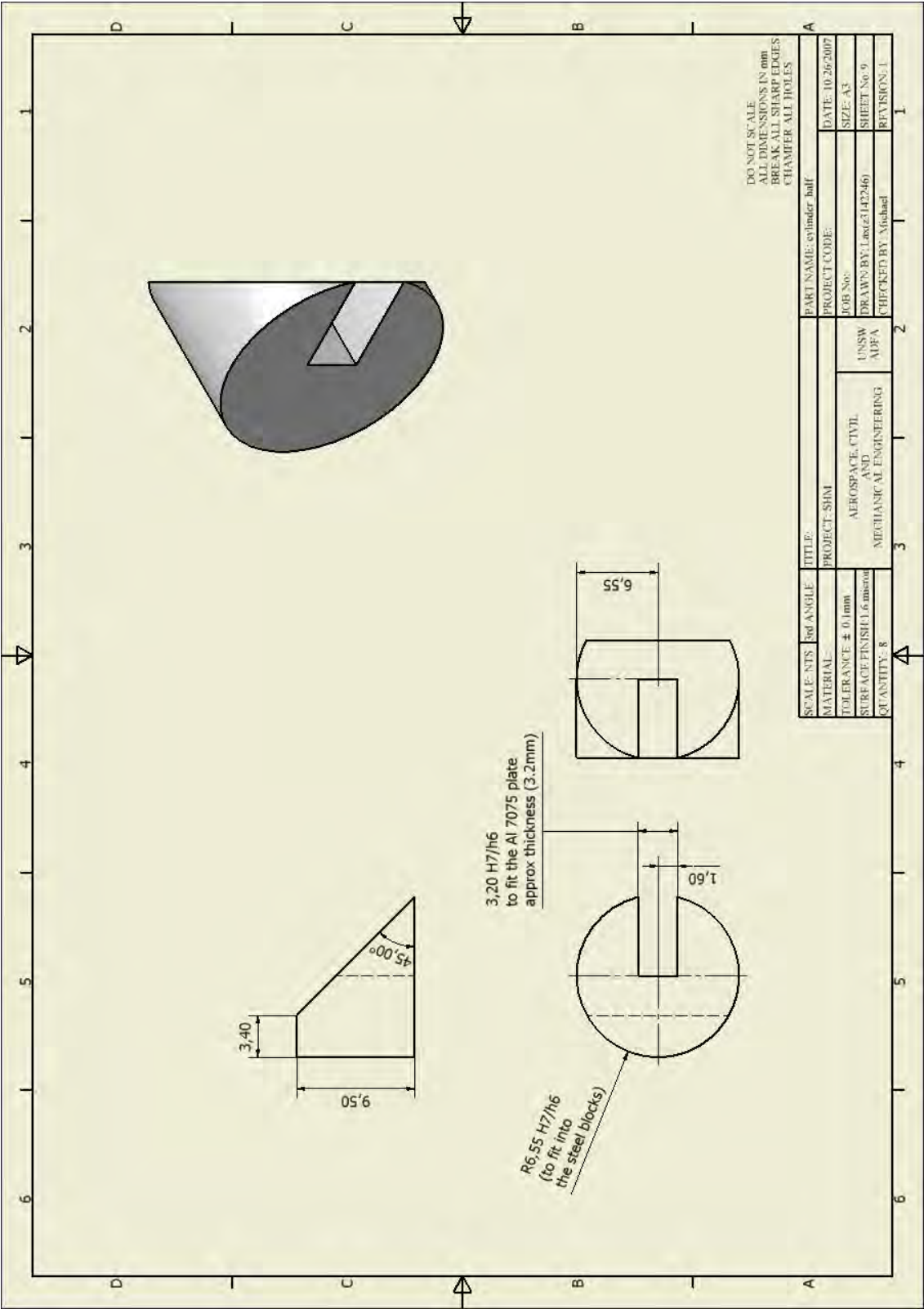
Figure G.9: Part drawings for test rig
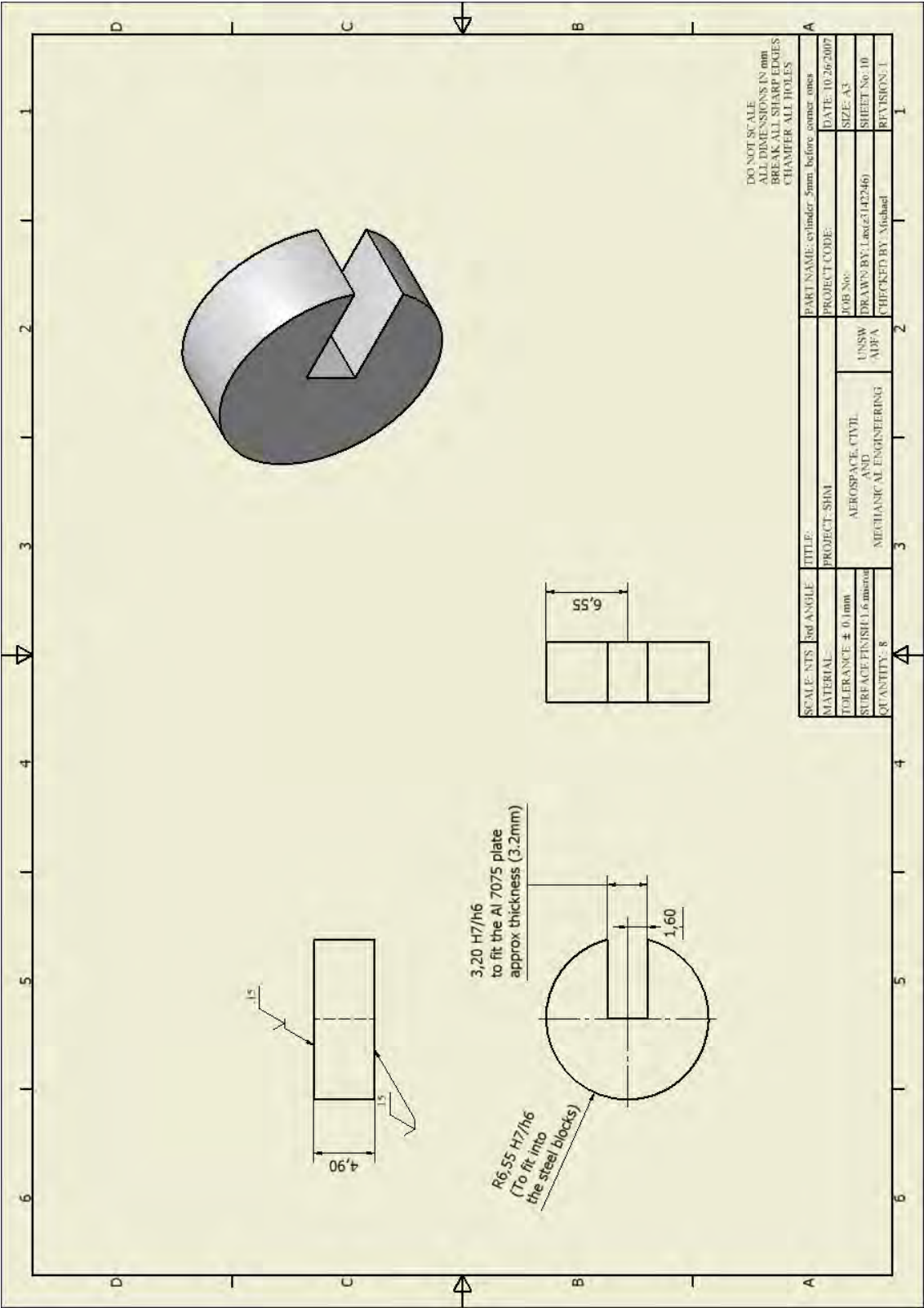
Figure G.10: Part drawings for test rig

Item number	Name	NOs	File name
1	Thick bottom plate	1 off	small_thick_plate
2	Thick top plate	1 off	Top_plate
3	Thin sheet	1 off	thin_sheet
4	Frame	4 off	height
5	Frame	4 off	breadth
6	Frame	2 off	length-1
7	Frame	2 off	length -2
8	Frame	1 off	middle

DO NOT SCALE
ALL DIMENSIONS IN mm
BREAK ALL SHARP EDGES
CHAMFER ALL HOLES

PART NAME: frame_vibration

PROJECT CODE:

JOB No:

DRAWN BY: Liu(z3142246)

CHECKED BY:

DATE: 10/26/2007

SIZE: A3

SHEET No: 11

REVISION: 1

UNSW ADFA

AEROSPACE, CIVIL AND MECHANICAL ENGINEERING

SCALE: NTS 3rd ANGLE

TITLE:

PROJECT:

MATERIAL=

TOLERANCE ± 0.1mm

SURFACE FINISH(1.6 micron)

QUANTITY: 1

750,00
650,00
50,00
950,00
800,00
350,00
850,00
75

Figure G.11: Frame to hold the set up

Figure G.12: Part drawings for frame

Figure G.13: Part drawings for frame
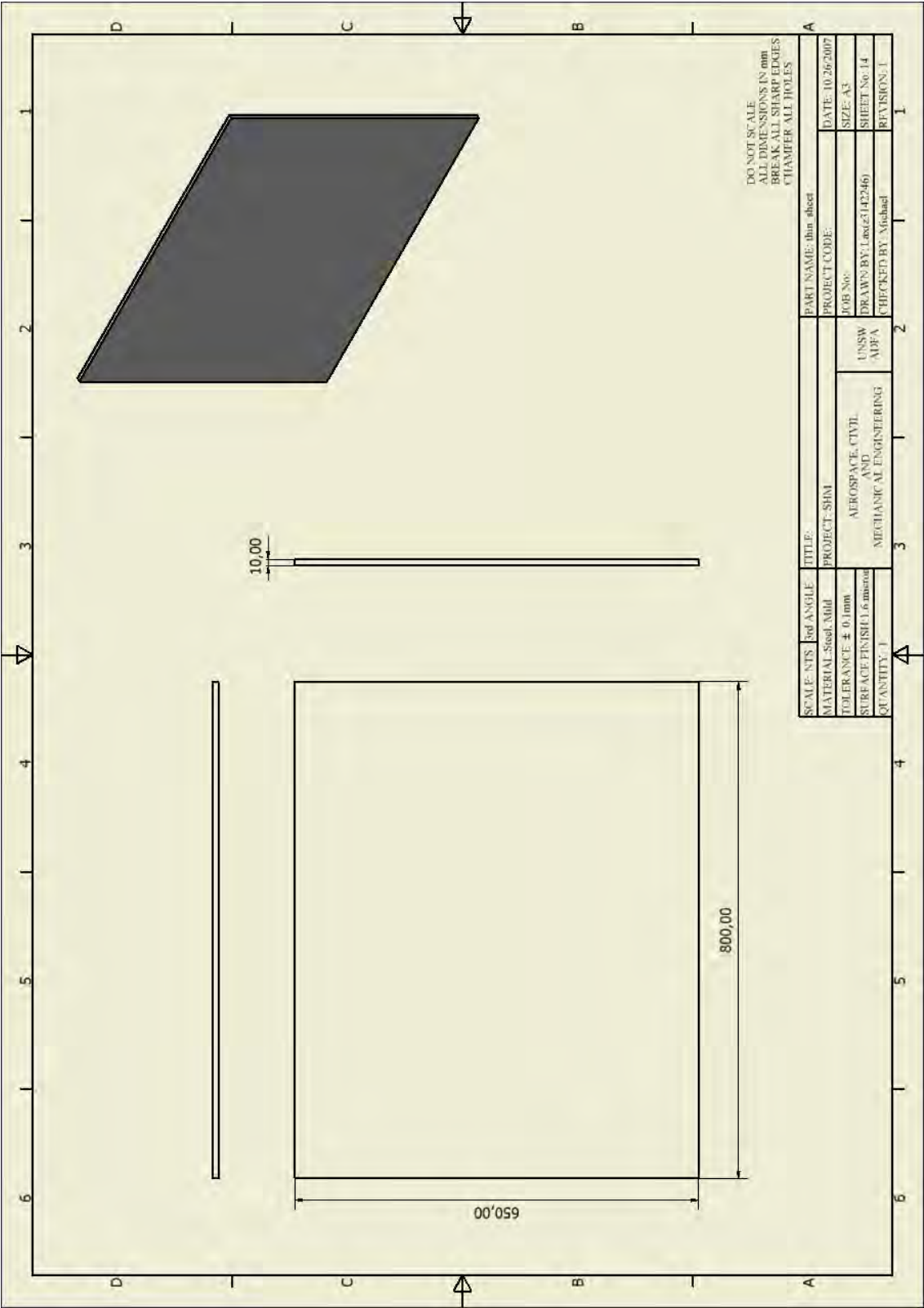
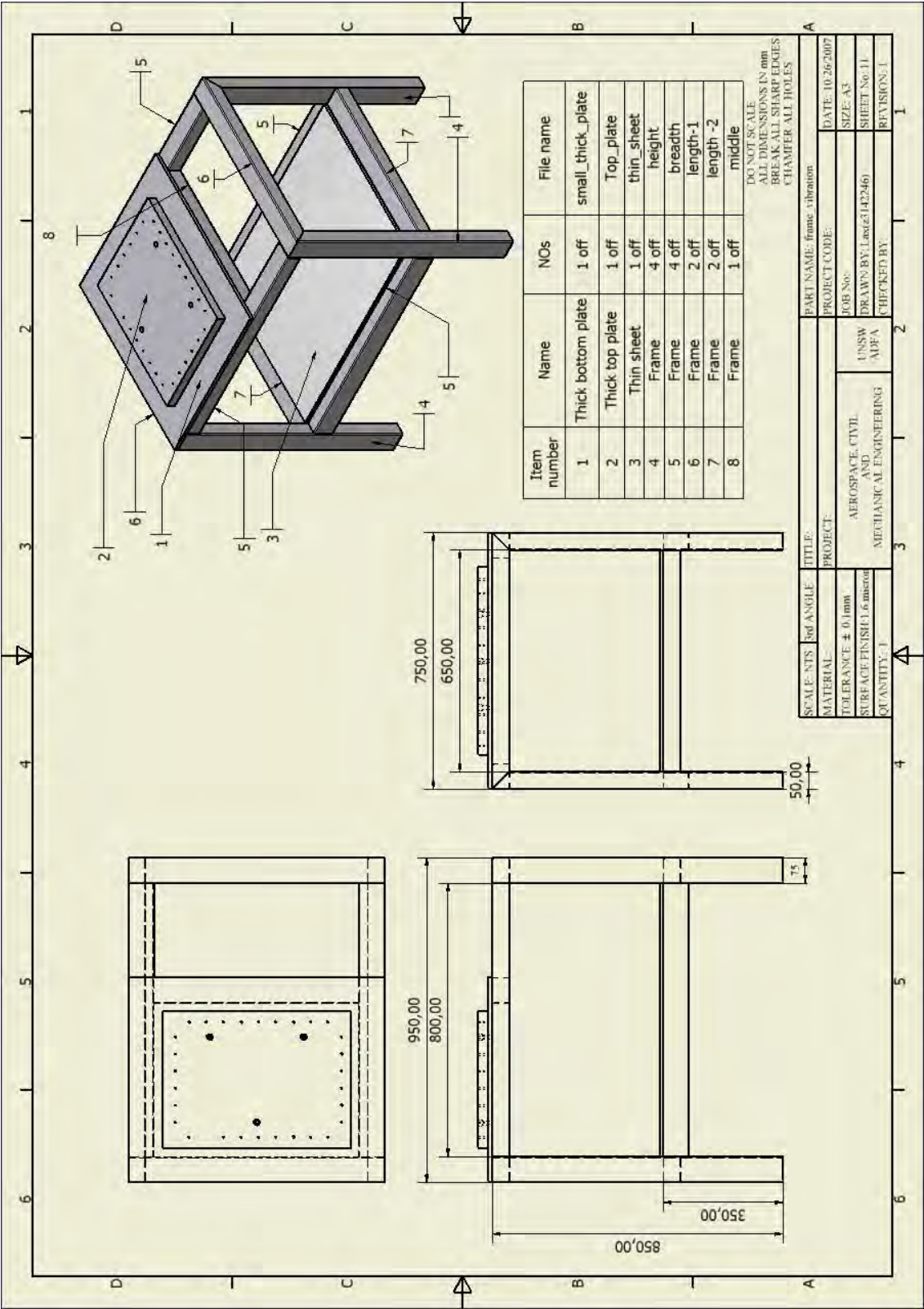Figure G.14: Part drawings for frame
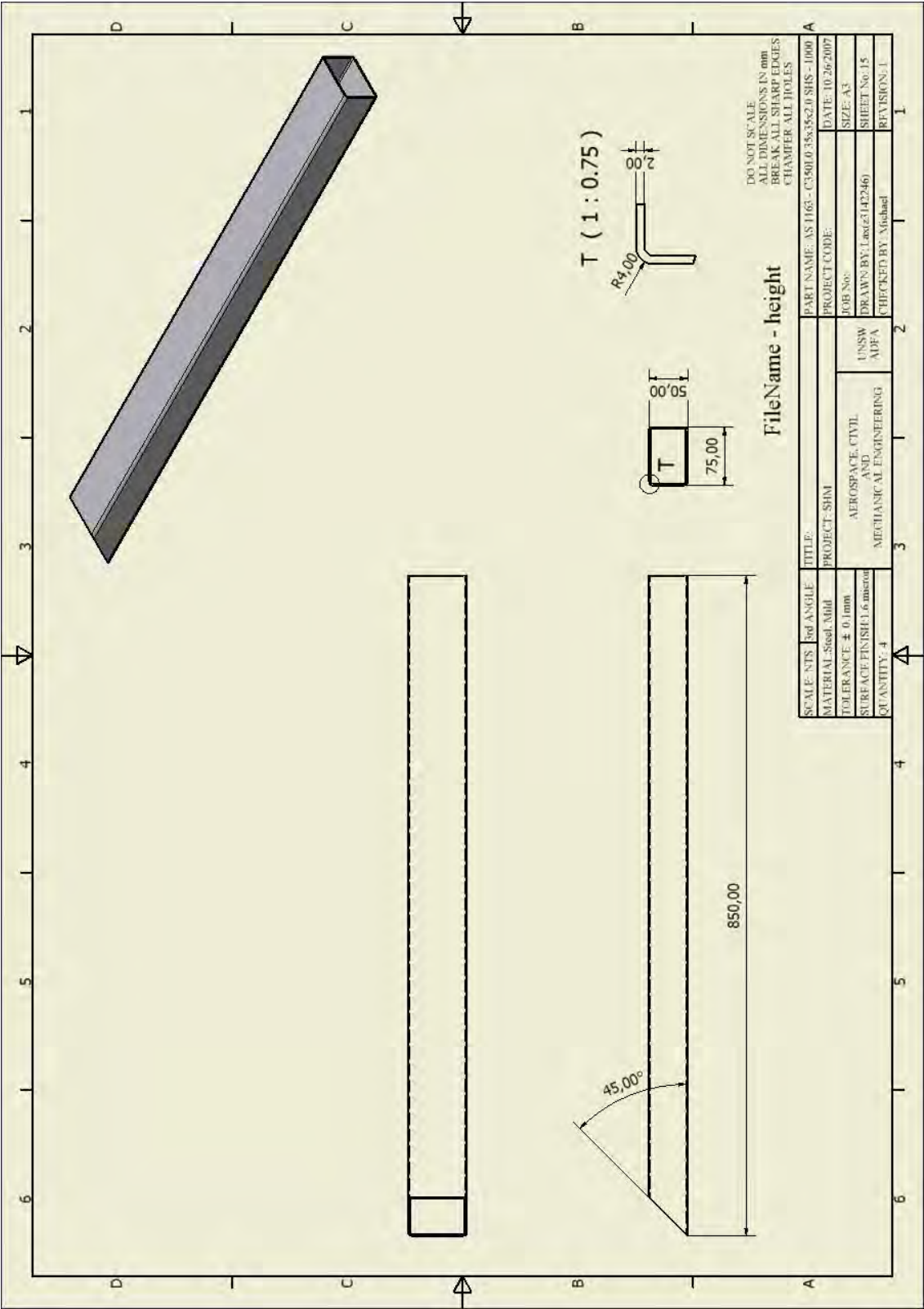
Figure G.15: Part drawings for frame
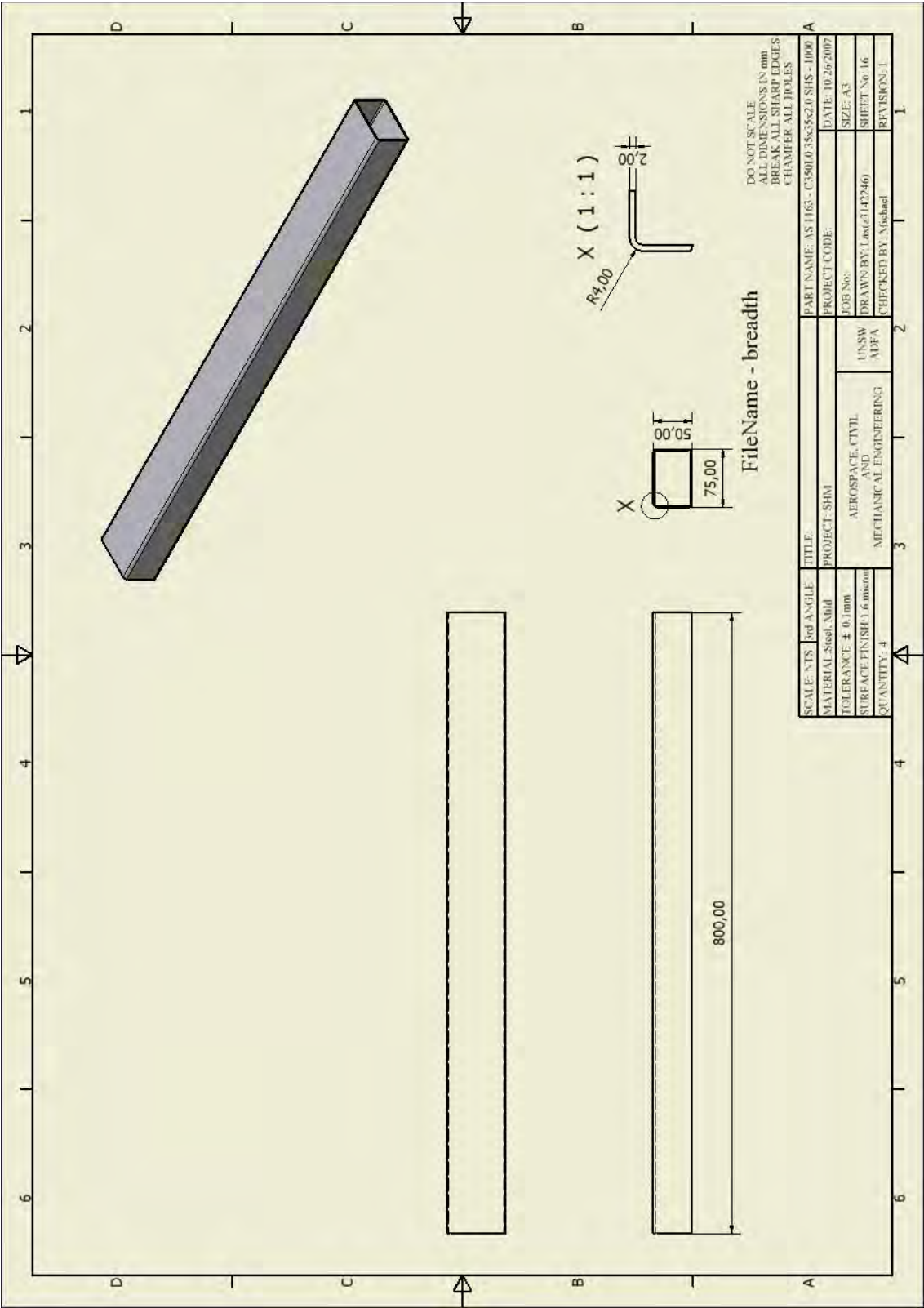
Figure G.16: Part drawings for frame
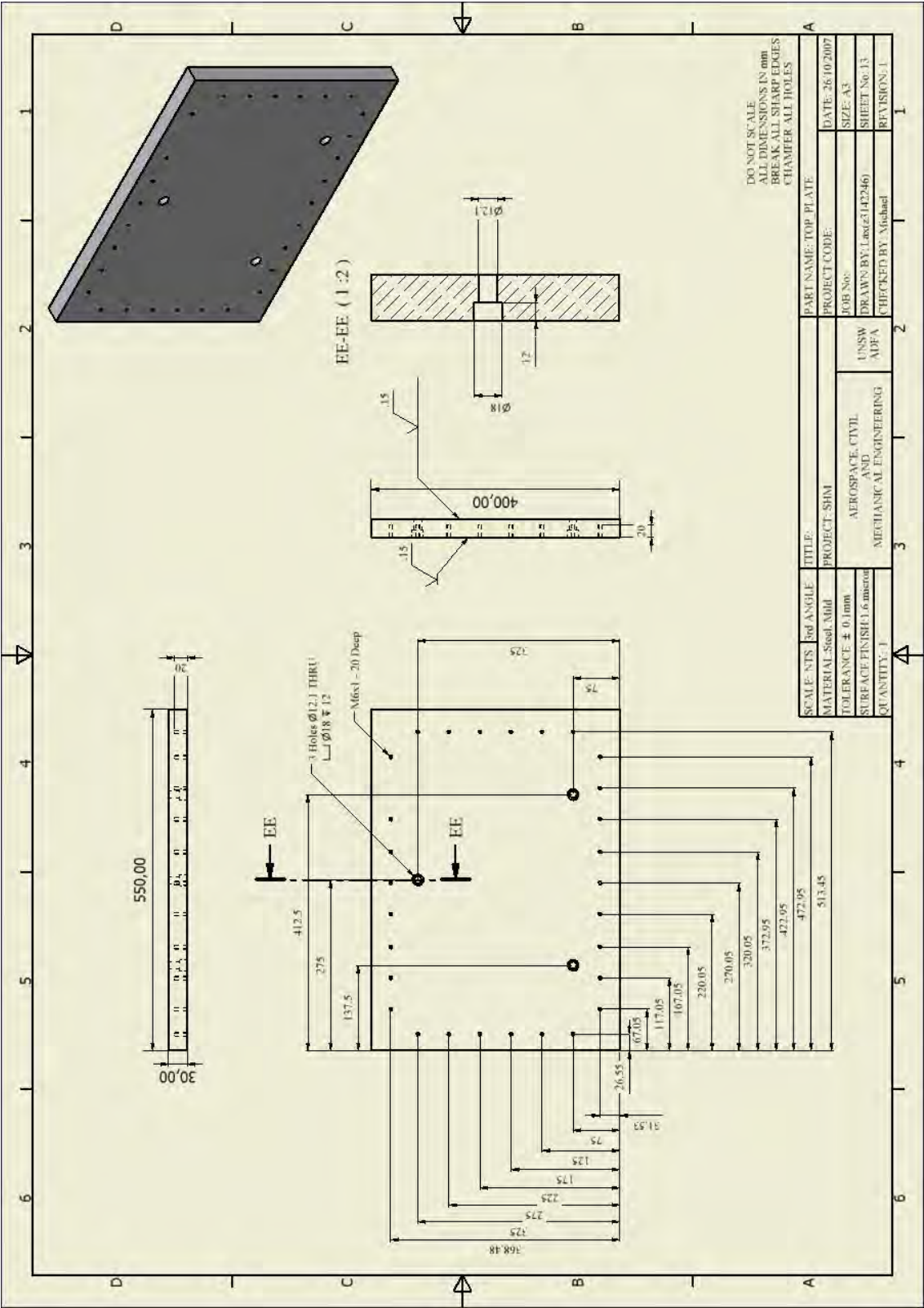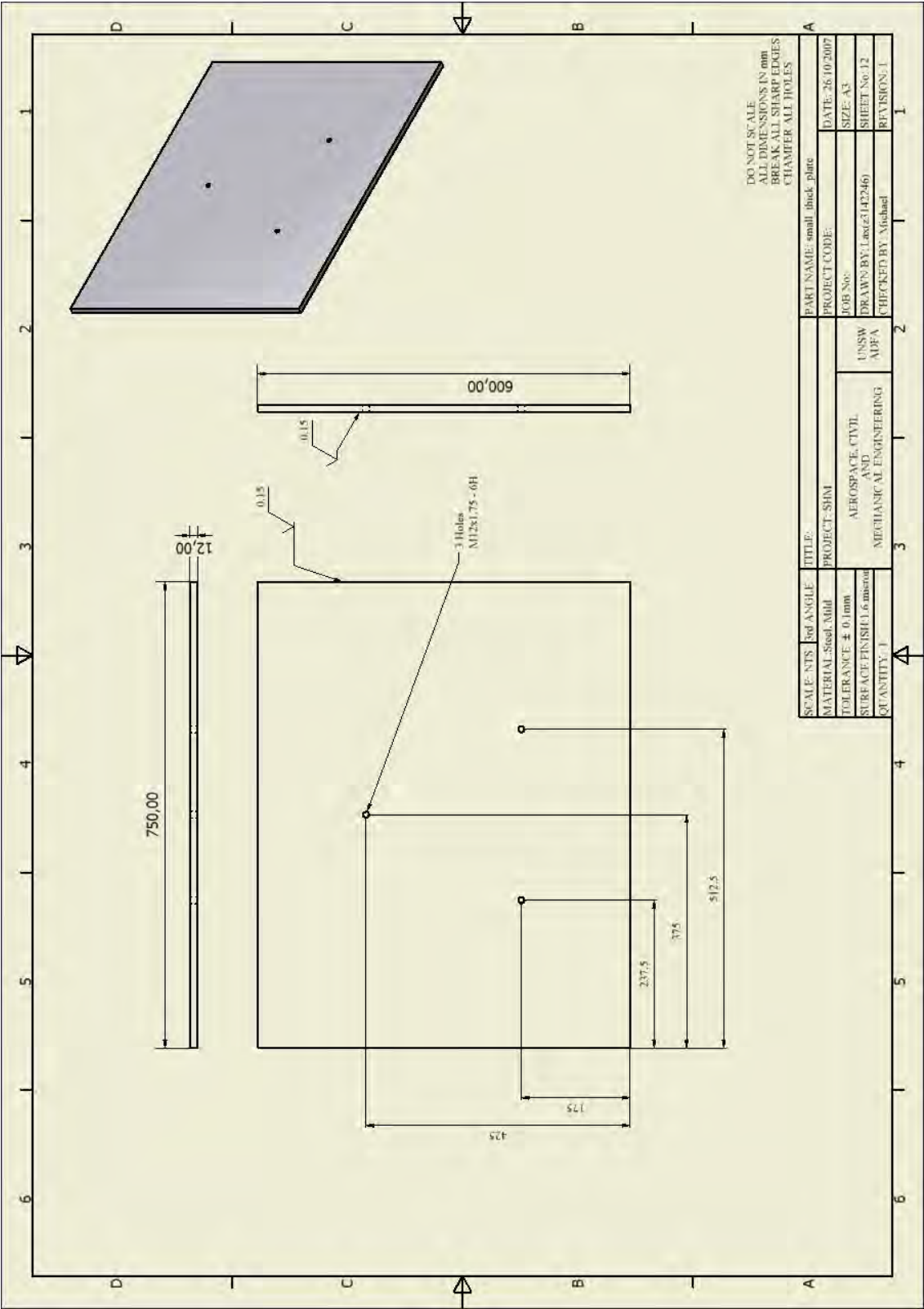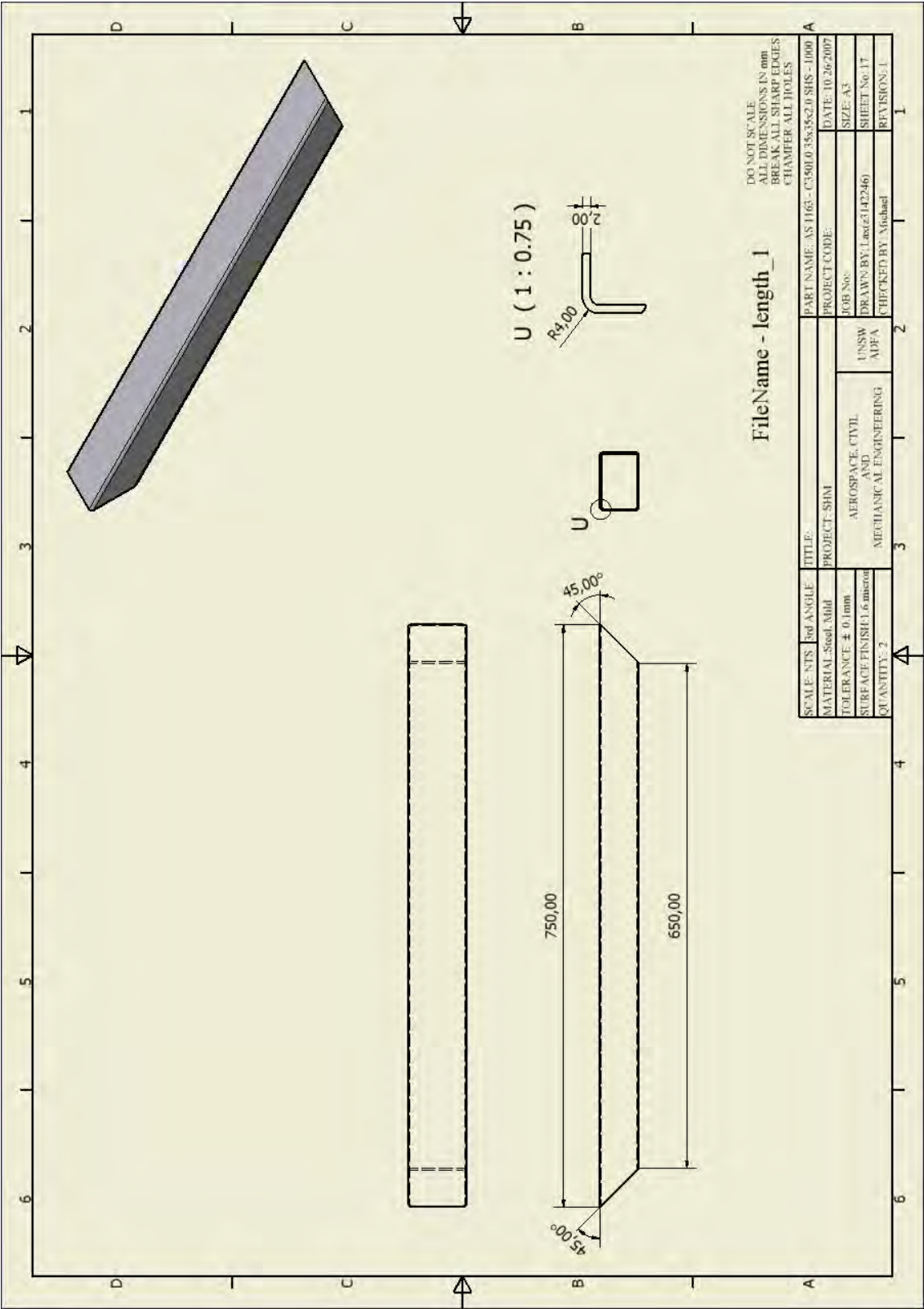
Figure G.17: Part drawings for frame
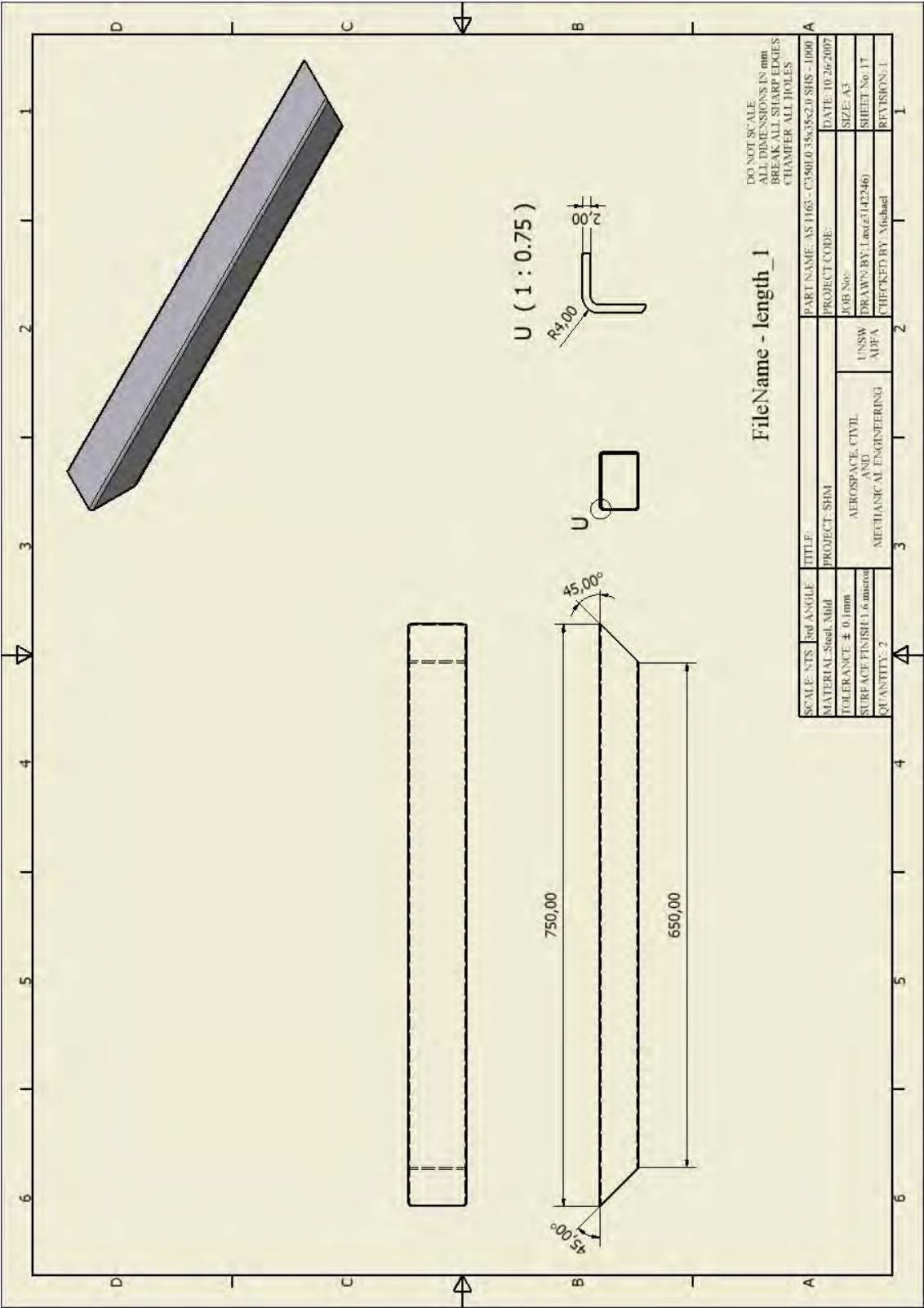
Figure G.18: Part drawings for frame
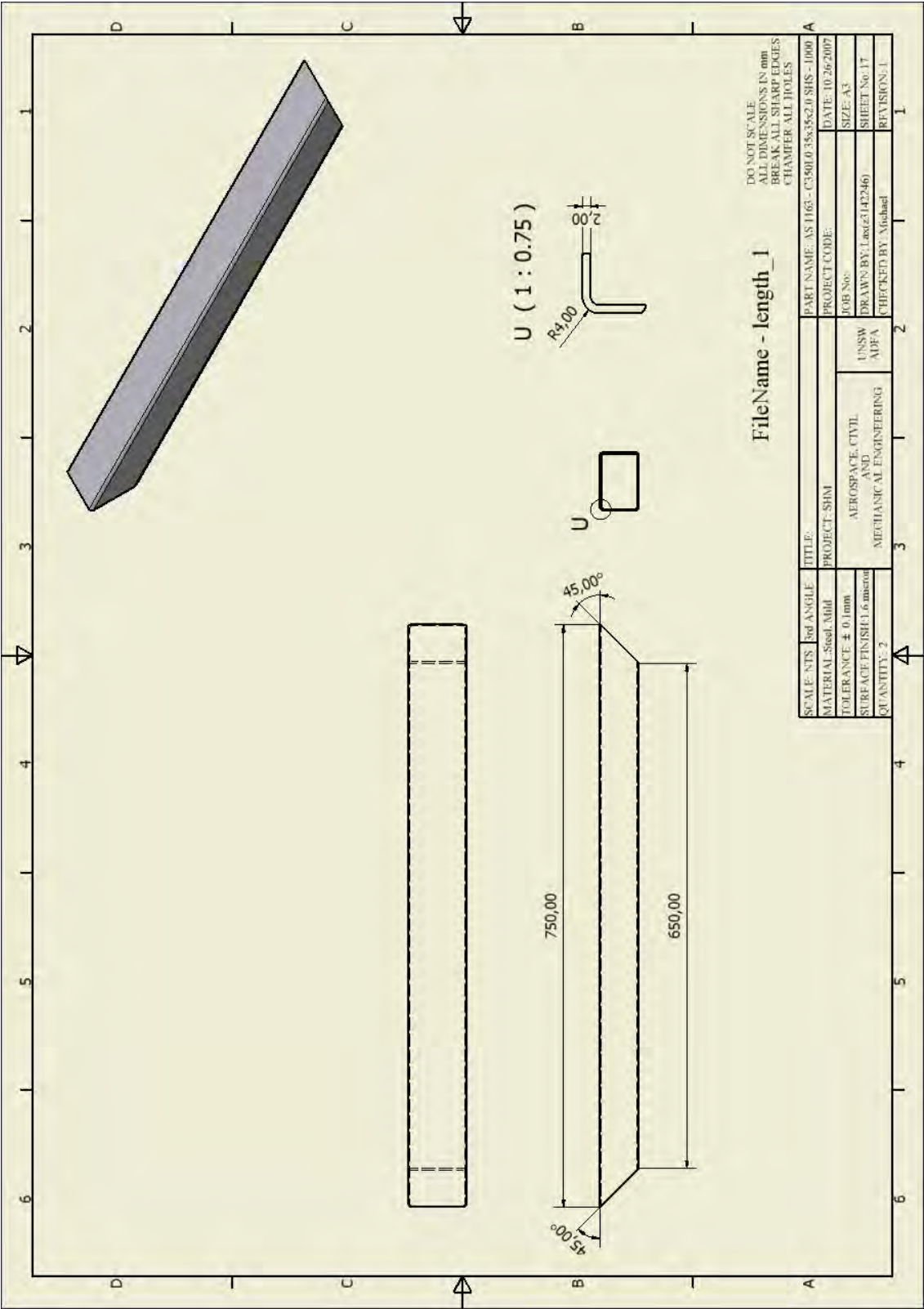
Figure G.19: Part drawings for frame

APPENDIX H

Results of the *hybrid technique* using frequency data from different sets of modes

The inverse problem for damage characterisation in plates using experimental data was presented in Chapter 9. Totally, frequencies in 8 modes were measured from the experiments. The results of the 14 damage cases presented in Table 9.4 in Section 9.4.1 was obtained using frequencies from modes 3 to 8. This section presents results from other combinations of frequencies used as input to the damage detection algorithm, *viz.* modes 1 to 6, 2 to 7, 1 to 8 and 2-8. Comparing these to the results in Table 9.4, it is seen that the best accuracies (least normalised discrepancies) are obtained with the data from modes 3 to 8. Note that in all cases the frequencies measured in the experiments were employed along with the corresponding mode-shapes obtained from *FEA* to predict the damage parameters.

Table H.1: Normalised damage parameters predicted with measured frequencies from modes 1 to 6

Damage	Actual crack parameters				Normalised discrepancy			
cases	α_c	β_c	ϕ	γ	α_c	β_c	ϕ	γ
1	0.30	0.33	38.99	0.13	0.1	3.4	43.3	6.7
2	0.37	0.30	36.34	0.18	6.7	0.1	40.4	8.2
3	0.30	0.33	37.80	0.21	0.1	3.1	42.0	5.8
4	0.30	0.33	37.18	0.25	0.1	3.0	41.3	5.0
5	0.37	0.30	37.38	0.15	6.7	0.1	8.2	8.5
6	0.30	0.33	39.55	0.17	0.1	2.7	10.6	6.7
7	0.30	0.33	39.43	0.19	0.1	2.9	10.5	4.3
8	0.30	0.33	39.13	0.24	0.1	2.9	10.1	3.6
9	0.30	0.35	39.58	0.14	0.1	5.1	22.7	7.5
10	0.37	0.30	36.64	0.19	6.7	0.0	26.0	8.7
11	0.37	0.30	36.91	0.21	6.7	0.1	25.7	6.5
12	0.37	0.30	37.78	0.25	6.7	0.1	24.7	4.8
13	0.17	0.70	40.78	0.17	3.3	10.2	12.0	7.1
14	0.50	0.30	33.53	0.17	0.1	10.0	3.9	7.0

Table H.2: Normalised damage parameters predicted with measured frequencies from modes 2 to 7

Damage	Actual crack parameters				Normalised discrepancy			
cases	α_c	β_c	ϕ	γ	α_c	β_c	ϕ	γ
1	0.29	0.36	15.21	0.13	1.1	6.3	16.9	6.1
2	0.29	0.36	8.68	0.16	1.1	6.0	9.6	6.1
3	0.29	0.37	13.31	0.20	1.4	6.8	14.8	5.1
4	0.29	0.36	15.08	0.24	1.2	6.0	16.8	4.4
5	0.30	0.33	21.60	0.14	0.2	3.2	9.3	6.9
6	0.30	0.33	19.16	0.16	0.4	3.2	12.0	6.4
7	0.30	0.33	22.25	0.19	0.1	3.2	8.6	4.0
8	0.30	0.34	25.72	0.23	0.3	3.8	4.8	3.2
9	0.31	0.36	29.89	0.14	0.5	5.6	33.5	7.5
10	0.30	0.35	33.74	0.17	0.5	5.3	29.2	6.8
11	0.31	0.36	34.49	0.19	0.8	5.9	28.3	4.3
12	0.30	0.38	38.45	0.22	0.3	7.7	23.9	1.9
13	0.20	0.60	29.59	0.14	0.2	0.1	0.5	3.9
14	0.52	0.30	24.24	0.17	1.6	9.9	6.4	7.3

Table H.3: Normalised damage parameters predicted with measured frequencies from modes 1 to 8

Damage cases	Actual crack parameters				Normalised discrepancy			
	α_c	β_c	ϕ	γ	α_c	β_c	ϕ	γ
1	0.27	0.25	45.23	0.15	3.3	4.9	50.3	8.4
2	0.27	0.25	44.41	0.19	3.3	4.9	49.3	9.1
3	0.27	0.25	45.41	0.23	3.3	4.9	50.5	8.0
4	0.27	0.25	46.69	0.27	3.2	4.9	51.9	7.4
5	0.27	0.25	45.48	0.16	3.3	4.9	17.2	9.1
6	0.27	0.25	45.57	0.19	3.3	4.9	17.3	8.7
7	0.27	0.40	40.47	0.19	3.3	10.5	11.6	3.7
8	0.27	0.25	48.82	0.26	3.1	4.9	20.9	5.8
9	0.27	0.41	41.47	0.14	3.3	11.0	20.6	7.1
10	0.27	0.41	42.93	0.17	3.3	11.0	19.0	6.6
11	0.27	0.41	43.59	0.19	3.3	11.2	18.2	4.1
12	0.27	0.42	44.22	0.22	3.3	11.5	17.5	2.1
13	0.17	0.70	43.49	0.15	3.3	10.2	15.0	5.2
14	0.50	0.40	38.07	0.15	0.1	0.1	9.0	4.7

Table H.4: Normalised damage parameters predicted with measured frequencies from modes 2 to 8

Damage cases	Actual crack parameters				Normalised discrepancy			
	α_c	β_c	ϕ	γ	α_c	β_c	ϕ	γ
1	0.29	0.35	16.40	0.13	0.7	5.1	18.2	6.2
2	0.29	0.36	9.21	0.16	1.0	5.6	10.2	6.2
3	0.29	0.36	13.69	0.20	1.3	6.5	15.2	5.1
4	0.29	0.35	16.09	0.25	0.8	4.9	17.9	4.6
5	0.30	0.33	21.55	0.14	0.3	2.8	9.4	7.0
6	0.30	0.33	19.37	0.16	0.2	2.9	11.8	6.4
7	0.30	0.33	22.18	0.19	0.2	2.6	8.7	4.2
8	0.30	0.33	25.72	0.24	0.3	2.7	4.8	3.5
9	0.33	0.29	29.17	0.16	3.4	1.2	34.3	8.9
10	0.32	0.32	34.77	0.17	1.9	2.4	28.0	7.4
11	0.32	0.32	36.04	0.20	2.4	2.5	26.6	5.0
12	0.32	0.35	41.12	0.22	1.5	4.9	21.0	2.4
13	0.20	0.60	29.72	0.14	0.2	0.2	0.3	3.9
14	0.50	0.38	31.00	0.14	0.0	2.4	1.1	4.5

H3